DERIVATION OF A LOOK-UP TABLE FOR TRANS-CRITICAL HEAT TRANSFER IN WATER-COOLED TUBES

by

Hussam A. M. Zahlan

Thesis submitted to the
Faculty of Graduate and Postdoctoral Studies
in partial fulfillment of the requirements
for the Doctorate in Philosophy degree in Mechanical Engineering

Ottawa-Carleton Institute for Mechanical and Aerospace Engineering
Faculty of Engineering
University of Ottawa

© Hussam Ali Mustafa Zahlan, Ottawa, Canada, 2015

ABSTRACT

This thesis describes the development and validation of a look-up table capable of predicting heat transfer to water flowing vertically upward in a circular tube in the trans-critical pressure range from 19 to 30 MPa. The table was based on an extensive and screened experimental database and its trends were smoothened to remove unrealistic scatter and physically implausible discontinuities. When compared to other prediction methods, the present look-up table approximated the experimental data closer in values and trends. Moreover, unlike existing prediction methods, the table applies not only to normal heat transfer conditions but also to conditions with heat transfer deterioration and enhancement. A separate multi-fluid look-up table for trans-critical heat transfer was also developed, which besides the existing water database incorporated new measurements in carbon dioxide; the latter were collected at the University of Ottawa supercritical flow loop under conditions of interest for the current Super-Critical Water-Cooled Reactor designs, for which few water data were available in the literature. Existing fluid-to-fluid scaling laws were tested and two additional sets of scaling laws were proposed, which are applicable not only to the supercritical pressure region, but also to the high pressure subcritical region. The multi-fluid table is applicable to water at conditions of normal and abnormal heat transfer, but its applicability to model fluids is restricted to the normal heat transfer mode.

ACKNOWLEDGEMENTS

First and above all, I praise ALLAH, the almighty for providing me this opportunity and granting me the capability and patience to proceed successfully.

Foremost, I would like to express my sincerest gratitude to Professor Dionysius Groeneveld and Professor Stavros Tavoularis, my advisors and research supervisors, for the continuous support, patient guidance and useful critiques of this research work.

I would like to thank my fellow in the University of Ottawa supercritical research group, Kai Jiang for the help in running the experimental program. I would like also to express my gratitude to Aurelian Tanase for providing the codes of the critical heat flux look-up table. I would also like to extend my thanks to the staff of the machine shop of the mechanical engineering department as well as contractor Dave Petry for their essential technical support.

Funding for this program by Natural Resources Canada through the Office of Energy Research and Development, Atomic Energy of Canada Limited, and Natural Sciences and Engineering Research Council of Canada is gratefully acknowledged.

I dedicate this thesis to my brother Jameel Zahlan.

Finally, I wish to thank my wife Areej Odwan and children Khaled, Hanin, Hala and Ahmad for their support and encouragement throughout my study.

TABLE OF CONTENTS

LIST OF FIGURES

LIST OF TABLES

NOMENCLATURE

c_p	heat capacity at constant pressure (J kg^{-1} K^{-1})
d, D	tube inner diameter (mm, m)
e	error (%)
e_{10}, e_{20}, *etc*.	% of data within specified error range ($\pm$ 10%, $\pm$ 20% etc.)
G	mass flux (kg m^{-2} s^{-1})
H	enthalpy (kJ kg^{-1})
L	heated length (m)
k	thermal conductivity (Wm^{-1}K^{-1})
P	pressure (kPa)
q	heat flux (kW m^{-2})
T	temperature (˚C or K)
z	axial distance from the inlet of the heated section (m)

Greek letters

μ	dynamic viscosity (N s m^{-2} = kg m^{-1} s^{-1})
ν	kinematic viscosity (m^2 s^{-1})
ρ	fluid density (kg m^{-3})
τ	shear stress (N m^{-2})

Subscripts

avg, rms	average, root mean square
b	bulk
c	critical
h	hydraulic
pc	pseudo-critical

w	wall

Dimensionless numbers

Ac^*	acceleration parameter ($= f(Q^*, \mathrm{Re}, \mathrm{Pr})$
Bo^*	buoyancy number ($= f(\overset{*}{\mathrm{Gr}}, \mathrm{Re}, \mathrm{Pr})$)
$\overset{*}{\mathrm{Gr}}$, $\overline{\mathrm{Gr}}$	modified Grashof number based on q ($= g\beta_b q_w d^4 / k_b v_b^2$)
Nu	Nusselt number (= hd/k)
Pr	Prandtl number ($=\mu C_p/k$)
Pr_{avg}, $\overline{\mathrm{Pr}}$	averaged or modified Prandtl number (= $(H_w-H_b)\mu_b/(k_b \times (T_w-T_b))$)
$\overset{+}{q}$	non-dimensional heat flux number (= (q/G) (β/c_p))
Q_b^*	thermal loading group ($= (Q_b^* = \beta_b q_w d / k_b$)
Re	Reynolds number (= $G\, D\, \mu^{-1}$)
β_b	thermal expansion coefficient $\beta_b = (-1/\rho)(\partial\rho/\partial T)_P$

Abbreviations

CHF	critical heat flux
h, HTC	heat transfer coefficient
ID	inner diameter
LUT	look-up table
NHT	normal heat transfer
SC	supercritical
SCHT	supercritical heat transfer
SCWR	Supercritical Water Cooled Reactor
TC LUT	trans-critical look-up table

CHAPTER 1

INTRODUCTION

1.1 Background

Super-Critical Water-cooled Reactor (SCWR) is one of six innovative nuclear reactor concepts selected from cooperative studies by the Generation IV International Forum. Canada adopted the SCWR because of existing opportunities to achieve high thermal efficiency (high coolant temperature) and considerable design simplification, which will give rise to improved plant economics. Reliable supercritical heat-transfer prediction methods are required for the thermal-hydraulic design and safety analysis of the SCWR. The Canadian SCWR pre-conceptual core design was completed at the beginning of 2011 and has been modified since then (McDonald et al., 2011, Leung et al., 2011, Leung, 2012). As described recently by Yetisir et al. (2013), the Canadian SCWR conceptual design of the reactor core (Figure 1.1) is a pressure-tube-type reactor oriented vertically and cooled by supercritical water; this design consists of 336 fuel channels, each of them containing a 5-meter long fuel assembly. Light water enters the fuel channel at an approximate temperature of 325˚C and a pressure about 26 MPa. Each fuel assembly has a central flow tube and two rings of fuel elements (Figure 1.2). At the bottom of each fuel channel, the coolant flows out of the central tube and changes its flow direction from downward to upward before passing through the fuel elements (Figure 1.2, a). While flowing up through fuel elements, light water temperature increases gradually and exceeds the critical temperature. The maximum outlet coolant temperature is 625˚C and the pressure at the outlet is 25 MPa.

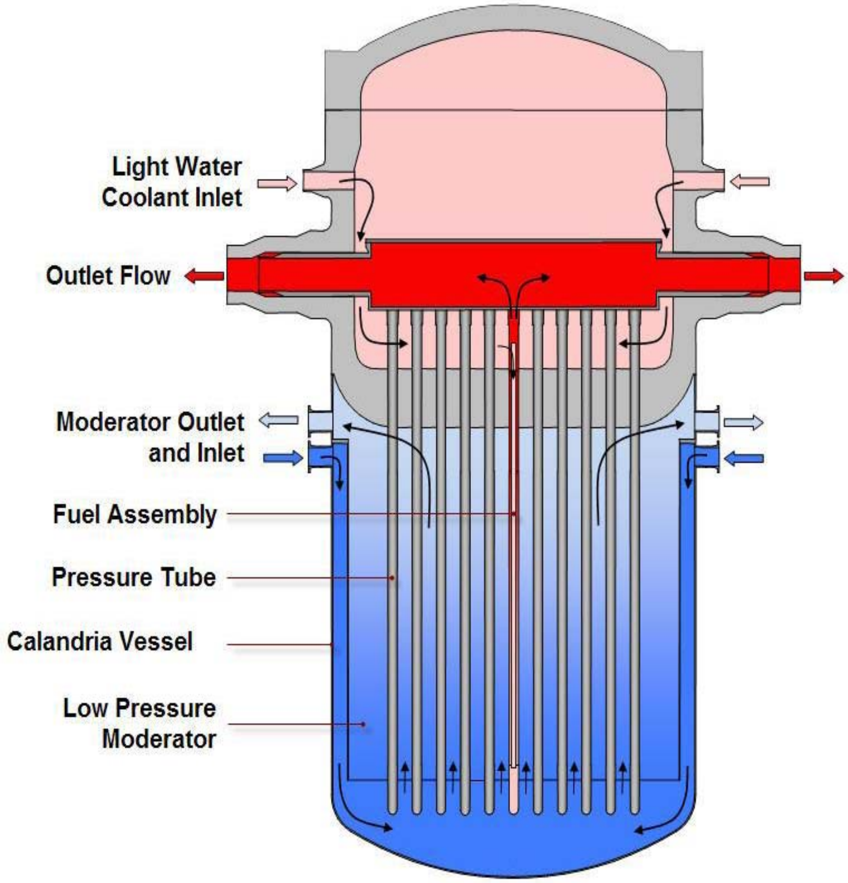

Figure 1.1: A schematic of the Canadian SCWR reactor core (Yetisir et al., 2013).

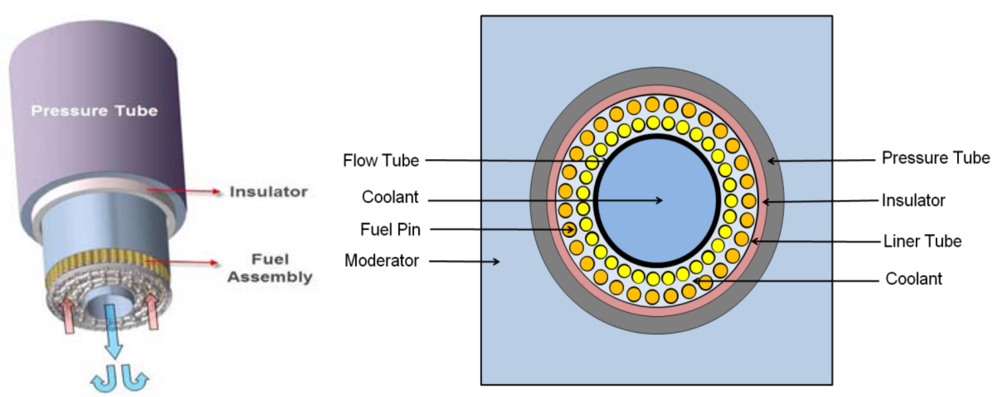

(a) Fuel channel (b) Fuel bundle

Figure 1.2: Canadian SCWR fuel channel and fuel bundle cross section (Yetisir et al., 2013).

1.2 Thermodynamics and heat transfer in the near-critical region

The thermodynamic behaviour of fluids at near critical and supercritical pressures is illustrated by Figures 1.3 and 1.4, which present various thermodynamic phases and processes of water at subcritical and supercritical conditions. A supercritical fluid is a fluid at a pressure higher than its critical pressure. The pseudo-critical line as shown in Figure 1.3 can be viewed as an extension of the saturation line beyond the critical pressure, hence separating supercritical liquid-like fluid from supercritical vapour-like fluid. Another important feature of this line is its relationship to supercritical heat transfer (SCHT), which is conventionally characterized by a pseudo-critical point[1] (described by T_{pc} for a particular pressure); at the pseudo-critical point, the fluid specific heat reaches a maximum value and the pseudo-critical line is the locus of these points within a range of pressures. It is worth noting that, at subcritical pressures, the maximum specific heat occurs at saturation. At the critical point of water, the specific heat reaches its maximum value, exceeding the specific heat value at standard pressure and temperature by three orders of magnitude (Cheng and Schulenberg, 2001). However, as the pressure is increased beyond the critical value, the peak value of the specific heat at the pseudo-critical temperature decreases.

Figure 1.4 demonstrates the differences between subcritical and supercritical states for water. This figure shows variations of pressure versus specific volume: at the triple point pressure, the difference in specific volume between saturated liquid and the saturated vapour is the largest; with increasing pressure this difference decreases and eventually vanishes when approaching the critical point. No distinct differences in phases are present beyond the critical point; water changes its behaviour from being liquid-like to gas-like along the trajectory A-A (Jackson, 2007). At subcritical pressures, isotherms display a discontinuity in slope when transitioning from a single phase to a two phase state compared to the isotherms at supercritical pressure which show a more gradual

[1] This point corresponds to a thermodynamic state of a fluid when its pressure and temperature become equal or higher than the critical values, and is characterized by a maximum specific heat for a given pressure.

change. When examining the behaviour of pressure versus volume along the isotherm $T = T_c$, one notes an inflection point with a zero slope (Figure 1.4); this inflection can be expressed by the two equations:

$$\left[\frac{\partial P}{\partial V}\right]_{T=Tc} = 0 \tag{1.1}$$

$$\left[\frac{\partial^2 P}{\partial V^2}\right]_{T=T_c} = 0 \tag{1.2}$$

These equations represent a definition for the critical point which is unique for a specific fluid (Kaye and Laby, 1973).

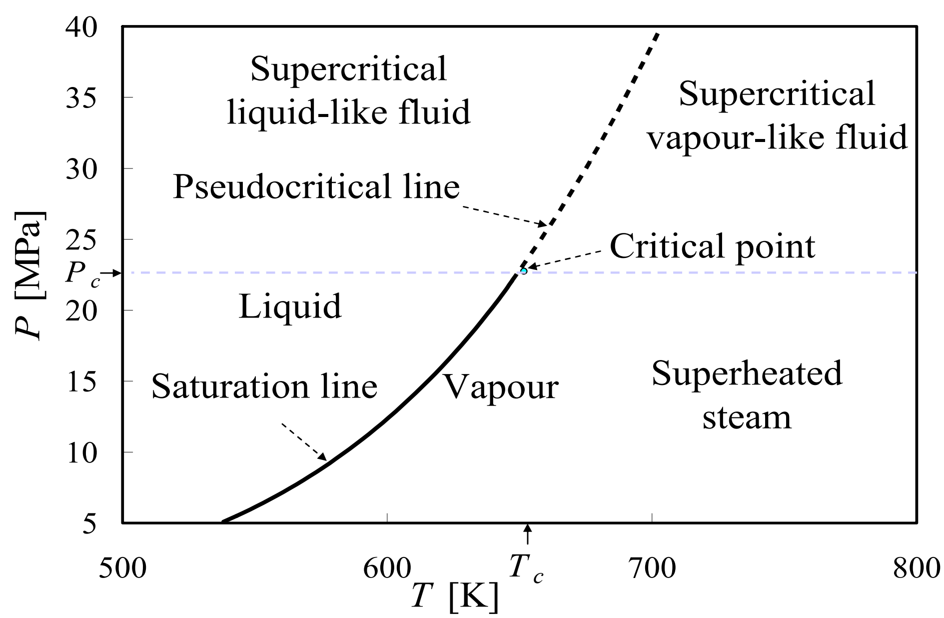

Figure 1.3: Pressure - temperature diagram. P_c = 22.064 MPa, T_c = 647.1 K.

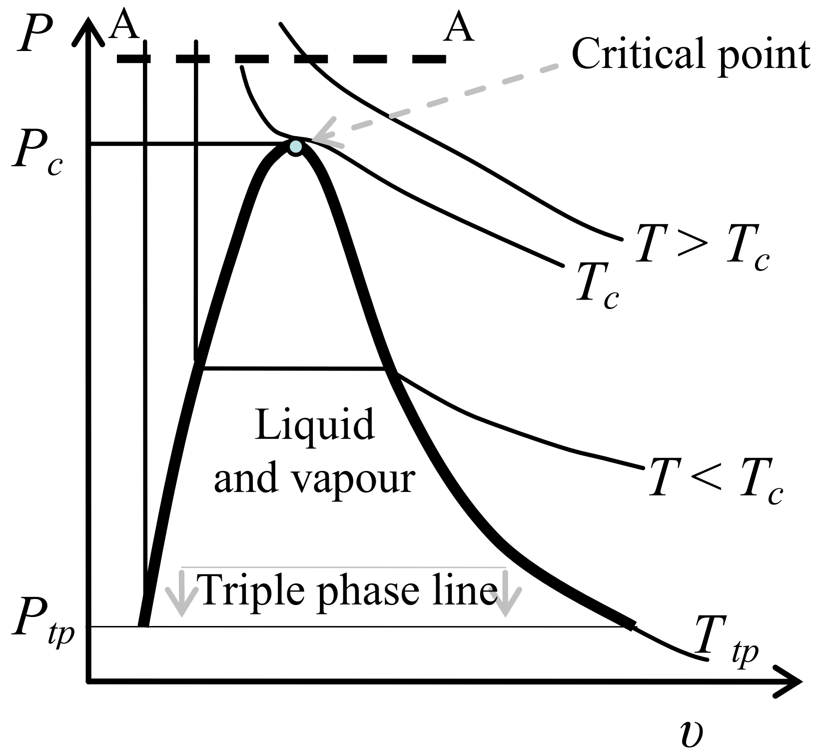

Figure 1.4: Pressure - specific volume diagram. The triple point pressure and temperature for water are, respectively, $P_{tp} = 6.117\times 10^{-4}$ MPa and $T_{tp} = 273.16$ K.

The effects of thermo-physical property variations on momentum and heat transfer near critical and/or pseudo-critical points include: (i) strong variations of the fluid thermodynamic and transport properties which influence the transport of energy and momentum, (ii) significant differences of velocity and temperature fields from those with uniform properties in a flow cross section, and (iii) under certain flow conditions, significant buoyancy and acceleration forces due to strong changes in density; these effects lead to complications in flow description (coupling of energy and momentum equations). As mentioned earlier in this section, specific heat varies significantly within a narrow range of temperature near the critical or pseudo-critical point. Sengers and Sengers (1968) attributed the large values of c_p to the increase in isothermal compressibility $\kappa = \frac{1}{\rho}\left(\frac{\partial\rho}{\partial P}\right)_{\mathrm{T}}$ which appears as a variable in the equation for c_p. Approaching the critical point, density becomes very sensitive to small changes in P and

T, as a result thermal expansion $\beta = -\frac{1}{\rho}\left(\frac{\partial \rho}{\partial T}\right)_P$ at the critical point, where the isotherm is horizontal (see Figure 1.4), becomes infinity. In addition to the specific heat, all other thermo-physical properties exhibit strong changes within a narrow range of temperature around T_c and T_{pc}; such variations of properties for water and carbon dioxide are discussed extensively in Appendix A, which also sheds light on the observed abnormal and irregular behaviour of the thermal conductivity k.

Another unusual physical phenomenon, called critical opalescence (Sengers and Sengers, 1968), occurs near the critical point. Critical opalescence refers to the turbid appearance of transparent fluids as they approach the critical point. Critical opalescence is attributed to light scattering, caused by local fluctuations in refractive index due to fluctuations in density for one-component fluid near the critical point. Critical opalescence is described in more detail in Appendix A.

1.3 Motivation

Reliable SCHT prediction methods are required for the thermal-hydraulic design and safety analysis of SCWR, however, the convective heat transfer coefficient is difficult to predict at near-critical and supercritical pressures, particularly when the fluid temperature approaches the critical or pseudo-critical temperature, where the fluid thermodynamic and transport properties change rapidly. A single correlation cannot be expected to adequately represent all possible heat transfer modes relevant to the SCWR. In the literature, there are more than twenty SCHT correlations available; these correlations all have limited ranges of validity; in addition, they usually do not predict heat transfer enhancement and deterioration that can be encountered at near critical conditions. Moreover, some of these correlations are based on experimental data from surrogate fluids such as CO_2 or Freon, and their validity for supercritical water has not been established.

A trans-critical look-up table (TC LUT) is expected to overcome some of these shortcomings and is a more promising prediction methodology compared to SCHT correlations and recently proposed SCHT LUTs[2] for the following reasons:

- look-up tables have been used successfully to predict complex heat transfer phenomena such as critical heat flux (Groeneveld et al., 2005) and film boiling heat transfer (Groeneveld et al., 2003) with an accuracy that is much higher than those of the best available prediction methods;
- the range of application of the proposed TC LUT is sufficiently wide to span all conditions for which conventional single-phase correlations do not apply;
- the proposed TC LUT will include the high-pressure subcritical region, thus providing the transitional heat transfer from the high subcritical to the supercritical pressure region, well beyond critical and pseudo-critical temperatures, and
- the proposed TC LUT is basically a normalized data bank, based on the world's largest trans-critical heat-transfer database and therefore includes heat transfer deterioration and enhancement.

1.4 TC LUT method and specifications

The development of the TC LUT employs similar construction steps to those used for the development of critical heat flux and film boiling look-up tables (Groeneveld et al.; 2003, 2005). Derivation of a reliable TC LUT requires a database which covers all conditions of interest for the SCWR. Look-up table development requires first the construction of a skeleton table based on predictions from leading heat transfer correlations to provide an initial estimate of the heat transfer coefficient (h, HTC) at specific values of flow conditions including pressure (P), mass flux (G), coolant enthalpy (H_b) and heat flux q or wall temperature T_w. For the current TC LUT, the difference

[2] Two supercritical heat transfer look-up tables, which address only normal heat transfer, have been proposed in recent years. The first table was developed by Loewenberg et al. (2008) for application within relatively narrow ranges of parameters, while the second one (Liu et al., 2011) is still under development.

between wall and bulk-fluid temperatures (T_w-T_b)[3] was chosen as an input parameter to the table: actually, this choice fits the way how thermal-hydraulic system codes perform calculations, particularly in running transient calculations for safety studies, which iterate for heat flux using wall temperature as an input parameter. Thus, the TC LUT heat transfer coefficient

$$h = f(P, G, H_b, T_w - T_b) \tag{1.3}$$

The skeleton table provides values of the heat transfer coefficient for a matrix of combinations of 11 values of pressure in the range from 19 to 30 MPa, 9 values of mass flux in the range from 100 to 5000 kg m^{-2} s^{-1}, 17 values of bulk-fluid enthalpy in the range from 1000 to 3000 kJ kg^{-1}, and 8 values of wall superheat in the range from 10 to 500 K. The final look-up table incorporates all available experimental data within the ranges of the table parameters, thus replacing the values of the skeleton table in the range of conditions of the experimental data. To minimize unrealistic sudden transitions (*i.e.*, transitions which are not based on experimental trends), HTC trends are smoothened. Figure 1.5 summarizes the development steps of the TC LUT.

[3] The maximum value of this TC LUT input parameter is 500 K, due to unavailability of thermo-physical properties data and estimation for water from NIST beyond the temperature of 1000˚C. Extrapolation of HTC by the TC LUT is not recommended beyond T_w-T_b = 500 K.

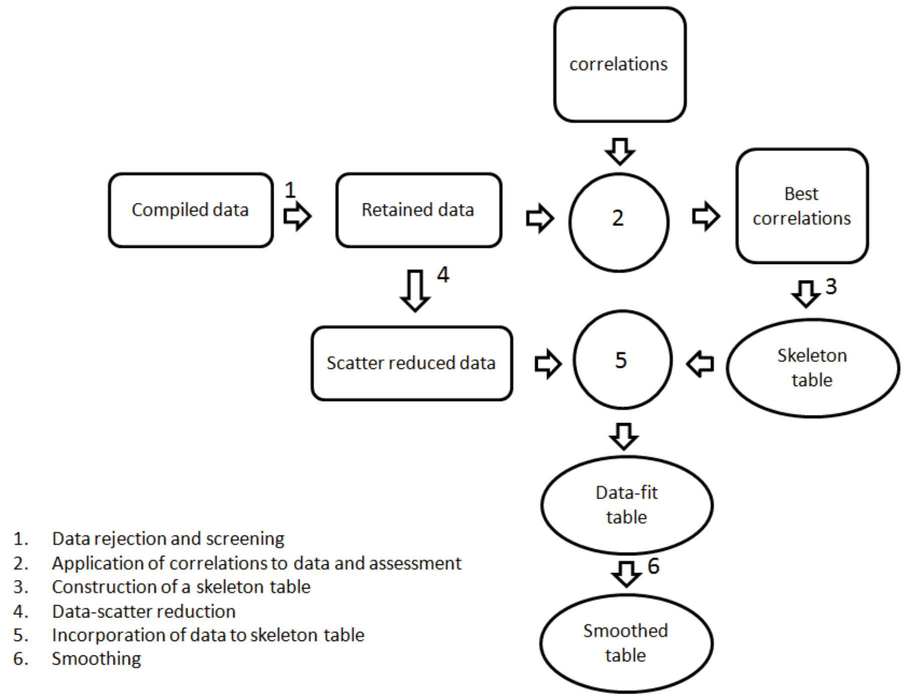

Figure 1.5: A flowchart showing the development steps of the TC LUT.

1.5 Objectives

The first objective of the thesis research is to construct a reliable, wide-range, trans-critical[4] heat transfer look-up table from experimental data applicable to water.

The second objective is to develop a multi-fluid trans-critical heat transfer look-up table applicable to water and other fluids. To achieve this objective, the following is also required:

- Acquire new, wide-range and reliable trans-critical heat transfer data. New measurements of heat transfer in tubes with 8 and 22 mm ID will be designed to cover wide range of flow conditions and to supplement the experimental database for CO_2 with measurements under conditions for which previous data are scarce or not available.

[4] The term trans-critical in this thesis refers to the heat transfer region bounded by the high subcritical pressure of 19 MPa and the supercritical pressure of 30 MPa.

- Evaluate existing fluid-to-fluid scaling laws and, if necessary, develop new ones.
- Use of collected CO_2 data to fill some gaps in the experimental database of the trans-critical heat transfer look-up table: CO_2 data will be incorporated in the trans-critical LUT database after their transformation into their water equivalent values using appropriate scaling laws.

The TC LUT was constructed to meet the following specifications: (i) good prediction accuracy, (ii) few independent parameters and (iii) smooth convergence with existing single phase and film boiling prediction methods.

1.6 Contributions to knowledge

The main product of this investigation is an improved trans-critical heat transfer prediction method which can be used for water and other fluids. The proposed prediction method is the first method applicable to both the high subcritical region and the supercritical region, extending well beyond the expected range of flow conditions for the SCWR. In addition, the new near critical and supercritical heat transfer table covers both deteriorated and enhanced heat transfer regimes, so that it can be a powerful tool to estimate the heat transfer coefficient for different heat transfer modes for wide ranges of conditions. Aside from reactor safety analysis, the new TC LUT can also be used in the thermal analysis of fossil-fuelled SC power stations, SC Brayton cycle analysis, and SC heat exchanger design calculations, especially those involving different fluids. The new reliable measurements of heat transfer to SC CO_2 in 8 and 22 mm tubes should be valuable for the study of normal and abnormal modes of heat transfer and the evaluation of the effect of tube diameter on heat transfer. The TC LUT is based on a large water and multi-fluid databank and is expected to be used as the primary heat transfer prediction method by the nuclear industry in thermal-hydraulic analyses of the SCWR. Tube-based prediction methods can be used as a basis for the estimation of maximum cladding temperature for rod bundles: an important example of the TC LUT application would be the prediction of the maximum sheath temperature of rod bundles of the SCWR, whose accurate estimation is crucial in determining the SCWR flow conditions and in choosing fuel sheath material.

1.7 Organization of the thesis

This dissertation is presented in the form of a manuscript-based thesis. Chapter 2 provides a general literature review of turbulent convective heat transfer at near critical and supercritical pressures including experimental, numerical, modeling and analytical studies.

Chapter 3 describes in detail the derivation of TC LUT for water as described in the following manuscript

Zahlan, H., Tavoularis, S., Groeneveld, D.C., 2014. A look-up table for trans-critical heat transfer in water-cooled tubes, as submitted in August 2014 to Nuclear Engineering and Design.
DOI: http://dx.doi.org/10.1016/j.nucengdes.2014.12.027
0029-5493/© 2015 Elsevier B.V. All rights reserved. Nuc. Eng. Des., 285 (2015) 109–125, 2015.

Chapter 4 reports measurements and analysis of heat transfer and pressure drop to CO_2 at near critical and supercritical pressure in the form of the following manuscript

Zahlan, H., Groeneveld, D.C., Tavoularis, S., Measurements of Convective Heat Transfer to Vertical Upward Flows of CO2 in Circular Tubes at Near-critical and Supercritical Pressures, as submitted in December 2014 to Nuclear Engineering and Design.
DOI: http://dx.doi.org/10.1016/j.nucengdes.2015.04.013
0029-5493/© 2015 Elsevier B.V. All rights reserved. Nuc. Eng. Des., 289 (2015) 92–107.

Chapter 5 describes the development of new fluid-to-fluid scaling laws of turbulent convective heat transfer at high subcritical and supercritical pressures and contains the manuscript

Zahlan, H., Groeneveld, D.C., Tavoularis, S., 2014. Fluid-to-fluid scaling for convective heat transfer in tubes at supercritical and high subcritical pressures, as submitted in October 2013 to International Journal of Heat and Mass Transfer.
DOI: **http://dx.doi.org/10.1016/j.ijheatmasstransfer.2014.02.018**
0017-9310/© 2014 Elsevier Ltd. All rights reserved. Int. J. Heat Mass Tran., 73 (2014), 274–283, 2014.

Author's contributions to the published research papers: H. Zahlan performed all analyses and experiments and prepared drafts of publications independently. Papers were subsequently reviewed and edited by supervisors/co-authors D. Groeneveld and S. Tavoularis.

Chapter 6 presents development stages of the multi-fluid TC LUT, which are similar to those applied for the development of the TC LUT.

Finally, a summary of the main findings of this thesis is presented in Chapter 7, which lists the novel contributions of this investigation and makes recommendations for future work. A description of fluid opalescence and the anomalous behaviour of thermal conductivity near the critical point are presented in Appendix A. An assessment of single-phase and SCHT correlations is presented in Appendix B. The tabulated values of heat transfer coefficient of the TC LUT are shown in Appendix C. The experimental data of the CO_2 tests are tabulated in Appendix D. An example of application of the multi-fluid table to carbon dioxide data is discussed in Appendix E. The heat transfer coefficient values of the multi-fluid look-up table are presented in Appendix F. Lastly, papers related to this thesis authored or co-authored by H. Zahlan are listed in Appendix G.

CHAPTER 2

LITERATURE REVIEW

2.1 Previous reviews

Among the first reviews of forced convection heat transfer to supercritical fluids are those of Bishop et al. (1962), Hall et al. (1968), Petukhov (1968, 1970) and Hendricks et al. (1970). These studies considered free, mixed and forced convective flow at near-critical and supercritical pressures. In addition, they presented basic equations and expressions for turbulent properties and some of them proposed heat transfer correlations. The early reviews also attempted to explain the normal, enhanced and deteriorated heat transfer modes. In addition, these reviews also discussed the analogy between nucleate boiling / film boiling at subcritical pressures, and the enhanced / deteriorated heat transfer at supercritical pressures (pseudo-boiling): SCHT enhancement is similar to the pre-CHF nucleate boiling regime with its very high HTCs, while SCHT deterioration is similar to the inefficient film boiling heat transfer. The similarity between subcritical nucleate boiling and enhanced heat transfer at supercritical conditions had been proposed by Goldmann (1961). He assumed that pseudo-boiling exists at supercritical heat transfer. As fluid temperature approaches the critical/ pseudo-critical point, c_p increases significantly allowing for much more heat to be absorbed by the SC fluid; this c_p increase may have similarity with the latent heat of vapourization associated with phase change at subcritical conditions. However, enhancement of heat transfer in subcritical nucleate boiling is much more pronounced than the enhancement of heat transfer under SC pressures (Wang et al., 2010). Because liquid and vapour phases do not exist at SC pressures, it was assumed that transient processes occur, where liquid-like fluid is heated by the much hotter surface; this contact may cause breakup of the liquid-like fluid into lower density vapour-like bubbles. The SCHT region is divided with respect to T_{pc} into three heat transfer regions; fluid is considered as vapour or vapour-like if $T_{pc} < T_b$, while fluid is considered as liquid or liquid-like if $T_b < T_{pc}$ and a near critical (NC) or pseudo-critical point fluid if $T_b < T_{pc} < T_w$. This analogy is based on the observation that deterioration and enhancement occur when $T_b < T_{pc}$ and $T_{pc} < T_w$. The popularity of the pseudo-boiling concept has diminished somewhat as it did not produce useful expressions for analogy-based SCHT models.

Recent comprehensive reviews on SCHT have been published by Bazargan (2001) and Pioro et al. (2002). Bazargan's review was presented chronologically and covered experiments, empirical correlations, horizontal flow and numerical models. Pioro et al. (2002) reviewed Russian and western publications on heat transfer and hydraulic resistance at near critical and supercritical conditions with the emphasis on Russian research.

2.2 SCHT deterioration

The terms enhancement and deterioration in convective SCHT refer to those modes for which the convective heat transfer coefficient is greater or less than that of a reference mode represented by a normal forced convective heat transfer mode with variable properties. The normal heat transfer (NHT) mode may exist in regions away from the critical or pseudo-critical temperature. In the context of this section, some discussions on SCHT enhancement will be presented. In the literature, SCHT enhancement is also presented in comparison with SCHT deterioration, because these effects develop along the test section. Therefore, enhancement and deterioration can be experienced simultaneously along the length of a heated section cooled by a supercritical fluid. However emphasis was generally on heat transfer deterioration studies: in mixed convection heat transfer, Lee (2006) and Jackson (2011) described enhancement onset as a sequel to an increase in the buoyancy number beyond the range required for the occurrence of deterioration which can ultimately end by laminarization of the flow ─ the enhanced HTC in this case can exceed the corresponding HTC for pure forced convection.

Discussions on improved and deteriorated heat transfer appeared in the early studies of Deissler (1954), Goldmann (1961) and Shitsman (1963) who first discovered improved and deteriorated supercritical heat transfer. Some investigators attributed heat transfer deterioration in the entry region of a turbulent pipe flow to development of the thermal boundary layer. Vikhrev et al. (1967, 1971) found that a kind of deterioration occurred within the entrance region (l/d < 40 – 60) particularly at high q and low G. Kirillov et al. (2005) found also that entrance effect on SCHT is significant within $l/d \leq$ 30. Pis'menny et al. (2005) showed that entry region effect on SCHT can vary within an l/d of 50 – 95 or less and is a function of q. The length of this thermal entry region decreases with increasing Re (Miropolski and Shitsman, 1957).

Petukhov et al. (1970, 1972) reported that heat transfer deterioration is related to changes in turbulent diffusivity caused by significant variations of thermo-physical properties at high heat fluxes over the flow cross section, in particular density and specific heat. In the near-wall region, the fluid density is much lower and the specific heat capacity is much higher than in the flow core. At high heat fluxes, the large thermo-physical property difference between fluid at the wall and that at the core causes a change in turbulent flow transport mechanisms; large density gradients cause natural convection transport. Petukhov and Polyakov (1988) attributed heat transfer deterioration to the suppression of turbulent transport by thermo-gravity (buoyancy affected flow) and by thermally-induced flow acceleration, which resulted from the sharp decrease in fluid density along the channel. They also noticed that effects leading to a local deterioration of the heat transfer may extend along the full length of the pipe. This was observed as an overall reduction of the heat transfer without the appearance of hot-spots on the wall.

Jackson et al. (1989), in their literature review of turbulent mixed convection heat transfer, found that heat transfer correlations for upflow should also be based on the distance from the start of the heated length expressed as l/d, which is opposite to downflows, for which the heat transfer correlations were successful when based only on local parameters. Interestingly laminar mixed convection causes enhancement for vertical upward flow and impairment for downflow.

Bazargan (2001) studied SCHT in horizontal tubes. He found that the occurrence of local hot spots was not restricted to the temperature range $T_b < T_{pc} < T_w$ or within the entry region of the pipe; temperature peaks appeared at the same location regardless of any small changes in flow conditions; deteriorated heat transfer data were not reproducible (presumably in temperature magnitudes and not in location). Decreasing the tube diameter d to below a certain size eliminates the buoyancy effects ($d \leq 2\,\mathrm{mm}$). For horizontal flows, effects of buoyancy and thermally-induced acceleration are usually coupled. For large tubes, buoyancy effects may dominate over the acceleration effects.

McEligot and Jackson (2004) described the effect of high heat flux on property variation and heat transfer: properties across the flow show variations, these changes adjust the fluid temperature distribution, so that the relation between the heat flux and the temperature difference, the convective HTC will be altered from the normal case (being enhanced or deteriorated). They also described acceleration and buoyancy effects on heat transfer: as the fluid is heated up along the tube, its density decreases and the velocity increases, this acceleration corresponds to an increased pressure drop. This effect is known to stabilize the laminar boundary layer. For turbulent flows and in analogy to the flow behaviour in laminar boundary layer, McEligot and Jackson (2004) hypothesized that acceleration of the fluid tends to reduce instability caused by the rapid expansion of the SC fluid near the wall, so that turbulent transport of the less dense fluid from the viscous layer is reduced. Laminarization occurs for flows that may be assumed at turbulent conditions; in addition laminarized flows show inferior heat transfer comparable to that of laminar flows. As buoyancy forces increase in turbulent flow, impairment of heat transfer can occur for vertical up flow, while for down flows heat transfer increases (these buoyancy effects on heat transfer for turbulent flow become opposite to those in laminar regime).

Jackson (2011) described two main mechanisms for heat transfer deterioration: (i) thermally-induced bulk flow acceleration (at high q) and (ii) mixed convection mechanism (buoyancy aided flow in vertical upward channels). Both types of deterioration cause reduction in turbulence transport of momentum and energy which can lead to partial laminarization of the flow. However, thermally-accelerated flow can lead to complete laminarization and suppression of turbulence. Jackson (2013) expanded his model on deterioration of SCHT by bulk flow acceleration due to thermal expansion (Jackson, 2011) to account for not only temperature effects but also pressure effects on density variation. Jackson's (2011, 2013) description of these two mechanisms and criteria for the onset of heat transfer deterioration are presented in following sections.

2.2.1 Bulk flow acceleration

This deterioration mechanism appears clearly at near critical and supercritical pressures in the vicinity of the pseudo-critical temperature for flows in tubes with relatively small size diameters, high mass fluxes and high heat fluxes. As the fluid progresses in a vertical tube, it gains enthalpy and its bulk temperature increases, while the pressure decreases. This increase in temperature and decrease in pressure causes a reduction in the fluid density. To maintain a constant mass flow rate, the fluid must accelerate while its density decreases. Extra pressure difference is needed to induce this acceleration and to overcome the additional frictional losses, however near the wall (within the boundary layer) fluid velocity is less than that at the core (viscous flow with no slip at the wall) and the magnitude of axial pressure gradient there becomes more than required for the flow acceleration. As a result, the shear stress modifies its magnitude to balance the excess pressure difference. The difference between shear stress distributions for a flow that is affected by thermal acceleration and that one that is free from this effect can be viewed as follows: with increasing radial distance from the wall, shear stress for an accelerated flow decreases faster than that for a fully developed flow at the same flow rate without acceleration effect. Reaching the buffer layer, the mean shear stress gradient is less than that for a normal flow at similar flow conditions. Consequently, production of turbulence is reduced, since the mean velocity gradient is lower in the buffer layer. This flow can also be viewed as an equivalent to a flow with less mass flow rate (less bulk Re and less turbulence production) having thicker viscous sub-layer with less turbulence production and less energy transport. Jackson (2011, 2013) applied this description of the flow behaviour into simplified conservation equations to produce his semi-empirical model that characterizes this type of deterioration. The mechanism can be summarized as follows:

- Heat transfer deterioration is related to strong variations of density along and across the flow, this density variation ultimately reduces turbulence generation.
- Re-distribution of wall shear stress results in a decrease in turbulent stresses; thus turbulence production and transport of heat are deteriorated.
- Non-dimensional parameters associated with the effects of pressure and temperature on density (compressibility and thermal expansion) causing the acceleration of fluid were identified. They include Reynolds number and Mach number for compressibility effects, and thermal expansion group[5], Reynolds number and Mach number for thermal expansion effects.
- Complete laminarization of the flow: the extra pressure gradient at the wall region is high enough that shear stress cannot adjust itself to maintain the viscous contact forces; bulk flow becomes nearly uniform with a flat velocity profile, the flow is laminar.

2.2.2 Buoyancy influenced flow

For vertical up flow in tubes (an assumed buoyancy aided flow), deterioration in SCHT starts at a point labeled as "the onset of buoyancy effect"; as buoyancy force increases, it reaches a point where a significant reduction in the heat transfer coefficient occurs; it can reach half of the corresponding normal heat transfer coefficient. A further increase in the buoyancy effect will result in a more effective heat transfer, thus the SCHT will recover itself to normal heat transfer mechanisms and with an additional increase in this effect, buoyancy forces will eventually cause enhancement to heat transfer. Buoyancy forces can cause deterioration in heat transfer and increase the radial extent to which the shear stress falls (caused by low density fluid near the wall); thus in the near wall region, where turbulent production mainly occurs, the shear stress is

[5] Thermal expansion group is a function of thermal expansion coefficient, heat flux, tube diameter and thermal conductivity.

reduced, fewer eddies are produced and the flow becomes less turbulent. However, for downward flow (buoyancy opposed flow), improvement in heat transfer occurs.

Some investigators described this development of buoyancy force for vertical upflow by the term "shear stress redistribution" and "shear stress distortion" and explained the subsequent mechanism of enhancement by shifting the point of maximum velocity ($\tau_{fluid} = 0$) close to the wall. The flattened and M-shape velocity profiles describing these development stages of buoyancy force are represented schematically by Figure 2.1. This figure shows buoyancy effects for vertical upward flow in circular tube geometry. The left side figure shows a flattened velocity profile and the corresponding shear stress distribution leading to deterioration in heat transfer, while the figure on the right side shows an increased effect of buoyancy (M velocity profile) and the corresponding shear stress distribution. In this case as the buoyant layer develops, it becomes thick enough that the shear stress in the core changes sign. This causes restoration of heat transfer followed by enhancement compared to that in pure forced convection. Figure 2.2 shows the effect of increasing heat flux on SCHT for a turbulent flow while the mass flux is kept constant. For $q \geq 698$ kW/m^2, noticeable increases in temperature can be noted in the wall temperature profile of the Schmidt (1959) data. This figure also shows the prediction of wall temperature profile by Jackson (2002) for q = 815 kW/m^2.

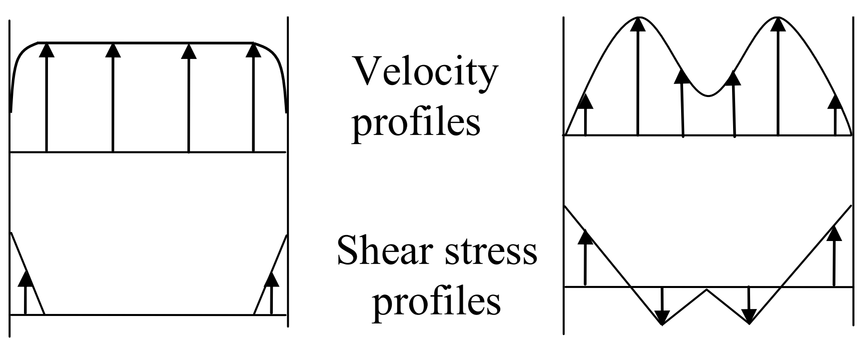

Figure 2.1: Schematic of velocity variation and the corresponding shear stress for flattened velocity profile resulting in reduced shear stress (left) and M-velocity profile leading to increased shear stress (W-profile) and heat transfer (Kraan et al., 2005).

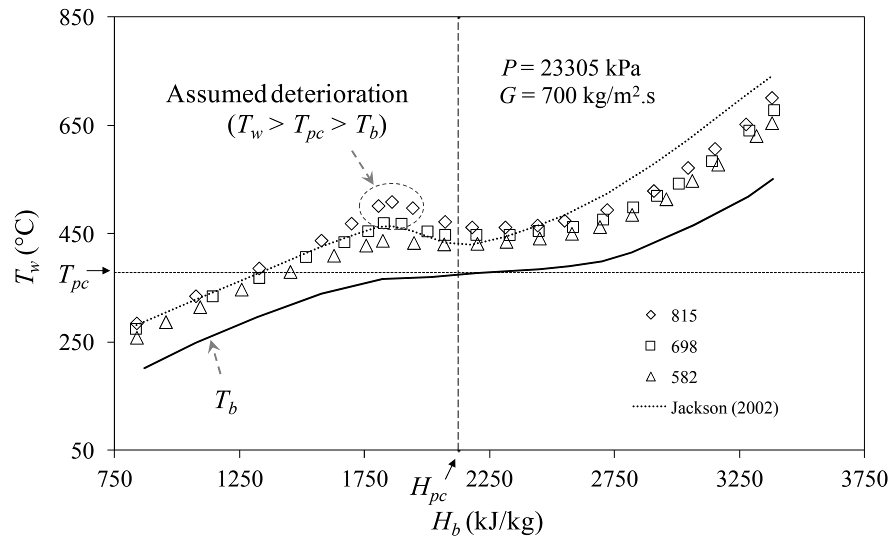

Figure 2.2: Heat flux effect on SCHT (Data of Schmidt, 1959), symbols indicate values of heat flux in kW/m^2.

2.2.3 SCHT deterioration criteria

Most of the early criteria predict heat transfer deterioration occurrence as a function of the ratio *q/G* (kJ/kg); *q* in kW/m^2 and *G* in kg/m^{2}s. Table 2.1 shows some of the SCHT deterioration criteria. These criteria predict the onset of heat transfer deterioration, but do not quantify the effect or the location. It is generally known that simple criteria of the form *q/G* are rough and lack accuracy. A more sophisticated criterion was developed by Mikielewicz et al. (2002) and subsequently by McEligot and Jackson (2004) and Jackson (2011); these criteria have a better physical basis than the criteria of the form *q/G*.

Jackson's (2011) criteria: the limits for the buoyancy number $Bo_b^* = f(\mathrm{Gr}, \mathrm{Re}, \mathrm{Pr})$ resulted from setting the buoyancy coefficient $\mathrm{C_B} = \sqrt{2}\delta^+ \mathrm{K}_1^{-3/2} = 10^5$. C_B is based on universal turbulent buffer layer thickness which has an approximated magnitude δ^+ = 30. The buoyancy coefficient is adjustable and not universal (Jackson, 2011). In a more recent study by Jackson (2012), C_B was estimated

5500. $K_1 = 0.079$ is the coefficient in the empirical equation for the friction coefficient, $f_b = K_1 \mathrm{Re}_b^{-m_1}$ and $m_1 = 0.25$. The lower bound in the inequality for Bo_b^* listed in Table 2.1 represents around 2% reduction in the Nusselt number ratio $= \frac{\mathrm{Nu}_b}{\mathrm{Nu}_{b0}}$, where Nu_b is the Nusselt number evaluated at bulk temperature and the subscript 0 in Nu_{b0} indicates normal heat transfer in a variable property flow, while the upper limit indicates partial laminarization of the mixed convection flow where the corresponding reduction in Nusselt number ratio ≈ 50%. N.B., the upper limit could include the region of recovery where heat transfer starts restoration but its value is still below the corresponding normal heat transfer for forced convective variable property flow. The overbar Pr number is the integrated average Pr number between T_b and T_w.

Table 2.1: Selected criteria for SCHT deterioration.

Reference	Criterion	Comments
Vikhrev et al. (1967)	$q/G \geq 0.4$	-
Alekseev et al. (1976)	$q/G \geq 0.8$	-
Kondratiev (1971)	$q \geq 5.815\times10^{-7}\mathrm{Re}_b^{1.7}(\frac{P}{0.1})^{4.5}$	-
Koshizuka and Oka (2000)	$q \geq 200G^{1.2}$	-
Mikielewicz et al. (2002)	$\overset{*}{Bo} = \frac{\overset{*}{\mathrm{Gr}}}{\mathrm{Re}^{3.425}\mathrm{Pr}^{0.8}} \geq 6\times10^{-7}$ where $\mathrm{Gr}_b^* = g\beta_b q_w d^4 / k_b \nu_b^2$ and $\beta_b = -\frac{1}{\rho}\left(\frac{\partial\rho}{\partial T}\right)_p$	$\overset{*}{Bo}$ modified buoyancy parameter Gr_b^* modified Grashof number at T_b β_b thermal expansion coefficient
Jackson (2011)	$Bo_b^* = \frac{\overset{*}{\mathrm{Gr}}_b}{\mathrm{Re}_b^{3.425}\mathrm{Pr}_b^{0.8}}$, where	$\overline{\mathrm{Pr}}$ averaged Prandtl number Ac_b^* acceleration parameter

Reference	Criterion	Comments
	$4\times10^{-6} \geq Bo_b^* > 4\times10^{-7}(\frac{\overline{\mathrm{Pr}}}{\mathrm{Pr_b}})^{0.4}$ $Ac_b^* = \frac{Q_b^*}{\mathrm{Re}_b^{1.625}\,\mathrm{Pr_b}} > 4\times10^{-6}$ where $Q_b^* = \frac{\beta_b q_w d}{k_b}$	Q_b^* thermal loading/expansion group

Concluding remarks: for turbulent upflow in vertical tubes, both mechanisms of heat transfer deterioration have similar origin and characteristics. Momentum transport and heat transfer affect each other: variations of density and other thermo-physical properties across and along the flow can cause these changes. Deterioration typically starts when $T_w > T_{pc} > T_b$. When the deterioration effect becomes relatively significant, then this point is referred to as the onset of deterioration and is described differently for each mechanism of deterioration. Under appropriate buoyancy conditions, as this force develops along the tube, partial laminarization of the mixed convection flow can occur and is believed to be followed by transition which is associated with instability induced by heating and restoration of turbulence generation and the recovery in heat transfer (Lee, 2006). Deterioration by acceleration is independent of flow direction, while deterioration by buoyancy is observed in vertical upflow in tubes (buoyancy aided). For vertical upflow, the buoyancy force is assumed to assist the flow (in the same direction); however the net effect is negative. While for vertical downflow, buoyancy hinders the flow and the net effect is positive (enhancement occurs). Deterioration by buoyancy is a mixed convection problem, where gravity and convective terms are comparable in the momentum equation (Jackson, 2011). The two deterioration mechanisms are similar: near the wall, density decreases while velocity increases, this alters the shear stress distribution causing a decrease in turbulence generation which is known to initiate from this region (Townsend, 1976). As a result of deterioration, the flow can be approximated by a less efficient turbulent or even laminar flow regime (this is equivalent to reducing the Reynolds number in normal heat transfer – HTC decreases as shown by many heat transfer correlations. This decrease is particularly pronounced at high heat fluxes, which generate large temperature gradient across the flow accompanied by the presence of drastic variations in properties in the vicinity of the critical/pseudo-critical point.

2.3 Experimental studies and simulations

2.3.1 Experimental tube data compilation at the University of Ottawa

Many heat transfer experiments using SC water have been reported during the past sixty years. Most of these heat transfer data were obtained in support of the SC fossil fired plants, which have been constructed around the world since the early nineteen sixties. Pioro and Duffey (2005) reviewed the literature of SCHT experiments in water and found more than a hundred data sets. Although these data should, in principle, be available to investigators worldwide, in practice data availability is a real problem for the following reasons:

- Several data sets have been lost, especially those data obtained prior to 1965, when computers were not used in the laboratory. Most of the early investigators have died or retired, and, in many cases, their data have never been properly archived. In other cases, the laboratories where the data were obtained have ceased to exist (e.g., UKAEA), making it very difficult to retrieve the archived data.
- The data are classified as proprietary or commercial.
- The data may still be available, but it would require significant motivation, effort, and expense to retrieve them from archives and have them restored in a usable form.
- The data are only available in graphical form, often created manually. Values can be extracted from the graphs using data digitization software, but they would generally be less accurate than tabulated values, because of loss of resolution in small-size graphs, averaging of data on plots, and averaging of flow conditions for each graph.

An exhaustive literature review was performed at the University of Ottawa and revealed 26 water data sets containing more than 6000 trans-critical heat transfer data points. The majority of the compiled data covered flows in a vertical tube; less data were obtained in a horizontal tube and a very limited number of experiments were reported for flow inside rod bundles. The compiled high subcritical pressure data were mainly from the database of the film boiling look-up table (Nakla, 2010) with 852 screened data points. The sources for these compiled data are Herkenrath et al. (1967), Subbotin et al. (1973) and Becker et al. (1983).

Table 2.2 provides a summary of the reviewed SCHT experiments performed in tubes; for each experimental investigation the table shows the range of flow conditions of the data, the data source (graph or table), and the number of SCHT data points extracted.

Table 2.2: University of Ottawa collection of SCHT data sets for water in circular tubes.

Reference	P MPa	T_b ˚C	q kW/m^2	G kg/m^{2}s	Tube ID (mm) / flow direction	Data availability	Number of data
Ackerman (1970)	22.75−31.03	90.7−405	158− (946)	407−1221	9.4−24.4/ vertical up	Graph	317
Alekseev et al. (1976)	24.5	101−341	270−580	380	10.4 / vertical up	Graph	99
Alferov et al. (1969)	25.3−30.4	152-261	474	342	20/ vertical up	Graph	78
Alferov et al. (1975)	26.5	76−248	480	447	20/ vertical up & down	Graph	63
Barulin et al. (1971)	24.5	320−381	480−490	467	3/ vertical up & down	Graph	45
Bishop et al. (1965)	24.2−27.06	324−441	694−3470	665−3390	2.5−5.1 a bit oval (5.1)/ vertical up	Graph	48
Dickenson and Welch (1958)	24.2−31.1	102−536	748−1844	2170−3418	7.6/ horizontal	Table	123
Glushchenko et al. (1972)	22.6	19−402	1050-1220	750	4, 6, 8 / vertical up	Graph	60
Goldmann (1961)	34.5	222−363	3533−3659	2034	1.6/ vertical up	Graph	26
Griem (1996)	25	351−416	300−600	500−2500	14 /vertical up	Graph	110
Herkenrath, (1970)	24	336−383	400	1000	10 / vertical up	Graph	32

Continued

Table 2.2							
Reference	P MPa	Tb ˚C	q kW/m^2	G kg/m^2s	Tube ID (mm) / flow direction	Data availability	Number of data
Ishigai et al. (1976) (in Russian)	25.3	207−531	151-698	500	3.92/ vertical up	Graph	169
Kirillov et al. (2005)	24−25	298−435	86−1056	198−1495	10/ vertical up	Table	2344
Krasyakova et al. (1977)	24.5	202−393	81−900	90−1000	20 / vertical down	Graph	216
Lee and Haller (1974)	24.1	266−382	315−1577	542−2441	38.1/ vertical up	Graph	270
Ornatsky et al. (1971)	25.5	24−384	395−1810	850−1530	3 / vertical up & down	Graph	90
Razumovskiy (2005)	23.5	17−325	76−496	248,249	6.28−9.5 / vertical up & down	Graph/table	380
Schmidt (1959)	22.3−30.4	192−564	291– 815	700	5/ horizontal	Graph	369
Shitsman (1963)	23.3−25.3	284−383	278−1083	323−1500	8/ vertical up	Graph/table	86
Shitsman (1968)	24.5−34.3	100−403	238−700	103-608	8,16 / vertical up & down	Graph	296
Swenson et al. (1965)	22.75−31	153–516	789−1735	2150	9.42 / vertical up	Graph	160
Vikhrev et al. (1967)	26.5	61−407	362−1160	493−1400	20.4 / vertical up	Graph	262
Watts and Chou (1982)	25	149−177	250	493	32.2/ vertical up	Graph	20
Yamagata et al. (1972)	24.5	334−477	233−698	1260	7.5/ vertical up & down	Graph	184
Yin et al. (2006)	26	286−434	200	600	29 / inclined upward, 20˚ from horizontal axis	Graph	34
Yoshida and Mori (2000)	24.5	241−466	233−698	1180	10/ vertical up & down	Graph	133
Total							6014

Concluded

2.3.2 SCHT studies in rod bundles

Chun et al. (2009) investigated experimentally pressure-transient effect on SCHT in a 5×5 rod bundle for a vertical upflow using R-134a as a coolant. Inner surface temperatures of the heater rods were measured using K-type thermocouples. The axial heat flux distribution was uniform for each rod, but not identical for all rods. This open bundle geometry (pitch /diameter > 1.2) used simple spacers without flow enhancing features with a radial distance of 12.85 mm and an inside diameter for the heated rod of 9.5 mm. During their pressure transient tests, the test section power, mass flow rate and inlet temperatures were kept constant. The pressure transients were generated by varying the nitrogen gas pressure in the pressurizer/ accumulator.

Dyadyakin and Popov (1977) performed measurements of surface temperature and pressure drop in a tight seven-rod bundle equipped with helical spacers cooled by SC water. The rods were wrapped with helical fins with a height of 0.6 mm, a thickness of 1 mm and a helical pitch of 400 mm; the test section heated length was 500 mm. The rod bundle is positioned inside a hexagonal shell, which is contained in a 42.6 mm pressure tube, with a pressure rating of 40 MPa. The test section failed more than once. The hydraulic diameter d_h was varied from 2.15 to 2.77 mm by changing the shell size. Dyadyakin and Popov (1977) measured internal surface temperature of the central rod using 10 chromel-alumel thermocouples having estimated uncertainty of $\pm$1˚C. They performed 59 tests with heated test sections and reported the occurrence of pressure and flow oscillations during the tests. The paper did not present experimental data or refer to any publication which may include their data. Dyadyakin and Popov (1977) reported that no sharp changes in surface temperature distribution were detected; the wall temperature always increased. The sharp changes observed in wall temperature in tubes under similar flow conditions were not observed in their experimental study. System pressure was 24.5 MPa. Flow direction was not specified, however from the context of the paper, flow direction is thought to be upwards. They generalized their data in a form of two correlations: a correlation for the coefficient of hydraulic resistance as a function of Re and a correlation for Nusselt number variation, Nu = f (Re, Pr, x/d_h). Similar non-dimensional parameters (correction factors) for density and viscosity were introduced in the two correlations: $(\frac{\rho_w}{\rho_b})_x^{0.2}$ $(\frac{\mu_b}{\mu_{in}})_x^{0.2}$ $(\frac{\rho_b}{\rho_{in}})_x^{0.1}$, where x is the axial location.

Grabezhnaya and Kirillov (2004) discussed SCHT deterioration caused by acceleration and buoyancy force. For forced convective SC flow in tubes, they recommended the correlation of Bishop (1965) and Swenson (1965) for normal mode of heat transfer and Popov (1964) correlation for hydraulic resistance. For rod bundles, the Dyadyakin and Popov (1977) correlations for heat transfer and hydraulic resistance were recommended.

2.3.3 Numerical methods for supercritical heat transfer

Chatharaju (2011) discussed the application of system codes to SCHT. System tools or computational codes were developed only for flows at subcritical pressures and currently undergo upgrades to address the supercritical conditions. Computational codes can be categorized in two groups: (i) one dimensional system codes and (ii) computational fluid dynamics codes. The first type includes thermal-hydraulic simulation codes which are commonly used in nuclear industry for safety analysis and design of light water reactor systems. These codes in general use a non-homogeneous, non-equilibrium two-fluid model to describe the behaviour of single and two-phase flow. They have been validated against sub-critical experimental data and are generally accepted for accident simulations in light water reactors.

Computational fluid dynamics codes are generally based on commercial software; these codes have the capability of modeling the flow in three dimensions compared to the first type. Computational power and turbulence models are the main source of limitations of these codes. Thermo-physical properties included in these two types of computational codes do not include the supercritical region; however efforts have been made recently to overcome this difficulty by developing external routines integrated with the code which correlate water properties at supercritical pressure as a function of temperature only for an assumed isobaric flow.

Yu et al. (2007a, b) reported the progress on development of a sub-channel thermal-hydraulic code to analyze the thermal behaviour of fuel bundles in a CANDU[6]-SCWR type reactor (horizontal flow). They compared predictions of the developed code and ASSERT-PV[7] at a sub-critical pressure for a reference fuel channel called TACR (similar to the Advanced CANDU Reactor (ACR 700)): the predictions of the developed code agreed with the ASSERT-PV predictions of sub-channel fluid temperatures/enthalpies, and channel pressure drop. Yu et al. (2007a, b) explored the possibility of implementing the derived code in analysis of CANDU-SCWR; this code uses the SCHT data obtained at Xi'an Jiaotong University and the correlation of Dyadyakin and Popov (1977). Yu et al. (2007a) found that the developed code would be able to estimate the steady state thermal-hydraulic characteristics of the CANDU-SCWR.

2.4 Prediction methods for the near-critical and supercritical heat transfer

Forced convective heat transfer for turbulent flows in tubes near the critical point is described by variable thermo-physical properties. Another difficulty appears when property variation becomes very large, this occurs near the critical and pseudo-critical temperature. At high heat fluxes, property change becomes very strongly dependent on temperature for a particular pressure. Similarly, experiments revealed that the mass flux effect on the heat transfer coefficient depends on heat flux. A decrease in mass flux showed a similar effect on the property variation across the flow as an increase in heat flux. Thus under these conditions, supercritical heat transfer becomes very complicated

---

[6] CANDU is CANada Deuterium Uranium, a registered trademark of AECL.

[7] a sub-channel thermal-hydraulic code developed at Chalk River Laboratories for single-and two-phase steady and transient flow; ASSERT-PV is based on the advanced drift flux model: considers unequal velocity and temperature profiles between phases and a drift flux correlation to account for the transverse flow.

and satisfactory analytical solutions have not yet been developed. Instead empirical and semi-empirical methods are used for solving supercritical heat transfer problems.

2.4.1 Empirical methods for circular tubes

Several reviews of SCHT prediction methods have been published: Hall et al. (1968), Jackson and Hall (1979a, 1979b) and Cheng and Schulenberg (2001) have presented overviews and assessments of SC heat transfer correlations against both SC water and SC CO2 data. Pioro et al. (2004) presented a more up-to-date review of such correlations that have been applied to SC conditions. In a more recent study, Zahlan et al. (2011) presented a review of SCHT correlations and an assessment against the University of Ottawa water databank.

Single-phase correlations: single-phase correlations have a form similar to the Dittus-Boelter (1930) equation, but with different exponents. The Dittus-Boelter (1930) equation was originally based on water data only and evaluates the fluid properties at the bulk fluid temperature, whereas the Sieder-Tate (1936) equation includes a viscosity ratio term to account for the difference in fluid viscosity at the wall and in the bulk flow. The Hadaller and Banerjee (1969) equation is based on high-pressure superheated steam data. The most recent single-phase heat transfer equation is that of Gnielinski (1976) for turbulent flows, which includes a friction factor term to account for the increase in heat transfer with an increase in friction factor. The Gnielinski (1976) correlation includes also a factor to account for the effect of boundary layer development on heat transfer coefficient enhancement.

SCHT correlations: one of the earliest SCHT correlations is that of Bishop et al. (1965) who modified the Dittus-Boelter (1930) equation by including a density ratio (ratio of the density at wall temperature and the density at bulk fluid temperature) and replacing the specific heat in the Prandtl number by the effective integrated specific heat capacity $\bar{c_p} = \frac{H_w - H_b}{T_w - T_b}$. The Swenson et al. (1965) correlation has similar parameters to those in the Bishop et al. (1965) correlation, except that T_w was used as the reference temperature for Nu, Re, and averaged Pr number. Krasnoscheckov and Protopopov (1966) proposed a modified version of a SCHT correlation previously derived in 1959 and 1960 based on CO_2 data. Data were predicted within 15% (for their database) with this correlation, which was recommended for the following ranges:

$2\times10^4 < \mathrm{Re_b} < 8.6\times10^5$,

$0.85 < \overline{\mathrm{Pr}}_b < 65$, $0.9 < \frac{\mu_b}{\mu_w} < 3.6$, $1.0 < k_b/k_w < 6.0$ and

$0.07 < \frac{c_p}{c_{p,b}} < 4.5$

Jackson's (2002) correlation is basically a modified form of the Krasnoscheckov et al. (1967) equation, the exponent n of the specific heat ratio is defined (with T in K):

$n = 0.4$, for $T_b < T_w < T_{pc}$ and $1.2T_{pc} < T_b < T_w$

$n = 0.4 + 0.2(T_w/T_{pc} - 1)$, for $T_b < T_{pc} < T_w$

$n = 0.4 + 0.2(T_w/T_{pc} - 1)(1 - 5(T_b/T_{pc} - 1))$, for $T_{pc} < T_b < 1.2T_{pc}$

Yamagata et al. (1972) introduced a correction factor to the Dittus-Boelter (1930) equation, which is a function of the Eckert number E (= $(T_{pc}-T_b)/(T_w-T_b)$) and the Prandtl number at the pseudo-critical temperature or the effective integrated specific heat capacity ratio. Watts and Chou (1982) correlated mixed convection water and CO_2 data for vertical upward and downward flows; they used the deterioration criterion of Jackson and Hall (1979b) in the development of their correlations for normal and deteriorated heat transfer. Jackson and Hall (1979b) criterion is dimensionless and is expressed by the ratio of averaged Grashof number $\overline{\mathrm{Gr}}$ based on averaged density to Reynolds number raised to the power of 2.7; if the ratio is less than 10^{-5}, the buoyancy effect is assumed to have negligible influence on heat transfer. Griem (1996) modified the Dittus-Boelter (1930) equation by considering c_p at five reference temperatures over the range from T_b to T_w; the selected $c_{p,sel}$ was based on excluding the largest two c_p values and averaging the remaining three; $c_{p,sel} = (\sum_{i=1}^{i=5} c_{p,i} - c_{p,1^{st}\max} - c_{p,2^{nd}\max})/3$. Griem (1996) also introduced a correction factor to cover the entire enthalpy range; this factor is a function of H_b. The correlation of Koshizuka and Oka (2000) was based on their earlier numerical study of SC water flow in a 10 mm tube (Cheng and Schulenberg, 2001); they proposed an empirical correlation, in which the "pseudo-CHF" (in analogy to subcritical heat transfer) is equal to $200G^{1.2}$; this parameter indicates the occurrence of heat transfer deterioration.

Kuang et al. (2008) used their SCHT databank for water in vertical upward flow in tubes to develop their correlation. They investigated the enhanced and deteriorated heat transfer regions based on the normal heat transfer coefficient predicted by Dittus-Boelter correlation (1930). Kuang et al. (2008) used the modified Grashof number $\overset{*}{\mathrm{Gr}}$ (there is a negative correlation between HTC and $\overset{*}{\mathrm{Gr}}$), which was first introduced by Jackson et al. (1989) to account for the buoyancy effect. In addition they used the McEligot and Jackson (2004) non-dimensional heat-flux number q^+ to consider the streamwise thermal acceleration effect from heating on the HTC.

Mokry et al. (2009) used the SCHT water data of Kirillov et al. (2005; 89 tests with 81 data points per test) in deriving their correlation. For the development of their correlation, Mokry et al. (2009) excluded heat transfer deterioration regions, and removed outliers as observed in wall temperature profiles of the Kirillov et al. (2005) database. Cheng et al. (2009) derived a simple SCHT correlation to predict the deviation from the normal heat transfer predicted by the Dittus-Boelter (1930) equation. This correlation is a function of the dimensionless acceleration number π_A; this number is a form of non-dimensional heat flux number and is similar to q^+ in the Kuang et al. (2008) correlation.

Recently, Gupta et al. (2010) modified the Swenson et al. (1965) correlation which evaluates the fluid properties in Nu, Re and average Pr at the wall temperature. Gupta et al. (2010) added a viscosity ratio term, to account for viscosity variations at the wall and at the bulk fluid. They included also a correction factor to account for the developing boundary layer effects at the entry region: this was an exponentially decreasing function with distance l from the entrance of the test section (expressed by the ratio *l/d* where *d* is the tube diameter). The correlations described above are listed in Table 5 of Appendix B.

Look up tables (LUT): Löwenberg et al. (2005) described the steps required for the development of a SCHT look-up table including procedures, interpolation considerations and smoothening of heat transfer trends. Löwenberg performed smoothening of experimental data using a MATLAB routine with smoothening splines. They demonstrated the problem of interpolation between two pressures involving different flow regimes around the critical point; e.g. for the same q, G, d at P = 21.5 and 22.5 MPa; wall temperature profiles are different. They concluded that simple interpolation between these two pressures is not possible without prior knowledge of the flow structure in between these interpolated pressures. They emphasized the importance of filling the gap in experimental data near the critical point. Löwenberg et al. (2008) presented their supercritical heat transfer LUT for water inside vertical upward smooth tubes. The table presents wall temperatures as a function of five parameters: P (22.5 – 25 MPa), G (700 – 3500 kg/m^{2}s), q (300 – 1600 kW/m^2), d (8 – 20 mm) and H_b (1200 – 2700 kJ/kg). The LUT was developed for SCHT and does not cover the heat transfer at high subcritical pressures; its parameters range is limited, particularly in heat flux, which does not cover consistently all combinations of LUT parameters. In addition, the table was not constructed for the prediction of heat transfer deterioration since its database was screened to remove data affected by buoyancy deteriorated heat transfer. Löwenberg et al. (2008) used 5744 fully developed (z/d > 50) forced convection data from twelve sources for its development. They used linear interpolation for predicting wall temperatures in regions between the table grid points. The mean error in wall superheat ($T_w - T_b$) of their LUT is -1.7%, and the standard deviation is 10.2% for all experimental wall superheats.

Liu et al. (2011) reported on their progress in developing a SCHT look up table for water upflow in tubes. The derived LUT has the form $T_w = f(P, G, q, H_b)$. It includes a main table for a reference tube diameter of 10 mm and 8 tables for different reference tube diameters ranging from 7 to 26 mm; these 8 LUTs were not were not finalized, since they needed further improvements. In the development of their LUT, Liu et al. (2011) did not exclude deteriorated heat transfer data from their database. The LUT was constructed for fully developed flow and uniform q. They assumed that local parameters can sufficiently describe relevant SCHT; total number of data used for the LUT update was 10764 data points from 11 sources. Liu et al. (2011) applied regression polynomials using commercial software for wall temperature over all experimental data within each interval of H_b. The functional dependence between T_w and P, G, q, H_b is a polynomial function of maximum 3rd degree. Heat transfer at grid points of the table was calculated using these established regression functions; when no experimental data covered a specific parameter range, then the LUT values were labeled appropriately; on the other hand if only one data point or a very limited number of data fell in a particular parameter range, then the LUT values were also labeled accordingly. Average errors and standard deviations in temperature prediction (in ˚C) for these tables were low. For all tables, the overall average error was -0.072% and the overall standard deviation was 2.12%. Only a section of the LUT for d = 10 mm was presented and parametric trends of the final LUT were not provided.

2.4.2 Semi-analytical models

Deissler (1954) and Goldmann (1954) were the first investigators to develop models for SCHT. Deissler (1954) used a turbulence model that was similar to the law of the wall and assumed analogy between momentum and heat transfer. Goldmann (1954) followed a similar approach, but used an expression for eddy diffusivity derived originally for a constant property flow; the eddy diffusivity was calculated at different radial locations considering property variations at these locations.

Analytical models for flow and heat transfer at supercritical conditions with variable fluid properties are complex and often result in mathematical and physical difficulties (Petukhuv; 1970). Mathematical difficulties can be attributed to the coupling of momentum and heat transfer; in addition these equations are nonlinear. Physical difficulties are associated with the unavailability of analytical expressions for turbulent diffusivity of momentum (eddy viscosity) and heat transfer for variable property flow.

Alternatively assumptions have been made to use the derived expressions for constant property flow. Petukhov (1970) studied turbulent flow with variable properties which fits characteristics of SC flow without the consideration of gravitational and acceleration effects. An analytical description of the heat transfer phenomena in a turbulent flow near the critical point requires consideration of variations of flow properties in time and space. This was also approximated by Petukhov (1970), who decomposed field properties (like velocity, pressure, temperature and density) into mean and fluctuating components for incompressible flow (although density varies, these variations are attributed to the strong gradients in temperature, whereas pressure gradients are assumed insignificant), quasi-steady flow (mean properties are nearly constant in time) and axisymmetric turbulent flow in pipes. Petukhov (1970) identified two controlling transport mechanisms: (i) molecular; which results in viscous stresses (proportional to mean velocity gradient) and heat fluxes (proportional to mean temperature gradient) and (ii) turbulent convective mechanism in analogy to the mechanisms mentioned above for turbulent flow (gradient transport concept): turbulent stresses (resulted from momentum transport; velocity fluctuations) and heat transfer (caused by velocity and temperature fluctuations) are proportional to mean velocity and temperature gradients, where the coefficient of proportionality is the turbulent diffusivity. Disagreement was noticed between semi-analytical methods and experimental data, this deviation is attributed to the approximation from assuming constant turbulent diffusivities. Jackson (2011) solved the momentum and energy equations and proposed a model to account for normal, enhanced and deteriorated heat transfer: Jackson's model features enhancement and deteriorated heat transfer and was described in Section 2.2. Recently Jackson et al. (2012) published a review of progress on the development of new empirical equations under the framework of the IAEA, the author of this thesis contributed to this study.

In general, semi-empirical models are often based on expressions for turbulent diffusivities that are questionable. In addition, the numerical coefficients included in Jackson's (2011) model are empirical and may have a limited range of validity.

2.5 Supercritical heat transfer similarity and scaling methods

The literature review pertaining to this topic is presented in Section 2.1 of the fluid-to-fluid scaling paper, which forms Chapter 5.

CHAPTER 3

A LOOK-UP TABLE FOR TRANS-CRITICAL HEAT TRANSFER IN WATER-COOLED TUBES

This chapter addresses the development and validation of the trans-critical heat transfer look-up table. This study is presented in the form of a manuscript entitled:

Zahlan, H., Tavoularis, S., Groeneveld, D.C., 2015. A look-up table for trans-critical heat transfer in water-cooled tubes, as submitted in August 2014 to Nuclear Engineering and Design.
DOI: http://dx.doi.org/10.1016/j.nucengdes.2014.12.027
0029-5493/© 2015 Elsevier B.V. All rights reserved. **Nuc. Eng. Des., 285 (2015) 109–125, 2015.**

The manuscript discusses the details of development of a trans-critical heat transfer look-up table for water including water data compilation and screening, data rejection and scatter reduction. Discussion was expanded on the source of scatter in the experimental data. Table construction steps are presented and discussed in detail: skeleton table construction, incorporation of experimental data into the skeleton table and smoothing of the table trends. Comparison of the table predictions against leading prediction methods is also presented.

A look-up table for trans-critical heat transfer in water-cooled tubes

H. Zahlan, S. Tavoularis and D.C. Groeneveld
Department of Mechanical Engineering, University of Ottawa, Ottawa, ON K1N 6N5, Canada

Abstract

This article describes the development and validation of a trans-critical heat transfer look-up table for water at high subcritical and supercritical pressures. As a basis for constructing the table, an extensive database of near-critical and supercritical heat transfer measurements was compiled and upgraded by the rejection of unreliable or inappropriate data, the removal of duplicates and outliers and the reduction of data scatter. A large number of available single-phase and supercritical heat transfer correlations were assessed against the database and the most accurate correlations for each heat transfer regime were identified. These correlations were then used to construct a skeleton table, which provides values of the heat transfer coefficient for a matrix of combinations of 11 values of pressure in the range from 19 to 30 MPa, 9 values of mass flux in the range from 100 to 5000 kg m^{-2} s^{-1}, 17 values of bulk enthalpy in the range from 1000 to 3000 kJ kg^{-1}, and 8 values of wall superheat in the range from 10 to 500 K. For the construction of the final table, the predictions of correlations were replaced by experimental values, adjusted following established trends to conform to the skeleton table value matrix. Unlike all previous prediction methods, the table applies not only to normal heat transfer conditions but also to conditions with heat transfer deterioration and enhancement, as it includes data obtained under such conditions. The table values were further adjusted so that apparent discontinuities that were not related to physically plausible changes in heat transfer were smoothened out. The predictions of the table were assessed statistically against the experimental database. When compared to predictions of other available methods, the predictions of the present table were found to be generally closer to the experimental values for wide ranges of conditions. Finally, the trends followed by the smoothened table predictions for different heat transfer modes were found to represent more closely the trends of experimental data than trends followed by other prediction methods.

1. Introduction

Reliable supercritical heat transfer (SCHT) prediction methods are required for the thermalhydraulic design and safety analysis of the Supercritical Water-cooled Reactor (SCWR), which is one of the leading candidates for the Generation IV nuclear power reactors. Such analysis also requires accurate prediction of heat transfer at high subcritical ("near critical") pressures. However, the convective heat transfer coefficient (HTC, h) is difficult to predict at near critical and supercritical pressures, because of the complexity of heat transfer phenomena that occur under such conditions. As Figure 1 illustrates, at supercritical pressures, the specific heat c_p of water under constant pressure reaches a peak value at a specific temperature called the pseudo-critical temperature T_{pc}. All other thermodynamic and transport properties of the fluid also change substantially following small changes of temperature near T_{pc}. Because of these abnormally large changes in the properties in the vicinity of T_{pc}, the heat transfer coefficient becomes very sensitive to the local conditions, especially when the mass velocity is relatively small and the wall heat flux is relatively large.

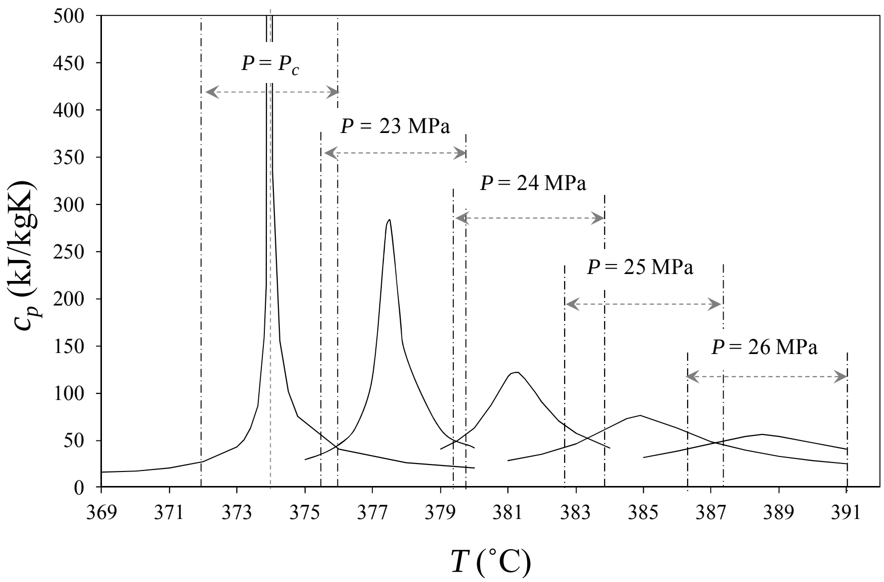

Figure 1: Variation of specific heat under constant pressure c_p with temperature for water under different pressures; dashed lines mark the boundaries of temperature ranges within which significant variations in c_p are present; the critical pressure of water is P_c = 22.1 MPa.

Several reviews of SCHT prediction methods have been published over the years. Hall et al. (1968), Jackson and Hall (1979a, 1979b), Cheng and Schulenberg (2001) and Pioro et al. (2004) have presented overviews of SCHT correlations and assessments of these correlations against measurements in pipe flows of water and carbon dioxide. More than twenty correlations are available in the literature for predicting the heat transfer in the near-critical and supercritical region, each with a limited range of validity. Most of these correlations are modified versions of the Dittus and Boelter (1930) equation and account for changes in properties in the near-critical region, but not for heat transfer abnormalities in the vicinity of the pseudo-critical temperature. Moreover, some of these correlations are based on experimental data collected in carbon dioxide or a refrigerant, and their validity for supercritical water has not been established. SCHT correlations contain thermodynamic and transport properties, which are evaluated at the bulk fluid temperature, the wall temperature, or some intermediate value. When these properties have strong variations across the test section, these correlations may give inaccurate predictions, as they cannot adequately represent all possible heat transfer modes that may occur under such conditions. In summary, it seems most unlikely that a single correlation would provide accurate heat transfer predictions over the entire range of conditions that are of interest in the operation and safety analyses of the SCWR.

An alternative approach that could potentially overcome some of these shortcomings is the use of a trans-critical look-up table (TC LUT). Look-up tables (LUT) have been used successfully to predict other complex heat transfer phenomena, including film boiling heat transfer (Groeneveld et al., 2003) and critical heat flux (Groeneveld et al., 2005), with an accuracy that is much higher than those of the best available correlations. The range of application of a TC LUT can be made sufficiently wide to include conditions with high subcritical, near-critical and supercritical pressures and temperature ranges that are very wide and include the critical and pseudo-critical values. Because the TC LUT is basically a normalized data bank, it may be expected to predict abnormal heat transfer variations. Two LUT relevant to SCHT have so far been developed, one by Loewenberg et al. (2008) and another by Liu et al. (2011), both for SC water flowing vertically upward in tubes. Although these tables were shown to have some advantages compared to correlations, their development procedures, range of validity and predictive capabilities were limited in scope, so that they leave significant room for improvement.

The objective of the present work was to develop a TC LUT capable of predicting heat transfer in vertical tubes containing water flowing upwards over much wider ranges of pressure and temperature and with higher prediction accuracy than current SCHT prediction methods. In particular, the present TC LUT was designed to span the complete range of flow conditions of interest to the SCWR development, including abnormal heat transfer conditions, and to have a form that is suitable for incorporation into system codes that are used for SCWR safety analysis. The latter requirement dictated the format of the TC LUT. Tube-based prediction methods are commonly used in subchannel codes, in particular when rod bundle data and heat transfer prediction methods are inadequate or unavailable, as is the case for the SCWR. The diameter of the reference 8 mm tube was chosen because it is close to the hydraulic diameter of the Canadian SCWR fuel channel. In experimental convective heat transfer studies, one usually sets the wall heat flux q to a desired value and then measures the wall temperature variation. Nevertheless, safety analysis codes require specification of the wall superheat $\Delta T_w = T_w - T_b$, which is the difference between wall T_w and bulk T_b temperatures, and calculate q by iteration. Consequently, the present TC LUT was structured as to predict the convective HTC from specified values of four properties: pressure P, mass flux G, wall superheat ΔT_w, and local fluid specific enthalpy H_b. The choice of these four table properties is also generally consistent with parameters used in other prediction methods. To avoid the additional complication of having to interpolate for five parameters, we did not include the tube diameter among the input parameters, however, we suggested and validated a diameter correction procedure. It is also important to mention that the TC LUT takes into consideration only local conditions on heat transfer and does not account for inlet temperature and other entrance effects; this was achieved by considering only data collected at distances longer than 50 tube diameters from the inlet of the heated section.

The procedure we followed to construct the TC LUT is illustrated on Figure 2 and may be summarised as follows. The first and most important step was to compile a databank of all available experimental data of interest and to screen all data in this databank to eliminate duplicates and problematic entries. Because the databank contained measurements that were reported without sufficient documentation and in some cases had appreciable scatter, all data were processed for scatter reduction. This databank was used to evaluate the accuracy of a large number of available SCHT correlations, which led to the selection of the most accurate correlation in each distinct subrange of conditions. Predictions of these "best" correlations were used to construct a "skeleton table", which served as a preliminary version of the TC LUT. The skeleton table was subsequently "data-fit" by the incorporation of experimental values from the databank, interpolated along appropriate trends to fit the table grid and replace only the skeleton table values that surrounded the experimental points. The final TC LUT was constructed by smoothing the predictions of the updated table to remove erroneous discontinuities and inconsistencies. The performance of the TC LUT was evaluated by comparing its prediction accuracy and parametric trends to those of previous SCHT prediction methods.

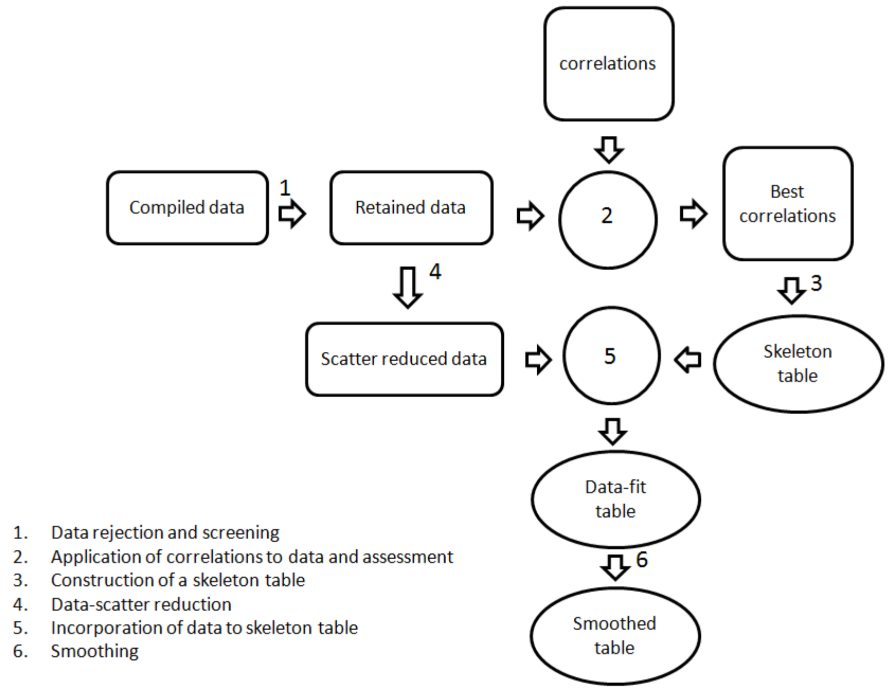

Figure 2: A flowchart showing the development steps of the TC LUT.

2. Compilation of a trans-critical heat transfer databank

The compilation of an initial database of heat transfer measurements at high subcritical and SC pressures in tubes and other channels containing water and other fluids has been described by Groeneveld and Zahlan (2009) and Zahlan et al. (2010); this will be referred to as the University of Ottawa (UO) database. The database consists of a large number of data points, which refer to a single set of measured values of pressure, mass flux, wall superheat, bulk fluid enthalpy, heat flux, tube diameter and axial location (when available). All data points provided by the specific source that conducted the experiments will be referred to as a dataset; a dataset may include one or more data points collected during one or more runs in the same laboratory. The UO database was subsequently enlarged by the incorporation of three additional SC water databases: the University of Stuttgart database, (Lowenberg et al., 2008), the Shanghai JiaoTong University (SJTU) database (Cheng, 2009), and the University of Ontario Institute of Technology (UOIT) database (Pioro, 2010; Kirillov et al., 2005). The combined databases will be referred to as the databank. It is noted that numerical values of some of these datasets were readily available in tables, however, many others were extracted from graphs using data digitization software, which introduced additional uncertainty (Zahlan et al., 2010). In several cases, more than one datasets were obtained under comparable flow conditions; this was considered to be beneficial, as it enhanced our confidence on the TC LUT accuracy for these conditions. Data reconstructed from graphs of poor quality and data for which the experimenter provided inadequate documentation regarding flow conditions or geometry and the missing information was extracted from secondary sources were excluded from the databank.

Although many types of data were collected, only those that were considered to be relevant to the objectives of the present TC LUT and sufficiently reliable were retained in the databank. All datasets were examined carefully, and many of them were rejected for the following main reasons.

a) *Fluid*: Data for fluids other than water were removed.
b) *Flow direction*: Data in flows with directions other than vertical upwards were removed. Although it is understood that for sufficiently high mass fluxes convective heat transfer would be independent of flow direction, available criteria for identifying conditions under which heat transfer would be independent of buoyancy effects have not been validated sufficiently and have not been accepted widely. To avoid unnecessary errors, we did not consider any data other than those in vertical upwards flows.
c) *Channel geometry*: Only data in circular tubes with inner diameters in the range from 5 to 16 mm were retained.
d) *Parameter ranges*: Data that did not fall within the range of the TC LUT parameters were excluded. These parameter ranges were set to conform to the needs of SCWR development and will be presented in section 3.
e) *Duplicates*: The four databases included many duplicate data from identical runs. Two types of duplicates were encountered, internal duplicates within each dataset, caused by errors in transcribing the data, and external duplicates between two different datasets. Duplicate data were identified using a methodology described by Zahlan et al. (2010) and removed. Roughly one third of all datasets collected were rejected as duplicates.
f) *Outliers*: Some data had values that were very different from the bulk of the data and could not be possibly reasoned as being correct. Such values were removed from the databank as their inclusion would introduce considerable inaccuracy to the TC LUT. Among the many possible sources of outliers would be errors in data transcribing or digitization and instrumentation malfunctioning. Roughly 1% of the data were removed as outliers.
g) *Heat balance inconsistencies:* A small number of data (less than 0.5%) were removed because the reported local or outlet enthalpies were incompatible with a simple heat balance (Zahlan et al., 2010).
h) *Conduction effects*: Measured axial temperature profiles frequently displayed sudden temperature changes at locations close to the test section inlet or outlet, which were attributed to significant axial conduction to a nearby heat sink, e.g., a copper power clamp with large power cables, or strong local heating caused by poor electrical contact of the power terminals. The proportion of data rejected for this reason was also less than 0.5%.
i) *Inlet effects*: Measurements collected at locations that were closer to 50 diameters from the inlet were excluded, as they are deemed to correspond to flows in which the boundary layers were not fully developed; in such cases, the local heat transfer would also depend on upstream conditions and not exclusively on local ones, as required for the present TC LUT.

The numbers of data sources and measurements in water-cooled tubes in each of the four databases and the final databank, after data screening was completed, are listed in Table 1. The ranges of reduced pressure P/P_c covered by the databank are shown in Figure 3 against the local bulk Reynolds number Re_b and the reduced bulk temperature T_b/T_c. Details about the parameter ranges for all datasets from all sources were presented by Zahlan et al. (2011b).

Table 1: Experimental databases and data points in the screened databank.

	High subcritical pressures		Supercritical pressures	
	Number of data sources	Number of data points	Number of data sources	Number of data points
UO Database	4	411†	28	2514
SJTU Database			11	3840
Stuttgart U Database	1	306	15	673
UOIT			20	5266
Databank	4	717	21	12293

†Most of these data are from the UO water database for the film boiling look-up table (Nakla, 2010).

The data points in the databank were separated into four regions, according to flow conditions.

a) The subcritical region, for $P < P_c$; only 717 data points were available in this region.
b) The high density state (liquid-like) SC region, for $P_c < P$ and T_w , $T_b < T_{pc} - \Delta T$.
c) The near-critical or near-pseudo-critical region, for $P_c < P$; $T_{pc} - \Delta T < T_w$ and $T_b < T_{pc} + \Delta T$; the half-width ΔT of this region, within which property changes were significant, was specified by the empirical relationship $\Delta T/T_{pc} = 3.1 \times 10^{-3}(P/P_c)$, where P_c is the critical pressure and the numerical values of all temperatures are in degrees K (Zahlan et al., 2011b).
d) The low density state (gas-like) SC region, for $P_c < P$ and $T_{pc} + \Delta T < T_w$, T_b.

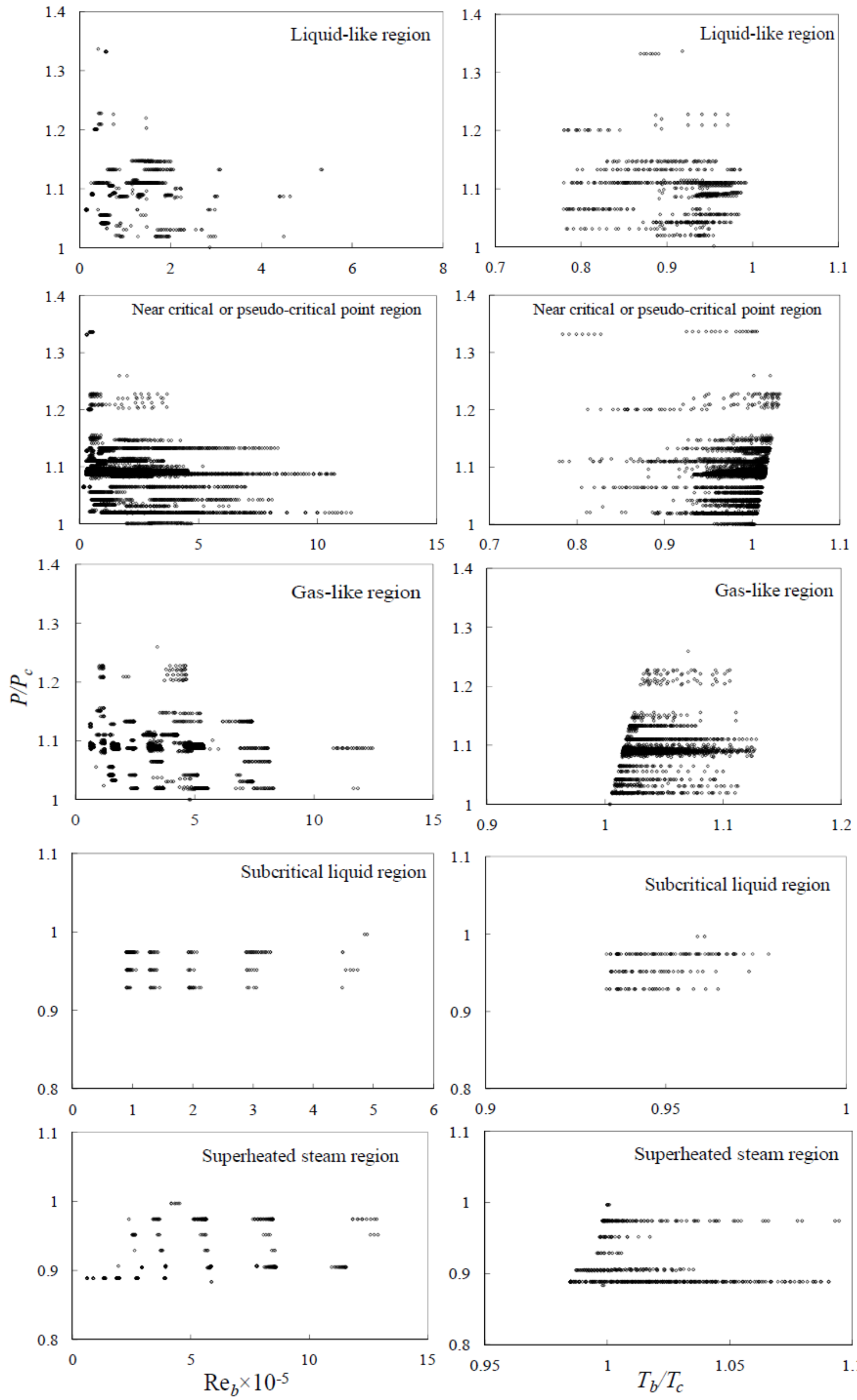

Figure 3: Ranges of parameters in the present databank.

3. Construction of the skeleton table

The construction of a trans-critical skeleton table was an essential step in the construction of the TC LUT. First, the desired ranges of the four input parameters, namely P, G, ΔT_w and H_b were specified as those that are relevant to SCWR needs, but also wide enough for use in other applications of SCHT. In view of the fact that the large majority of the data in our databank were collected in tubes with diameters in the range from 5 to 10 mm, the skeleton LUT was constructed for a diameter of 8 mm[1]. Then, a grid having nodes corresponding to combinations of values of the four input parameters was constructed. The spacing between nodes varied in each direction and within the parameter range so that it was denser in regions in which the HTC shows relatively high sensitivity to a particular input parameter. Table 2 presents the ranges of parameters and grid nodes of the skeleton table, which are identical to those used for the TC LUT. In total, there were 13,464 nodes, each of which corresponded to a different combination of 11 values of P, 9 values of G, 8 values of ΔT_w and 17 values of H_b.

Table 2: Range of parameters and grid nodes of the skeleton table and the TC LUT.

P kPa	G kg/m^{2}s	ΔT_w K	H_b kJ/kg
19000	100	10	1000
20000	200	20	1400
21000	400	50	1600
22000	700	100	1800
22500	1000	200	1900
23000	1500	300	2000
24000	2000	400	2050
25000	3000	500	2100
26000	5000		2150
28000			2200
30000			2250
			2300
			2400
			2500
			2600
			2700
			3000

Values of HTC at the grid nodes were then calculated with the use of the best available heat transfer correlations in each heat transfer region to form the skeleton table. Because the databank included all parameters that were necessary for evaluating the correlations, this task was straightforward. It is reminded, however, that in practice correlations are used to predict the HTC from information that does not include wall temperature. The latter is usually calculated by iteration as follows: a) the iteration starts from an assumed value of T_w, which is used to calculate

[1] A reference 8 mm diameter was chosen for the TC LUT because this diameter is close to the SCWR fuel channel hydraulic diameter and also because the critical heat flux and film boiling LUTs also used an 8 mm tube as a reference.

the values of thermophysical properties that appear in the correlation; b) the correlation is used to calculate the Nusselt number, from which, together with the specified value of the wall heat flux, a new value of T_w is determined; c) if the assumed and determined values of T_w nearly coincide, the iteration stops, otherwise the procedure is repeated using the new value of T_w. This procedure may lead to more than one solution for T_w under certain ranges of SC conditions, because of the strong non-linear dependence of thermophysical properties on local temperature (Churkin and Deev, 2013). This problem did not affect the present evaluation procedure because wall superheat is an input parameter in the table and so the correlations were applied without iteration for T_w. Nevertheless, it can introduce difficulties in the application of heat transfer correlations through automated algorithms, such as subchannel codes.

Well established heat transfer correlations and LUT are available for conventional heat transfer modes at low and moderate subcritical pressures and these were used for the appropriate ranges of parameters for the construction of the skeleton table. Nevertheless, only limited performance tests of such correlations have been published for the high subcritical and SC regions. In order to reduce unnecessary uncertainties, we performed our own assessment of the available correlations against data in our databank. We considered twelve SCHT correlations and four single-phase correlations, which may also be used for predicting the HTC in high-subcritical and/or SC flows. These correlations have been summarized by Zahlan et al., 2011b. The HTC h_p predicted by each of these correlations for each data point in the databank was calculated and compared to corresponding value h that was calculated directly from the measurements. The percentage difference between the predicted and the experimental HTC was than calculated as

$$e = 100\frac{h_p - h}{h} \tag{1}$$

for all trans-critical heat transfer data and analyzed statistically to compute the corresponding average e_{avg} and root mean square e_{rms} errors for specific heat transfer regions. It is noted that a non-zero value of e_{avg} represents a bias, whereas e_{rms} is a measure of the overall uncertainty, which includes both bias and precision uncertainty (Tavoularis, 2005). The average and rms errors for all correlations, calculated for data from a partially screened version of the present databank, were presented by Zahlan et al. (2010, 2011b). An evaluation of the most promising correlations against data from the screened databank that was described in the previous section was performed and its results are summarized in Tables 3 and 4.

Table 3: Average and rms errors in the high subcritical region.

Correlation	Liquid water (157 data points)		Superheated steam (560 data points)	
	e_{avg} (%)	e_{rms} (%)	e_{avg} (%)	e_{rms} (%)
Dittus-Boelter (1930)	11.0	15.4	73.1	123.1
Sieder and Tate (1936)	26.7	30.0	81	132.1
Hadaller and Banerjee (1969)	31.1	34.6	18.4	32.1
Gnielinski (1976)	-4.6	10.0	79.1	126.3
Mokry et al. (2009)	4.5	13.3	-5.0	17.4

Table 4: Average and rms errors in the three supercritical regions.

Prediction method	Liquid-like region (743 data points)		Gas-like region (3075 data points)		Near-critical/pseudo-critical region (8475 data points)	
	e_{avg} (%)	e_{rms} (%)	e_{avg} (%)	e_{rms} (%)	e_{avg} (%)	e_{rms} (%)
Swenson et al. (1965)	-7.2	22	-14.3	19.6	4.4	21.3
Mokry et al. (2009)	-8.0	20.6	-7.3	15.2	1.8	15.8
Gupta et al. (2010)	-24	29.1	-10.4	18.5	0.5	16.5

Table 3 shows that, at high subcritical pressures, the correlation of Gnielinski (1976) had the best overall performance for liquid water, whereas the Mokry et al. (2009) correlation was by far the best for superheated steam. Table 4 shows that the Mokry et al. (2009) correlation had the lowest e_{rms} in all three SCHT regions, as well as fairly small e_{avg}. The correlations and other prediction methods that were used for the construction of the skeleton table are listed in Table 5. It is noted that the skeleton table does not account for heat transfer deterioration and enhancement. The parametric trends of the skeleton table were compared against the experimental data trends to ensure consistency (Zahlan et al., 2011a).

Table 5: Prediction methods used for the construction of the skeleton table.

Pressure range	Heat transfer regime	Prediction method
Subcritical	Subcooled liquid	Correlation of Gnielinski (1976)
	Nucleate boiling	Correlation of Thom et al. (1965)
	Critical heat flux	CHF LUT of Groeneveld et al. (2005)
	Transition boiling	Method of Groeneveld et al. (1986) and Groeneveld and Stewart (1982)
	Film boiling	Film boiling LUT of Groeneveld et al. (2003)
	Superheated steam	Correlation of Mokry et al. (2009)
Supercritical	All three regimes	Correlation of Mokry et al. (2009)

4. Construction of the trans-critical look-up table

4.1 Dataset scatter reduction

Most of the datasets exhibited scatter in the reported wall temperature measurements and in the calculated HTC values. In some cases, the scatter was very large and its source was not identified by the authors reporting these data. Scatter may be the result of oscillations in flow conditions, which can be especially severe when they are caused by flow instability in the near-critical/pseudo-critical region; it may also be the result of small changes in experimental conditions during each test, or during repeated measurements that are reported together, as well as noise in the acquired signals. Because scatter may influence significantly the accuracy of the TC LUT, we are going to discuss its sources in more detail.

Some of the reviewed papers (Shitsman, 1963; Bishop et al. 1965; Yamagata et al., 1972) reported the encountering of relatively low frequency oscillations under certain conditions, but they generally did not seem to include oscillatory data in the reported datasets. Zahlan et al. (2013) also reported that, under certain conditions, their SCHT flow loop at the University of Ottawa using CO_2 as medium experienced low frequency oscillations in flow rate, which were accompanied by oscillations in wall temperatures; this occurred despite the presence of accumulators that were connected to the loop with the objective to dampen possible oscillations, and appeared to be specific to the loop design and settings, as it was possible to eliminate these oscillations by changing the loop configuration, for example by changing valve settings. Although we put effort into identifying oscillatory datasets and exclude them from the databank, it is possible that a very small number of such datasets might be present; if such datasets exist, their effects on the table should be insignificant, first because their number would be very small and second because the resulting fluctuations of data values would be dampened by the applied scatter reduction algorithm as well as by the table smoothing procedure, which will be discussed in Section 4.4.

Scatter in data due to small changes in experimental conditions can be especially large under conditions of heat transfer deterioration. A small change in inlet temperature may shift the location of deterioration onset and thus affect the wall temperature variation. Such scatter would be very difficult to account for and may be treated as random. Ubiquitous sources of scatter that contaminate all measurements, and particularly thermocouple signals, include electronic (thermal) noise and interference of electromagnetic fields, which is exacerbated by the proximity of large electric power supplies and transmission lines. Such noise can sometimes be reduced by grounding and/or shielding of various components and by low-pass filtering, but the degree by which such techniques were used effectively in the various sources of our data is generally unknown. Inspection of the compiled datasets identified several of them that had large scatter. These included not only older data (e.g., by Shitsman, 1963), but also some more recent ones (Kirillov et al., 2005). Considering that SCHT measurements in water are scarce and that deteriorated heat transfer is very sensitive to experimental conditions, we decided to include some of these datasets in the databank, which would otherwise be too sparse for certain ranges of conditions. Nevertheless, inclusion of scattered data in the TC LUT was found to distort its parametric trends by creating false maxima and minima and interfere with the TC LUT smoothing process (see Section 4.4). For this reason, scattered datasets were processed by a scatter reduction algorithm, following which they generally showed more obvious and useful trends and were deemed to be more suitable for TC LUT construction.

All experimental datasets were subjected to smoothing using a Gaussian smoothing kernel (Data Curve Fit Creator, http://www.srs1software.com/DataCurveFitCreator.aspx), which weighs neighbouring points using a Gaussian-shape function. The objective was to reduce drastically the scatter in the data without removing relatively abrupt changes in wall temperature that characterize the near-critical heat transfer region. The smoothing window was selected to be as small as possible, which for many cases amounted to curve-fitting. Each of the datasets was checked carefully by plotting h *vs.* H_b before and after smoothing, to ensure that experimental trends were not eliminated by smoothing. To evaluate this smoothing process, the percentage difference between the smoothed h_s and measured h values of the HTC was calculated for each data point in the dataset as

$$e_s = 100\frac{h_s - h}{h} \quad . \qquad (2)$$

Then, the scatter removal effectiveness for each dataset was quantified by the corresponding rms value $e_{s,rms}$. Figure 4 shows two examples of datasets with scatter and the smooth curves fitted to them. The first example (upper pair of plots) is a dataset with rather extreme scatter (Shitsman, 1963), having $e_{s,rms} =$ 35.6%. The author provided plots with highly scattered wall temperatures, which may be conjectured to be composites of measurements obtained from tests with different inlet specific enthalpies. The scatter was amplified when these temperatures were used to calculate the local heat transfer coefficient, also shown in Figure 4. Nevertheless, the smooth curve preserved the average trend of the data and the presence of a minimum. This is one of very few cases in the database with a very high scatter in HTC. These test data were not rejected because they were among the few datasets that showed very strong heat transfer deterioration in their range of conditions. During the data scatter reduction process, HTC and wall temperature profiles were compared before and after smoothing, to ensure that the reduction of scatter of the experimental data did not distort strongly the heat transfer coefficient trends. It is easier to see the general trend and to detect the extremes in wall temperature profiles rather than in HTC profiles. Shitsman (1963) also reported a representative curve for these test data, which is similar to the present smoothing line and shows a single peak in T_w at the same location as in the presently fitted curve. However, in this special case, smoothing resulted in a significant increase in HTC for the scatter reduced data at the location of the peak in T_w, which would probably affect the prediction uncertainty of the TC LUT for the location of the peak. The second example is a more representative case of datasets in the databank, which had moderate amounts of scatter (Kirillov et al., 2005; $e_{s,rms}$ = 5.3%).

It is important to emphasize that, unless stated otherwise, error analyses in this study were performed against HTC calculated from data before scatter reduction was applied to them, so that prediction errors were not reduced artificially.

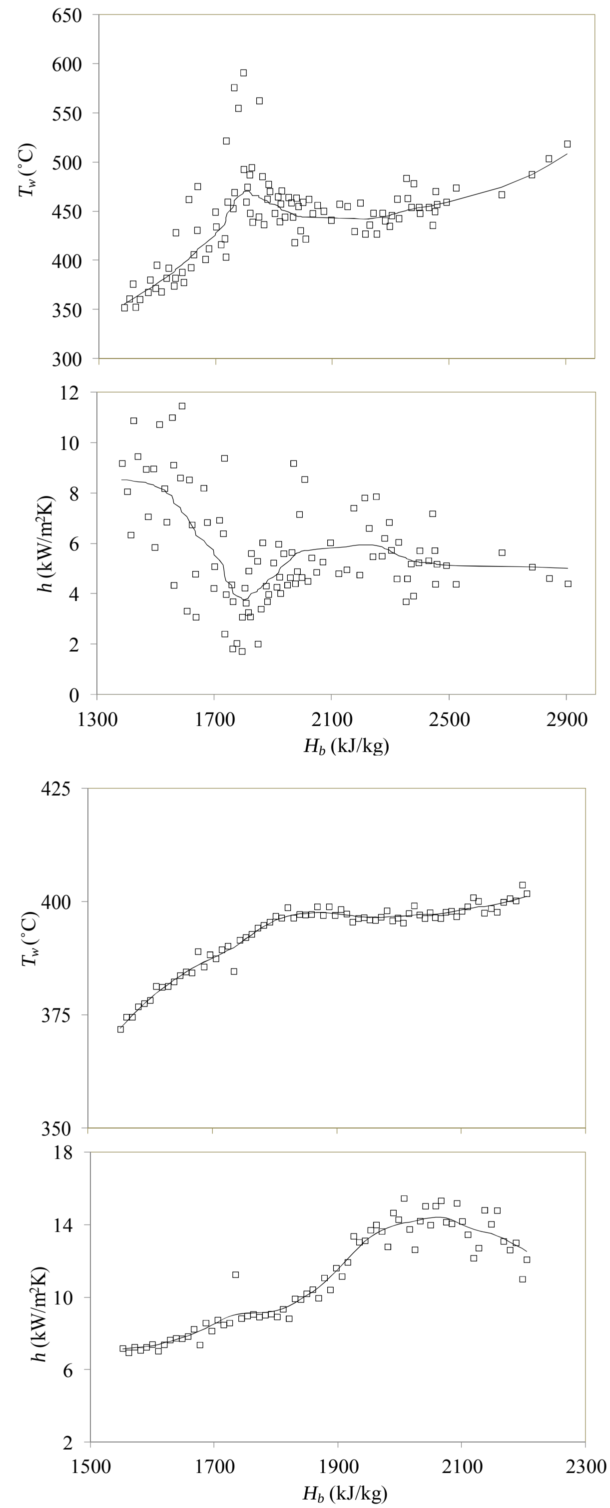

Figure 4: Two examples of datasets with scatter (square symbols) and their representations by smooth lines (solid lines). Upper pair of plots: data reported by Shitsman (1963); d =10 mm, P = 23300 kPa, G = 430 kg/m^{2}s, q = 384 kW/m^2. Lower pair of plots: data reported by Kirillov et al. (2005); d = 10 mm, P = 24030 kPa, G = 496 kg/m^{2}s, q = 239 kW/m^2.

4.2 Scaling of HTC in tubes of different diameters

As mentioned previously, the skeleton table was constructed for a tube with an inner diameter d = 8 mm. To avoid rejecting too many datasets from the databank, experiments were retained for tubes with diameters in the range from 5 to 16 mm. The distribution of data points collected in tubes of different diameters and retained in the final databank is shown in Table 6.

Table 6: Numbers of data points collected in tubes of different diameters.

Tube diameter (mm)	Number of data points
5	727
6	134
8	765
9	125
10	10487
14	619
15	73
16	80
All sizes	13010

Tube size is known to have an effect on heat transfer, and so it was necessary to scale all experimental HTC to values corresponding to an 8 mm tube., The reviewed single-phase and SCHT correlations, as well as the 2003 film boiling LUT (Groeneveld et al., 2003), generally predict that HTC would be roughly proportional to d^{-n} with $0.1 \leq n \leq 0.2$). Nevertheless, it is also known that the tube size effect is much more significant in the deteriorated and enhanced heat transfer regions, where HTC in tubes with different diameters may be impossible to reconcile by geometric scaling; for example, it is possible to have normal heat transfer (NHT) in a tube with a small diameter and deteriorated heat transfer in a larger tube under the same conditions. In any case, because the tube diameter range in our database was fairly narrow, errors introduced exclusively by the tube size effect, at least under NHT conditions, are expected to be small by comparison to other types of error.

A direct test of the tube diameter effect was performed as follows. Values of h that were determined from measurements in tubes with diameters different from the reference diameter d_{ref} = 8 mm were converted to reference values h_{ref} in an 8 mm tube as

$$h_{ref} = h\left(\frac{d}{d_{ref}}\right)^{n}, \qquad (3)$$

with the exponent n given the values 0.075, 0.09, 0.10, 0.12, 0.15, 0.20 and 0.25. All scaled HTC values, including those in 8 mm tubes, were incorporated in the skeleton table (as described in Appendix A) to construct a TC LUT. Then, the TC LUT for the corresponding value of n was used to predict the HTC for each of the 13010 data points. This value of HTC was scaled back to the actual tube diameter for each data point using the same value of n. The average and rms errors (i.e., the differences between TC LUT predictions and measurements, as will be discussed in section 5) were calculated for each value of n. The sensitivity of both errors on n was very weak, making the determination of an optimal n quite uncertain. Among the various choices, we selected the value n = 0.20 for use in the final TC LUT. This value produced relatively low errors as well as being consistent with single-phase correlations, such as the Dittus-Boelter relationship. It is also noted that the TC LUT is not sensitive to the exact choice of this exponent, as the change in HTC by the application of Equation (3) would be lower than 5% for tubes with diameters in the range from 6 to 10 mm, which represent nearly 90% of the data points in the databank.

4.3 Estimation of local HTC slopes and data incorporation in the skeleton table

The prediction accuracy of the skeleton table is comparable to that of the correlations on which it was based. To improve the prediction accuracy of the current skeleton look-up table, only the skeleton table values surrounding the experimental data were replaced by the normalized data. First the HTC data for tubes with different diameters were converted to the reference 8 mm diameter tube by assuming that the HTC is proportional to $d^{-0.2}$. The procedure for the estimation of the local HTC slopes and the incorporation of experimental data in the skeleton table is presented in Appendix A.

4.4 TC LUT smoothing and off-setting

For some nodes, the HTC in the data-fit table changed abruptly from one node to the next, following incremental changes in P, G, ΔT_w and/or H_b. Some of these abrupt changes were clearly not corresponding to experimental trends and are attributed to differences in data values of different datasets under comparable experimental conditions, residual data scatter, and secondary effects, such as upstream heated length and surface conditions. Abrupt HTC changes were also observed between pairs of nodes, one of which had an "experimental" value, while the other maintained the value of the skeleton table. Similarly, in the liquid region at high subcritical pressures, discontinuities were observed between pairs of nodes at each of which different prediction methods were used to compute the HTC. Such discontinuities in the table are undesirable, as they have no physical significance. Moreover, abnormal fluctuations of HTC values may introduce algorithm instability and multiple solutions in TC LUT applications employing iteration, such as subchannel codes. To reduce these adverse effects, it is necessary for the table value variation to be rendered relatively smooth. One needs to be careful, however, not to flatten HTC peaks and abrupt changes in certain particular regions of the table, where these were the result of physical causes. This was the case in regions in which the temperature was near the critical or pseudo-critical value, where sharp variations in fluid properties occur; to preserve the experimental trends in these regions,, the local spacing between nodes was reduced. Abrupt changes that corresponded to changes in heat transfer also occurred at the boundaries between different heat transfer regions, *i.e.*, between normal/deteriorated heat transfer/enhanced heat transfer for SC pressures and single-phase heat transfer/nucleate boiling/ transition/film boiling for subcritical pressures.

At an early stage of this work, the smoothing procedure that was developed by Huang and Cheng (1994) was applied to the data-fit table as follows. Regions with discontinuities in HTC values in the direction of one or more input variables were identified and the discontinuities were reduced by replacing the values at affected nodes by weighted averages of values on two nodes on either side of the affected node in the direction of interest. It was found, however, that this procedure resulted in inadequate smoothing, particularly in the direction of pressure.

Subsequently, B-spline smoothing procedures were applied to the TC LUT, but these were also found to result in inadequate smoothing. The technique that was found to be most efficient for smoothing of the TC LUT was the application of the Gaussian smoothing kernel, which has already been discussed in section 4.1. The main steps of this procedure will be summarized in the following paragraph.

Smoothing was first applied in the P direction, and then sequentially in the G, ΔT_w and H_b directions. The table value of HTC at each node (the "central node") was replaced by a weighted average value, calculated by dividing the sum of the weighted HTC values at the central and the neighbouring nodes by the sum of their weights. Because the TC LUT grid was non-uniform, it was impractical to calculate distances between nodes in terms of differences in the corresponding input parameter values. For this reason, distances between nodes were determined in terms of numbers of nodes (*i.e.,* in dimensionless form). This approach distorted the shape of the Gaussian function, giving higher weights to closely spaced nodes than widely spaced ones; even so, it is actually appropriate for smoothing of the TC LUT values, because node spacing was set to be closer in parts of the table where the sensitivity of HTC to the corresponding input parameter was relatively high. Weight for each node decreased with increasing distance (in number of nodes) from the central node according to a normalized Gaussian function, with the central node being assigned a weight of 1. The relative width of the Gaussian smoothing function was controlled by a parameter σ, corresponding to the standard deviation of a normalized Gaussian random variable and measured in number of nodes. To avoid contamination of the value at the central node by values at nodes that are widely separated in terms of an input parameter, σ was assigned values that were as small as possible. The choice of σ was made by trial and error and separately for each input parameter, but each value was kept fixed for the entire table. Smoothing with $\sigma = 1$ was applied first and the resulting HTC profile was compared to the one before smoothing. Then, σ was adjusted by small amounts upwards or downwards and the minimum value that resulted in relatively smooth and continuous HTC variations was chosen for the final smoothing. During this process, effort was made to avoid the elimination of true experimental trends. In particular, special attention was given to table regions near the critical and pseudo-critical points and regions with heat transfer deterioration and enhancement, where the HTC is expected to undergo rapid variations. As a consequence of smoothing, local extremes of HTC in these regions were reduced but not eliminated. The final values of σ were 1.3, 0.8, 1 and 1.3 for the P, G, ΔT_w, and H_b directions, respectively. For the weighted average calculation, the number of nodes considered on either side of the central node was equal to the highest between two values, either the integer that was closest to 3σ or 3. In the present case, the total number of nodes (including the central node) considered for the weighted average were, respectively, 9, 7, 7 and 9, for the P, G, ΔT_w, and H_b directions.

Representative examples of HTC variations in the P, G, ΔT_w and H_b directions in the data-fit table, in intermediate tables generated during the smoothing process, and in the final TC LUT are shown in Figure 5. In cases for which HTC did not change significantly from one node to the next, the smoothing procedure acted essentially like curve-fitting and the data were represented quite well both in values and trends. A notable exception is the vicinity of the critical pressure P_c (Figure 5a). When $P = P_c$ and the mass flux is relatively small, HTC has a prominent global minimum, which is represented clearly by the data-fit table nodal values; following smoothing in the P direction, the minimum remained prominent, but its value increased by approximately 35%; after smoothing in all directions was complete, the value of this minimum increased by 50% from the data-fit value. Such a distortion is deemed to be tolerable for this extreme case, in view of the fact that smoothing essentially eliminated a local HTC maximum at P = 20 MPa and a local minimum at P = 26 MPa, which are most likely the result of experimental scatter.

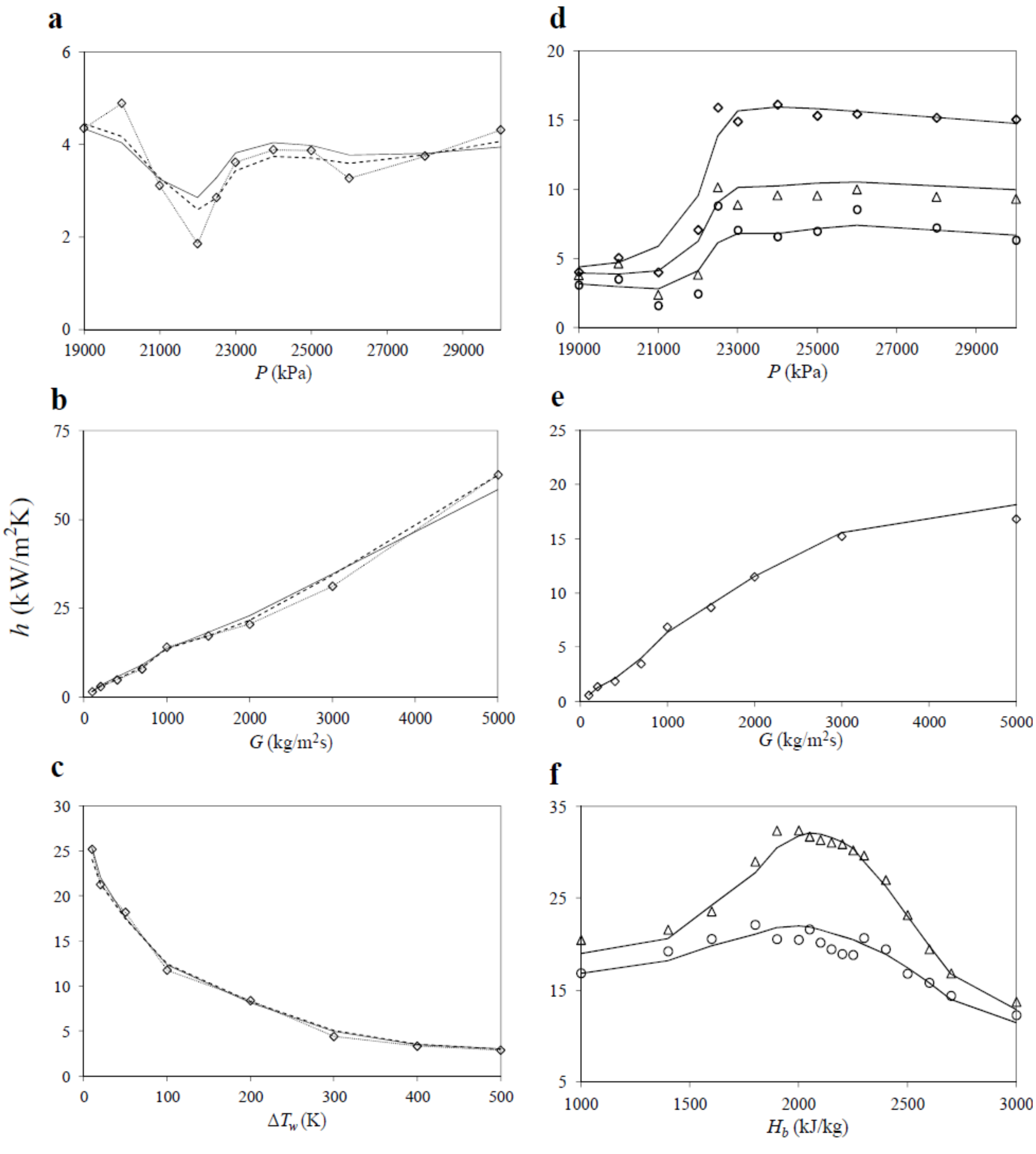

Figure 5: Representative variations of HTC in the P, G, ΔT_w and H_b directions in the data-fit LUT (symbols), intermediate tables before and after the smoothing process (dotted lines connecting symbols and dashed lines, respectively) and final TC LUT (solid lines). a) G = 400 kg/m^{2}s, ΔT_w = 100 K and H_b = 1000 kJ/kg. b) P = 22.5 MPa, ΔT_w = 50 K and H_b = 2050 kJ/kg. c) P = 22.5 MPa (P/P_c =1.02), G = 1500 kg/m^{2}s and H_b = 1400 kJ/kg. d) G = 700 kg/m^{2}s, H_b =

2100 kJ/kg, and ΔT_w = 20 (diamonds), 50 (triangles) and 100 (circles). e) P = 20 MPa, ΔT_w= 50 K and H_b 1900 kJ/kg. f) P = 25 MPa, G = 1500 kg/m^{2}s and ΔT_w = 20 (triangles) and 50 (circles).

Following smoothing, the overall average difference between each data point in the databank and the TC LUT prediction was 4.6% (see error analysis in the next section). If this were not corrected, it would entail an unnecessary bias to all TC LUT predictions. To remove such bias, all HTC in the table were multiplied by the factor 0.96, so that the average error was reduced to zero. This step is referred to as TC LUT off-setting.

4.5 TC LUT structure

The TC LUT is a four-dimensional table that provides values of the HTC for water flowing vertically upward in a tube with a diameter of 8 mm. HTC values are provided at 13,464 nodes, which are combinations of specific values of the input variables $P, G, H_b, \Delta T_w$, as listed in Section 3 with reference to the skeleton table. Table 7 shows, as an example, a section of the TC LUT for the supercritical pressure of 25 MPa (P/P_c =1.13), which is close to the projected operating pressure of the SCWR. Each of the 1,224 nodes for this pressure corresponds to a different combination of values of G, H_b and ΔT_w. HTC values in kW/m^{2}K that appear in bold and italic font correspond to "experimental" values, whereas entries in roman font are smoothed values of the skeleton table. In the presented example, the HTC values have been truncated to two significant digits; the same precision has been retained in the complete TC LUT, which is attached to this article in electronic form.

To use the table, one should start by specifying values of $P, G, H_b, \Delta T_w$ and d in the same units as those used in the table. If the tube diameter is different from 8 mm, then the TC LUT would provide a reference HTC, from which the desired value can be found with the use of Equation (3) with n = 0.20. Then, one should identify the 16 nodes that bound the element of the four-dimensional grid that encloses the point in question. Finally, one should estimate the value of HTC at the point of interest by performing a series of linear interpolations among the 16 nodes, each with respect to a particular input variable, in a manner similar to the one described in Appendix A.

Table 7: Representative section of the TC LUT for a pressure of 25 MPa (P/P_c =1.13).

H_b → kJ/kg / ΔT_w K ↓	1000	1400	1600	1800	1900	2000	2050	2100	2150	2200	2250	2300	2400	2500	2600	2700	3000
									G = 100 kg/m²s								
10	1.3	1.6	2.1	2.7	3.3	3.6	3.7	3.7	3.6	3.5	3.3	3.0	2.6	2.2	1.8	1.4	0.9
20	1.3	1.5	1.9	2.3	2.6	2.8	2.9	2.9	2.8	2.8	2.6	2.4	2.1	1.8	1.5	1.3	0.9
50	1.2	1.3	1.4	1.6	1.8	1.9	1.9	2.0	2.0	1.9	1.8	1.7	1.6	1.4	1.3	1.1	0.8
100	1.0	1.0	1.0	1.1	1.1	1.2	1.3	1.3	1.4	1.4	1.3	1.3	1.3	1.2	1.1	0.9	0.7
200	0.7	0.7	0.7	0.7	0.7	0.8	0.8	0.9	1.0	1.0	1.0	1.1	1.1	1.0	0.9	0.7	0.6
300	0.5	0.5	0.5	0.5	0.5	0.6	0.6	0.7	0.7	0.8	0.8	0.8	0.8	0.8	0.7	0.6	0.5
400	0.4	0.4	0.4	0.4	0.4	0.5	0.5	0.5	0.5	0.6	0.6	0.6	0.6	0.6	0.5	0.5	0.5
500	0.3	0.3	0.4	0.4	0.4	0.4	0.4	0.4	0.5	0.5	0.5	0.5	0.5	0.5	0.5	0.5	0.5
									G = 200 kg/m²s								
10	2.9	3.4	4.3	5.3	6.2	6.7	6.8	6.7	6.4	6.1	5.8	5.4	5.1	4.6	4.1	3.3	2.3
20	2.9	3.2	3.9	4.5	5.0	5.2	5.1	5.1	5.0	4.9	4.8	4.6	4.5	4.2	3.7	3.1	2.3
50	2.8	3.0	3.2	3.4	3.4	3.4	3.4	3.4	3.3	3.3	3.3	3.3	3.3	3.2	3.0	2.7	2.2
100	2.2	2.3	2.4	2.4	2.3	2.3	2.3	2.3	2.3	2.3	2.3	2.3	2.3	2.2	2.1	2.0	1.7
200	1.4	1.6	1.6	1.6	1.6	1.6	1.6	1.6	1.6	1.6	1.6	1.6	1.6	1.5	1.4	1.3	1.2
300	0.9	1.1	1.2	1.2	1.2	1.1	1.2	1.2	1.3	1.3	1.3	1.4	1.3	1.3	1.1	1.1	1.0
400	0.7	0.8	0.9	0.9	0.9	0.9	0.9	1.0	1.0	1.1	1.1	1.1	1.1	1.1	1.0	1.0	1.0
500	0.7	0.7	0.7	0.7	0.8	0.8	0.8	0.9	0.9	0.9	0.9	1.0	1.0	0.9	0.9	0.9	0.9
									G = 400 kg/m²s								
10	5.9	7.1	8.7	10.4	11.9	12.8	13.1	12.8	12.3	11.7	11.0	10.4	9.7	9.0	8.1	7.0	5.6
20	5.5	6.5	7.7	8.8	9.6	10.0	10.1	10.0	9.8	9.6	9.3	9.0	8.6	8.1	7.4	6.5	5.3
50	5.1	5.7	6.1	6.4	6.5	6.6	6.6	6.6	6.6	6.7	6.7	6.7	6.6	6.4	6.1	5.7	4.8
100	4.0	4.2	4.3	4.3	4.4	4.4	4.5	4.5	4.5	4.5	4.5	4.4	4.4	4.4	4.3	4.1	3.5
200	2.6	2.8	2.9	2.9	2.9	3.0	3.0	3.0	3.0	2.9	2.9	2.8	2.8	2.7	2.6	2.5	2.3
300	1.8	1.9	2.0	2.1	2.0	2.0	2.0	2.1	2.1	2.2	2.2	2.2	2.2	2.1	2.0	2.0	1.9
400	1.4	1.4	1.5	1.5	1.6	1.6	1.7	1.7	1.8	1.9	1.9	1.9	1.9	1.9	1.8	1.8	1.7
500	1.2	1.2	1.3	1.3	1.4	1.5	1.5	1.6	1.7	1.7	1.7	1.7	1.7	1.7	1.7	1.7	1.6
									G = 700 kg/m²s								
10	9.2	10.8	13.2	16.0	18.5	20.1	20.7	20.6	20.2	19.7	19.1	18.0	16.2	14.0	12.0	10.3	8.4
20	8.9	10.3	11.9	13.5	14.9	15.6	15.9	15.8	15.6	15.3	14.9	14.3	13.2	12.0	10.7	9.6	8.2
50	8.6	9.3	9.8	10.1	10.3	10.4	10.4	10.4	10.4	10.3	10.2	10.0	9.7	9.3	8.7	8.1	7.1
100	6.9	7.1	7.2	7.1	7.1	7.1	7.2	7.1	7.1	7.0	6.9	6.8	6.7	6.5	6.3	6.0	5.3
200	4.6	4.7	4.8	4.9	4.9	5.0	5.0	5.0	4.9	4.8	4.6	4.5	4.4	4.3	4.2	4.1	3.9
300	3.1	3.2	3.4	3.4	3.4	3.4	3.4	3.5	3.6	3.5	3.5	3.4	3.4	3.3	3.2	3.2	3.1
400	2.3	2.4	2.4	2.5	2.6	2.6	2.7	2.9	3.0	3.0	3.0	3.0	3.0	2.9	2.9	2.9	2.8
500	2.0	2.0	2.1	2.1	2.2	2.4	2.5	2.6	2.7	2.7	2.8	2.8	2.8	2.8	2.7	2.7	2.6
									G = 1000 kg/m²s								
10	14.7	15.6	18.8	22.8	26.4	28.6	29.5	29.8	30.0	30.0	29.5	27.5	23.8	19.8	16.7	14.4	11.5
20	13.6	14.7	17.0	19.5	21.6	22.7	23.0	22.9	22.8	22.5	22.0	20.9	19.0	16.8	14.6	12.6	10.0
50	12.1	12.9	13.8	14.6	15.0	15.1	15.0	14.9	14.7	14.5	14.2	13.9	13.3	12.4	11.4	10.3	8.6
100	9.1	9.7	9.9	9.9	9.9	9.8	9.6	9.6	9.5	9.3	9.2	9.0	8.8	8.5	8.2	7.9	7.1
200	6.1	6.4	6.5	6.5	6.5	6.5	6.4	6.4	6.5	6.4	6.3	6.1	5.8	5.6	5.5	5.6	5.6
300	4.2	4.3	4.4	4.4	4.5	4.6	4.6	4.7	4.8	4.8	4.6	4.4	4.2	4.0	4.0	4.2	4.5
400	3.2	3.3	3.3	3.4	3.6	3.7	3.9	4.0	4.1	4.2	4.2	4.1	4.0	4.0	3.9	3.9	4.0
500	2.8	2.8	2.9	3.0	3.2	3.3	3.5	3.7	3.8	3.9	3.9	3.9	3.9	3.9	3.8	3.8	3.7

H_b → kJ/kg	1000	1400	1600	1800	1900	2000	2050	2100	2150	2200	2250	2300	2400	2500	2600	2700	3000
ΔT_w K ↓	G = 1500 kg/m^{2}s																
10	20.6	22.3	27.0	32.4	36.9	39.6	40.6	40.9	40.8	40.4	39.5	36.9	32.3	27.0	22.5	19.0	14.6
20	19.0	20.6	24.2	27.8	30.5	31.8	32.1	32.0	31.6	31.1	30.4	29.0	26.3	23.0	19.8	16.8	12.9
50	16.8	18.2	19.8	21.1	21.8	22.0	21.9	21.6	21.2	20.8	20.5	20.0	18.9	17.4	15.8	14.0	11.4
100	13.2	14.0	14.4	14.6	14.5	14.2	14.0	13.8	13.5	13.4	13.2	12.9	12.5	12.0	11.4	10.7	9.5
200	8.5	8.9	9.2	9.4	9.5	9.3	9.2	9.1	9.0	9.0	8.9	8.6	8.4	8.1	8.0	7.8	7.4
300	5.7	5.8	6.0	6.2	6.4	6.5	6.7	6.8	6.9	6.9	6.8	6.5	6.2	6.1	6.0	6.0	6.1
400	4.5	4.5	4.6	4.8	5.0	5.2	5.5	5.7	5.9	6.0	6.0	5.9	5.8	5.7	5.6	5.6	5.6
500	3.9	4.0	4.1	4.2	4.5	4.7	4.9	5.2	5.3	5.4	5.5	5.5	5.5	5.5	5.4	5.4	5.3
	G = 2000 kg/m^{2}s																
10	22.7	26.3	34.6	42.7	48.8	51.8	52.9	52.9	51.8	50.0	48.1	45.9	42.3	37.0	31.1	24.9	17.2
20	21.8	24.6	30.1	35.1	38.4	39.5	39.7	39.5	39.1	38.5	38.0	37.2	35.2	31.8	27.8	23.3	16.7
50	21.4	23.0	25.0	26.5	27.1	27.1	26.8	26.5	26.3	26.2	26.1	25.9	25.1	23.7	21.9	19.6	16.0
100	17.4	18.4	18.9	19.0	18.7	18.3	17.9	17.6	17.4	17.3	17.2	17.1	16.9	16.4	15.8	14.8	12.9
200	11.2	12.0	12.6	12.8	12.6	12.4	12.2	12.1	12.0	12.0	12.0	11.9	11.8	11.7	11.4	11.0	9.9
300	7.5	7.9	8.2	8.4	8.6	8.7	9.0	9.2	9.4	9.5	9.5	9.4	9.3	9.2	9.0	8.8	8.3
400	6.0	6.1	6.2	6.4	6.7	7.0	7.4	7.7	7.9	8.1	8.1	8.1	8.1	8.0	7.9	7.7	7.5
500	5.3	5.3	5.5	5.7	6.0	6.3	6.6	6.9	7.1	7.3	7.4	7.4	7.4	7.4	7.3	7.2	7.1
	G = 3000 kg/m^{2}s																
10	31.6	37.2	48.4	60.0	69.7	75.5	78.2	79.1	78.7	77.3	74.6	69.9	62.3	53.0	43.5	34.4	24.2
20	30.6	36.1	43.6	50.6	55.7	58.2	59.1	59.6	59.9	59.8	59.0	56.8	52.2	45.9	39.1	32.4	24.0
50	29.4	32.5	35.6	37.8	39.0	39.2	39.0	38.9	38.9	39.1	39.1	38.4	36.5	33.7	30.4	27.1	22.7
100	24.5	26.0	27.1	27.4	27.2	26.7	26.4	26.2	26.0	25.9	25.8	25.5	24.7	23.7	22.4	20.9	18.5
200	16.4	17.8	19.0	19.5	19.3	18.9	18.8	18.7	18.7	18.7	18.5	18.2	17.9	17.4	16.9	16.2	14.7
300	11.2	11.7	12.3	12.6	12.8	13.1	13.4	13.8	14.0	14.2	14.2	14.1	13.9	13.7	13.4	13.0	12.2
400	8.7	8.9	9.1	9.4	9.8	10.3	10.7	11.2	11.5	11.8	11.9	11.9	11.8	11.7	11.5	11.3	10.9
500	7.6	7.8	8.0	8.3	8.7	9.2	9.6	10.1	10.4	10.6	10.8	10.8	10.8	10.7	10.6	10.5	10.3
	G = 5000 kg/m^{2}s																
10	45.1	55.6	72.3	89.8	105.1	115.8	121.8	123.4	121.7	117.5	110.9	101.4	88.7	74.7	60.9	47.7	32.7
20	43.7	54.7	67.0	77.9	86.2	90.8	92.7	92.7	91.5	89.7	87.0	82.5	75.0	65.1	54.3	43.5	30.8
50	40.3	48.6	54.7	58.8	60.9	61.7	61.8	61.6	61.1	60.7	60.2	58.7	55.2	49.6	43.2	36.4	27.8
100	32.3	36.5	38.2	38.7	38.8	39.1	39.6	40.2	40.6	40.8	40.6	39.8	38.0	35.5	32.6	29.2	24.3
200	22.1	23.4	23.9	24.2	24.6	25.3	26.2	27.0	27.6	28.0	27.9	27.5	26.8	25.8	24.6	23.1	20.8
300	15.9	16.5	16.8	17.3	18.0	18.8	19.6	20.4	20.9	21.3	21.4	21.3	21.0	20.6	20.0	19.4	18.2
400	13.1	13.4	13.7	14.2	14.8	15.6	16.3	17.0	17.5	17.9	18.1	18.1	18.0	17.8	17.5	17.2	16.6
500	11.7	11.8	12.1	12.6	13.2	14.0	14.7	15.3	15.8	16.2	16.4	16.5	16.4	16.3	16.2	16.0	15.7

5. Error analysis of the TC LUT

The prediction accuracy of the TC LUT was quantified by comparing the HTC value calculated from the experimental data before and after scatter removal to the corresponding value from the TC LUT, obtained by linear interpolation as discussed in Appendix A. 15 linear interpolations were performed for finding the TC LUT prediction for each data point. HTC values in tubes with diameters different from 8 mm were corrected according to Equation (3) with n = 0.20. For each data point, the percent difference between the value h_{LUT} predicted by the TC LUT and the value h calculated from the measurements was computed as

$$e = 100\frac{h_{LUT} - h}{h} \quad . \tag{4}$$

Then, the average e_{avg} and root mean squared (rms) e_{rms} values were calculated separately for the subcritical and supercritical ranges as well as for the entire databank. It is reminded that, following off-setting of all HTC values in the TC LUT, the overall average error was forced to be zero.

Table 8 summarizes the prediction accuracies of the entire TC LUT, as well as its SC and subcritical regions separately. The overall rms error in the predictions of all experimental data was 14.2%; this error decreased to 12.6% when the same data but subjected to scatter removal were considered. If off-setting had not been performed, the error would have been 15.3%; this means that off-setting both removed the bias and lowered the precision error. Table 9 and 10 present the average and rms errors of the TC LUT in the two subcritical regions and the three supercritical regions, respectively. It is evident that the TC LUT is more accurate than any of the leading heat transfer correlations in the superheated steam region (Table 3) and all three SCHT regions (Table 4). However, for single-phase liquid heat transfer, the correlation of Gnielinski (1976) appeared to be slightly more accurate than the TC LUT; the small (0.8%) difference is attributed to the corrections made to the TC LUT values for inconsistencies in the trends at boundaries between subregions with values originating from different predictions methods.

Table 8: Average and rms errors for the entire TC LUT.

	All data (13010 data points)		Subcritical data (717 data points)		SC data (12293 data points)	
	e_{avg} %	e_{rms} %	e_{avg} %	e_{rms} %	e_{avg} %	e_{rms} %
Data without scatter removal	0.0	14.2	-1.9	11	0.36	14.3
Data with scatter removal	0.0	12.6	-2.0	10.7	0.34	12.7

Table 9: Average and rms errors for the TC LUT in the high subcritical region.

	Subcritical liquid (157 data points)		Superheated steam (560 data points)	
	e_{avg} %	e_{rms} %	e_{avg} %	e_{rms} %
Data without scatter removal	-0.5	11.2	-0.1	10.9
Data with scatter removal	-1.6	10.8	-0.6	10.7

Table 10: Average and rms errors for the TC LUT in the three supercritical regions.

	Liquid-like region (743 data points)		Gas-like region (3075 data points)		Near-critical/pseudo-critical region (8475 data points)	
	e_{avg} %	e_{rms} %	e_{avg} %	e_{rms} %	e_{avg} %	e_{rms} %
Data without scatter removal	-0.8	16.3	-0.1	11.2	0.16	15.0
Data with scatter removal	-1.6	14.6	1.4	11.0	0.12	13.1

6. Predictive capability of the TC LUT and comparisons with other prediction methods

The use of semi-empirical heat transfer correlations is the most common method of predicting HTC at SC pressures. Before comparing the predictions of the TC LUT with those of correlations, we would like to expose certain potential weaknesses of most correlations, some of which are not present in the TC LUT. To begin with, the datasets that were available for the development of SCHT prediction methods were collected under diverse conditions and with different experimental uncertainties. As explained in section 2, the TC LUT databank contained data from many different sources, but it was screened for inappropriate and problematic datasets, which were identified and removed. As far as we can discern from the published literature, most correlations have not been based on very extensive as well as thoroughly screened databanks and may, therefore, be restricted to limited ranges or possibly contaminated by the inclusion of inappropriate datasets. A related limitation of correlations, but not of the TC LUT, is the inclusion of highly scattered data in their databanks, which unnecessarily increased their prediction uncertainties. Most of the SCHT correlations were intended to describe NHT, however, it is not always clear whether the experimental data used for the development of these correlations were obtained exclusively under NHT conditions. In addition, it is possible that some near-critical results may have been collected under unstable conditions, and so contain pressure and wall temperature fluctuations. Even if effort was made to remove deteriorated and enhanced heat transfer data from the databases used, the absence of universally valid criteria for identifying such conditions makes the process open to questions. Mokry et al. (2009) attempted to screen their database only for heat transfer deterioration; they excluded evident deteriorated heat transfer data points from their correlation database, however, they did not exclude enhanced heat transfer data. Some correlations are very sensitive to local thermophysical property values, which have sharp variations with temperature in the vicinity of the critical and pseudo-critical points. When applied to scattered wall temperature data at near-critical and near-pseudo-critical temperatures, such correlations may produce highly scattered HTC predictions, due to the strong variation of thermophysical properties with wall temperature in these ranges of conditions. This may be the consequence of fitting empirical expressions to inadequately screened data, thus contaminating the correlation parameters (*e.g.*, property ratios raised to certain powers) by data not collected under NHT conditions (Jackson, 2014). As the TC LUT includes explicitly wall temperature difference as an independent parameter, the scatter of temperature data will also introduce scatter in the predicted HTC profiles, however the table scatter is milder than that of the corresponding data on which the table is based because of the averaging of the HTC values in the databank and the subsequent smoothing of the HTC trends with respect to each of the four input parameters.

When applied to cases with very strong heat transfer deterioration, the table may overestimate the minimum HTC by up to 100%. Moreover, the tube diameter correction, which was based on normal heat transfer data, may introduce additional uncertainty when applied in the deteriorated heat transfer region. To avoid the possibility of excessively large uncertainty by tube size scaling, the intended range of application of the table was restricted to tubes with sizes from 5 to 16 mm. For tubes with diameters near the lower limit of this range, an underestimation of the deteriorated HTC might occur for deterioration by buoyancy (relatively low mass flux and high heat flux conditions) and an overestimation of HTC for deterioration by acceleration (high mass flux and high heat flux conditions). The opposite would be true for tubes with diameters near the upper limit of this range.

Heat transfer correlations for low subcritical pressure are conventionally evaluated based on a reference temperature, which is the bulk temperature; however for the case when radial variation of properties exists, it is the film temperature (*i.e.*, the mean between wall and bulk temperatures) that is usually considered. Most near-critical and SCHT correlations are based on conventional subcritical single-phase correlations, modified by the inclusion of multipliers in the form of property ratios to account for the effects of strong radial variation of properties on heat transfer. As an alternative, Li et al. (2011) proposed to compute average instantaneous local properties near the critical and pseudo-critical point using probability density functions to account for the strong non-linear dependence of these properties on instantaneous temperature. This approach was introduced by Laurien (2010) in his development of wall functions for SCHT and results in smoothing the property variations. Li et al. (2011) also showed that, although the Dittus-Boelter (1930) correlation overpredicted significantly the peak value of experimental HTC in carbon dioxide near the pseudo-critical temperature (P = 7.5 MPa, G = 762 kg/m^{2}s), the same correlation predicted fairly accurately this peak value when the properties were averaged by the proposed method. Kruizenga et al. (2012) also reported that different SCHT correlations showed different amount of scatter. It must be emphasized that, unlike low subcritical pressure correlations, which generally predict smooth HTC trends (mainly because the method for evaluation of properties described above suffices), poorly developed SCHT correlations may lead to highly scattered predictions. It is noted that the HTC profiles predicted by the TC LUT also have scatter due to the explicit use of the wall temperature difference as an input parameter; however, this scatter is lower than the scatter in the corresponding data.

A comparison of the prediction accuracy of the TC LUT and those of three correlations that were found to give the best predictions for each region of the TC LUT is presented in Table 11. For this comparison, all data that were used for the construction of the TC LUT were considered without scatter removal, so that the reported errors refer to differences between predictions and actual data values. Table 11 shows percentages of these data for which the corresponding errors fell within bands of $\pm$10% (e_{10}), $\pm$20% (e_{20}), $\pm$30% (e_{30}), and $\pm$50% (e_{50}) of the experimental values. The table clearly illustrates that the TC LUT predictions are at least as accurate as, and in most cases significantly more accurate than, any of the leading correlations. Moreover, the TC LUT was constructed from data covering the entire range of conditions of interest, whereas each correlation was meant to cover a specific range. It may be seen that, although all four predictions fall within the $\pm$50% error band for essentially all data considered, the TC LUT is clearly superior to the others with respect to predictions that fall within the ±10% error band. Among the available correlations, the best overall performance is shown by the Mokry at al. (2009) correlation; even though this correlation was developed against SCHT data, it has a fair predictive ability for high subcritical superheated steam cases as well.

Table 11: Percentages of all data predicted within various error bands for the TC LUT and leading correlations.

Error band	Near-critical/pseudo-critical region (8475 data points)			
	Mokry et al. (2009)	Gupta et al. (2010)	Swenson et al. (1965)	TC LUT
e_{10}	51	55	49	56
e_{20}	82	82	75	85
e_{30}	93	93	88	95
e_{50}	100	99	96	99
	Liquid-like region (743 data points)			
	Mokry et al. (2009)	Bishop et al. (1965)	Kuang et al. (2008)	TC LUT
e_{10}	41	35	40	48
e_{20}	69	64	71	79
e_{30}	87	83	86	93
e_{50}	97	98	97	100
	Gas-like region (3075 data points)			
	Mokry et al. (2009)	Gupta et al. (2010)	Bishop et al. (1965)	TC LUT
e_{10}	51	36	46	67
e_{20}	82	73	77	92
e_{30}	95	91	90	99
e_{50}	100	99	97	100
	Subcritical liquid (157 points)			
	Mokry et al. (2009)	Gnielinski (1976)	Dittus-Boelter (1930)	TC LUT
e_{10}	57	69	43	69
e_{20}	89	94	83	94
e_{30}	96	99	95	99
e_{50}	100	100	100	100
	Subcritical superheated steam (560 data points)			
	Mokry et al. (2009)	Hadaller and Banerjee (1969)	Dittus-Boelter (1930)	TC LUT
e_{10}	50	18	10	54
e_{20}	73	45	21	86
e_{30}	89	68	33	98
e_{50}	100	88	55	100

Following a statistical evaluation of the TC LUT predictive accuracy, we will now present a few representative examples of the TC LUT predictions of the HTC and compare them to corresponding values of HTC computed from experimental data, both without and with scatter removal. In addition, we will compare these predictions with predictions of the Mokry et al. correlation and the LUT by Loewenberg et al. (2008). The TC LUT predicts the HTC from specified values of P, G, ΔT_w and H_b. Subsequently, one may further estimate a hypothetical wall temperature $T_{w,LUT}$ from the HTC predicted by the TC LUT and the experimental values of the heat flux and bulk temperature as $T_{w,LUT} = T_b + q/h_{LUT}$. $T_{w,LUT}$ may then be compared to the experimental wall temperature to demonstrate, among other things, possible effects of strong property variations on the wall temperature in the vicinity of T_c and T_{pc}.

Figure 6 shows HTC and wall temperature profiles from a near-critical (P/P_c = 1.056) experimental dataset by Shitsman (1963), which covers the three SCHT regions with respect to T_w, T_b and T_{pc}; data without and with scatter reduction are shown in the figure. As distance from the inlet, or equivalently H_b, increased, T_w increased to a sharp peak, followed by a decrease to a mild minimum at H_b = H_{pc}, and a gradual increase till the exit of the heated section; the HTC followed the opposite trends. Such behaviour may be attributed to heat transfer deterioration and recovery caused by buoyancy force development. Predictions of the HTC and $T_{w,LUT}$ profiles by the TC LUT and the Mokry et al. correlation are shown together with the measurements. Both types of predictions had a fair agreement with the measurements, but it is evident that the TC LUT predictions were generally closer to the experimental values. Moreover, the Mokry et al. correlation predicts a second HTC peak at H_b = 1600 kJ/kg, which is not present in the data or the TC LUT predictions. Figure 7 shows similar comparisons of HTC and T_w predictions with a group of two near-critical (P/P_c = 1.031) datasets by Ackerman (1970); these two datasets had comparable flow conditions, except for a difference in the inlet temperature. The dataset with the lower inlet temperature, only three points of which overlapped with the range of the TC LUT, corresponded to normal heat transfer, but the other set showed two peaks in wall temperature (and corresponding local minima in the HTC), which were referred to by Ackerman as pseudoboiling and film boiling, respectively. The TC LUT followed the general trend of the data, but only predicted the first and largest peak in T_w. The Mokry et al. correlation provided a less satisfactory prediction of the experimental trends, missing either of these peaks and in fact predicting a local minimum in T_w at the location of the first peak.

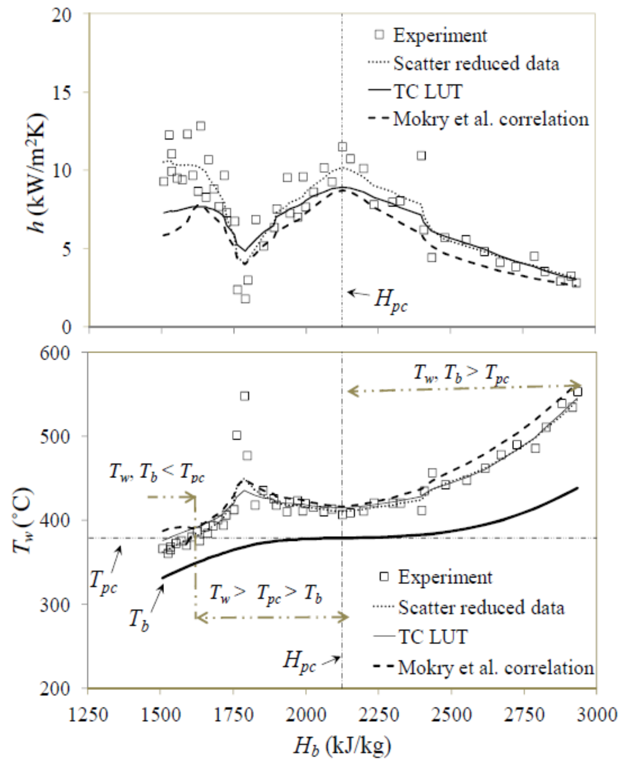

Figure 6: Comparison of experimental values of h and T_w by Shitsman (1963) and predictions by the TC LUT and the Mokry et al. (2009) correlation; P = 23300 kPa (P/P_c = 1.056), G = 430 kg/m^{2}s, q = 326 kW/m^2 and d = 10 mm.

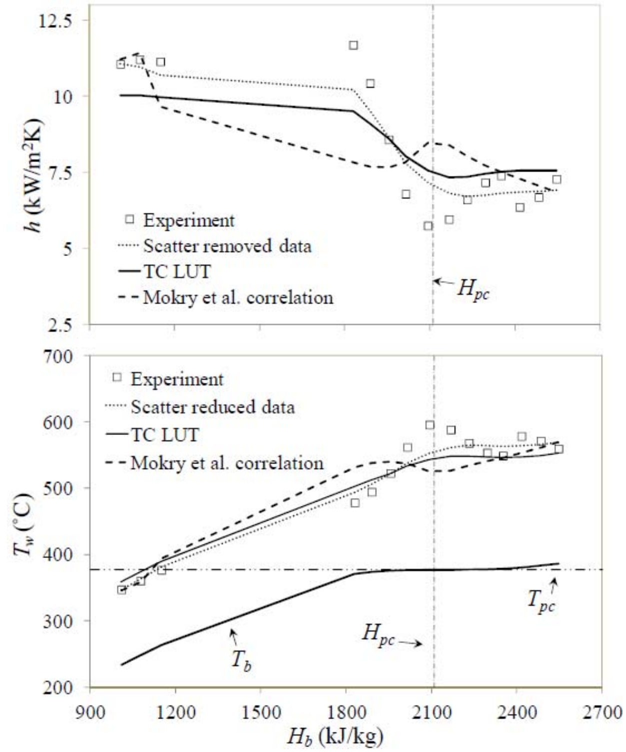

Figure 7: Comparison of experimental values of h and T_w by Ackerman (1970) and predictions by the TC LUT and the Mokry et al. (2009) correlation; P = 22754 kPa (P/P_c = 1.031), G = 1220 kg/m^{2}s, q = 1260 kW/m^2 and d = 9.4 mm.

Among the two SC LUT that have been reported in the literature, only the one by Loewenberg et al. (2008), to be referred to hereafter as SU LUT (with SU standing for Stuttgart University), has been reported with sufficient information to permit comparisons with the present TC LUT. Such comparisons, however, are not straightforward and cannot be performed for the full range of parametrs of the SU LUT, because it has a structure and a range of conditions that are different from those of the TC LUT. The SU LUT has five input parameters, namely, P, G, q, H_b and d and so one would need to calculate T_w before comparison with the TC LUT predictions can be made. Moreover, the range of heat flux in the SU LUT only partially overlaps with that in the TC LUT, which complicates the finding of table regions that can be compared. To simplify matters, we digitized the T_w values from the five figures presented by Loewenberg in his thesis (Loewenberg, 2007, Figures 6.2 – 6.6), in which he compared the SU LUT predictions with correlations and experimental data. Figure 8 reproduces data by Herkenrath et al. (1967) from two of these figures and compares them with predictions of the SU LUT, the TC LUT and the Mokry et al. (2009) correlation. Figure 8a corresponds to the case with the best agreement of the SU LUT predictions with the measurements; the TC LUT predictions are somewhat less accurate than those of the SU LUT, but they are also faithful to the experimental trends. On the contrary, In Figure 8b, it is the TC LUT predictions that are the closest to the measurements, whereas the SU LUT predictions are visibly less accurate. An important point for the data in this figure is that they were collected in a tube with a diameter of 20 mm, which is outside the range of conditions of the databank that was used for the TC LUT construction; this proves first that the sensitivity of the HTC to the tube diameter in the range considered is very weak and second that equation

(3) adequately accounts for the diameter effect. The Mokry et al. correlation predictions are not far from the experimental values and in some cases have an accuracy that is comparable with those of either or both LUT. Nevertheless, this correlation also predicts some unrealistic trends, most notably the presence of a local minimum of T_w at H_b = H_{pc}, which is absent from the measurements and the LUT predictions.

In addition to the previous comparisons, we reorganised a section of the SU LUT with d = 10 mm to make it suitable for comparisons with the TC LUT. We also selected one set of data in a 10 mm tube diameter by Yoshida and Mori (2000), which was in the range of application of the SU LUT. Figure 9 shows the experimental values of the HTC and the T_w, as well as the corresponding predictions of the SU LUT, the TC LUT and the Mokry et al. correlation. None of the three methods predicted the HTC variation accurately, with the SU LUT predictions being much worse than those of the two other methods. The TC LUT prediction trends agreed qualitatively with the experimental trends, but the Mokry et al. correlation prediction showed some unrealistic trend in HTC in the range of H_b = 1500 – 2000 kJ/kg.

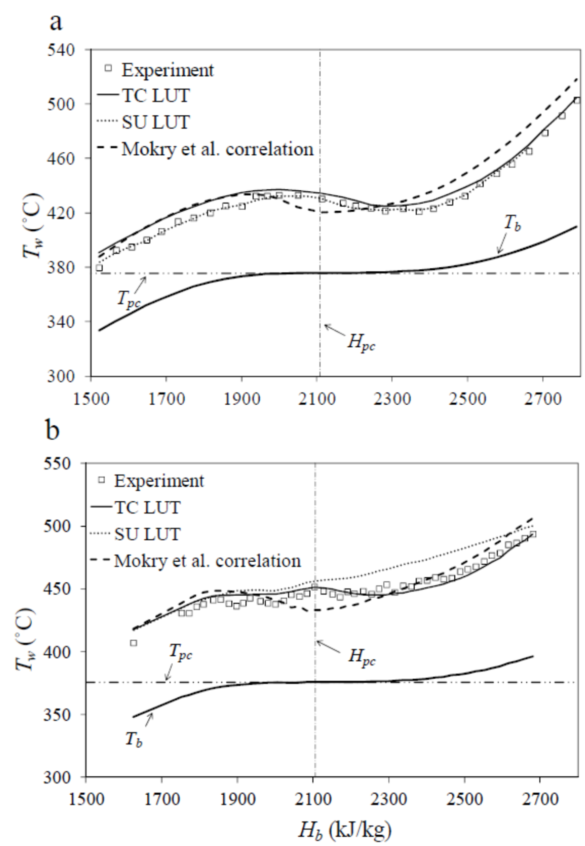

Figure 8: Comparison of experimental values of T_w by Herkenrath et al. (1967) and predictions by the SU LUT, the TC LUT and the Mokry et al. (2009) correlation. a) P = 22500 kPa, G = 700 kg/m^{2}s, q = 500 kW/m^2 and d = 10 mm. b) P = 22500 kPa, G = 1000 kg/m^{2}s, q = 700 kW/m^2 and d = 20 mm.

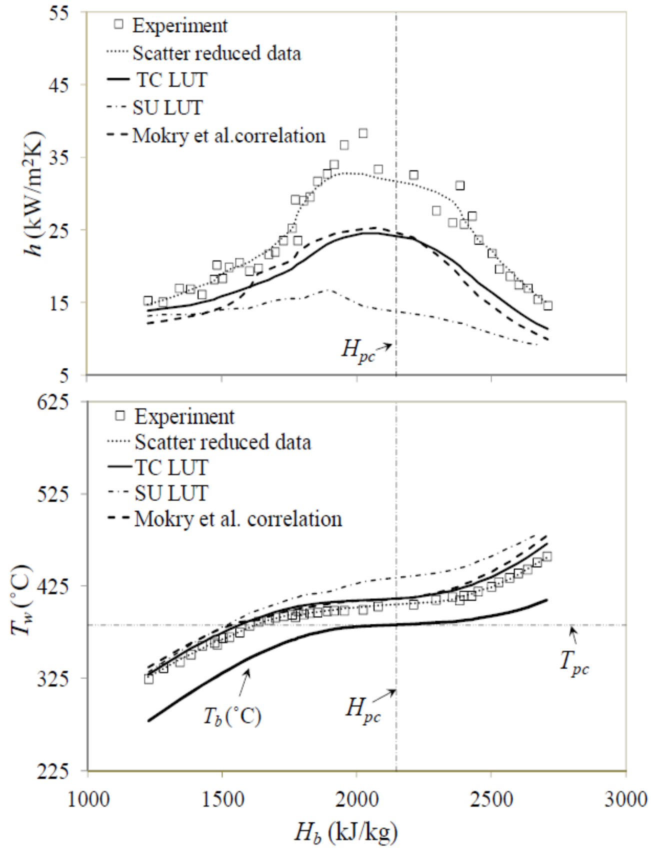

Figure 9: Comparison of experimental values of h and T_w by Yoshida and Mori (2000) and predictions by the SU LUT, the TC LUT and the Mokry et al. (2009) correlation; P = 24500 kPa, G = 1180 kg/m^{2}s, q = 698 kW/m^2 and d = 10 mm.

In summary, all tests performed have proved that the HTC predicted by the TC LUT over the entire trans-critical pressure range is at least as accurate as, and in most cases significantly more accurate than, any previous prediction method.

7. Updating and extended uses of the TC LUT

The present version of the TC LUT was based on the available experimental databases, after a number of restrictions were imposed to exclude data that did not meet several strict criteria. The final databank used for constructing the TC LUT included only datasets for downward flows of water in tubes with diameters in the range from 5 to 16 mm. Unfortunately, certain regions of this databank were fairly sparse, or even void of any experimental data. Consequently, some nodal values of the TC LUT were based on leading SC heat transfer correlations and/or extrapolations from the database using the parametric trends of the correlation, rather than experimental values. A convenient feature of the TC LUT is that it can be easily updated with additional water data, if such become available in the future. Moreover, following validation of appropriate scaling methods, the TC LUT may also be updated with data in other fluids and different channel geometries and orientations. In fact, some of these options are being currently pursued by the present authors.

As a substitute for the scarcity of water data in the high subcritical regime and in some SC ranges of conditions, we have collected extensive CO_2 data in an 8 mm tube under equivalent water conditions and we have developed accurate scaling laws between water and CO_2 for normal heat transfer at high subcritical and SC pressures (Zahlan et al., 2014). We are also in the process of performing similar tests for refrigerant R134a. Our intention is to incorporate such NHT data for CO_2 and R134a into the TC LUT, thus improving its accuracy in regions in which sufficient water data were not available. The same scaling laws may be used to convert the HTC in water from the TC LUT to values that pertain to these two other fluids, and possibly to additional fluids as well, thus creating a multi-fluid TC LUT that may be used in a wide range of applications.

The TC LUT databank included 13010 data points for tubes with diameters in the range from 5 to 16 mm. Nevertheless, the databases that were available to us included a total of 18359 acceptable data points in tubes with diameters in the range from 2 to 39 mm. When the expanded databank was considered, following application of Equation (3) to scale the HTC for NHT in tubes in the extended diameter range, the rms prediction error of the TC LUT increased from 14.2% to 17.4%, whereas the bias remained unchanged at 0.0%. This means that the effect of diameter on the HTC in the NHT mode is weak and one can use the TC LUT for the prediction of normal heat transfer in tubes with diameters within the extended range with only a small increase in uncertainty.

Another extension of the TC LUT on which we work currently is the inclusion of the effect of flow orientation, particularly the prediction of HTC in downward flows. We may plausibly hypothesise that, as the mass flux increases and/or the heat flux decreases, the HTC would become independent of flow direction for flows in tubes with diameters in the range of the TC LUT. For conditions for which flow orientation makes a difference, we will consider the use of an empirical HTC correction factor K_{DF} that accounts for this effect. Our intention is to restrict this correction procedure to conditions with normal heat transfer, as the description of HTD by such a simple method would be inappropriate.

Finally, we are investigating empirical correction methods to make the TC LUT applicable to flows in non-circular channels, specifically annular channels and rod bundles, as well as to channels that contain obstructions, particularly grid- and wire-wrapped spacers.

Because the TC LUT is by construction easy to update and modify, it has excellent potential to evolve into a tool that would be useful not only for SCWR design and safety analysis purposes, but also in a variety of other applications involving different channel geometries, fluids and operating conditions. TC LUT versions that would be fine-tuned to the needs of a particular application would also be relatively easy to construct by restricting the ranges of conditions of the general TC LUT; in such cases, it would be possible to improve the prediction accuracy of the specialised TC LUT by considering only the most relevant experimental data.

8. Conclusions

A trans-critical look-up table has been constructed as a new prediction method for near-critical and supercritical heat transfer of water flowing upwards through tubes. By comparison to existing SCHT and high pressure subcritical prediction methods, the new method has a much wider range of application, higher prediction accuracy, and a capability to reproduce more faithfully the experimental trends; unlike previous methods, the table is capable of predicting not only normal, but also deteriorated heat transfer. Careful screening of the experimental databases used for the construction of the table and the application of data scatter reduction and HTC smoothing procedures were found to improve measurably the accuracy of the look-up table. With the application of a correction factor for the tube diameter effect, the table can be used for flows in tubes having a fairly wide range of diameters. Further improvement of the table accuracy is possible by the incorporation of additional experimental results, as they become available. Moreover, the use of empirical scaling laws and correction factors permits the extension of the present table to applications involving different fluids, channel geometries and flow orientations.

Acknowledgements

Funding to the Canada Gen-IV National Program was provided by Natural Resources Canada through the Office of Energy Research and Development, Atomic Energy of Canada Limited, and Natural Sciences and Engineering Research Council of Canada. We are thankful to Professors I. Pioro, X. Cheng and E. Laurien for providing us their supercritical heat transfer data compilations. We also thank Drs. A. Vasic and M. Nakla for providing us the FORTRAN codes used for the film boiling look-up table construction.

References

Ackerman, J.W., 1970. Pseudoboiling heat transfer to supercritical pressure water in smooth and ribbed tubes. J. Heat Transfer, Trans. ASME, 92(3), 490–498 (P69–WA/HT-2).

Bishop, A.A., Sandberg, R.O., Tong, L.S., 1965. Forced convection heat transfer to water at near-critical temperatures and supercritical pressures. AIChE – I. Chem. E. Sym. Series. 2, 77−85.

Cheng, X., 2009. Private communication.

Cheng, X., Schulenberg, T., 2001. Heat transfer at supercritical pressures–literature review and application to an HPLWR. Wissenschaftliche Berichte (Technical Report) FZKA6609, Forschungszentrum Karlsruhe, May 2001.

Churkin, A.N., Deev, V.I., 2013. Ambiguity of calculation results of heat transfer to water using empirical correlations in the region of supercritical pressure. Proc. 6th Int. Sym. SCWR (ISSCWR-6), Shenzen, Guangdong, China, March 3–7.

Dittus, F.W., Boelter, L.M.K., 1930. Publications on Engineering, University of California, Berkeley. 2, 443–461.

Gnielinski, V., 1976. New equation for heat and mass transfer in turbulent pipe and channel flow. Intern. Chem. Eng. 16 (2), 359–366.

Groeneveld, D.C., Zahlan, H.Z., 2009. SCWR data compilation and LUT. Progress Report to AECL.

Groeneveld, D.C., Shan, J.E., Vasic, A.Z., Durmayaz, A., Yang, J., Cheng, S.C., Tanase, A., 2005. The 2005 CHF look-up table. NURETH-11, P166, Avignon, France, October 2−6.

Groeneveld, D.C., Leung, L.K.H., Vasic, A., Guo Y.J., Cheng, S.C., 2003. A look-up table for fully developed film-boiling heat-transfer. Nuc. Eng. Des. 225, 83–97.

Groeneveld D.C., Snoek, C., 1986. A comprehensive examination of heat transfer correlations suitable for reactor safety analysis. Multiphase Sci & Technol. 2, 181–274.

Groeneveld, D.C., Stewart, J.C., 1982. The minimum film boiling temperature for water during film boiling collapse. Proc. of the 7th IHTC, Munich, FRG. 4, 393–398.

Gupta, S., Mokry, S. Farah, A., King, K. , Peiman, W., Pioro, I., 2010. Developing a heat-transfer correlation for supercritical-water flow in bare vertical tubes and its application. UOIT, unpublished report.

Hadaller, G., Banerjee, S., 1969. Heat transfer to superheated steam in round tubes, AECL Report.

Hall, W.B., Jackson, J.D., Watson, A., 1968. A review of forced convection heat transfer to fluids at supercritical pressures. Proc. I. Mech. E., 182, Part 3I, Bristol Sym., HTFS 3907.

Herkenrath, H., Mörk-Mörkenstein, P., Jung, U., and Weckermann, F. J., 1967. Wärmeubergung an Wasser bei Erzwungener Strömung in Drückbereich von 140 bis 250 Bar", EUR-3658d.

Huang, X. C., Cheng, S. C., 1994. Simple method for smoothing multidimensional experimental data with application to the CHF and PDO Look-up Table, Numer. Heat Trans., Part B. 26, 425– 438.

Jackson, J.D., 2014. Approach for validating an improved semi-empirical model of turbulent mixed convection heat transfer to fluids at supercritical pressure. International Meeting of Specialists in Heat Transfer to Fluids at Supercritical Pressure, Manchester, UK, June 30 - July – 1, 2014.

Jackson, J.D., 2013. Fluid flow and convective heat transfer to fluids at supercritical pressure. Nuc. Eng. Des., 264 , 24–40.

Jackson, J.D., 2011. A Model of developing mixed convection heat transfer in vertical tubes to fluids at supercritical pressure. Proc. of the 5th Int. Sym. SCWR (ISSCWR-5), P104, Vancouver, British Columbia, Canada, March 13-16.

Jackson, J.D., Hall, W.B., 1979a. Forced convection heat transfer to fluids at supercritical pressure, in: Kakaç, S., Spalding D.B. (eds.), Turbulent forced convection in channels and bundles. Hemisphere Publishing Corp., Washington, USA, 2, pp. 563–611.

Jackson, J.D., Hall, W.B., 1979b. Influences of buoyancy on heat transfer to fluids flowing in vertical tubes under turbulent conditions, in: Kakaç, S., Spalding D.B. (eds.), Turbulent forced convection in channels and bundles. Hemisphere Publishing Corp., Washington, USA, 2, pp. 613–641.

Kuang, B., Zhang, Y. Cheng, X., 2008. A New, Wide-ranged heat transfer correlation of water at supercritical pressures in vertical upward ducts, NUTHOS-7, Seoul, Korea.

Kruizenga, A., Li, H., Anderson, M., Corradini, M., 2012. Supercritical carbon dioxide heat transfer in horizontal semicircular channels. J. of Heat Transfer, Vol. 134 / 081802-1.

Laurien, E., 2010. Development of numerical wall functions to model the heat transfer of supercritical fluids, Proc. ICAPP'10, International Congress on Advances in Nuclear Power Plants, June 13-17, San Diego, California, USA.

Lemmon, E.W., M'cLinden, M.O., Friend, D.G., 2002. Thermophysical Properties of Fluid Systems, NIST Standard Reference Database Number 69, REFPROP: Version 7.0.

Li, H., Kruizenga, A., Anderson, M., Corradini, M., Luo, Y., Wang, H., Li, H., 2011. Development of a new forced convection heat transfer correlation for CO2 in both heating and cooling modes at supercritical pressures. Int. J. Therm. Sci., 50, 2430–2442.

Liu, X., Kuang, B., Ni, C., Cheng, X, 2011. Look-up table establishment of supercritical water heat transfer in vertical upward flow and tube-size effect investigation. 5th Int. Sym. SCWR (ISSCWR-5), Vancouver, Canada, March 13–16.

Löwenberg, M., Starflinger, J., Laurien., E., Class, A., Schulenberg, T., 2008. Supercritical heat transfer in vertical tubes, a look-up table. Prog. Nucl. Energy, 50, 532−538.

Löwenberg, M., 2007. Heat transfer from water in vertical pipe flows at supercritical pressure, Doctoral Dissertation, Institute for Nuclear and Energy Technologies, Faculty of Mechanical Engineering, University of Stuttgart, Stuttgart, Germany.

Mokry, S., Gospodinov, Ye., Pioro, I., Kirillov, P., 2009. Supercritical water heat-transfer correlation for vertical bare tubes. Proc. ICONE-17, Brussels, P76010, 8 pages.

Nakla, M., 2010. Private communication.

Pioro, I.L., 2010. Private communication.

Pioro, I.L., Khartabil, H.F., Duffey, R.B., 2004. Heat transfer to supercritical fluids flowing in channels – empirical correlations (survey). Nuc. Eng. Des., 230 (1–3), 69–91.

Seider, N.M., Tate, G.E., 1936. Heat transfer and pressure drop of liquids in tubes. Ind. Eng. Chem., 28(12), 1429–1435.

Shitsman, M.E., 1963. Impairment of the heat transmission at supercritical pressures, 1963. Teplofiz. Vysokikh Temperatur (High Temperatures), 1(2), 237-244.

Swenson, H.S., Carver, J.R., Kakarala, C.R., 1965. Heat transfer to supercritical water in smooth-bore tubes, J. of Heat Transfer, Trans. ASME Series C. 87 (4), 477–484.

Tavoularis, S., 2005. Measurement in Fluid Mechanics. Cambridge University Press, Cambridge, UK.

Thom, J.R.S., Walker, W.M., Fallon, T.A., Reising, G.F.S., 1965. Boiling in sub-cooled water during flow up heated tubes or annuli. Proc. Inst. Mech. Eng., Manchester.

Watts, M. J., Chou, C.T., 1982. Mixed convection heat transfer to supercritical pressure water. Proc. 7th, IHTC, Munich, Germany. 495–500.

Yamagata, K., Nishikawa, K. Hasegawa, S., Fujii, T., Yoshida, S., 1972. Forced convective heat transfer to supercritical water flowing in tubes. Int. J. Heat Mass Transfer, 15 (12), 2575–2593.

Yoshida, S., Mori, H., 2000. Heat transfer to supercritical pressure fluids flowing in tubes. Proc. 1st Int. Symposium on SCWR Design and Technology, University of Tokyo, 72–78.

Zahlan, H., Jiang, K., Tavoularis, S., Groeneveld, D.C., 2013. Measurements of heat transfer coefficient, CHF and heat transfer deterioration in flows of CO_2 at near-critical and supercritical pressures. 6th Int. Symposium on Supercritical Water-Cooled Reactors (ISSCWR-6), March 3-7, 2013, Shenzhen, Guangdong, China.

Zahlan, H., Groeneveld, D.C., Tavoularis, S., 2010. Look-up table for trans-critical heat transfer, the 2nd CCSC-2010, Toronto, Canada, April 25 – 28, 18 pages.

Zahlan, H., Groeneveld, D.C., Tavoularis, S., 2011. Derivation of a look-up table for trans-critical heat transfer for water-cooled tubes. NURETH-14, Toronto, Ontario, Canada, September 25 – 30.

Zahlan, H., Groeneveld, D.C., Tavoularis, S., 2014. Fluid-to-fluid scaling for convective heat transfer in tubes at supercritical and high subcritical pressures. Int. J. Heat Mass Tran.73, 274 – 283.

Zahlan, H., Groeneveld, D.C., Tavoularis, S., Mokry, S., Pioro, I., 2011b. Assessment of supercritical heat transfer prediction methods. Proc. 5th Int. Sym. SCWR (ISSCWR-5), Vancouver, British Columbia, Canada, March 13 – 16, 20 pages.

Appendix A: Estimation of the local HTC slopes and incorporation of experimental data in the skeleton table

A.1 Estimation of the local HTC slopes

The partial derivatives of the HTC with respect to each of the four input parameters $P, G, \Delta T_w, H_b$ at each data point in the databank, to be referred to in the following as the local slopes, were estimated for use in the construction and error analysis of the TC LUT. Each local slope was estimated by performing 14 linear interpolations between values at the nodes of the skeleton table and one finite difference, so that 60 operations were performed for obtaining all four local slopes at each data point. The detailed procedure will be illustrated by an example, with the operations discussed in reverse order.

Consider a data point with input parameter values $P, G, \Delta T_w, H_b$ and an HTC value *h*. The first step was to identify the four-dimensional element of the skeleton table grid that contained the experimental point. This element was defined by 16 grid nodes, at which the skeleton table parameter values bounded the corresponding experimental values, *i.e.*, $P_l < P < P_{l+1}$, $G_k < G < G_{k+1}$, $\Delta T_{w,j} < \Delta T_w < \Delta T_{w,j+1}$, $H_{b,i} < H_b < H_{b,i+1}$, where, for example, the values $P_l, G_k, \Delta T_{w,j}, H_{b,i}$ correspond to the node *ijkl*. The local slope of HTC with respect to *P* was estimated as

$$\frac{\partial h}{\partial P} \cong \frac{h(P_{l+1}, G, \Delta T_w, H_b) - h(P_l, G, \Delta T_w, H_b)}{P_{l+1} - P_l} \quad . \qquad (1)$$

This expression cannot be evaluated directly from the skeleton table, because its right-hand-side contains values which are not at the nodes. These values were estimated by linear interpolation as, for example,

$$h(P_l, G, \Delta T_w, H_b) \cong h(P_l, G_k, \Delta T_w, H_b) + [h(P_l, G_{k+1}, \Delta T_w, H_b) - h(P_l, G_k, \Delta T_w, H_b)] \frac{G - G_k}{G_{k+1} - G_k} \quad . \qquad (2)$$

Two such interpolations were performed to account for changes in *G*. For each of these expressions, two linear interpolations were performed to account for changes in ΔT_w, and for each of the resulting expressions two more linear interpolations were performed to account for changes in H_b. In summary, to estimate the local slope with respect to *P*, the algorithm performed eight linear interpolations for H_b, four linear interpolations for ΔT_w, two linear interpolations for *G*, and one finite difference for *P*. Similar procedures were followed to estimate the three other local slopes.

A.2 Incorporation of experimental data in the skeleton table

To generate a table with predictions that would be as closely as possible to the measurements, the skeleton table values of HTC were replaced by projections of HTC values that were calculated directly from measurements corresponding to one or more data points. This procedure was applied to nodes in the vicinity of which data points were available in the databank, but, if additional data become available in the future, they can be easily incorporated in the table by the use of the same procedure. In past LUT literature, the table that resulted from the incorporation of the experimental data to the skeleton table has been referred to as the "updated table", but in the present article it will be referred to as the "data-fit table", as the latter name describes more clearly the procedure. Following data incorporation, the TC LUT was finalized by smoothing and slightly off-setting all HTC values, as will be described in the following subsection. The methodology for data incorporation in the skeleton table is similar to the one used by Groeneveld et al. (2003) for the construction of the film boiling LUT (2003 FB-LUT) and has also been described by Zahlan et al. (2011a). Its main steps are described in the following paragraphs.

The first step was to project the HTC value $h(P, G, \Delta T_w, H_b)$ at each data point in the databank to each of the 16 nodes at which the four input parameters had values that bounded those of the data point so as to generate an "experimental" HTC value at each node. For example, at node *ijkl*, the "experimental" value was calculated as

$$h_{node}\left(P_l, G_k, \Delta T_{w,j}, H_{b,i}\right) = h(P, G, \Delta T_w, H_b) + \Delta h \ , \qquad (3)$$

where the correction Δh was determined from the local slopes of the input parameters as

$$\Delta h = \frac{\partial h}{\partial P}(P_l - P) + \frac{\partial h}{\partial G}(G_k - G) + \frac{\partial h}{\partial \Delta T_w}\left(\Delta T_{w,j} - \Delta T_w\right) + \frac{\partial h}{\partial H_b}\left(H_{b,i} - H_b\right) \ . \qquad (4)$$

When only a single data point was found to be in the vicinity of a skeleton table node, the value at that node was simply replaced by the "experimental" value. If, however, more than one data points were identified near the node, the data-fit value was essentially a weighted average of all relevant data and it was calculated according to the following procedure. Let us consider a four-dimensional element of the skeleton table grid and assume that M data points have input parameter values that fall within that element. We are going to consider, as an example, the incorporation of these points into node *ijkl* in the sequence $m = 1, 2, \dots, M$. Let $h^{(m)}$ be the HTC for data point m and $h_{node}^{(m)}$ the "experimental" value at the node, updated by the incorporation of the first *m* data points. It is obvious that $h_{node}^{(1)} = h^{(1)}$. For the incorporation of subsequent points, weights that accounted for the proximity of each data point to the skeleton table node *ijkl* were defined as

$$W^{(m)} = \left(\frac{P_{l+1} - P^{(m)}}{P_{l+1} - P_L}\right)\left(\frac{G_{k+1} - G^{(m)}}{G_{k+1} - P_k}\right)\left(\frac{\Delta T_{w,j+1} - \Delta T_w^{(m)}}{\Delta T_{w,j+1} - \Delta T_{w,j}}\right)\left(\frac{H_{i+1} - H^{(m)}}{H_{i+1} - H_i}\right), m = 1, 2, \dots, M \ . \qquad (5)$$

Similar weights were assigned to each of the remaining 15 nodes of the grid element and the sum $S^{(m)}$ of all weights of the m experimental point for the 16 nodes of the grid element was calculated. Then, each weight was divided by $S^{(m)}$ to provide the normalized weight

$$w^{(m)} = \frac{W^{(m)}}{S^{(m)}} \quad . \qquad (6)$$

It is obvious that, when the data point values P, G, ΔT_w and H_b coincided with those at the skeleton table node *ijkl*, this weight would be equal to 1, whereas, when these data point values coincided with those in any other node of the grid element, this weight would be equal to zero. To incorporate the experimental point *m*, the "experimental" value at node *ijkl* was updated as

$$h_{node}^{(m)} = h_{node}^{(m-1)} \frac{\sum_{n=1}^{m-1} w^{(n)}}{\sum_{n=1}^{m} w^{(n)}} + h^{(m)} \frac{w^{(m)}}{\sum_{n=1}^{m} w^{(n)}} \ , \ \ m = 2,\ 3, \dots , M \ . \qquad (7)$$

The same process was repeated for all 16 nodes of the grid element. As the number of data incorporated to a specific node increased, the confidence in the value at that node and the overall TC LUT increased as well. The incorporation of several data points at a particular node also acted as a sort of smoothing.

CHAPTER 4

MEASUREMENTS OF CONVECTIVE HEAT TRANSFER TO VERTICAL UPWARD FLOWS OF CO_2 IN CIRCULAR TUBES AT NEAR-CRITICAL AND SUPERCRITICAL PRESSURES

This chapter addresses the measurements of heat transfer and pressure drop in vertical upward flow of CO_2 in circular geometry, also results of the analysis of the collected data is presented. This investigation is presented in the form of a manuscript entitled:

Zahlan, H., Groeneveld, D.C., Tavoularis, S., Measurements of Convective Heat Transfer to Vertical Upward Flows of CO2 in Circular Tubes at Near-critical and Supercritical Pressures, as submitted in December 2014 to Nuclear Engineering and Design.
DOI: http://dx.doi.org/10.1016/j.nucengdes.2015.04.013
0029-5493/© 2015 Elsevier B.V. All rights reserved. **Nuc. Eng. Des., 289 (2015) 92–107.**

This manuscript discusses the observed parametric trends and identifies an interesting heat transfer phenomenon encountered at low heat fluxes and high subcritical and supercritical conditions.

Measurements of Convective Heat Transfer to Vertical Upward Flows of CO_2 in Circular Tubes at Near-critical and Supercritical Pressures

H. Zahlan[a,b,*], D. Groeneveld[a,b] and S. Tavoularis[b]

[a]*Canadian Nuclear Laboratories, Chalk River, K0J 1J0, Canada*

[b]*Department of Mechanical Engineering, University of Ottawa, Ottawa, ON K1N 6N5, Canada*

ABSTRACT

An extensive experimental program of heat transfer measurements has been completed recently at the University of Ottawa's supercritical pressure test facility (SCUOL). Thermalhydraulics tests were performed for vertical upflow of carbon dioxide in directly heated tubes with inner diameters of 8 and 22 mm, at high subcritical, near-critical and supercritical pressures. The test conditions, when converted to water-equivalent values, correspond to conditions of interest to current Super-Critical Water-Cooled Reactor designs, and include many measurements under conditions for which few data are available in the literature. These data significantly complement the existing experimental database and are being used for the derivation and validation of a new heat transfer prediction method in progress at the University of Ottawa. The same data are also suitable for the assessment of the accuracy of other heat transfer prediction methods and fluid-to-fluid scaling laws for near-critical and supercritical pressures. In addition, they permit further examination of previously suggested relationships describing the critical heat flux and post-dryout heat transfer coefficient at high subcritical pressures and the boundaries of the deteriorated/enhanced heat transfer regions for near-critical and supercritical pressures. The measurements reported in this paper cover several subcritical heat transfer modes, including single phase liquid heat transfer, nucleate boiling, critical heat flux, post-dryout heat transfer, and superheated vapor heat transfer; they also cover several supercritical heat transfer modes, including heat transfer to liquid-like supercritical fluid and heat transfer to vapour-like supercritical fluid, which occurred in the downstream sections of the tubes. The collected data were reduced and compiled. The reported heat transfer database consists of more than 17,000 data points in the 8 and 22 mm tubes, along with pressure drop data for the 8 mm tube. The table of heat transfer data is provided as separate file in electronic format. The results are presented in plots of wall temperature and heat transfer coefficient *vs.* bulk fluid enthalpy. The parametric trends of diameter, mass flux, pressure and heat flux on these wall temperature and heat transfer coefficient profiles have been plotted and discussed. The present supercritical heat transfer measurements are in good agreement with corresponding results reported by other investigators.

Keywords:

Convective heat transfer

Supercritical pressure

Experimental data

Carbon dioxide

Pressure drop

1. INTRODUCTION

Experimental studies on heat transfer in supercritical (SC) water and other fluids have been reported since the 1950s and they were initially in support of SC fossil-fuelled power plants. This topic has recently received renewed attention in the nuclear energy field, because the Super-Critical Water-cooled Reactor (SCWR) concept is one of the potential new nuclear energy systems recommended by Generation IV International Forum. The attractive features of these new innovative nuclear energy systems include increased safety, more compact size, lower cost of energy production and reduced volume of nuclear waste, compared to existing systems. The present research is in support of the Canadian National Program for the development of the SCWR.

Heat transfer in a fluid at near-critical and supercritical pressures has distinct characteristics, which are not present at subcritical pressures. When the SC fluids are near their critical values, small changes in temperature cause large changes in the thermophysical properties and the heat transfer may undergo enhancement or deterioration. This abrupt change in the thermophysical properties extends to supercritical pressures in the vicinity of pseudocritical temperature, but decreases with increasing SC pressure. Of particular importance for the safety of SCWR is the phenomenon of heat transfer deterioration (HTD). Various investigators have attempted to predict the presence or absence of HTD at SC conditions. Early experimental studies in upward flow in tubes had revealed the occurrence of peak(s) in wall temperature indicating local heat transfer deterioration, however, most of the attempts to explain the associated mechanisms were made on the basis of analogy of SC heat transfer and subcritical boiling phenomena (critical heat flux (CHF) and film boiling), which ultimately did not produce useful expressions. Wall temperature peaks appearing close to the start of the heated length have been attributed to heat transfer degradation associated with the development of the thermal boundary layer (Pioro and Duffey, 2007), whereas peaks observed at locations that are distant from the thermal entry region have been attributed to buoyancy effects in mixed convection flow (Fewster and Jackson, 2004). The wall temperature drop following a temperature rise has been attributed to further development of buoyancy effects, which result in heat transfer enhancement (Lee, 2006; Jackson, 2011). It has also been reported that HTD can be caused by acceleration of near-wall fluid due to the local decrease in its density (Jackson, 2011), particularly at relatively high mass fluxes (Licht et al., 2008). Under certain conditions, HTD may extend along the entire length of the heated test section, without the appearance of hot-spots on the wall (Petukhov and Polyakov, 1988).

Experiments in SC water are necessary for the development of SCWR, however, they are difficult and expensive to perform. As a contribution towards an improved understanding of SC heat transfer under wide ranges of flow conditions, we report the results of a series of experiments using carbon dioxide as a modeling fluid, which, by comparison to corresponding experiments in water, were easier, safer and less expensive to perform. One objective of the present work was to supplement the experimental database for CO_2 with measurements under conditions for which previous data are scarce or not available. These data will be used to fill some gaps in the experimental database of the trans-critical heat transfer look up table (Zahlan et al., 2014b); CO_2 data will be incorporated in the trans-critical look up table database after their conversion to water equivalent values using appropriate scaling laws (Zahlan et al., 2014a). In addition, data obtained at high subcritical pressures will be used to fill some gaps in the experimental database that can be used for developing and validating CHF and film boiling look up tables and boiling heat transfer correlations. It is noted that data at near-critical pressures are particularly scarce in the literature. We hope that the present results will help improve our understanding of deterioration and enhancement of heat transfer and facilitate the testing of the accuracy of existing heat transfer correlations in the near-critical pressure regime.

2. SUPERCRITICAL TEST FACILITY AND PROCEDURES

2.1 Super-Critical University of Ottawa Loop (SCUOL)

The Super-Critical University of Ottawa Loop (SCUOL) was designed to operate with carbon dioxide as a coolant at a maximum operating pressure of 10 MPa. A schematic diagram of the loop is shown in Figure 1. The CO_2 was circulated through the loop by means of two gear pumps connected in parallel. Five bellow-type accumulators, using nitrogen as the secondary fluid, were connected to the loop to dampen flow and pressure oscillations and to provide a means for pressure adjustment. Electrical power for the direct heating of the test section was provided by a rectified power supply, rated at a maximum voltage of 60 V DC and a maximum current of 2833 A. The fluid exiting the test section was passed through two heat exchangers connected in series, where it was cooled by a centrally supplied chilled water stream and/or ethylene glycol supplied from a separate refrigeration system. The operating procedures for the loop were developed based on best practices with objectives highlighting safety of personnel, reliability and quality assurance of collected data.

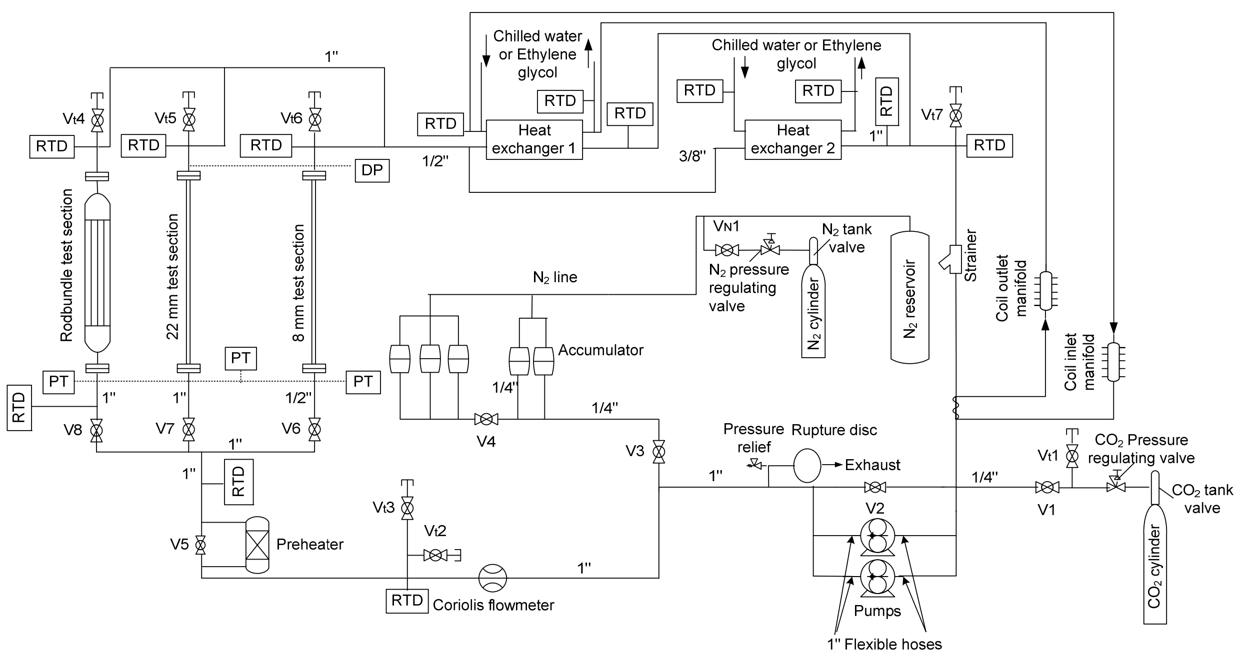

Figure 1: Schematic diagram of the flow loop**.**

2.2 Test sections

Measurements were collected in two directly heated circular tubes, mounted vertically with CO_2 flowing upwards. The first tube had an inner diameter of 8 mm and a wall thickness of

1 mm and was made of Inconel 600, whereas the second tube had an inner diameter of 22 mm and a thickness of 1.5 mm and was made of Inconel 625. The heated lengths L_h of the two tubes were, respectively, 1940 and 2000 mm and were preceded by unheated sections with lengths of 890 and 728 mm, respectively, which ensured that the flow entering the heated section was essentially fully developed and free of entrance effects. Each test section was insulated thermally by two or three layers of fibreglass cloth tape with a thickness of 0.8 mm; additional insulation was provided by rubber-foam insulation tubes, surrounding the fiberglass tape. Figures 2 and 3 show schematic diagrams of the two test sections with the locations of the thermocouples and other instrumentation.

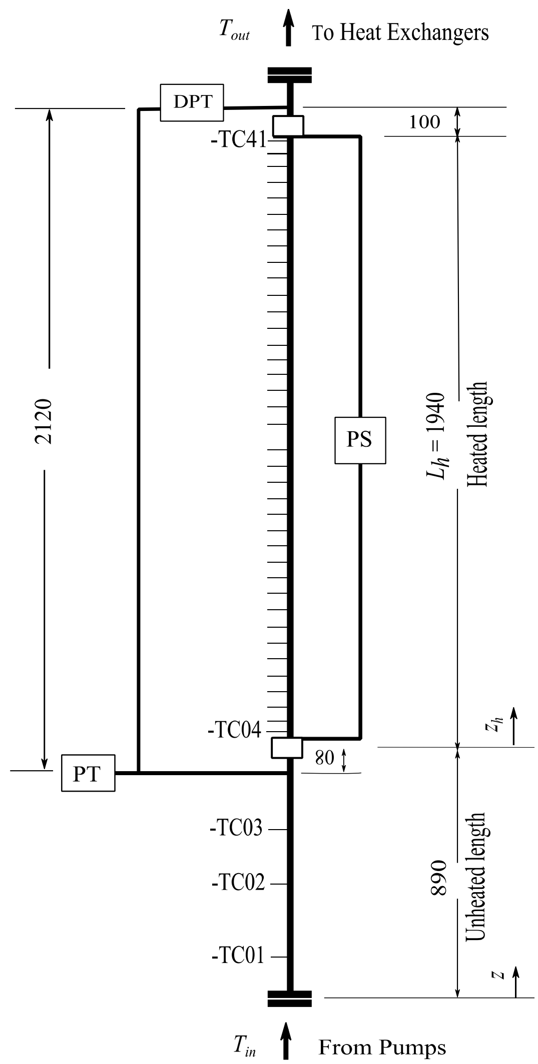

Figure 2: Schematic diagram of the 8 mm test section, showing the locations of thermocouples; PS: power supply; PT: pressure transducer; DPT: differential pressure transducer; dimensions in mm.

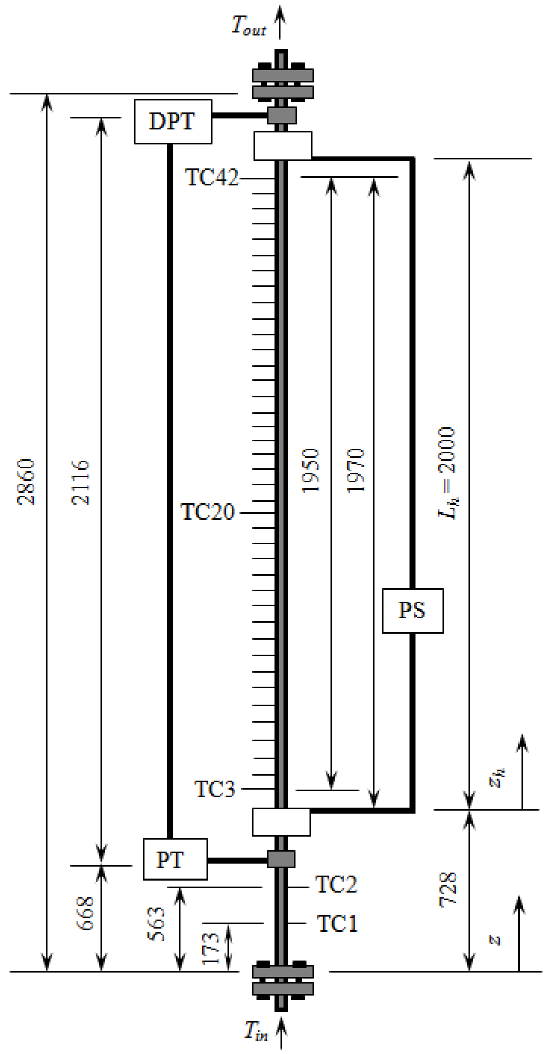

Figure 3: Schematic diagram of the 22 mm test section, showing the locations of thermocouples; PS: power supply; PT: pressure transducer; DPT: differential pressure transducer; dimensions in mm.

2.3 Instrumentation

Measurements of test section wall temperature were made using T-type (Copper-Constantan) thermocouples (Omega SA1XL-T-SRTC), having an uncertainty of 0.5 K (all reported precision uncertainties are at the 95% confidence level, namely, equal to two standard deviations of repeat values) and a time constant of less than 0.15 s. The thermocouples were attached to the exterior wall of each test section using a silicone-based adhesive, which can withstand temperatures up to 260˚C. The bulk fluid temperatures at the inlet and outlet of the test sections and other locations of the loop were measured with ultra-precise immersion RTD sensors (Omega P-M-1/10-1/8-5-1/2-G-15), having an uncertainty of 0.35 K within the range from 0 to 100˚C. The 8 mm test section inlet pressure was measured by a pressure transducer (Omega PX01C1-3KA5T) with an uncertainty of 21 kPa, whereas the 22 mm test section inlet pressure was measured by a different pressure transducer (Rosemount

3051TG4M2B21AM5C6Q4), made from low carbon stainless steel 316L with a full range from −101 to 27580 kPa, but calibrated in the range from 0 to 10342 kPa with a maximum uncertainty of 7.8 kPa. The pressure drop across the heated length of each test sections was measured with a differential pressure transmitter (Omega PX771A-300DI), having an uncertainty of 75 Pa. The pressure drop readings were corrected for the elevation difference between the transmitter and the pressure taps. The CO_2 mass flow rate was measured with a Coriolis flow meter (Micro Motion® ELITE® CFM050M320N0A2E2ZZ), having an uncertainty of 0.05% for liquid flow. The instantaneous voltage drop across the heated length of the test section was measured with a 24-bit digital voltage measurement module (National Instrument NI 9225), having a range of ±300 V and an uncertainty of 0.034 V. The rectified voltage fluctuated at a frequency of 360 Hz and was sampled at a much higher sampling rate. The electrical power supplied to the test section was calculated from the measured time-averaged voltage and the measured electrical resistance of the test section. A dedicated computerized data acquisition system was used to monitor and control different loop operations and to record data. A chassis (NI PXIe-1065 PXI Express chassis) was used to connect different modules for different input signal types.

3. DATA REDUCTION

3.1 Heat transfer data reduction

The volumetric heat flux in the test section wall was calculated as

$$q^v = \frac{Q_e}{\pi(r_o^2 - r_i^2)\mathrm{L_h}} \quad , \tag{1}$$

where Q_e is the measured electrical power supplied to the test section, r_o and r_i are the tube outer and inner radii, respectively, and L_h is the heated length. The inner wall temperature T_w was calculated from the measured outer wall temperature $T_{w,o}$ using the heat diffusion equation with uniform internal energy generation in cylindrical coordinates (Incropera et al., 2007), as

$$T_w = T_{w,o} + \frac{2q_{loss} r_o - q^v r_o^2}{2k} \ln\frac{r_o}{r_i} + (r_o^2 - r_i^2)\frac{q^v}{4k} \quad , \tag{2}$$

where the heat loss q_{loss} to the surroundings was neglected and k is the thermal conductivity of Inconel 600 or 625, evaluated at the local $T_{w,o}$.

The wall heat flux through the test section was calculated as

$$q = \frac{Q_e}{\pi d L_h} \quad , \tag{3}$$

assuming no losses to the environment or axial conduction effects. It must be pointed out, however, that the readings of the two thermocouples that were located the closest to either end of the heated test section were affected by axial heat conduction towards the large copper power clamps. The result was that these thermocouples read lower temperatures than would have been the case in the absence of conduction; this error was clearly noticeable at high wall temperatures but was insignificant otherwise. Then, the bulk fluid specific enthalpy along the heated test section was calculated using the simplified energy equation as

$$H_b = H_{in} + \frac{Q_e}{\dot{m}} \frac{z_h}{L_h} \quad , \tag{4}$$

where H_{in} is the specific enthalpy at the inlet, $\dot{m}$ is the mass flow rate and z_h is the axial distance along the heated section. The corresponding local bulk fluid temperature T_b and the thermophysical properties of carbon dioxide were calculated using NIST software (Lemonn et al., 2002). Finally, the local heat transfer coefficient (HTC) h was calculated as

$$h = \frac{q}{T_w - T_b} \, . \tag{5}$$

3.2 Pressure drop data reduction

The average friction factor f for each of the tests was calculated as

$$f = \frac{\Delta P_{fr}}{\left(\frac{L}{d}\right)\left(\frac{1}{2}\rho_b {U_b}^2\right)_{avg}} \, , \tag{6}$$

where L = 1.94 and 2.00 m are, respectively, the heated lengths of the 8 and 22 mm tubes, U_b is the bulk fluid velocity and ΔP_{fr} is the frictional pressure drop along the heated length. The latter was obtained from the application of the momentum equation to a control volume along the heated length of the tube as

$$\Delta P_{fr} = [P(0) - P(L)] - \mathrm{g}\int_0^L \rho_b(z)dz - G[U_b(L) - U_b(0)] \, . \tag{7}$$

In this equation, $[P(0) - P(L)]$ is the total pressure drop across the heated length of the test section; this was measured with the differential pressure transmitter and was corrected for the elevation difference between the transmitter and the pressure taps. The term $\mathrm{g}\int_0^L \rho_b(z)dz$ is the hydrostatic pressure difference between the inlet and the outlet of the heated length; the local bulk density ρ_b was determined from the NIST thermodynamic property tables (Lemmon *et al.*, 2002). The term $G[U_b(L) - U_b(0)]$ is the pressure drop due to acceleration of fluid resulted from changes in density due to heating. The average kinetic energy in Equation (6) was calculated as

$$\left(\frac{1}{2}\rho_b {U_b}^2\right)_{avg} = \frac{1}{2L}\int_0^L \rho_b {U_b}^2 dz \, . \tag{8}$$

The calculated average friction factor was presented in normalized form as $f^* = f/f_F$, where f_F is the friction factor value predicted by the following correlation (Filonenko, 1954)

$$f = 1/(1.82\log_{10}(\mathrm{Re}) - 1.64)^2 \quad , \tag{9}$$

which is valid for pipe flows at near-atmospheric pressures and for a wide range of Re that includes the range in the present study.

3.3 Measurement procedure and data collection

After establishing the desired operating conditions P, G, q and T_{in} according to the test plan, sufficient time was allowed for the loop and the instrumentation to reach steady state conditions. Data were sampled at a rate of 10 samples/s and each data record had a duration of at least 10 s. The collected data were averaged following removal of outliers whose values differed from the average by 3 or more standard deviations of the sample.

4. RESULTS

The complete data for heat transfer obtained in the present tests have been linked to this paper in an electronic format.

4.1 Flow conditions

Table 1 lists the ranges of the present experimental flow conditions and their water-equivalent values. The pressure was in the high subcritical and supercritical regions and the condition ranges include water-equivalent conditions that are of interest to the Canadian SCWR.

Table 1: Ranges of experimental flow conditions

Parameter	Range			
	Subcritical		Near-critical and supercritical	
	CO_2	Water equivalent*	CO_2	Water equivalent*
P [MPa]	5.91 − 7.17	17.67 − 21.44	7.44 − 8.67	22.24 − 25.94
P/P_c [−]	0.80 − 0.97		1.01 − 1.18	
T_{in} [˚C]	7.3 – 12.2	325 − 335	7.1 – 13.8	325 – 335
T_b/T_c [K/K]	0.92 – 1.00		0.92 − 1.17	
G [kg/m² s]	193 − 2041	325 − 3450	197 − 2027	300 – 3100
q [kW/m²]	2.9 – 280	30 − 3000	5.1 – 436	55 − 4600

* Scaling of CO_2 conditions to their water equivalent values followed the method proposed by Zahlan et al. (2014a).

4.2 Comparisons with previous measurements and quality assurance tests

Commissioning tests of SCUOL were reported recently by Jiang et al. (2012). Additional commissioning tests were performed to check the capability of the SCUOL to replicate previously measured supercritical heat transfer (SCHT) data collected in CO_2 loops in different laboratories. These included one set of results reported by Fewster and Jackson (2004) for a supercritical pressure slightly exceeding the critical value (P/P_c = 1.03) and two sets by Song et al. (2008) for a supercritical pressure that is relevant to the SCWR operation (P/P_c = 1.10).

Table 2 shows that the present experimental conditions approximated fairly closely those in the previous tests, although an exact match was not possible because of differences in the designs of the loops, diameters and lengths of the test sections and inlet temperatures, which resulted in differences in the experimental bulk-enthalpy ranges.

Table 2: Conditions in selected tests from the literature and in present tests

P/P_c	Authors	D mm	L_h mm	P MPa	G kg/s m^2	q kW/ m^2	T_{in} ºC	T_{pc} ºC	H_{pc} kJ/kg
1.03	Fewster & Jackson (2004)	7.9	1,185	7.58	398	33.6	14.5	32.2	337.7
	Present	8.0	1,940	7.61	402	33.9	13	32.3	337.8
1.10	Song *et al.* (2008) - Case B1	9.0	2,650	8.12	400	30	7.5	35.3	339.3
	Present	8.0	1,940	8.14	405	29.9	13.4	35.4	339.4
	Song *et al.* (2008) - Case B3	9.0	2,650	8.12	1200	50	6.4	35.3	339.3
	Present	8.0	1,940	8.14	1210	50.1	9.0	35.4	339.4

The wall temperatures measured by Fewster and Jackson (2004) showed significant heat transfer deterioration and had a sharp first peak that moved upstream as the inlet temperature was increased. Figure 4 demonstrates that our results were in excellent agreement with these. As shown in Figure 5, present measurements of wall temperature and heat transfer coefficient were also in fair agreement with the corresponding results of the two test runs by Song et al. (2008). In conclusion, it is evident that heat transfer results in the present loop can be treated with confidence, as they demonstrate good reproducibility with results from the literature.

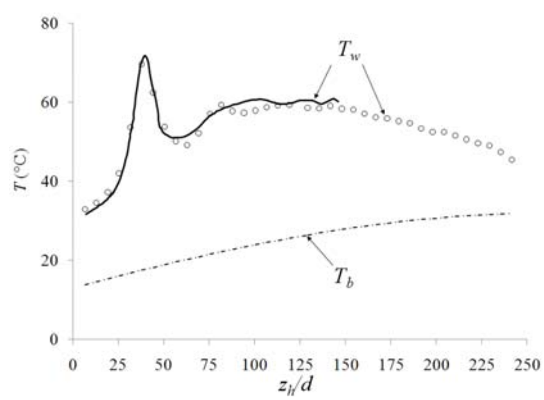

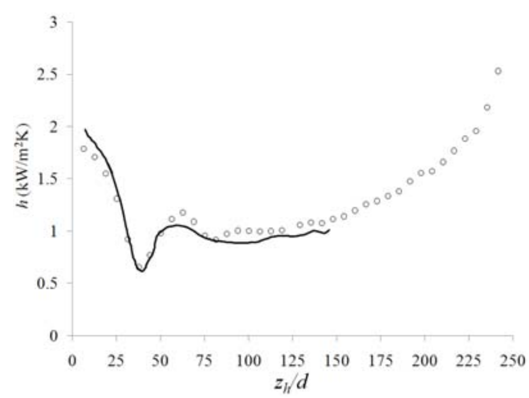

Figure 4: Wall and bulk fluid temperature variations (left) and corresponding heat transfer coefficients (right) in the present study (circles) and as reported by Fewster and Jackson (2004; solid lines).

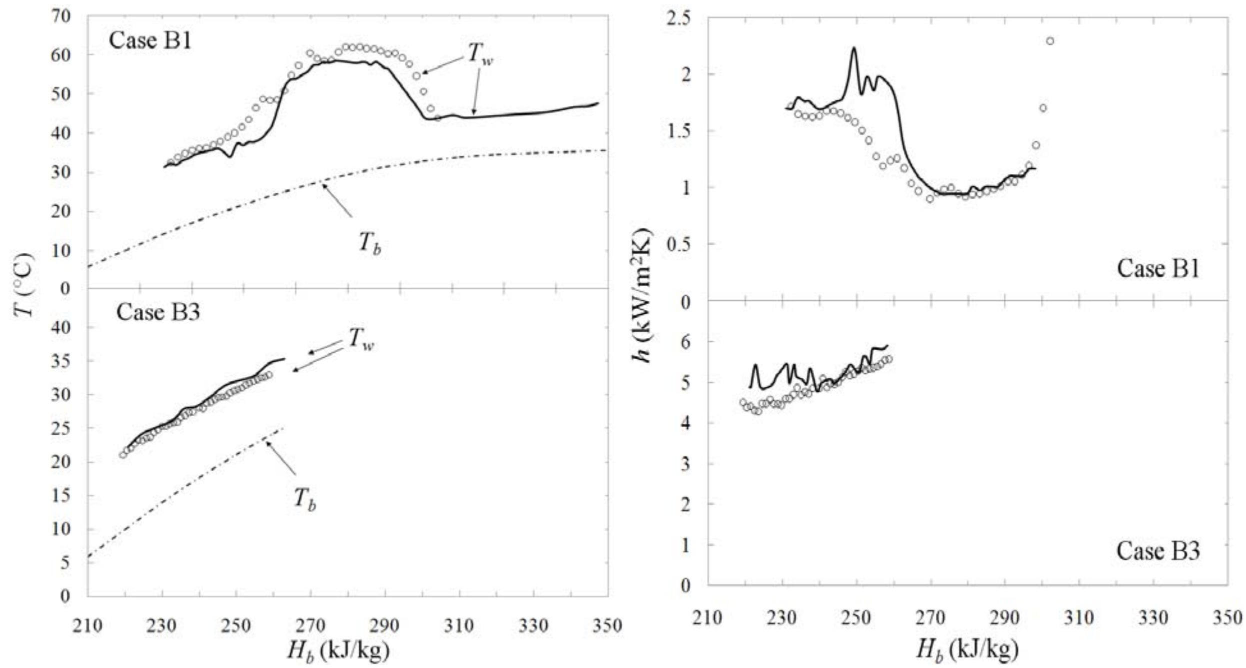

Figure 5: Wall and bulk fluid temperature variations (left) and corresponding heat transfer coefficients from the present study (circles) and as reported by Song et al. (2008) (solid lines).

Quality assurance (Q/A) tests: The difference between the electric power Q_e provided to the test section and the rate of heat transferred to the fluid Q_t, estimated from the energy equation, was calculated in real time during each test as

$$\Delta Q = Q_e - Q_t = Q_e - \dot{m}\,(H_{out} - H_{in}) \quad , \tag{10}$$

where the inlet and outlet fluid specific enthalpies were calculated from linked NIST CO_2 property tables at the measured test section inlet and outlet fluid temperatures. Figure 6 shows that the heat balance discrepancy $e_Q = \Delta Q / Q_e$ was less than 4% in magnitude. As a different Q/A test, we examined the pressure and temperature readings for the flows at subcritical pressures encountering saturated boiling. Differences between the fluid temperature at saturation state as measured by an RTD at the inlet/outlet of the test section and the corresponding saturation temperature evaluated from the measured inlet/outlet pressure were within the uncertainty of the pressure and temperature measurements.

During some tests, the loop experienced low-frequency oscillations (at approximately 0.05 Hz) in flow rate, accompanied by oscillations in the recorded temperatures. Similar flow oscillations have been reported occasionally in the literature (Zahlan et al., 2014b). Further investigation is needed to clarify the cause of this phenomenon. These cases were excluded from the present database, so that all results reported in the following sections were obtained during steady operation of the loop.

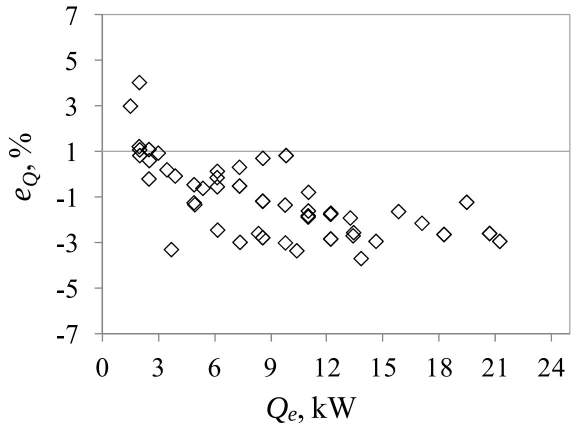

Figure 6: Heat balance discrepancy e_Q as a function of the power supplied to either the 8 mm or the 22 mm test section.

4.3 Supercritical heat transfer measurements

This and the following section contain representative results of heat transfer tests, presented as plots of the wall temperature T_w and the corresponding heat transfer coefficient h *vs.* the bulk fluid enthalpy H_b. Some figures also include plots of T_w and h *vs.* distance z_h from the inlet of the heated section. Dashed lines in these plots indicate the pseudocritical enthalpy or temperature for the SC cases or the saturation temperature for the subcritical cases. Flow conditions reported on the plots are averages of the conditions of the presented test data; pressure, mass flux and heat flux variations from the reported average values were within ±1% and inlet temperature differences from the reported average value were typically within ±0.5 ºC.

Tube diameter size effect: Tests performed with relatively low or moderate heat fluxes were, in general, characterized by monotonically increasing wall temperature profiles that were free of local peaks, as is typical for normal heat transfer. As an exception to this categorization, tests in the 22 mm tube at the low mass flux of 200 kg/m^{2}s and at low heat fluxes revealed the presence of peaks in wall temperature close to the entry of the heated section; these cases will be discussed further at the end of this section. Typical examples of tube diameter size effect are presented in Figure 7, which shows variations of measured T_w and h *vs.* H_b for the 8 and 22 mm tube obtained at similar flow conditions. For q = 50 kW/m^2, the heat transfer appears to be normal in both tubes and the trends in T_w and h were very similar; at comparable flow conditions, the HTC in the 8 mm tube was slightly higher than that in the 22 mm tube, in agreement with the predictions of the single-phase heat transfer correlation of Jackson (2009). In contrast, for q = 70 kW/m^2, some heat transfer deterioration appears to have occurred in the 22 mm tube but not in the 8 mm tube, whereas, for q = 125 kW/m^2, significant HTD occurred in both tubes.

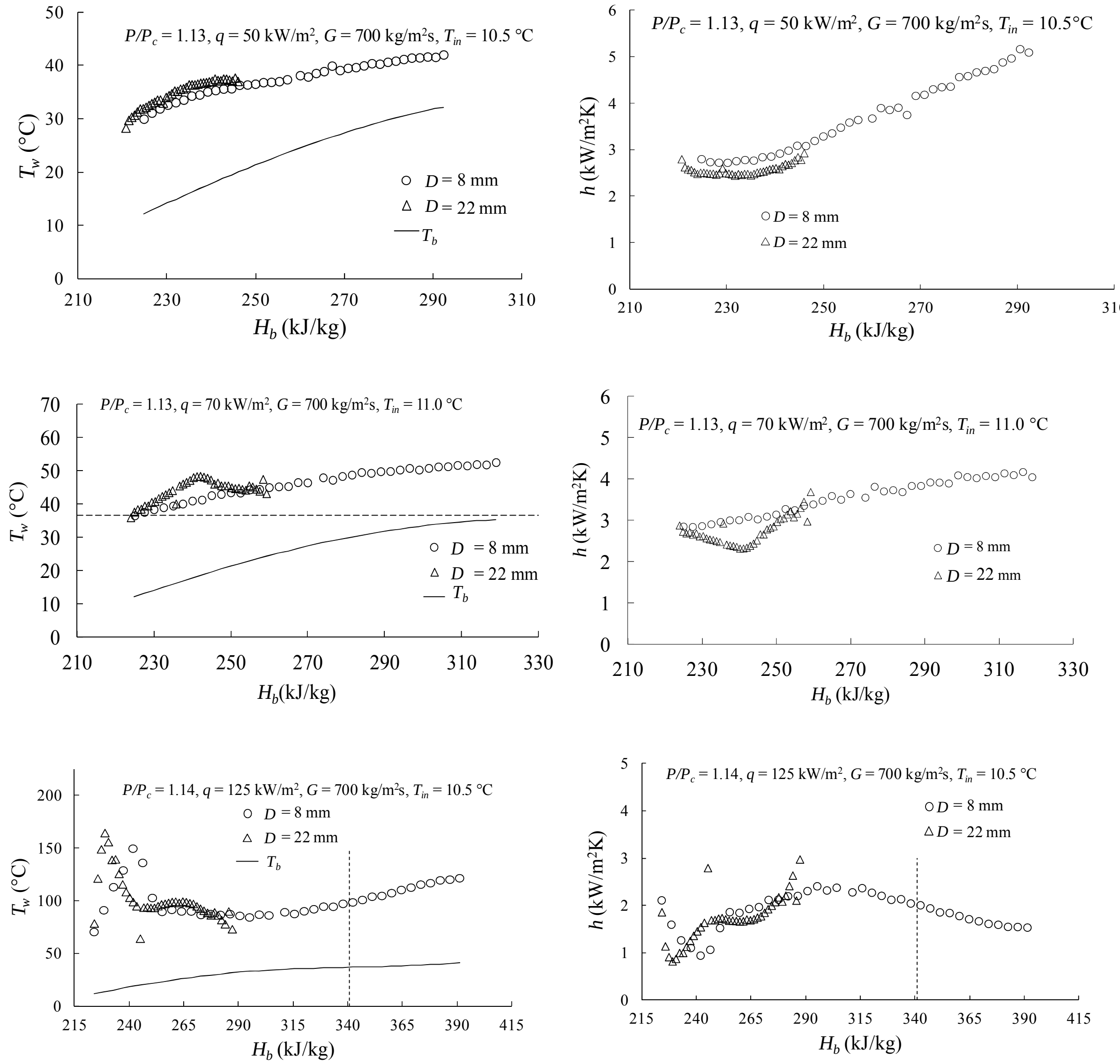

Figure 7: Tube diameter size effect on T_w and h at a supercritical pressure and different heat fluxes; dashed lines indicate T_{pc} or H_{pc}.

Inlet temperature effect: Figure 8 shows the variations of measured T_w and h *vs*. H_b for three different inlet temperatures in the normal heat transfer regime. The effect of varying inlet temperature from 10.6˚C to 12.4˚C on the profiles of both properties was small. This is compatible with the expectation that the local HTC would depend primarily on the local bulk enthalpy.

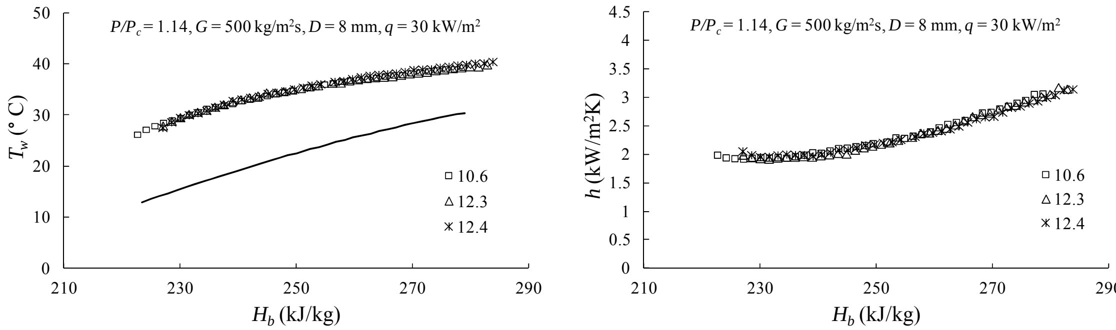

Figure 8: Inlet temperature effect on T_w and h for relatively low heat fluxes; the numbers in the legend indicate inlet temperature in ˚C.

Pressure effect: Figure 9 shows variations of T_w and h measured in both the 8 and 22 mm tubes for three different SC pressures. These results show that, for the same test conditions other than loop pressure, the differences between heat transfer profiles were small.

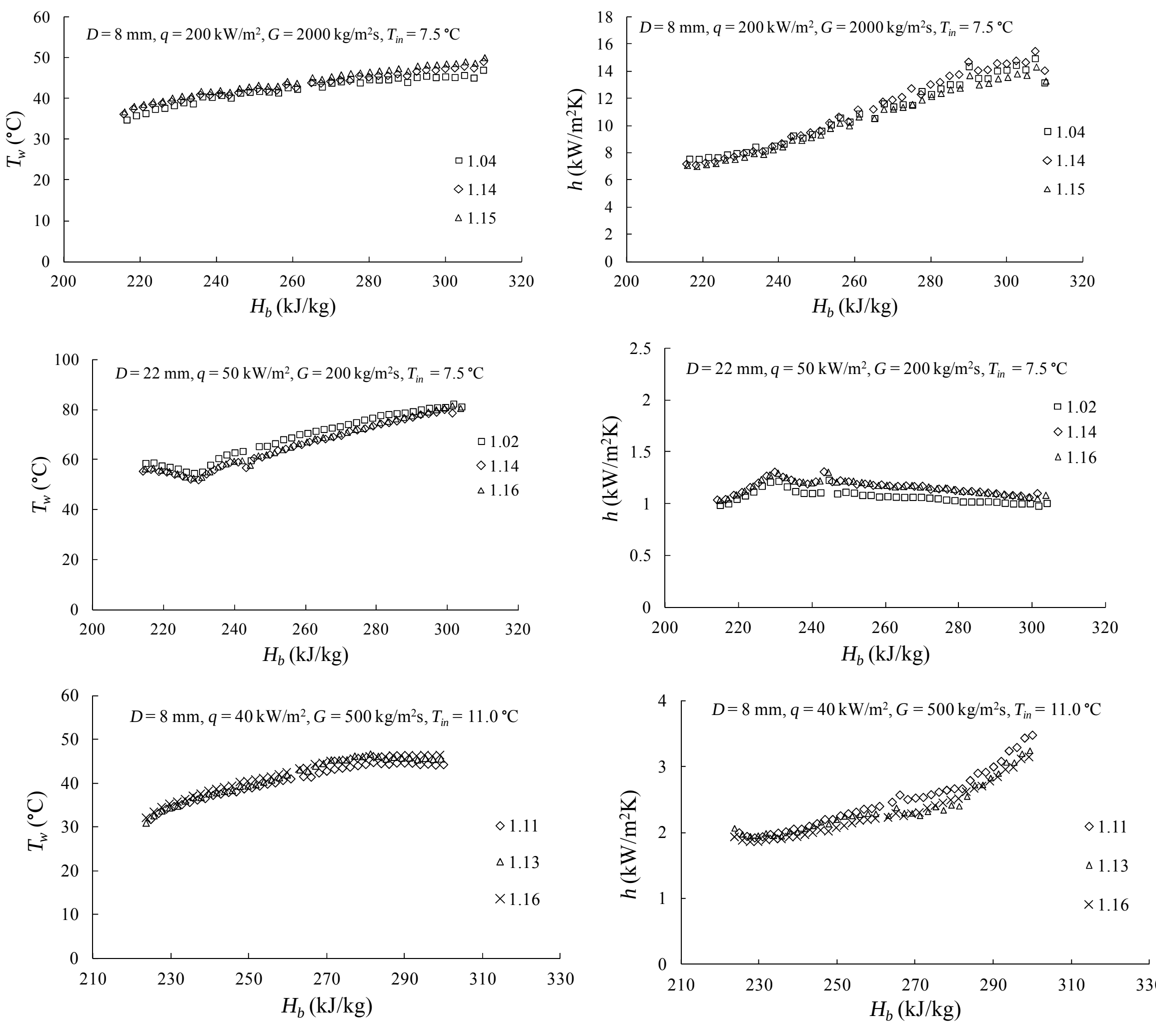

Figure 9: Variations of T_w and h *vs*. H_b in the 8 and 22 mm tubes for three different pressures; numbers in the legends indicate reduced pressures.

Mass flux effect: Figure 10 shows plots of T_w and h *vs.* H_b along the 8 and 22 mm tubes for a fixed heat flux in each tube and different mass fluxes. T_w tended to decrease and HTC tended to increase with increasing mass flux, as long as the heat transfer remained in the normal mode. This trend is in agreement with expectations based on physical arguments and with predictions of heat transfer correlations (e.g., Jackson, 2009). In such cases, T_w increased gradually along the heated tube. However, in the case with G = 701 kg/m^{2}s and q = 125 kW/m^2 for the 8 mm tube, the T_w profile showed a strong peak at z_h/D = 31, which corresponds to a minimum in the HTC profile and is evidence of HTD. The available data for the 22 mm tube and the same heat flux do not show HTD, but this cannot lead to any conclusion, because these data were obtained for a much smaller heat flux (q = 40 kW/m^2). The available measurements for the lowest mass fluxes tested in each of the tubes (G = 496 kg/m^{2}s for the 8 mm tube and G = 201 kg/m^{2}s for the 22 mm tube) showed a mild peak in T_w just downstream from the inlet of the heated test section, which resulted in a very small variation of the local HTC.

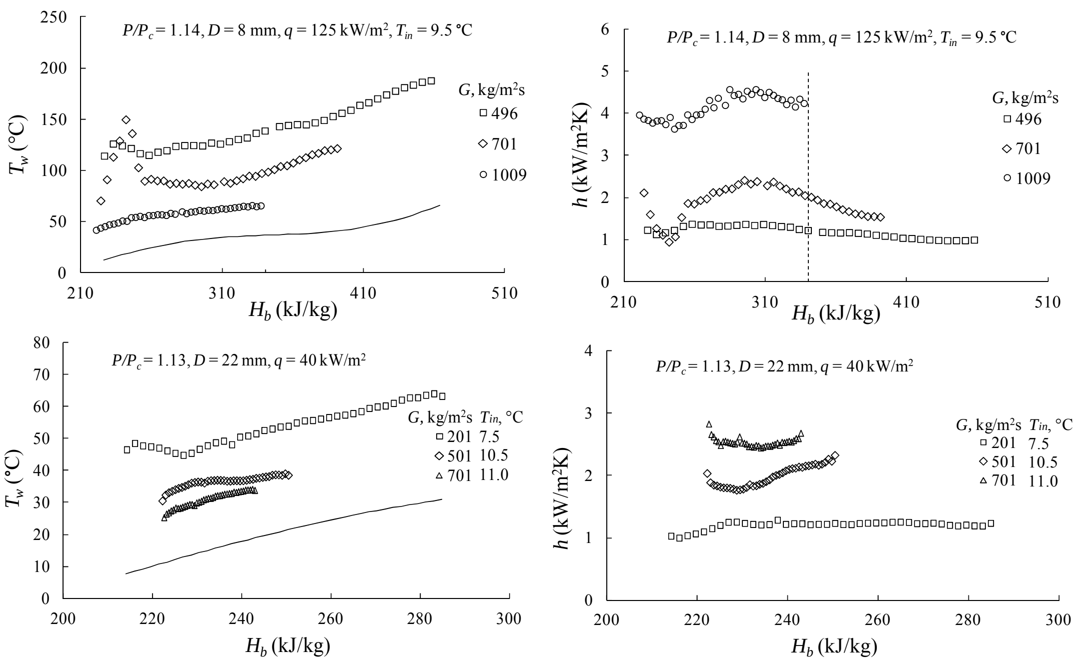

Figure 10: Variations of T_w and h *vs.* H_b in the 8 and 22 mm tubes for different mass fluxes.

Heat flux effect and the onset of heat transfer deterioration: Figure 11 shows two representative sets of measurements for the 8 and 22 mm tubes at pressures that were comparable to the design operating pressure of the Canadian SCWR. In each of the sets, all cases had the same pressure, mass flux, and inlet temperature but different heat fluxes. The cases with sufficiently low heat fluxes had wall temperature profiles with gradually and monotonically increasing shapes; in such cases, heat transfer was classified as normal. In contrast, at higher heat fluxes, local peaks appeared in these profiles; we classified the heat transfer in such cases as deteriorated. Jackson's studies (e.g., 2011) on onset of heat transfer deterioration criteria provided physical insight and identified key non-dimensional parameters characterizing this heat transfer phenomenon; it is noted, however, that these criteria include numerical coefficients, whose values have not yet been determined conclusively. Two important issues for SCHT predictions which need further investigation are the identification of flows with deteriorated heat transfer and the determination of flow conditions at the onset of HTD. The literature contains many different approaches for the identification of HTD and some authors even discuss HTD without ever describing the criterion by which they distinguished it from normal heat transfer. In most cases, HTD was assumed to occur when the measured HTC deviated in some way from a heat transfer correlation that was based on normal heat transfer measurements. Such approaches, however, are indirect and, besides having little, if any at all, physical significance, they often lead to inconsistent conclusions. Similarly, the onset of HTD has been described by different types of empirical correlations, which are necessarily specific to particular sets of experiments and do not seem to be of general validity. We have already presented some preliminary thoughts on the onset of HTD in an earlier paper (Zahlan et al., 2013) and we intend to examine it in detail in a future study. In the present article, we will restrict our presentation to a few cases with HTD onset that was detected directly by inspection of the wall temperature profile. To enable this, we performed several series of tests in which the pressure, mass flux and inlet temperature were kept constant and the wall heat flux was adjusted by small increments. The conditions at the onset of HTD were identified as those for the case with the highest heat flux for which the wall temperature profile showed no tendency to have one or more peaks. From Figure 11, one may identify two specific sets of conditions for the onset of HTD. These conditions are listed in Table 3, together with five additional sets of conditions at HTD onset at pressures comparable to those in the operating SCWR. Two pairs of sets had comparable conditions and were included as tests of reproducibility.

Table 3: Sets of conditions corresponding to the onset of heat transfer deterioration

P/P_c	D mm	z_h/D -	G kg/s m^2	q kW/ m^2	T_{in} ºC	T_w ºC	H_b kJ/kg	h kW/m^2 K
1.17	8	82	510	50	12.5	56	258	1.6
1.12	8	88	506	50	11.0	53	256	1.7
1.13	8	75	700	85	11.0	57.5	255	2.5
1.13	8	69	700	90	8.5	63.6	252	2.2
1.16	8	154	975	225	9.5	159	360	1.9
1.16	22	28	500	48	11.5	75	236	0.84
1.13	22	46	703	70	11.5	48.5	242	2.3

In the remainder of this section, we will present three more examples showing the diversity of heat flux increase effects on heat transfer. Figure 12 shows two sets of plots of T_w and h *vs.* H_b with different heat fluxes in the 8 mm tube. The first set of data was obtained at the slightly supercritical pressure of P/P_c = 1.05 and the relatively low mass flux of 500 kg/m^{2}s. In this set, which includes three cases with relatively small differences in heat flux, all wall temperature profiles had two peaks, one fairly close to the heated section inlet (z_h/D < 20) and another further downstream ($z_h/D \approx 55$). The second set of data in Figure 12 was obtained at the nominal SCWR pressure of P/P_c = 1.15 and the high mass flux of 2000 kg/m^{2}s. These data, obtained for six different heat fluxes show no clear evidence of HTD, as the T_w profiles generally increased monotonically; nevertheless, the trend of these profiles indicates that HTD might have occurred if q were increased above the highest tested value of 436 kW/m^2, a condition that was not possible in our loop because the wall temperature would have exceeded the desired maximum level of about 200ºC. The HTC profile shows visible heat transfer enhancement at some intermediate position in the test section, upstream of the position where HTD was likely to have occurred at higher q; this enhancement became more intense and moved upstream with increasing q.

Figure 13 shows the variations of T_w and h in the 22 mm tube at the near-critical pressure of P/P_c = 1.03 and a mass flux of 200 kg/m^{2}s, which was the case with the lowest mass flux examined in the present experiments. All T_w profiles showed a peak close to the inlet of the tube heated section, which moved upstream and became less sharp as q was increased. This is evidence of heat transfer deterioration, but it is unusual because it occurred even for very low heat flux values, for which both the wall and the bulk temperatures were lower than the pseudocritical temperature. This phenomenon seems to be caused by buoyancy effects in the thermal entry region of the test section.

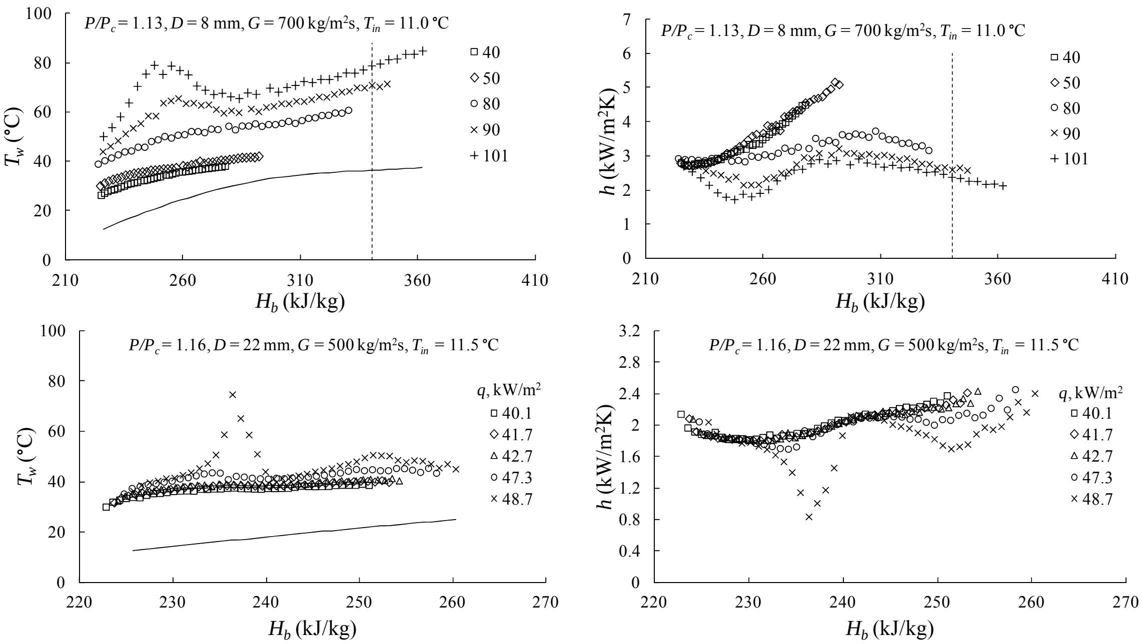

Figure 11: Variations of T_w and h *vs*. H_b at different heat fluxes for the 8 and 22 mm tubes; solid lines indicate the bulk temperature and dash lines indicate the pseudocritical specific enthalpy.

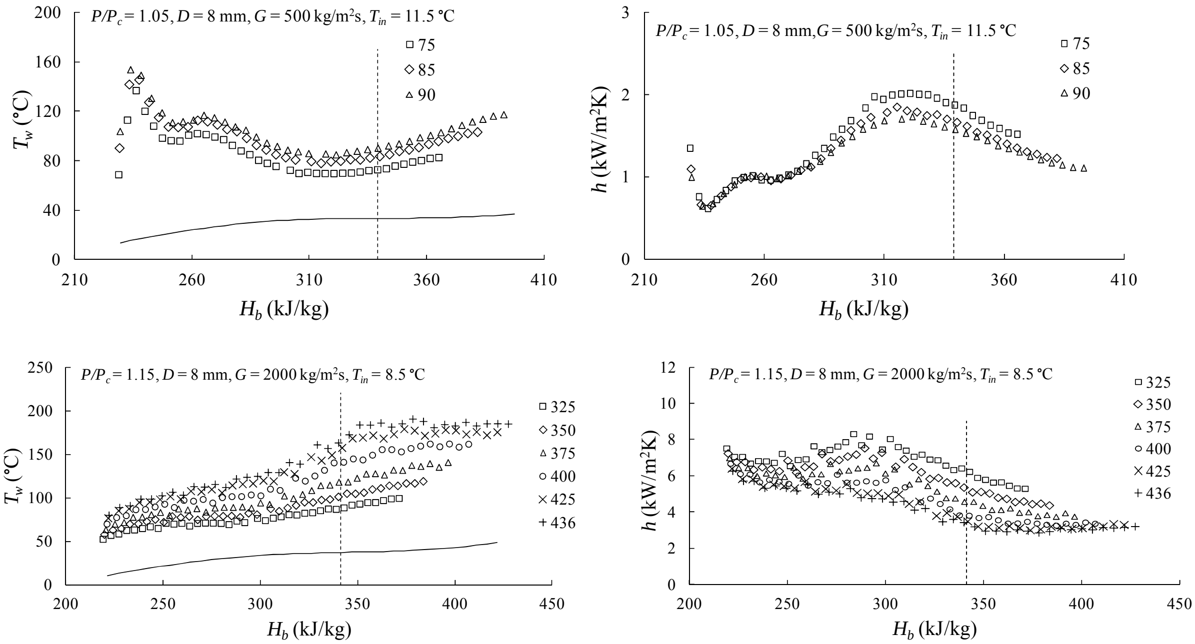

Figure 12: Wall temperature and HTC variations *vs.* bulk fluid enthalpy in the 8 mm tube at different heat fluxes (in kW/m^2, specified by the symbols in the legend). Solid lines indicate the bulk temperature and dashed lines indicate the pseudo-critical specific enthalpy.

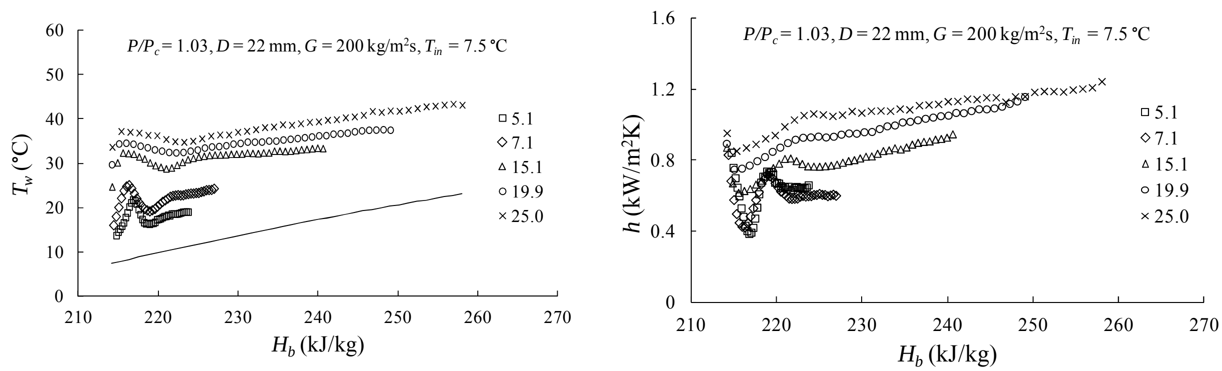

Figure 13: Variations of wall temperature and HTC *vs.* bulk fluid enthalpy in the 22 mm tube for different heat fluxes, specified (in kW/m^2) by the symbols in the legend. The solid line indicates bulk fluid temperature.

4.4 Heat transfer measurements in the high subcritical pressure region

Tube diameter size effect: Figure 14 compares the pre-CHF (LHS plots) and post-CHF (RHS plots) trends of the measured wall temperature and the corresponding HTC in the 8 and 22 mm tubes, obtained at comparable flow conditions. In the subcooled forced convective heat transfer regime, the trends were similar to those observed for SCHT (Figure 7); as predicted by single-phase heat transfer correlations, the HTC in the 8 mm tube was slightly higher than the HTC in the 22 mm tube. In the pre-CHF nucleate boiling regime (note that this HTC plot has semi-logarithmic axes), the impact of the diameter was negligible, as expected, and the CHF occurred at approximately the same local conditions. Because of the lack of post-CHF data in the 22 mm tube, it was not possible to determine the diameter effect on post-CHF temperatures.

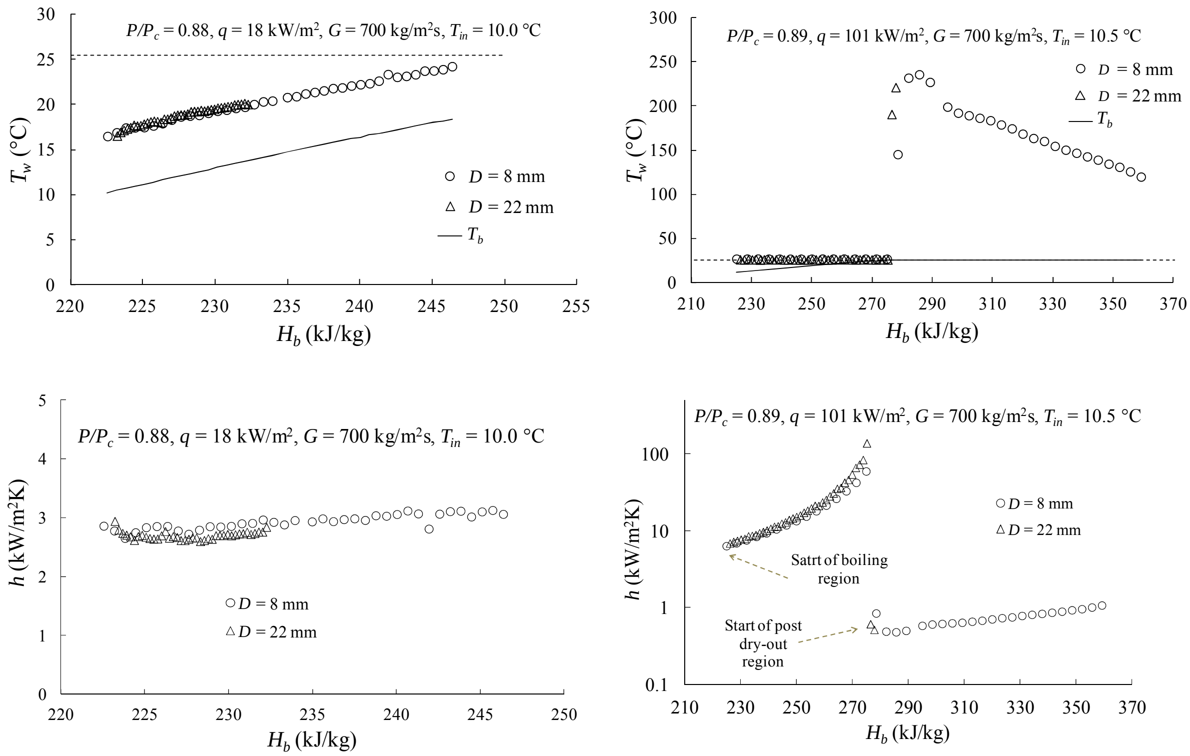

Figure 14: Variations of wall temperature and HTC *vs.* bulk fluid enthalpy in the single-phase liquid (left) and boiling (right) regimes; the dashed line indicates the saturation temperature.

Pressure effect: Figure 15 shows some representative plots of the pressure effect on heat transfer in the two test sections in the high subcritical pressure region. In the RHS plots, which correspond to a flow in the 8 mm tube with the relatively large mass flux of 1000 kg/m^{2}s, the fluid appears to be entirely subcooled liquid and heat transfer is normal and essentially independent of pressure within the considered range. The LHS plots, obtained in a 22 mm tube show almost self similar profile with a downstream shift due to the increase in inlet fluid temperature (Fewster and Jackson, 2004). This indicates small effect of pressure for these flow conditions. However, these plots show distinct peaks in the T_w profiles even though the heat flux is very low and the coolant is subcooled. This deterioration in single-phase heat transfer at low heat fluxes occurred only at low mass velocities (Re ≈ 50,000), suggesting that this phenomenon may be caused by mixed convection/buoyancy effects. When the HTC is plotted *vs.* heated length as shown in the last plot, the minima in HTC (or peaks in temperatures) occurred at the same location along the test section and the curves for different pressures appear to collapse on each other. This phenomenon is very similar to the behaviour described earlier at the end of the Section 4.3 (Figure 13), except the location of the peak is different in the two cases. In the present case temperature peak occurred at z_h/D = 32, compared to the peak location noted in the SC pressure case at z_h/D = 12. This topic will be discussed further later.

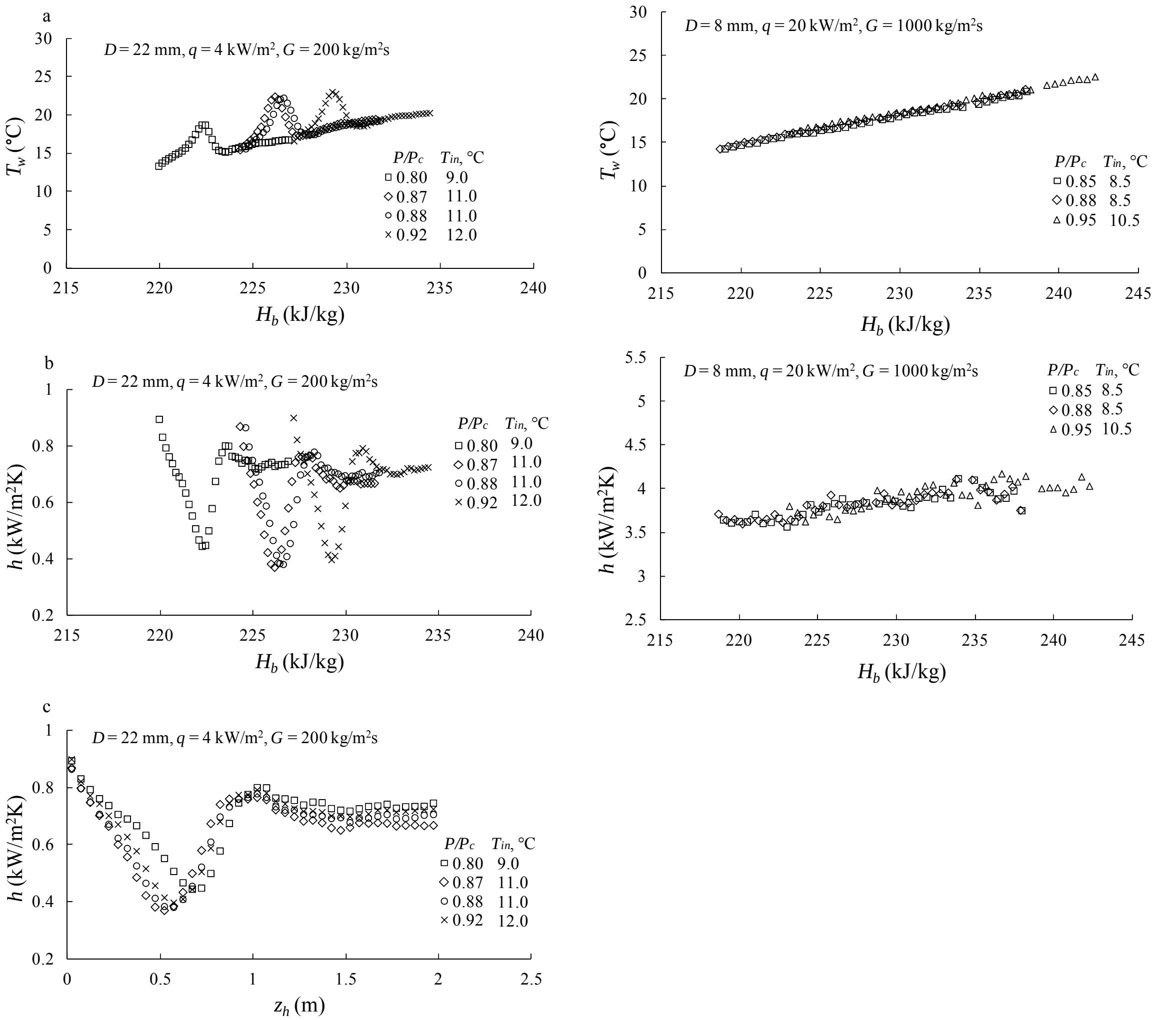

Figure 15: Pressure effect on the variations of the wall temperature and the HTC at high subcritical pressures.

Mass flux effect: Figure 16 shows two pairs of plots for different mass fluxes in the two test sections at high subcritical pressures. It is known that surface tension and bubble size decrease with subcritical pressure increase and vanish when $P/P_c = 1$. We would also expect that, under the conditions of these two groups of tests, bubbles in the 8 mm tube would be smaller than those in the 22 mm tube. In both cases, when the mass flux was sufficiently large, T_w remained lower than the saturation temperature and the fluid remained subcooled liquid in the entire test section. However, at lower mass fluxes, the wall temperature exceeded the saturation temperature at some location along the test section and subcooled nucleate boiling occurred near the wall. Had the HTC been calculated with respect to the saturation temperature (namely, as $h = \frac{q}{T_w - T_{sat}}$), as it is commonly done for this heat transfer mode (Collier and Thom, 1994), it would have been much larger than the range of values shown in these plots.

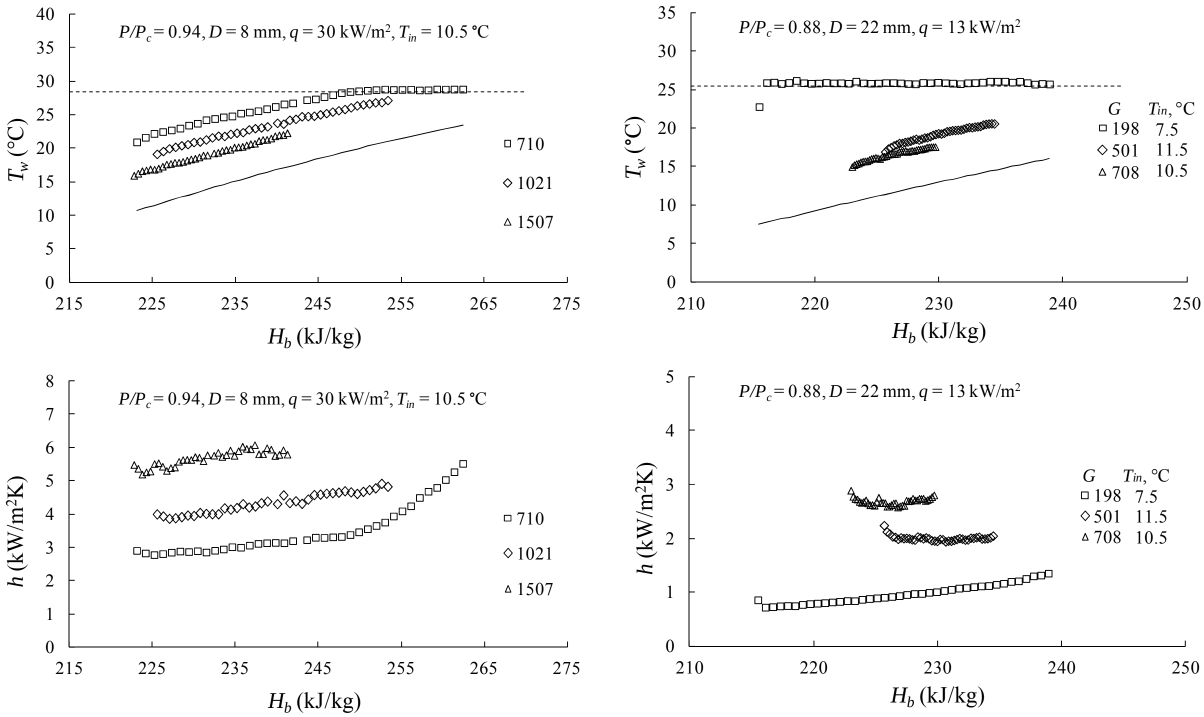

Figure 16: Variations of T_w and h *vs*. H_b in the two test sections for different mass fluxes at high subcritical pressures; dashed lines indicate the saturation temperature.

Heat flux effect: In the present experiments, we were able to generate flows spanning the entire range of heat transfer modes at the downstream end of the test section. We started with liquid CO_2 in the entire test section and gradually increased the heat flux while keeping all other conditions fixed, we observed the heat transfer mode undergo the following changes along the test section: starting with single-phase heat transfer to liquid CO_2 for sufficiently low q, it switched to nucleate boiling, then to boiling crisis and dryout at the critical heat flux, followed by film boiling and eventually by single phase heat transfer to superheated CO_2 vapour.

Figure 17 demonstrates clearly the changes in wall temperature variation that occurred along the 22 mm test section as the heat flux increased from a very low value to the highest permissible one. To enable the entire range of phenomena, the mass flux was set at a very low value. For q = 2.9 kW/m^2, T_w increased monotonically, indicating that heat transfer to liquid CO_2 was normal. For 4.0 kW/m^2 $\leq q \leq$ 9.0 kW/m^2, T_w developed a peak, followed by a minimum and then a monotonically increasing part to the test section exit, while never reaching the saturation value (similar behaviour to the one described earlier and for the same test section, Figure 15). Following a slight further increase in q, the near-peak T_w values, as well as those in the far downstream part of the test section, nearly matched the saturation temperature, while elsewhere T_w remained lower than T_{sat}. In all these cases, heat transfer appears to have deteriorated in parts of the test section, presumably as a result of buoyancy effects. For q = 15.8 kW/m^2, essentially the entire heated test section was at the saturation temperature, which indicates that nucleate boiling was present throughout. For 41.8 kW/m^2 $\leq q \leq$ 79.8 kW/m^2, nucleate boiling occurred essentially at the inlet of the heated test section and the flow reached CHF at some downstream location, beyond which film boiling occurred; with increasing q, the CHF location moved upstream and the maximum post dryout temperature increased. The occurrence of CHF is described more clearly in Figure 18, which shows three representative sets of wall temperature and HTC for the 8 mm test section at a higher mass flux. It can be seen that the HTC increased to very large values while nucleate boiling was maintained and then dropped to a low value while film boiling occurred. Such boiling and boiling related phenomena look qualitatively similar to those observed at low subcritical pressures.

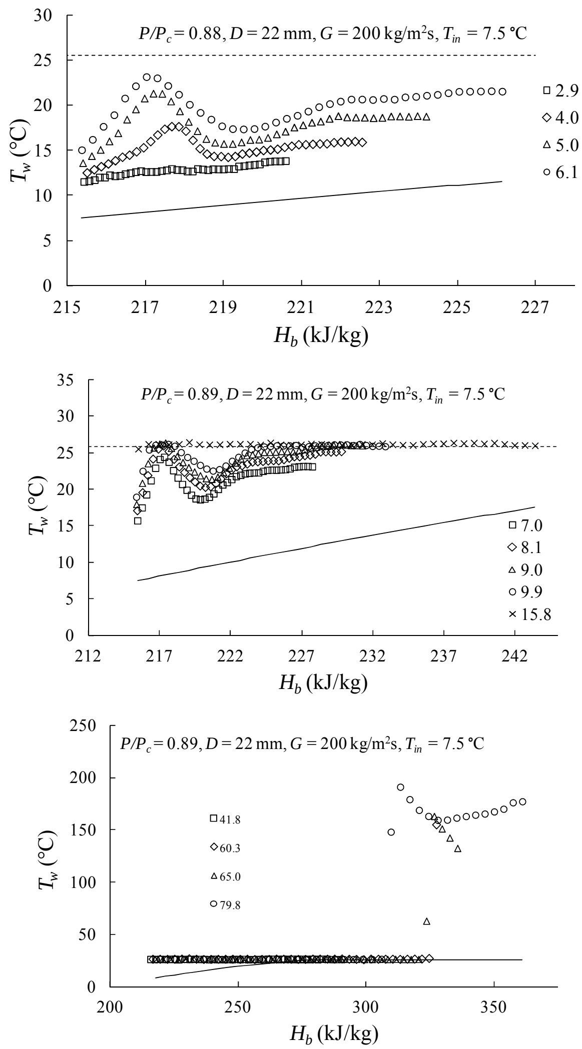

Figure 17: Variations of T_w *vs.* H_b for different heat fluxes at a high subcritical pressure, showing both normal and deteriorated single phase heat transfer, nucleate boiling, CHF and film boiling heat transfer in the 22 mm tube; the dashed line indicates the saturation temperature and the solid line indicates the bulk fluid temperature; numbers in the legend indicate heat flux in kW/m^2.

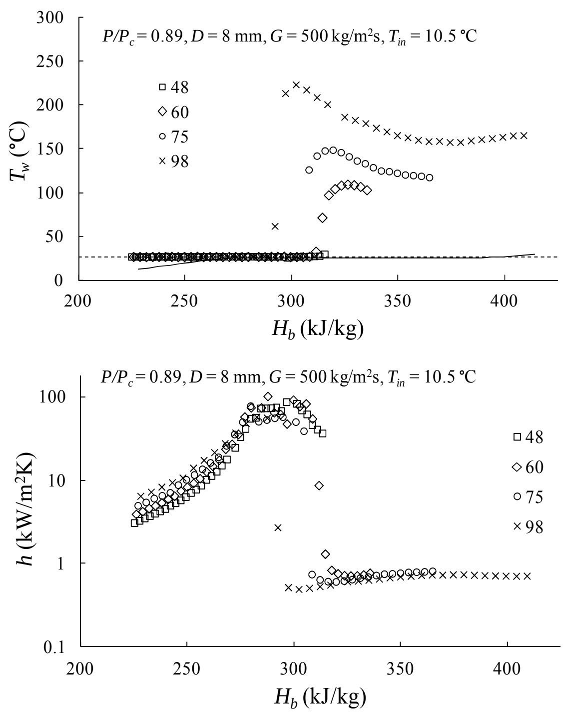

Figure 18: Variations of T_w and h *vs.* H_b for different heat fluxes at a high subcritical pressure, showing nucleate boiling, CHF and film boiling heat transfer in the 8 mm tube; numbers in the legend indicate heat flux in kW/m^2; the dashed line indicates the saturation temperature and the solid line indicates the bulk fluid temperature; note that the HTC axis has a logarithmic scale.

Two additional interesting sets of results are shown in Figure 19. The plots on the LHS, which correspond to a high mass flux, show the suppression of deterioration in the liquid regime until the heat flux increased sufficiently to induce nucleate boiling and, eventually, CHF. The plots on the RHS show that, for a low mass flux and high heat fluxes, the entire test section experienced film boiling and the wall temperature had a very small peak near the inlet of the heated section. Both sets of plot show that the HTC for nucleate boiling was up to two orders of magnitude larger than that for film boiling.

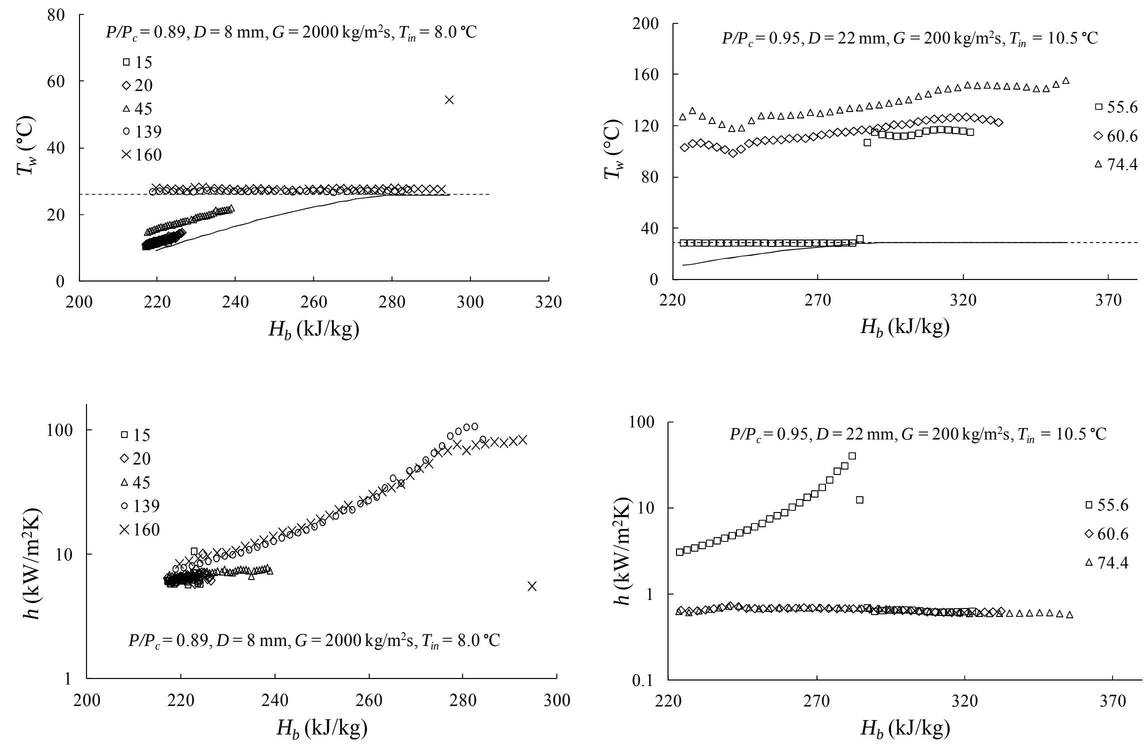

Figure 19: Variations of T_w and h *vs.* H_b in the 8 and 22 mm tubes at high subcritical pressures for different heat fluxes; numbers in the legend indicate heat flux in kW/m^2; the dashed line indicates the saturation temperature and the solid line indicates the bulk fluid temperature; note that the HTC axes have logarithmic scales.

4.5 Pressure drop measurements

Figure 20 shows the variation of the normalised friction factor f * *vs.* Reynolds number evaluated at inlet conditions in the 8 mm tube. The LHS plot includes all high subcritical and supercritical data in different heat transfer modes, while the RHS plot includes only data in tests with normal heat transfer (Zahlan, 2014a). A general observation from these plots is that the friction factor in most of the present tests exceeded the corresponding one for incompressible flow, which was based on measurements at low subcritical pressures. A second observation is that the friction factor ratio decreases with increasing Re and seems to have a trend towards unity as Re → ∞. Power laws fitted to both sets of data were not very different from each other, but it is evident that the normal heat transfer measurements had a much lower scatter. Some scatter was anticipated, because the plotted values correspond to cases with different heat transfer modes, different pressures and a wide range of heat fluxes. In addition, at low mass fluxes frictional losses were small compared to losses due to gravity and acceleration, which increased the uncertainty in the calculated friction factor for the data in the low range of Re. One is also reminded that the measured friction factor was an overall value for the entire heated test section and therefore masks local variations corresponding to changes in heat transfer mode in the flow direction. A more detailed study of pressure losses under high subcritical and supercritical pressures would require pressure measurement along the test section, which was not possible in the present facility. To assist future work, we have summarised the conditions of the present measurements in Table 4.

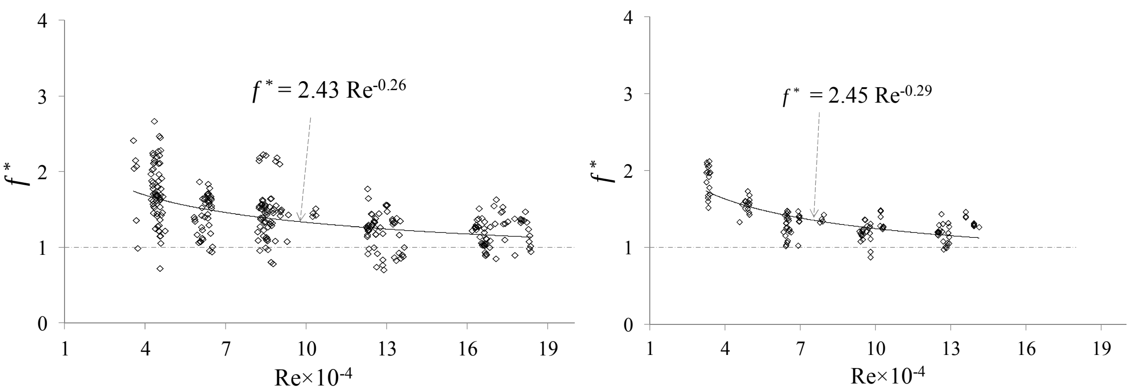

Figure 20: Variation of the normalised friction factor with Reynolds number; LHS plot shows all data while RHS plot shows only normal heat transfer data.

Table 4: Pressure drop database for the 8 mm tube

P/Pc	T_{in} °C	*q* kW/m²	*G* kg/m²s	Re_{in}	*f**	*P/Pc*	T_{in} °C	*q* kW/m²	*G* kg/m²s	Re_{in}	*f**
0.81	8.8	49.3	2010	179974	1.33	1.09	7.6	74.5	1501	124187	1.28
0.83	9.2	159.7	1901	170811	1.63		9.3	40.2	493	42092	1.97
0.84	9.2	169.3	1897	169958	1.55		7.6	125.0	1002	82966	1.39
0.85	8.5	20.3	1009	89057	2.19		7.3	250.1	2001	164710	1.14
	9.3	10.9	1006	90098	2.10	1.10	10.1	44.8	414	35806	2.05
0.88	10.0	10.0	701	63308	1.69		9.0	49.9	500	42381	1.88
	8.5	20.7	1012	88714	1.56		7.1	125.2	2001	164017	1.28
	10.0	13.9	703	63434	1.84		9.0	50.1	1210	102360	1.41
	11.0	15.0	698	64379	1.68		12.3	19.8	503	45267	2.22
	11.1	13.7	694	63973	1.79		13.4	29.9	405	37178	0.99
	10.8	39.9	709	65019	1.01		9.9	75.1	1005	86467	1.31
	10.3	92.2	494	44825	2.28	1.11	8.9	39.8	1004	84810	1.34
	10.6	30.2	692	63270	1.71		10.2	75.1	1007	87068	1.29
	10.0	17.9	707	63714	1.60		10.2	49.6	412	35568	2.41
	8.5	31.0	1010	88430	1.09		7.8	100.1	1504	124454	1.44
0.89	11.0	24.2	703	64606	1.52		7.9	274.9	1994	165283	1.06
	10.3	75.1	498	45200	2.47		7.2	125.5	2006	164421	1.52
	8.6	41.1	1010	88544	2.14		11.1	39.7	497	43671	1.71
	10.3	59.9	710	64303	1.19		9.4	99.6	1000	85106	1.14
	11.1	18.1	700	64440	1.65		9.0	50.2	500	42219	1.63
	7.6	9.7	1513	130126	1.48		9.0	20.3	1002	84605	1.57
	9.7	79.8	693	62117	1.64		8.7	49.8	993	83412	1.56
	10.3	97.9	495	44931	1.88		12.3	24.7	506	45385	2.12
	8.1	139.4	2006	174010	1.10		9.0	50.2	1009	85282	1.50
	8.0	19.6	1997	173017	1.48	1.12	7.4	250.6	1502	123366	0.98
	9.7	85.3	698	62443	1.58		8.9	29.8	1003	84547	1.53
	9.7	100.9	707	63306	1.39		9.6	20.0	501	42760	2.25
	9.7	96.2	707	63235	1.44		10.4	79.8	704	60989	1.42
	8.0	45.3	1992	172592	1.46		7.7	150.4	995	82037	1.09
	7.6	19.9	1516	130203	1.56		8.8	60.0	509	42840	1.62
	7.5	37.0	1513	129821	1.55		8.9	40.0	1014	85316	1.47
	11.1	22.7	703	64631	1.55		10.8	50.0	508	44224	1.62
	7.5	30.4	1512	129738	1.57		7.9	100.2	1502	124246	1.45
	8.3	160.4	2012	175111	1.34		7.8	99.8	1508	124630	1.30
	10.3	74.6	503	45548	2.45		11.6	39.5	704	62198	1.66
	8.0	14.9	2001	173258	1.54	1.13	11.1	69.9	712	62164	1.40
	8.9	102.0	1001	87994	1.51		11.2	80.0	695	60945	1.27
0.90	7.7	169.4	1464	125910	1.18		8.6	75.2	999	83615	1.54
	8.9	113.0	993	87324	1.32		11.1	90.0	700	61283	1.23

P/Pc	T_{in} ˚C	*q* kW/m^2	*G* kg/m^{2}s	Re in	*f**	*P/Pc*	T_{in} ˚C	*q* kW/m^2	*G* kg/m^{2}s	Re in	*f**
0.91	8.1	131.1	2004	173430	1.31	1.13	7.9	299.9	2001	165640	1.03
	8.3	180.2	2005	174114	1.32		7.2	149.9	2001	163322	1.30
	8.4	220.4	1937	168555	1.27		11.1	60.0	687	60166	1.87
	8.9	122.2	998	87650	0.78		8.9	74.8	1001	84276	1.33
	7.6	120.5	1484	127091	1.45		8.8	49.9	995	83687	1.40
	8.5	225.2	2041	177756	0.90		11.1	101.2	700	61208	1.12
	8.4	201.1	1962	170352	1.31		7.5	274.8	1499	122943	0.92
0.92	9.0	81.5	999	87701	1.46		7.8	225.3	1000	82468	1.55
0.93	9.1	94.9	990	86736	1.34		10.7	40.1	499	43359	2.15
	9.8	20.9	1505	133674	1.39		11.3	50.2	699	61345	1.65
0.94	10.6	60.4	1995	179832	1.38		9.0	74.7	1005	84616	1.34
	11.0	109.4	1992	181104	1.36		9.1	124.9	1009	85142	1.10
	11.3	30.2	1021	93315	1.43		12.3	29.9	504	45062	1.97
	9.7	70.2	1497	132472	1.33		7.5	325.0	1498	122866	1.78
	11.0	150.9	2013	182836	1.24		8.5	89.0	697	58179	1.40
	10.5	15.9	1005	90375	1.47		11.0	110.2	704	61426	1.11
	10.6	50.6	1971	177666	1.38		7.5	350.8	1500	123130	1.65
	10.0	135.6	1511	134531	0.93		8.6	90.1	699	58411	1.37
	10.2	19.8	706	63185	1.70		11.1	69.9	699	61080	1.53
	10.3	29.6	1507	135016	1.35	1.14	12.9	29.9	406	36679	2.07
	10.7	70.0	1998	180238	1.37		8.8	90.6	697	58514	1.35
	10.9	79.1	1991	180167	1.35		7.8	175.1	1002	82654	0.96
	9.4	40.3	1501	132111	1.35		7.5	125.4	1520	124618	1.31
0.95	10.5	28.5	1010	90774	1.50		9.3	125.1	1007	85106	1.14
	9.5	52.0	1500	132311	1.31		10.1	125.2	496	42554	2.03
	10.5	20.4	1007	90458	1.49		9.1	100.9	704	59291	1.17
	10.3	14.9	707	63268	1.61		10.3	24.8	500	43037	2.11
	10.3	29.7	710	63502	1.72		7.7	199.7	994	81862	1.21
	10.6	40.1	1004	90286	1.42		7.2	175.1	2007	163647	1.37
	11.1	140.3	1998	181660	1.47		7.5	149.6	2002	164139	1.38
	9.6	50.1	1507	132983	1.33		9.3	125.6	1010	85478	1.09
	11.6	179.5	2003	183731	0.95		10.2	40.2	497	42725	1.82
	10.4	53.6	508	45460	0.72		12.6	20.1	509	45721	2.29
	10.4	51.0	722	64568	1.63		12.4	30.0	406	36344	2.15
	9.8	99.9	1493	132118	1.38		9.9	124.7	701	59893	1.07
	10.5	57.4	724	64836	0.94		8.6	225.0	1002	83658	1.63
	10.5	80.0	713	63933	0.96		7.4	174.9	1500	122726	1.14
0.96	10.2	150.6	1497	133510	0.83		10.5	130.0	701	60550	1.08
	11.4	84.0	1018	92846	1.08		8.0	250.3	998	82406	1.52
	10.3	114.3	1509	134656	1.17		10.7	124.9	698	60512	1.08
	11.6	169.6	2002	183192	0.99		7.4	150.5	1499	122665	1.25

P/P_c	T_{in} °C	q kW/m^2	G kg/m^{2}s	Re_{in}	f^*	P/P_c	T_{in} °C	q kW/m^2	G kg/m^{2}s	Re_{in}	f^*
0.96	11.6	219.7	1997	183054	1.08	1.14	12.4	39.5	508	45359	1.63
	11.7	200.3	2002	183608	1.02		12.3	50.1	514	45899	1.43
	10.6	160.3	1481	132842	0.87		8.8	229.8	995	83406	1.58
	11.2	170.3	1499	136096	0.88		10.6	29.9	503	43460	2.12
	10.8	60.4	708	63715	1.30		8.2	349.9	2008	166400	1.02
	10.4	58.9	712	63643	1.62		7.3	200.5	1999	163022	1.27
0.97	10.7	145.7	1507	135244	0.86		8.0	271.9	1004	82984	1.38
	10.5	100.6	712	63689	1.56		7.5	175.2	2006	164225	1.28
	11.5	279.9	1998	182203	1.33		12.6	29.9	514	46067	1.92
	11.6	239.7	2007	183301	1.16		7.5	300.2	1502	122858	1.26
	11.3	189.6	1503	136513	1.00	1.15	9.3	150.2	1013	85504	1.11
	11.2	164.3	1500	135771	0.90		8.9	99.8	1012	84825	1.00
1.01	10.6	19.6	507	44911	2.11		10.9	50.0	505	43906	1.69
1.02	7.1	99.9	2001	166459	1.34		8.3	100.6	997	82775	1.28
	8.5	74.8	1005	85675	1.27		8.0	324.8	2007	165789	1.06
	12.0	50.7	520	47358	1.22		8.7	99.8	1006	84090	1.23
	8.7	275.1	1509	128896	0.71		8.4	375.0	2005	166538	1.05
	8.6	249.9	1506	128513	0.84		9.3	175.1	1015	85703	0.97
	7.4	275.1	2002	167180	1.11		7.4	200.7	2000	163222	1.27
	7.1	149.8	2003	166349	1.20	1.15	7.4	225.0	1995	162914	1.27
1.03	7.7	20.3	1499	125788	1.39		8.5	400.0	2024	168376	1.00
	7.1	75.0	1996	165482	1.39		8.6	425.1	2000	166678	0.94
	7.5	324.8	2000	166962	0.92		10.4	50.2	508	43733	1.25
	7.2	180.1	2000	166302	1.25		10.4	60.1	504	43338	1.53
	10.0	19.6	492	42940	2.04		7.6	225.3	1500	122815	1.17
	12.1	33.9	402	36610	1.36		7.2	249.7	1989	161810	1.22
	10.5	29.7	503	44384	1.81		12.4	50.2	512	45603	1.63
	7.7	149.8	1495	125222	1.00		7.7	149.7	1503	123324	1.23
	8.4	50.4	1005	85242	1.44		9.5	249.8	1005	84959	2.22
	7.7	180.5	1509	126493	0.92		10.7	50.2	504	43592	1.73
	9.2	50.2	1203	103525	1.51	1.16	7.3	299.6	2003	162985	1.27
	7.7	199.6	1505	126173	0.74		12.5	40.2	513	45823	1.78
	7.6	124.5	1505	125896	1.17		12.4	30.0	496	44188	2.20
1.04	7.3	199.5	2008	166995	1.12		10.2	50.0	500	42799	1.86
	8.3	20.2	1000	84694	1.55		7.4	199.5	1508	123045	1.29
	7.3	225.4	2027	168521	1.09		7.8	175.1	1501	123234	1.30
	9.6	180.0	1001	86861	0.81		10.3	50.1	501	42963	1.71
	10.5	39.7	501	44162	1.69		8.7	436.4	2000	166796	0.89
	9.7	200.0	994	86319	1.54		9.8	70.0	506	43022	1.46
	8.8	325.2	1494	127554	1.27		7.8	125.1	1492	122498	1.28
	7.6	99.6	1506	125676	1.26		7.4	225.1	2003	163263	1.27

P/Pc	T_{in} °C	*q* kW/m^2	*G* kg/m^{2}s	Re $_{in}$	*f**	*P/Pc*	T_{in} °C	*q* kW/m^2	*G* kg/m^{2}s	Re $_{in}$	*f**
1.04	11.7	75.2	504	45431	1.37	1.16	7.2	275.4	2010	163334	1.24
	8.9	400.3	1999	170724	0.85		12.4	75.2	502	44632	1.28
	7.6	50.2	1501	125328	1.34		10.8	39.8	496	42889	2.22
	11.7	84.7	508	45743	1.06		9.4	225.0	977	82391	2.15
	8.9	349.9	1505	128529	1.19		9.4	199.7	994	83782	1.62
1.05	7.3	250.9	2012	166979	1.05		12.4	40.8	501	44594	1.80
	7.6	75.2	1504	125456	1.33		12.3	74.9	514	45653	1.15
	7.5	350.5	2008	167178	0.90	1.17	10.1	70.0	502	42874	1.57
	8.7	299.8	1509	128481	0.77		7.8	199.9	1502	123089	1.22
	9.2	50.0	1207	103585	1.43		12.2	99.8	507	44998	1.22
	9.8	225.6	998	86619	1.65		12.5	50.5	509	45301	1.66
	9.9	275.0	1007	87524	1.49		10.0	49.9	504	42882	1.78
	7.7	99.8	1007	84005	1.15		8.5	124.9	1003	83273	1.51
	7.4	300.1	2002	166344	1.04		10.4	60.2	502	43086	1.55
	9.8	249.9	1002	86949	1.65		13.7	55.8	502	45643	1.70
	11.7	90.3	506	45435	1.15		13.8	59.4	511	46546	1.67
1.06	12.1	100.3	500	45203	1.21		13.7	70.0	509	46358	1.46
	12.2	109.7	498	45135	1.29		9.5	274.3	978	82555	2.19
	12.2	120.4	499	45121	1.62		12.3	125.2	501	44389	1.45
	12.2	128.8	492	44557	1.69		13.8	70.0	499	45455	1.54
1.07	9.1	50.2	1202	102486	1.45		12.2	125.3	502	44434	1.41
1.08	8.1	75.2	1499	125265	1.35	1.18	9.6	274.8	994	83925	2.23
	8.8	20.2	1000	84624	1.46		7.8	199.8	1503	123048	1.24

5. CONCLUSIONS

This article presents and discusses a new database of CO_2 heat transfer measurements at high subcritical and supercritical pressures, obtained in 8 mm and 22 mm tubes; the corresponding pressure drop database for the 8 mm tube is reported as well.

The present measurements of wall temperature variations and CHF values in tubes cooled by CO_2 at high subcritical pressures are similar to previous results obtained in water at lower subcritical pressures. The present data can be used to improve fluid-to-fluid scaling methods at high subcritical pressures and, after transformation into water-equivalent data, to supplement the water database for conditions for which water data are not available.

The present supercritical heat transfer data are in good agreement with data from previous investigators obtained at similar experimental conditions, thus demonstrating the reproducibility of such measurements.

An examination of various parametric trends (pressure, mass flux, heat flux, inlet temperature and diameter) on the HTC and wall temperature *vs.* bulk enthalpy profiles has been made for conditions equivalent to those of interest to SCWR.

An interesting phenomenon was observed at high subcritical and SC pressures in the 22 mm tube in the single phase liquid and liquid-like regions. Peaks in wall temperature profile were observed near the start of the heated length at very low heat and mass fluxes, for which a monotonically increasing temperature profile was expected. A similar phenomenon was reported by Jackson et al. (1989) and was attributed to buoyancy effects. The observed temperature peaks at subcritical pressures were suppressed by the occurrence of nucleate boiling.

In general, the friction factor for convective flows at high subcritical and supercritical pressure exceeded that for incompressible flow at low subcritical pressures and seemed to approach the incompressible value with increasing Re.

ACKNOWLEDGEMENTS

This investigation is part of the Canadian Gen-IV National Program. Funding for this program was provided by Natural Resources Canada through the Office of Energy Research and Development, Atomic Energy of Canada Limited, and Natural Sciences and Engineering Research Council of Canada. We thank Kai Jiang for his assistance with the SCUOL experiments and Michael Coyle for his assistance in processing and plotting the CO_2 measurements.

REFERENCES

Bae, Y.Y., Kim, H.Y., Kang, D. J., 2010. Forced and mixed convection heat transfer to supercritical CO2 vertically flowing in a uniformly-heated circular tube, Exp. Therm. Fluid Sci., 34, 1295–1308.

Collier, J. G., Thome, J.R., 1994. Convective boiling and condensation, 3rd ed., Oxford Science Publications.

Fewster, J., Jackson, J.D., 2004. Experiments on supercritical pressure convective heat transfer having relevance to SPWR. Proc. ICAPP'04, Paper 4342, Pittsburgh, PA, USA, June 13−17.

Filonenko, G.K., 1954. Hydraulic resistance of pipelines, (In Russian). Thermal Engineering, 4, 40–44.

Incropera, F.P, DeWitt, D.P., Bergman, T.L., Lavine, A.S., 2007. Fundamentals of Heat and Mass Transfer, 6th ed., John Wiley and Sons.

Jackson, J.D., 2009. Validation of an extended heat transfer equation for fluids at supercritical pressure, Proc. 4th Int. Sym. Supercritical Water-Cooled Reactors (ISSCWR-4), Heidelberg, Germany, March 8-11.

Jackson, J.D., 2011. A Model of developing mixed convection heat transfer in vertical tubes to fluids at supercritical pressure. Proc. of the 5th Int. Sym. SCWR (ISSCWR-5), P104, Vancouver, British Columbia, Canada, March 13-16.

Jackson, J.D., 2013. Fluid flow and convective heat transfer to fluids at supercritical pressure. Nuc. Eng. Des., 264 , 24–40.

Jackson, J.D., Jiang, P.X., Liu, B., Zhao, C.R., 2011. Interpreting and categorizing experimental data on forced and mixed convection heat transfer to supercritical pressure fluids using physically-based models. Proc. 5th Int. Sym. Supercritical Water-Cooled Reactors (ISSCWR-5), Vancouver, British Columbia, Canada, March 13–16.

Jiang, K., Zahlan, H., Tavoularis, S., Groeneveld, D.C., 2012. Commissioning tests of the University of Ottawa Supercritical CO_2 Facility. Proc. of the 3rd Annual Conference of the Canadian Nuclear Society, Saskatoon, Saskatchewan, June 10 – 13.

Jiang, K, 2014. An experimental facility for studying heat transfer in supercritical fluids. MASc thesis, Ottawa-Carleton Institute for Mechanical and Aerospace Engineering, University of Ottawa, Canada.

Kim, J.K., Jeon, H.K., Yoo, J.Y. Lee, J. S., 2005. Experimental study on heat transfer characteristics of turbulent supercritical flow in vertical circular/non-circular tubes. NURETH-11, Avignon, France.

Lee, J, 2006. The flow structure under mixed convection in a uniformly heated vertical pipe. M.Sc. thesis, Department of Nuclear Science and Engineering, Massachusetts Institute of Technology.

Lemmon, E.W., McLinden, M.O., Friend, D.G., 2002. Thermophysical properties of fluid systems, NIST Standard Reference Database Number 69, REFPROP: Version 7.0.

Licht, J., Anderson, M., Corradini, M., 2008. Heat transfer to water at supercritical pressures in a circular and square annular flow geometry. Int. J. Heat Fluid Flow, 29, 156 –166.

Petukhov, B.S., Polyakov, A.F, 1988. Heat Transfer in Turbulent Mixed Convection (edited by B.E. Launder), Hemisphere Publishing Corporation.

Pioro, I. L., Duffey, R.B., 2007. Heat Transfer and Hydraulic Resistance at Supercritical Pressures in Power-Engineering Applications. ASME Press, New York.

Song, J.H., Kim, H.Y., Kim, H., Bae, Y.Y., 2008. Heat transfer characteristics of a supercritical fluid flow in a vertical pipe. J. Supercritical Fluids, 44, 164–171.

Zahlan, H., Groeneveld, D.C., Tavoularis, S., 2014a. Fluid-to-fluid scaling for convective heat transfer in tubes at supercritical and high subcritical pressures. Int. J. Heat Mass Tran.73, 274–283.

Zahlan, H., Tavoularis, S., Groeneveld, D.C., 2014b. A look-up table for trans-critical heat transfer in water-cooled tubes. Nuc. Eng. Des., submitted for publication.

Zahlan, H., Jiang, K., Tavoularis, S., Groeneveld, D.C., 2013. Measurements of heat transfer coefficient, CHF and heat transfer deterioration in flows of CO2 at near-critical and supercritical pressures. ISSCWR-6, March 03-07, Shenzhen, Guangdong, China.

CHAPTER 5

FLUID-TO-FLUID SCALING FOR CONVECTIVE HEAT TRANSFER IN TUBES AT SUPERCRITICAL AND HIGH SUBCRITICAL PRESSURES

This chapter describes the development of new fluid-to-fluid scaling laws of turbulent convective heat transfer at high subcritical and supercritical pressures and contains the manuscript entitled

Zahlan, H., Groeneveld, D.C., Tavoularis, S., 2014. Fluid-to-fluid scaling for convective heat transfer in tubes at supercritical and high subcritical pressures, as submitted in October 2013 to International Journal of Heat and Mass Transfer.
DOI: http://dx.doi.org/10.1016/j.ijheatmasstransfer.2014.02.018
0017-9310/© 2014 Elsevier Ltd. All rights reserved. **Int. J. Heat Mass Tran., 73 (2014), 274–283, 2014.**

This article reviews available scaling methods and their limitations and proposes two methods of scaling that introduce no bias and have better precision uncertainties than those of the previous scaling methods.

Fluid-to-fluid scaling for convective heat transfer in tubes at supercritical and high subcritical pressures

H. Zahlan[a], D.C. Groeneveld[a], S. Tavoularis[a,*]

[a]*Department of Mechanical Engineering, University of Ottawa, Ottawa, ON K1N 6N5, Canada*

Highlights

- We have evaluated two sets of scaling laws for water-to-carbon dioxide modelling of convective heat transfer at supercritical and high subcritical pressures.
- We have proposed modified scaling laws for normal heat transfer in tubes.
- We have demonstrated that the proposed scaling laws have a good accuracy.

ABSTRACT

Following a review of two recent sets of fluid-to-fluid scaling laws for supercritical heat transfer and a discussion of their possible limitations, we have proposed two additional sets of scaling laws, which take into account empirically adjustable versions of the Dittus-Boelter correlation and which are applicable to both the supercritical and the high subcritical flow regions. We have compiled a database of heat transfer measurements in carbon dioxide flowing upwards in vertical heated tubes that are free of deterioration or enhancement. We then applied the four sets of scaling laws to these data to compute values of the water-equivalent heat transfer coefficient and compared these values to predictions of a transcritical look-up table, which was earlier shown to represent well a large compilation of measurements in water at supercritical and high subcritical pressures. It was shown that the two earlier methods systematically overestimated the heat transfer coefficient in water and also introduced significant imprecision. In contrast, the two proposed methods of scaling introduce no bias and have lower precision uncertainties than those of the previous scaling methods.

Keywords:
Convective heat transfer
Fluid-to-fluid scaling
Supercritical pressure
Look up table
Carbon dioxide
Water

NOMENCLATURE

d	tube inner diameter
e	relative difference between the scaled and predicted heat transfer coefficients
H	specific enthalpy
h	heat transfer coefficient
k	thermal conductivity
Nu	Nusselt number
Pr	Prandtl number
Re	Reynolds number
z	axial distance from the inlet of the heated section

Greek symbols

θ	parameter in the Cheng *et al.* scaling laws
μ	viscosity

Subscripts

b	bulk
c	critical
in	inlet
LUT	look-up table
pc	pseudo-critical
sat	saturation
SC	scaled
SL	scaling law
w	wall

Other notation

$\langle\ \rangle$	average
$(\ )'$	rms value

Acronyms

CHF	critical heat flux
HTC	heat transfer coefficient
NHT	normal heat transfer
SC	supercritical
SCUOL	supercritical University of Ottawa loop
SCWR	supercritical water-cooled reactor
TC LUT	trans-critical look-up table

1. INTRODUCTION

Supercritical heat transfer experiments in water require high-pressure test facilities which are very expensive to construct. It is therefore more economical to perform test in a modelling fluid at water-equivalent conditions and transform the modelling fluid data into water. Supercritical test facilities using modelling fluids such as CO_2 operate at much lower pressures, temperatures and powers and are less costly to construct. However the accuracy of transforming SCHT data obtained in modelling fluids into water-equivalent values has yet to be determined in a systematic manner.

Starting in the 1950s, heat transfer in supercritical (SC) water and other fluids was investigated in support of SC fossil-fuelled power plants. This topic has recently received renewed attention because of its relevance to Super Critical Water-cooled Reactors (SCWR), which are among the designs considered by the Generation IV International Forum as innovative nuclear energy systems with increased safety, more compact size, lower cost of energy production and reduced volume of nuclear waste, compared to existing systems. The present work is part of ongoing multi-faceted research at the University of Ottawa (UO) in support of the Canadian National Program for the development of the SCWR (Nava-Dominguez *et al.*, 2013).

Prediction and modelling of the flow and heat transfer at SC pressures remain topics of intense research worldwide and are commonly described by empirical correlations that are fitted to measurements within suitable ranges of conditions. As an alternative to correlations, look-up tables (LUT) have been used successfully to predict complex heat transfer phenomena such as critical heat flux (CHF) and film boiling heat transfer with an accuracy that is much higher than the best available prediction methods (Groeneveld *et al.*, 2003, 2005). The UO team is in the process of finalizing a trans-critical look-up table (TC LUT) for convective heat transfer at high subcritical and SC pressures (Zahlan *et al.*, 2012). The TC LUT is based on a large database of reliable near-critical and SC heat transfer measurements for water and other fluids, which includes compilations from three other universities (Zahlan *et al.*, 2011). It was found that the uncertainty in predicting the heat transfer coefficient using the TC LUT is much lower than that of the assessed correlations and so the use of the TC LUT is recommended for design and analysis of SCWR as a more accurate alternative to the use of correlations.

Experiments in SC water are necessary for the development of SCWR, however, they are difficult and expensive to perform. We have constructed a supercritical heat transfer flow loop (SCUOL) and conducted a series of experiments using carbon dioxide as a surrogate fluid (Zahlan *et al.* 2013). One objective of this work is to supplement the available experimental database for CO_2 with measurements under conditions for which previous data are sparse or unavailable; moreover, these data are intended to fill some gaps in the experimental database of the TC LUT as well as in the databases for CHF and film boiling LUT and boiling heat transfer correlations for high subcritical pressures. In order to convert CO_2 data into water-equivalent values, it is necessary to use appropriate fluid-to-fluid scaling laws. Scaling laws for convective heat transfer at supercritical pressures were first developed for the purpose of estimating heat transfer to a fluid at some conditions from available values at different conditions but in the same fluid. Following customary dimensional analysis practices, the independent and dependent parameters were normalized by appropriate scales to form a set of dimensionless groups. The application of this concept was extended to scale convective heat transfer in two different fluids, in which case assumptions concerning the thermodynamic similarity of the two fluids needed to be introduced. Kirillov (2009) described briefly the thermodynamic similarity of fluids and referred this similarity to the Van der Waals equation of state in terms of pressure, temperature and specific volume "reduced" by the critical values; he then discussed its known applicability to different fluids, including fluids at supercritical pressures.

The objective of this article is to assess the accuracy of available and newly suggested fluid-to-fluid modelling (or fluid scaling) methods for heat transfer at high subcritical and supercritical pressures. The method that is deemed to be most appropriate will be used to convert the CO_2 experimental data that were obtained in SCUOL into their water equivalent values and then incorporate these values into the TC LUT.

Two previously suggested sets of scaling laws were evaluated in this work, namely the modified Jackson's (2008) scaling laws, as proposed by Zwolinski *et al.* (2011), and the Cheng *et al.* (2011) scaling laws. Some limitations of these laws were discussed and new sets of scaling laws were developed by modifying earlier relationships; these laws contained an empirical coefficient, which was fitted to the TC LUT predictions separately for the SC region and for the high subcritical region.

2. SCALING LAWS

In accordance with general scaling procedures, scaling of convective heat transfer is based on a set of dimensionless groups, which can be derived from dimensionless forms of the governing equations or by application of the Buckingham π theorem. In either case, the choice of appropriate scales for the independent and dependent variables, the specification of the ranges of conditions to which such scaling is intended to apply, and possibly physical constraints that must be satisfied for a meaningful application of scaling are essential parts of the process. Scaling may refer to the same fluid in different channels or under different conditions, to different fluids or to a combination of these cases. The interest of the present work is on scaling heat transfer in different fluids. In this section, we will first summarize previously suggested scaling laws, then comment on their suitability for our specific objectives, and finally modify some of these laws to improve the accuracy of scaling heat transfer data in CO_2 to equivalent water values not only in the supercritical pressure region but also in the high subcritical one.

2.1 Previous scaling laws

Jackson's scaling laws for the same fluid: Jackson and Hall (1979) and Jackson (2007, 2008) analysed the dimensionless equations for flow and heat transfer and specified the requirements for strict similarity between two geometrically-similar vertically-upward flows cooled by the same fluid at SC pressures. This similarity was restricted to steady-state forced convection in uniformly heated tubes. He specified that the pressure P_{in} and temperature T_{in} at the inlet of the heated section should be the same between the two cases considered and that the dimensionless distance z/d (z is the distance from the inlet and d is the tube diameter, to be replaced by the hydraulic diameter for channels with non-circular cross sections) along the tube should also be the same. This analysis specified that the Reynolds numbers Re_{in}, evaluated at inlet conditions, should be matched and further provided a scaling law for the wall heat flux q, which also contained properties at inlet conditions. Jackson did not identify a range of tube diameters to which this analysis would apply, but mentioned that the tube diameter should be small enough for the buoyancy effects to be small and large enough for viscous pressure losses not to have a significant effect on property variation. Jackson further noted that the presence of strong buoyancy, compressibility or viscous losses would make complete similarity unachievable. Although Jackson did not explicitly scale the HTC, one may calculate a scaled local HTC by the application of the energy equation in a control volume between the inlet and the location with *z/d* of interest at the scaled conditions. For the correlation of experimental data, Jackson specified a functional form of the local Nusselt number Nu_b, in which non-dimensional scaling relationships were based on local bulk properties, *i.e.*, $\mathrm{Nu}_b = f\left(\frac{z}{d}, \frac{P_{in}}{P_c}, \mathrm{Re}_b, \mathrm{Pr}_b, \frac{qd}{k_b T_b}\right)$. In this expression, P_c is the critical pressure, Pr is the Prandtl number, k is the thermal conductivity of the fluid and T is the temperature.

Zwolinski *et al.*'s extension of Jackson's laws: The scaling laws of Jackson (2008) for same-fluid similarity were adapted by Zwolinski *et al.* (2011) for scaling SC heat transfer between water and CO_2. These scaling laws will be referred to in the following as *modified Jackson laws*. The requirements of matching *z*/*d*, reduced pressure and temperature and Reynolds number at the inlet were maintained. Wall heat flux was also matched in a manner similar to that by Jackson (2008). This method does not model local conditions. To estimate local bulk fluid enthalpy in the modelled fluid, one needs to calculate the scaled inlet temperature, heat flux and mass flux and then apply the energy equation in a control volume bounded by the inlet and the local cross-section. The modified Jackson scaling requirements for water and carbon dioxide are as follows

$$\left(\frac{z}{d}\right)_{\mathrm{CO_2}} = \left(\frac{z}{d}\right)_{\mathrm{H_2O}} \tag{1}$$

$$\left(\frac{P_{in}}{P_c}\right)_{\mathrm{CO_2}} = \left(\frac{P_{in}}{P_c}\right)_{\mathrm{H_2O}} \tag{2}$$

$$\left(\frac{T_{in}}{T_{pc}}\right)_{\mathrm{CO_2}} = \left(\frac{T_{in}}{T_{pc}}\right)_{\mathrm{H_2O}} \tag{3}$$

$$\left(\frac{Gd}{\mu_{in,b}}\right)_{\mathrm{CO_2}} = \left(\frac{Gd}{\mu_{in,b}}\right)_{\mathrm{H_2O}} \tag{4}$$

$$\left(\frac{qd}{k_{in,b}\,T_{in}}\right)_{\mathrm{CO_2}} = \left(\frac{qd}{k_{in,b}\,T_{in}}\right)_{\mathrm{H_2O}} \tag{5}$$

where T_{pc} is the pseudo-critical temperature, G is the mass flux and μ is the fluid viscosity. Provided that the above five equalities are satisfied, then the HTC in water can be calculated from

$$\left(\frac{h\,d}{k_{in,b}}\right)_{\mathrm{CO_2}} = \left(\frac{h\,d}{k_{in,b}}\right)_{\mathrm{H_2O}} \tag{6}$$

which implies that $\mathrm{Nu} = f\left(\frac{z}{d}, \frac{P_{in}}{P_c}, \frac{T_{in}}{T_{pc}}, \mathrm{Re}_{in}, \frac{qd}{k_{in}T_{in}}\right)$.

Cheng *et al.*'s scaling laws: Cheng *et al.* (2010, 2011) also analysed the dimensionless governing equations and boundary conditions and suggested similarity conditions for SC flows in vertical circular tubes with a constant heat flux. This analysis was based on the condition that the tube diameter *d* would be the same, thus eliminating possible tube size effects. Moreover, all conditions in the resulting scaling laws are evaluated locally, without the need to refer to the inlet conditions or to match *z/d*. To model the local bulk temperature conditions, Cheng *et al.* (2010, 2011) introduced the dimensionless group $\theta_b = (T_b\text{-}T_{pc})/(T_{pc}\text{-}T_c)$ where T_b, T_c and T_{pc} are, respectively, the bulk, critical and pseudo-critical temperatures. They derived a scaling law for the wall heat flux *q* by matching the corresponding dimensionless boundary conditions for the energy equation. Mass flux *G* was not scaled by requiring Reynolds number equality, but by matching values of an empirical expression that includes both the Reynolds number and the Prandtl number, namely the Dittus-Boelter (1930) correlation for convective heat transfer. Finally, a scaling law for the HTC *h* was derived by imposing equality of the Nusselt numbers. When applied to scaling convective heat transfer in water to that in carbon dioxide, or *vice versa*, the Cheng et al. scaling requirements are as follows

$$d_{\mathrm{CO_2}} = d_{\mathrm{H_2O}} \tag{7}$$

$$\left(\frac{P}{P_c}\right)_{\mathrm{CO_2}} = \left(\frac{P}{P_c}\right)_{\mathrm{H_2O}} \tag{8}$$

$$\left(\frac{T_b - T_{pc}}{T_{pc} - T_c}\right)_{\mathrm{CO_2}} = \left(\frac{T_b - T_{pc}}{T_{pc} - T_c}\right)_{\mathrm{H_2O}} \tag{9}$$

$$\left(\frac{qd}{k_b\,(T_{pc} - T_c)}\right)_{\mathrm{CO_2}} = \left(\frac{qd}{k_b\,(T_{pc} - T_c)}\right)_{\mathrm{H_2O}} \tag{10}$$

$$\left(\frac{Gd\mathrm{Pr}_{\mathrm{b}}^{5/12}}{\mu_b}\right)_{\mathrm{CO_2}} = \left(\frac{Gd\mathrm{Pr}_{\mathrm{b}}^{5/12}}{\mu_b}\right)_{\mathrm{H_2O}} \tag{11}$$

Provided that the previous five equalities are satisfied, one may calculate the HTC in water from

$$\left(\frac{h\,d}{k_b}\right)_{\mathrm{CO_2}} = \left(\frac{h\,d}{k_b}\right)_{\mathrm{H_2O}} \tag{12}$$

The functional dependence of Nusselt number for the Cheng *et al.* method is $\mathrm{Nu}_b = f\left(\frac{P}{P_c}, \theta_b, \mathrm{Re}_b\mathrm{Pr}_b^{5/12}, \frac{qd}{k_b(T_{pc}-T_c)}\right)$.

Discussion of previous scaling laws: A general limitation of the previous scaling laws for the purposes of scaling heat transfer in the transcritical pressure regime is that they were developed strictly for supercritical pressures. At the least, these laws would need to be modified for application to the high subcritical region; while doing so, one should keep in mind that heat transfer phenomena at subcritical pressures are different from those at supercritical ones and so empirical relationships in the two regions would most likely differ from each other. The modified Jackson scaling laws have two additional limitations, which were not actually present in Jackson's original concept of scaling heat transfer in the same fluid. First, all properties in these scaling laws are evaluated at inlet conditions; in an arbitrarily long channel, inlet conditions would become irrelevant far downstream, where one would expect that local heat transfer would depend primarily on local conditions. Second, although the original Jackson scaling laws for the same fluid ensure equality of the Prandtl numbers, at least at the inlet, their modified form for different fluids cannot account for differences in Prandtl numbers, which in general would not be negligible. Cheng *et al.*'s laws are not subjected to these two limitations, however, they also present some problems as far as their suitability to the present objectives is concerned. First, temperature differences are scaled by $T_{pc} - T_c$, which vanishes at the critical pressure, thus introducing a singularity within the transcritical pressure region. Second, mass flux scaling is based on the original form of the Dittus-Boelter correlation, which is an empirical expression fitted to heat transfer data in the low subcritical pressure region. There is no reason to expect that the same expression would apply to both the high subcritical as well as the supercritical regions. On the contrary, previously developed empirical Nusselt number correlations for normal SC heat transfer have optimal exponents of the Reynolds and Prandtl numbers that differ from the Dittus-Boelter values. Therefore, it seems logical that one should at least allow some empirical adjustment to the Dittus-Boelter correlation, so it can describe more accurately, albeit piecewise, the entire transcritical region. In view of these considerations, we introduced some modifications to the previous scaling laws, in an effort to reduce or eliminate unnecessary inconsistencies and uncertainties and thus to achieve a higher scaling accuracy for the fluids and ranges of conditions of interest in the present study.

2.2 Additional scaling laws

The following considerations were made for the development of alternative scaling laws. These laws are meant to apply to normal convective heat transfer only, and should not be used for conditions of heat transfer deterioration or enhancement. Although some generalization may become possible in the future, at this time diameter and cross-sectional shape effects will be eliminated by restricting the scaling laws to circular tubes with equal diameters. A survey of the literature and our own analysis demonstrated that scaling of normal heat transfer at SC pressures should depend on local values of the various parameters. Consequently, we will disregard the inlet conditions and the distance along the heated length, which in any case may not be available for many experimental results reported, and evaluate all parameters and thermophysical properties locally. Finally, the proposed methods should be suitable for application to convective heat transfer at both the supercritical and the high subcritical pressure ranges. In this work, we will assume that laws developed for supercritical pressures apply to high subcritical pressures provided T_{pc} is replaced by the corresponding T_{sat} at that pressure.

Modified Cheng *et al.*'s scaling laws: The Cheng *et al.* method meets most of our requirements, with the exception that it does not allow for an inclusion of the Prandtl number effect in a fashion that can be optimized separately in the subcritical and supercritical regions. In convective heat transfer, the Nusselt number is known to depend on both the Reynolds number and the Prandtl number. This relationship may be expressed empirically by a generalized Dittus-Boelter-type equation

$$\mathrm{Nu} = C\,\mathrm{Re}_b^{\alpha}\mathrm{Pr}_b^{\beta} \qquad (13)$$

where C, α and β are empirical constants. By equalizing the Nusselt numbers for the two fluids, one may eliminate the constant C; further raising both sides to a power $1/\alpha$ and letting $\gamma = \beta/\alpha$, one may derive a simplified condition for Re and Pr as

$$(\mathrm{RePr}^{\gamma})_{\mathrm{CO_2}} = (\mathrm{RePr}^{\gamma})_{\mathrm{H_2O}} \qquad (14)$$

The exponent of Prandtl number can be determined empirically for a best match of predictions and measurements of HTC. It is noted that Cheng *et al.* (2011) recommended a similar law, but they assumed validity of the Dittus-Boelter correlation to fix γ to the value 5/12, which does not allow empirical adjustment. For convenience in scaling experimental results, one may rewrite Equation (14) in terms of the mass flux G, which is related to the Reynolds number as $\mathrm{Re} = Gd/\mu_b$. This results in the scaling law

$$\left(\frac{Gd\mathrm{Pr}_\mathrm{b}^{\gamma}}{\mu_b}\right)_{\mathrm{CO_2}} = \left(\frac{Gd\mathrm{Pr}_\mathrm{b}^{\gamma}}{\mu_b}\right)_{\mathrm{H_2O}} \quad (15)$$

Therefore, in addition to the previous two sets of scaling laws, we propose to consider the *modified Cheng et al. laws*, which consist of Equations (7-10), (15) and (12). The functional dependence of Nusselt number for the modified Cheng *et al.* method is $\mathrm{Nu}_b = f\left(\frac{P}{P_c}, \theta_b, \mathrm{Re}_b\mathrm{Pr}_b^{\gamma}, \frac{qd}{k_b(T_{pc}-T_c)}\right)$. For the high subcritical region, $T_{pc} - T_c$ will be replaced by $T_c - T_{sat}$.

Alternative scaling laws: An additional modification to these laws that appears to be suitable for transcritical heat transfer scaling is to scale the bulk temperature and the heat flux by T_{pc} (or T_{sat}), rather than $T_{pc} - T_c$ (or $T_c - T_{sat}$). This set of laws will be referred to in the following as *alternative scaling laws*. In summary, these laws are as follows.

$$d_{\mathrm{CO_2}} = d_{\mathrm{H_2O}} \quad (16)$$

$$\left(\frac{P}{P_c}\right)_{\mathrm{CO_2}} = \left(\frac{P}{P_c}\right)_{\mathrm{H_2O}} \quad (17)$$

$$\left(\frac{T_b}{T_{pc}}\right)_{\mathrm{CO_2}} = \left(\frac{T_b}{T_{pc}}\right)_{\mathrm{H_2O}} \quad (18)$$

$$\left(\frac{qd}{k_bT_{pc}}\right)_{\mathrm{CO_2}} = \left(\frac{qd}{k_bT_{pc}}\right)_{\mathrm{H_2O}} \quad (19)$$

$$\left(\frac{Gd\mathrm{Pr}_\mathrm{b}^{\gamma}}{\mu_b}\right)_{\mathrm{CO_2}} = \left(\frac{Gd\mathrm{Pr}_\mathrm{b}^{\gamma}}{\mu_b}\right)_{\mathrm{H_2O}} \quad (20)$$

$$\left(\frac{h\,d}{k_b}\right)_{\mathrm{CO_2}} = \left(\frac{h\,d}{k_b}\right)_{\mathrm{H_2O}} \quad (21)$$

This implies that $\mathrm{Nu}_b = f\left(\frac{P}{P_c}, \frac{T_b}{T_{pc}}, \frac{q\,d}{k_b\,T_{pc}}, \mathrm{Re_b}\mathrm{Pr}_b^{\gamma}\right)$.

If one is not interested in scaling experimental results in two fluids, but in comparing measurements with predictions of the TC LUT, as in the present case, it would be more convenient to use wall temperature T_w as an independent variable instead of heat flux, because the table has been constructed using this parameter as independent variable. The two parameters are equivalent, as they are related to each other through the scaled dimensionless groups. Noting that

$$q = h(T_w - T_b) = \left(\frac{h\,d}{k_b}\right)\left(\frac{T_w - T_b}{T_{pc}}\right)\frac{k_bT_{pc}}{d} \quad (22)$$

one can derive a scaled form for T_w as

$$\frac{T_w}{T_{pc}} = \frac{T_b}{T_{pc}} + \frac{qd}{k_b T_{pc}} / \frac{h\,d}{k_b} \tag{23}$$

which indicates that the scaling relationship

$$\left(\frac{T_w}{T_{pc}}\right)_{CO_2} = \left(\frac{T_w}{T_{pc}}\right)_{H_2O} \tag{24}$$

is equivalent to the heat flux scaling law, Equation (19) and so it can be used instead. In consequence, the relationship among dimensionless groups would be written as $\mathrm{Nu}_b = f\left(\frac{P}{P_c}, \frac{T_b}{T_{pc}}, \frac{T_w}{T_{pc}}, \mathrm{Re}_b \mathrm{Pr}_b^{\gamma}\right)$.

3. COMPILATION OF A DATABASE FOR NORMAL HEAT TRANSFER

At present, development of fluid-to-fluid scaling laws that would be of general use for all possible heat transfer conditions in SC fluids seems to be beyond reach since we found that the HTC scaling in the deteriorated heat transfer region required different scaling relationships than scaling in the "normal" heat transfer region. A more realistic goal is to develop scaling laws that apply only to normal heat transfer (NHT). Unfortunately, there is no general agreement in the literature on the criteria identifying normal, enhanced or deteriorated SC heat transfer (Zahlan *et al.*, 2012). Nevertheless, for scaling laws evaluation, it was necessary to select among the available experimental results those that were taken under NHT conditions. At an initial stage, we followed a simple method that has been used in past literature, which compares the measured HTC with the corresponding one that is predicted by an empirical correlation for NHT. We chose Jackson's (2009) correlation for fluids with variable properties, because the database for this correlation included data in CO_2. We tested this approach for our CO_2 database and concluded that it did not provide a proper means for the identification of NHT data. To ensure that our scaling laws evaluation would not be contaminated by data taken under heat transfer deterioration or enhancement conditions, we adopted a direct approach for identifying NHT data. For each set of results, we inspected visually the wall temperature variation along the heated length and considered as NHT only cases showing a monotonically increasing temperature that was free of local peaks and sudden rises that exceeded 2K. Similarly, only subcooled liquid flows with gradually and monotonically increasing wall temperature were selected in the high subcritical pressure region. We further excluded a small number of subcritical results in CO_2, for which the maximum wall temperature variation was so small that its water-equivalent value dropped below the wall temperature superheat resolution of our TC LUT, namely 10 K.

To illustrate this approach, we present three representative examples in Figure 1, two for SC pressures (P/P_c = 1.11 and 1.16) and one for a high subcritical pressure (P/P_c = 0.95). All these tests were conducted in SCUOL, using a vertical 8 mm ID tubular (8 mm was also the reference diameter for the TC LUT) test section in which CO_2 flowed upwards. For each of the three tests, the pressure, mass flux and inlet temperature were kept constant, whereas the wall heat flux was increased from relatively low values, at which wall temperature increased monotonically and gradually, to sufficiently high values for the wall temperature to present fairly sharp changes in rate of change with downstream distance. The results are plotted versus bulk enthalpy H_b, which increases linearly upwards and the plots include the variation of the calculated local bulk temperature.

The tests at P/P_c = 1.11 were made at the relatively small mass flux G = 500 kg/m^{2}s, which is significantly lower than the equivalent mass flux in the current Canadian SCWR design. For the two tests at q = 20 and 40 kW/m^2, the wall temperature showed monotonic increases from the inlet to the outlet of the heated length and the heat transfer coefficients were found not to vary significantly along the test section; these results were deemed to correspond to NHT and were included in the scaling law evaluation analysis. In contrast, for the test with q = 50 kW/m^2, the wall temperature presented two significant peaks, which clearly indicated deterioration in heat transfer; these results were excluded from the scaling law evaluation analysis.

The tests at P/P_c = 1.16 were made at the relatively high mass flux G = 2000 kg/m^{2}s. The tests at q = 225, 275 and 300 kW/m^2 were included in the NHT classification for the reason described previously. The test at q = 436 kW/m^2 showed a sharp local rise in wall temperature, which was of the order of 10 K and also displayed a clear curvature in the profile. This test was not included in the current compilation of NHT data.

Finally, representative results are presented for the high subcritical pressure region (P/P_c = 0.95), in which very few, if any at all, previous data are available. These measurements were taken for the moderate mass flux G = 700 kg/m^{2}s and six different heat fluxes. The wall temperature variations for q = 15 and 20 kW/m^2 indicate that single phase convective heat transfer to subcooled liquid occurred along the entire heated tube, in which T_w was always lower than T_{sat}. For these two tests, T_w and T_b increased monotonically and gradually and heat transfer was considered to be normal; consequently, these results were included in the database for scaling law evaluation. For the test at q = 30 kW/m^2, the wall temperature increased gradually downstream from the inlet value up to the location where H_b = 248 kJ/kg, at which subcooled nucleate boiling occurred at the heated wall and beyond which the wall temperature maintained a constant value, while the bulk temperature kept increasing; for this test, only data from the inlet up to the location of boiling onset (24 points) were considered to be NHT and included in the database. For the test at q = 51 kW/m^2, subcooled nucleate CO_2 boiling occurred close to the inlet of the heated tube section and so all data from this test were excluded from the NHT data compilation. For the tests with q = 57 and 80 kW/m^2, CO_2 essentially entered the temperature measurement section of the tube in the subcooled nucleate boiling mode and heat transfer continued in this mode until CHF occurred at locations with H_b = 291 and 248 kJ/kg, respectively, beyond which film boiling occurred; the results of these two tests were also excluded from the NHT database.

The conditions of all CO_2 tests that were used for the evaluation of scaling laws are listed in Table 1. All these results were deemed to have been collected under normal heat transfer conditions.

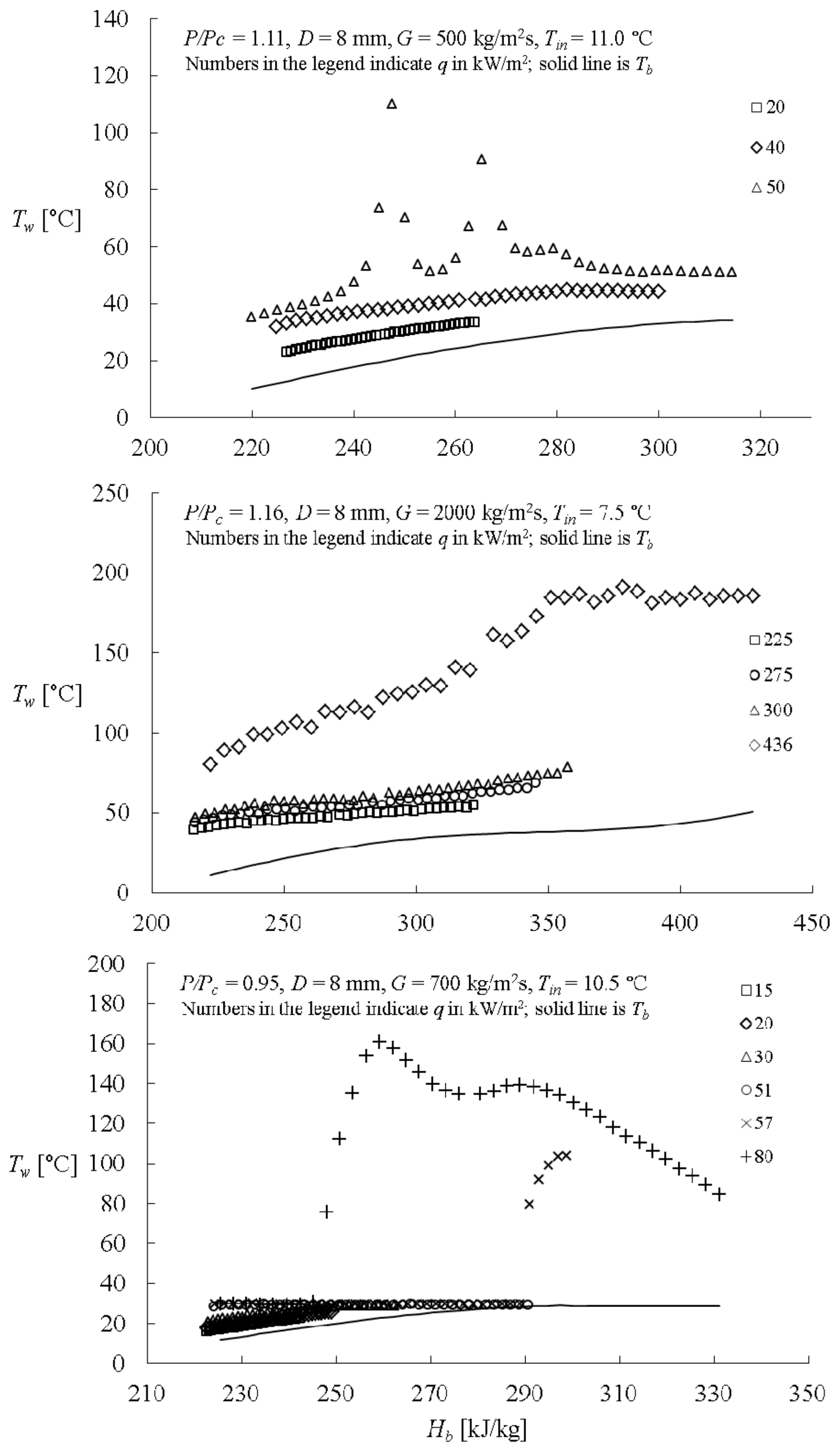

Figure 1: Representative examples of wall temperature variation in upward flows of CO_2 along a vertical 8 mm ID tube at supercritical and high subcritical pressures.

Table 1: Conditions of “normal” heat transfer tests in carbon dioxide.

P/P_c [-]	G [kg/m^{2}s]	q [kW/m^2]	T_b [˚C]
0.81	2000	49	9-17
0.85	1000	11	9-14
		20	9-16
0.88	500	5	10-15
		10	10-18
	700	10	10-16
		14	11-18
		14	10-17
		15	11-19
		18	10-19
		24	11-22
		30	11-24
	1000	21	9-16
		31	9-19
0.89	500	15	10-20
	700	18	11-20
		23	11-22
	1000	41	9-22
	1500	10	8-10
		20	8-13
		30	8-15
		37	8-16
	2000	15	8-11
		20	8-12
		45	8-16
0.94	700	20	10-20
	1000	16	11-17
		29	11-20
		30	11-21
	1500	30	10-17
		40	9-19
		70	10-24
	2000	51	11-19
		60	11-21
		70	11-22
		79	11-24
		109	11-26
0.95	700	15	10-18
		30	10-24
	1000	20	11-18
		40	11-23
	1500	50	10-21
		52	10-21
1.01	500	20	11-24
1.02	1000	75	9-30

P/P_c [-]	G [kg/m^{2}s]	q [kW/m^2]	T_b [˚C]
1.02	2000	100	7-24
		150	7-29
		275	7-32
1.03	500	20	10-24
		30	11-28
	1000	50	8-25
	1200	50	9-24
	1500	20	8-13
		125	8-31
		150	8-32
		181	8-32
		200	8-33
	2000	75	7-21
		180	7-31
1.04	1000	20	8-16
	1500	50	8-20
		100	8-28
	2000	200	7-32
		225	7-32
1.05	1000	100	8-32
	1200	50	9-24
	1500	75	8-25
1.05	2000	251	7-33
1.07	1200	50	9-24
1.08	1000	20	9-17
	1500	75	8-25
1.09	500	40	9-32
	1000	125	8-34
	1500	74	8-25
	2000	250	7-34
1.10	500	20	12-26
	1000	75	10-32
	1200	50	9-24
	2000	125	7-28
1.11	500	25	12-29
		40	11-33
	1000	20	9-17
		40	9-23
		50	9-27
		50	9-26
		75	10-32
		100	9-34
	1500	100	8-30
	2000	126	7-28
		275	8-36

P/P_c [-]	G [kg/m^{2}s]	q [kW/m^2]	T_b [˚C]
1.12	500	20	10-25
	700	40	12-29
		80	10-36
	1000	30	9-20
		40	9-23
	1500	100	8-30
1.13	1000	50	9-26
		75	9-32
		125	9-36
	2000	150	7-31
		300	8-37
1.14	500	20	13-26
		25	10-28
		30	13-31
		30	11-30
		40	12-34
	1000	125	9-36
	1500	125	8-32
		150	7-35
		175	7-36
	2000	150	8-31
		175	7-33
		200	7-35
1.15	1000	100	9-35
		101	8-35
	1500	150	8-35
		225	8-38
	2000	201	7-35
		225	7-36
		250	7-37
1.16	500	20	11-27
		30	12-31
		40	11-34
		40	12-34
		41	12-35
	1500	125	8-33
		175	8-37
		199	7-37
	2000	225	7-36
		275	7-37
		300	7-38
1.17	1000	125	9-37
	1500	200	8-38
1.18	1500	200	8-38

4. SCALING LAW ASSESSMENT

4.1 Approach

To assess the validity of a set of fluid-to-fluid scaling laws, it is preferable to use a direct method. This means to select pairs of corresponding measurements of independent variables in the two fluids, such that the values in one set, when scaled according to the laws considered, match the values in the other set. Then, the accuracy of the scaling method would be determined by comparing the measurement of the HTC in one fluid with the scaled measurement of the HTC in the other. Zwolinski *et al.* (2011) reported a plan to perform an experimental study with CO_2 (27 data points) to assess the validity of Jackson's (2008) scaling laws. They transformed test conditions and HTC of the water experiments that were obtained previously at the University of Wisconsin to CO_2 equivalent values and planned to perform experiments in CO_2 at the scaled conditions for a direct comparison of the scaled and measured HTC. No update on this work is known so far. When a match between the scaled test conditions and the corresponding experimental conditions is not possible, however, an indirect assessment becomes necessary. Cheng *et al.* (2011) used empirical correlations to estimate the value of HTC in one fluid, which was then compared to the corresponding value that was obtained by scaling the HTC measured in the other fluid. Obviously, this approach has the disadvantage of including the uncertainty of the correlation, which could be considerable, in the uncertainty of scaling.

In the present study, we had available a vast database of water data reported by various authors, which were represented quite well by our TC LUT (Zahlan *et al*., 2012), as well as a database of our own carbon dioxide data, obtained in SCUOL (Zahlan *et al*., 2013). At first, we attempted to use the direct method by selecting some water data as candidates for possible matching of their test conditions and the water-equivalent conditions of data in the CO_2 database. Conditions imposed on the selected water data were that they must be for upward vertical flow in a 8 mm tube and must specify values of the axial distance from the inlet of the heated length, so that all conditions for the testing of both selected scaling methods could be met. The inlet temperature in the water data, which in most cases was not reported by the authors, was estimated by assuming a linear variation of fluid enthalpy with axial distance from the inlet. In addition, only data with normal heat transfer were chosen. To find matching data points in the CO_2 database, we imposed the condition that the tube diameters as well as z/d for the two sets of results should be the same. Unfortunately, the values in CO_2 corresponding to available water data after scaling by either method could not be matched, even approximately, by any data in the CO_2 database and so the direct method could not be applied at the present. We plan to extend our studies of fluid-to-fluid scaling by conducting additional experiments in CO_2 as well as in Refrigerant 134a, for which effort will be made to produce sets of data in two, or even three, fluids at matched scaled conditions. In the meantime, we assessed the scaling laws indirectly with the use of our TC LUT. To do so, a data point was selected from our CO_2 database and the scaling laws were applied to it to calculate the water-equivalent values of pressure, mass flux and wall temperature difference $T_w - T_b$ based on the appropriate scaling laws or combinations of them. The input parameters were then inserted in the TC LUT, which provided a value of the water HTC, which was compared with the corresponding scaled HTC. It is noted that accurate values of all thermophysical properties for both CO_2 and water, determined from the NIST tables (Lemmon *et al.*, 2002) for the corresponding pressure and temperature, were inserted in all scaling relationships. Although the use of the TC LUT has the same limitation as the use of heat transfer correlations, namely of introducing its own uncertainty into the uncertainty of scaling laws, it is noted that the uncertainty of TC LUT for normal heat transfer at SC and high subcritical pressures was found to be significantly lower than those of all tested correlations (Zahlan *et al.*, 2011).

4.2 Evaluation of the scaling laws

An indirect assessment of the uncertainty of the three scaling methods considered was performed using the TC LUT. First, 3990 NHT data in the SC pressure region and 1491 data points in the high subcritical region of our CO_2 database in the 8 mm tube were selected for the assessment. Then, the scaling laws under consideration were applied to each CO_2 data point to calculate water-equivalent input parameters to the TC LUT, namely pressure, mass flux and wall temperature superheat, as well as a scaled HTC h_{SC}. Substitution of these input parameters to the table rendered an "experimental" value h_{LUT} for the water HTC. The percent difference between the two HTC values was then calculated as

$$e = 100\,\frac{h_{SC}-h_{LUT}}{h_{LUT}}\% \qquad (25)$$

These values were analysed statistically for the supercritical cases and for the subcritical ones, first separately and then for all cases together, to compute the corresponding averages $\langle e \rangle$ and root mean squares (rms) e'. It is noted that $\langle e \rangle$ represents a bias, whereas e' is a measure of the overall uncertainty, which includes both bias and precision uncertainty (Tavoularis, 2005). For empirical optimizations of the modified Cheng *et al*. and alternative scaling methods, the process was repeated for different values of the Prandtl number exponent γ and for each of the two pressure regions and the value of γ that resulted in elimination of the corresponding $\langle e \rangle$ was selected. This removed bias from the scaling method, leaving only precision uncertainty, which cannot be further reduced. It is noted that, by the method of its construction, the TC LUT introduces no bias. The overall uncertainty of the present procedure is a combination of the uncertainty of the TC LUT, expressed in rms value as e'_{LUT} and the corresponding uncertainty e'_{SL} of the scaling laws. e'_{LUT} was calculated to be approximately 13% for the SC region, 8% for the high subcritical region and 13% overall; it is noted that the overall value was close to that in the SC region, because 18640 data points were used for constructing the TC LUT in this region, whereas only 726 data points were available for the high subcritical region. Assuming statistical independence between the two uncertainties, it is possible to estimate the scaling law uncertainty as

$$e'_{SL} = \sqrt{e'^2 - e'^2_{LUT}} \qquad (26)$$

Figure 2 shows the variations of the ratio h_{SC}/h_{LUT}, determined by each of the four scaling methods considered and plotted *vs.* h_{LUT}. For the modified Cheng *et al.* and alternative methods, the results were plotted by using the optimal exponents γ of the Prandtl number in the corresponding mass flux scaling laws, whose values are listed in Table 2. It is clear that all values are significantly higher than the value corresponding to the Dittus-Boelter correlation and included in the Cheng *et al.* scaling laws. It is also clear that the optimal values of γ are higher in the high subcritical region (nearly twice the Dittus-Boelter value) than in the SC region (approximately 50% higher than the Dittus-Boelter value). Remarkably, the values of γ for the modified Cheng *et al.* and alternative methods in each of the two regions were essentially the same. These observations lead to the conclusion that the Prandtl number effect is significant in the range of conditions considered and must be accounted for separately in the high subcritical and supercritical regimes.

We now proceed to evaluate the accuracies of the four scaling methods based on observation of the results plotted in Figure 2 and on comparison of uncertainty indicators listed in Table 3. To illustrate the possible dependence of uncertainty on the HTC value, Figure 2 also shows dashed lines fitted by the linear-least-squares method to the HTC ratios over the range of results. A general observation is that the ranking of the four scaling methods is the same for the SC and high subcritical regions, which indicates that, at least as far as CO_2-to-water scaling of NHT is concerned, the choice of scaling parameters by each method produces consistent results. Moreover, the conclusions remain the same irrespectively of whether TC LUT uncertainty is included or removed from the overall uncertainty.

Among the four methods considered, the modified Jackson method is clearly significantly less accurate, resulting in both relatively large bias (71% overall) and large imprecision (91% overall). The corresponding values for the Cheng *et al.* method were lower, albeit not negligible (16.5 and 23%, respectively). Both previous methods overestimate systematically the water-equivalent HTC. The two newly proposed methods have, by construction, no bias with respect to TC LUT predictions and also have relatively low imprecisions (13% and 14% overall, respectively) by comparison to the two other methods. The differences in performance between the modified Cheng *et al.* and alternative methods are statistically insignificant, which leads to the conclusion that, once the Prandtl number affect has been taken into consideration in an optimal manner, it is immaterial whether temperatures are scaled by T_{pc}-T_c or T_{pc}. For the purposes of integrating CO_2 data into our TC LUT, we will use the alternative scaling method, which is free of singularity at the critical pressure, but it is acknowledged that the use of the modified Cheng *et al*. method would produce equally plausible results.

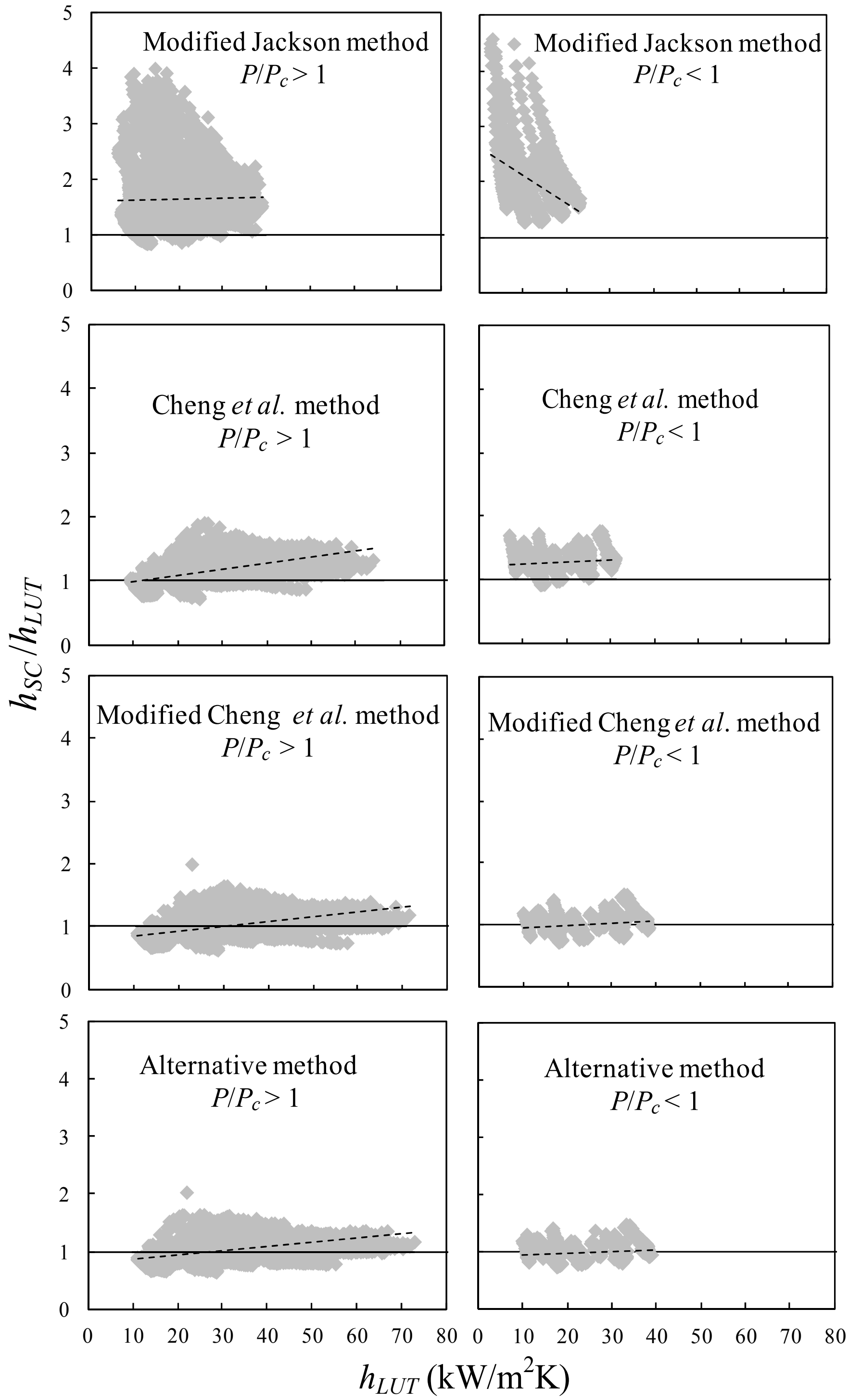

Figure 2: Variations of the ratio of the water-equivalent heat transfer coefficient for upward flow in a 8 mm ID tube, scaled from carbon dioxide data by four different methods, and the heat transfer coefficient predicted by the transcritical look-up table; the dashed lines are linear-least-squares fits through the HTC ratios.

Table 2: Optimal Prandtl number exponent in mass flux scaling law.

Scaling method	High subcritical region ($0.81 \leq P/P_c \leq 0.95$)	Supercritical region ($1.01 \leq P/P_c \leq 1.18$)
Cheng *et al.* method	0.42	0.42
Modified Cheng *et al.* method	0.82	0.63
Alternative method	0.77	0.66

Table 3: Scaling law uncertainties.

Scaling method	High subcritical region ($0.81 \leq P/P_c \leq 0.95$)			Supercritical region ($1.01 \leq P/P_c \leq 1.18$)			Transcritical region ($0.81 \leq P/P_c \leq 1.18$)		
	⟨e⟩ [%]	e´ [%]	e'_{SL} [%]	⟨e⟩ [%]	e´ [%]	e'_{SL} [%]	⟨e⟩ [%]	e´ [%]	e'_{SL} [%]
Modified Jackson method	101	118	118	63	84	83	71	92	91
Cheng *et al.* method	27	32	31	14	25	21	16.5	26	23
Modified Cheng *et al.* method	-0.2	14	12	-0.2	19	14	-0.2	18	13
Alternative method	0.1	13	10	0.0	20	15	0.0	19	14

As a final note, we would like to re-emphasize that the range of conditions in the present CO_2 tests were meant to be usable for the design and safety analysis of SCWR. As Table 4 indicates, this objective was met for the normal operating conditions of the current Canadian SCWR design and, to a large extend, for conditions under accident and transient scenarios.

Table 4: Water-equivalent ranges of conditions in the present experiments and conditions in the current Canadian SCWR design.

	Pressure [MPa]	Mass flux [kg/m2s]	Heat flux [kW/m2]	Inlet temperature [°C]	Bulk temperature [°C]
Present experiments[1]	17.9–25.9	760–3700	50–3420	322–335	324–388
Normal SCWR operating conditions[2]	25.0	1112	1008	350	350–625
SCWR conditions under accident and transient scenarios[2,3]	23–30 (24–26)	0–2200 (660–1500)	0–1530	300–400 (330-370)	

[1] Scaled with the use of the alternative method.
[2] Specified by the Atomic Energy of Canada Ltd. through private communication.
[3] Values in parentheses indicate focus areas of safety analysis.

5. CONCLUSIONS

In this article, we have summarized two sets of fluid-to-fluid scaling laws for supercritical heat transfer from recent literature and have proposed two new ones, which are based on an empirically adjusted version of the Dittus-Boelter correlation. We have applied these scaling laws to our normal heat transfer measurements in carbon dioxide flowing upwards in vertical heated tubes to compute a water-equivalent heat transfer coefficient, which we compared to predictions of our transcritical look-up table. These comparisons have demonstrated that, unlike the two earlier methods, which overestimate the heat transfer coefficient in water, the two newly proposed methods of scaling introduce no bias, as well as having a precision uncertainty, which is significantly lower than those of the previous scaling methods.

ACKNOWLEDGEMENTS

Funding to the Canada Gen-IV National Program was provided by Natural Resources Canada through the Office of Energy Research and Development, Atomic Energy of Canada

Limited, and Natural Sciences and Engineering Research Council of Canada. We thank Kai Jiang for his assistance with the SCUOL experiments and Michael Coyle for his assistance in processing and plotting the CO_2 measurements. We also thank Dr. Nihan Onder for providing us information on the Canadian SCWR design.

REFERENCES

Cheng, X., X.J. Liu and H.Y. Gu. Fluid-to-Fluid Scaling of Heat Transfer in Supercritical Fluids, 2nd Canada-China Joint Workshop on Supercritical Water-Cooled Reactors, Toronto, Canada, April 25–28, 2010.

Cheng, X., X.J. Liu and H.Y. Gu. Fluid-to-Fluid Scaling of Heat Transfer in Circular Tubes Cooled with Supercritical Fluids, Nuclear Engineering and Design 241, 498–508, 2011.

Groeneveld, D.C., J.E. Shan, A.Z. Vasic, A. Durmayaz, J. Yang, S.C. Cheng and A. Tanase. The 2005 CHF Look-up Table, log166, 11th International Topical Meeting on Nuclear Reactor Thermal – Hydraulics (NURETH-11), Avignon, France, October 2−6, 2005.

Groeneveld, D.C., L.K, Leung, A. Vasic, Y.J. Guo and S.C. Cheng. A Look-up Table for Fully Developed Film-boiling Heat Transfer, Nuclear Engineering and Design 225 (2003) 83–97, 2003.

Jackson, J.D. Requirements for Similarity in the Case of Heat Transfer to Fluids at Pressures above the Critical Value and an Approach to the Correlation of Experimental Data, Paper G3, Proceedings of the 10th UK National Heat Transfer Conference, Edinburgh, September 2007.

Jackson, J.D. A Semi-empirical Model of Turbulent Convective Heat Transfer to Fluids at Supercritical Pressure, 16th International Conference on Nuclear Engineering, Orlando, USA, May 11–15, 2008.

Jackson, J.D. Validation of an Extended Heat Transfer Equation for Fluids at Supercritical Pressure, 4th International Symposium on Supercritical Water-Cooled Reactors (ISSCWR-4), Heidelberg, Germany, Paper No. 24, March 8-11, 2009.

Jackson, J.D. and W.B. Hall. Forced Convection Heat Transfer to Fluids at Supercritical Pressure, in "Turbulent Forced Convection in Channels and Bundles", S. Kakaç and D.B. Spalding (editors), Hemisphere Publishing Corp., Washington, USA, Vol. 2, 563–611, 1979.

Kirillov, P. Experimental and Numerical Researches of Supercritical Water Heat Transfer in Rod Bundles, IAEA Progress Report, IAEA Research Contract No. 15221, 2009.

Lemmon, E.W., M.O. McLinden and D.G. Friend. Thermophysical Properties of Fluid Systems, NIST Standard Reference Database Number 69, NIST Reference Fluid Thermodynamic and Transport Properties Database: Version 7.0, 2002.

Nava-Dominguez, A., E.N. Onder, J. Pencer and D. Watts. Canadian SCWR Bundle Optimization for the New Fuel Channel Design, 6th International Symposium on Supercritical Water-Cooled Reactors (ISSCWR-6), Shenzhen, Guangdong, China, March 3-7, 2013.

Tavoularis, S. *Measurement in Fluid Mechanics*, Cambridge University Press, Cambridge, UK, 2005.

Zahlan, H., Groeneveld, D.C. Tavoularis, S., Mokry, S. and I. Pioro. Assessment of Supercritical Heat Transfer Prediction Methods, 5th International Symposium on Supercritical Water-Cooled Reactors (ISSCWR-5), Vancouver, March 2011.

Zahlan, H., D.C. Groeneveld and S. Tavoularis. A Look-up Table for Trans-Critical Heat Transfer for Water Cooled Tubes, 3rd China-Canada Joint Workshop on Supercritical Water-Cooled Reactors (CCSC-2012), Nanyang Hotel, Xi'an, Shaanxi, China, April 18-20, 2012.

Zahlan, H., K. Jiang, S. Tavoularis and D.C. Groeneveld. Measurements of Heat Transfer Coefficient, CHF and Heat Transfer Deterioration in Flows of CO_2 at Near-critical and Supercritical Pressures, 6th International Symposium on Supercritical Water-Cooled Reactors (ISSCWR-6), Shenzhen, China, March 3-7, 2013.

Zwolinski, S., M. Anderson, M. Corradini and J. Licht. Evaluation of Fluid-to-Fluid Scaling Method for Water and Carbon Dioxide at Supercritical Pressure, 5th International Symposium on Supercritical Water-Cooled Reactors (SCWR5), Vancouver, Canada, March 2011.

CHAPTER 6

DEVELOPMENT OF A MULTI-FLUID TRANSCRITICAL HEAT TRANSFER LOOK-UP TABLE

6.1 Introduction

The available water data do not span the full ranges of flow conditions of interest for the TC LUT. Two options are available for covering the TC LUT regions for which water data do not exist: (i) employing the predictions from the skeleton table, that are based primarily on SCHT correlations, or (ii) using the University of Ottawa carbon dioxide database after scaling the data to water conditions. The primary objective for development of the multi-fluid TC LUT (referred to as the multi-fluid table) is the expansion of the TC LUT water database by including experimental data obtained in model fluids at conditions, for which water data are unavailable. A second objective of the multi-fluid table is the development of a look up table capable of predicting trans-critical heat transfer for fluids other than water. Note that, in Chapter 5, the developed scaling laws, which were referred to as "the alternative scaling laws" with Equations (16) − (21) and (24), are applicable to water, CO_2 and R-134a and will be used in this chapter for converting the CO_2 data into water-equivalent values and *vice versa*. In Chapter 5 we also indicated that the recommended alternative scaling laws are valid for normal heat transfer (NHT) (defined in Section 3 of Chapter 5). Consequently only NHT data will be used in the construction of the multi-fluid table. The multi-fluid table is applicable directly to water for normal or abnormal heat transfer, however, its application to fluids other than water is accomplished with the use of the alternative scaling laws for conversion of flow conditions of the model fluid to water-equivalent values and *vice versa*. As a result, the application of this multi-fluid table to modeling fluids is restricted to NHT conditions.

This chapter is organized as follows: Section 6.2 shows the development steps of the multi-fluid table; Section 6.3 compares parametric trends of the updated and smoothened multi-fluid table; Section 6.4 presents results of uncertainty analyses including distributions of the uncertainty numbers of the multi-fluid table in different heat transfer regions and comparisons against leading prediction methods**.** Section 6.5 presents comparisons of HTC variations for the multi-fluid table, experimental data in water and CO_2, and leading SCHT prediction methods; and Section 6.6 discusses the subdivision of the multi-fluid TC LUT into regions according to the corresponding uncertainty levels, which have been indicated by different colours.

How to use the multi-fluid table*:* To predict HTC using the multi-fluid table, one should follow the following procedure. If the fluid is water, then the use of scaling laws is skipped; otherwise, flow conditions of the model fluid of interest, in terms of the multi-fluid table input parameters, should be transformed into their water-equivalent values using the alternative scaling laws. The multi-fluid table then provides a water-equivalent HTC. The value of the HTC from the multi-fluid table at water-equivalent conditions should subsequently be scaled back into conditions of the model fluid using the same scaling laws. An example of how to use the multi-fluid table for predicting HTC in CO_2 is presented in Appendix E.

6.2 Development of a multi-fluid TC LUT

The University of Ottawa CO_2 database of NHT for the 8 mm tube with 5481 data points was scaled to water conditions using the alternative scaling method, described earlier. These data were then used to fill some gaps in the water database in regions where water data are unavailable. Normal heat transfer data of CO_2 at high subcritical and SC pressures were identified based on the method discussed in Chapter 5, Section 3 and transformed into their water-equivalent values using the alternative scaling method. Since these scaling laws require identical geometries, only the 8 mm tube data were used in the table construction. The selected NHT data were relatively smooth and did not require scatter reduction (which was an essential process for the water data prior their incorporation into the TC LUT). The smoothened TC LUT developed in Chapter 3 for vertical upward flows and uniform heat fluxes was considered as the skeleton table for the multi-fluid LUT; therefore parameter ranges and their matrix (LUT regions) for the multi-fluid LUT remained the same as those of the TC LUT. Also, the tube diameter correction factor for the multi-fluid LUT remained unchanged from the original TC LUT table ($h \sim d^{-0.2}$). The applied methods for estimation of local HTC slopes and the incorporation of experimental data are as described earlier in Chapter 3, Section 4.3. This skeleton table was improved by the incorporation of the water-equivalent CO_2 data of the 8 mm tube in regions where water data were unavailable. Some of these water equivalent data did not fall within the range of parameters of the multi-fluid skeleton table, and were therefore not used (475 points). Also 2933 scaled data points were not used as water data existed in their range of conditions. The total number of scaled water data points incorporated in the skeleton table is 2073. However, most of the remaining scaled water data (2933 points) were subsequently used in the error analysis of the final multi-fluid table as will be shown in Section 6.4. The smoothing procedure applied to the water TC LUT (described in Chapter 3, Section 4.1 and 4.4) was also used for the present table, the Gaussian smoothing kernel was applied for smoothing the multi-fluid table trends in its four directions. The smoothing process was also controlled by the width of the smoothing window (see Chapter 3, Section 4.4), however, for the present multi-fluid table, the window width was narrower than the one used for smoothing the TC LUT. The final values of σ were 0.9, 0.8, 0.9 and 1.2 for the P, G, ΔT_w, and H_b directions, respectively. As a result, the smoothened trends were practically curve fitting approximations, especially in the heat transfer enhancement and deterioration regions; this will be demonstrated by comparing trends of the updated and smoothened multi-fluid table, and the uncertainty analysis. The complete multi-fluid table is presented in Appendix F. The table average error (or bias) was reduced to zero using the same off-setting procedure described in Chapter 3.

6.3 Parametric trends of the multi-fluid table

This section compares the parametric trends in two versions of the multi-fluid table: the updated and the smoothed table. The updated multi-fluid table is based on the TC LUT, which was updated with scaled water data. The parametric trends of the updated table and the smoothened multi-fluid trans-critical LUT for identical parameter ranges are shown in Figures 6.1 – 6.4. In general, the differences between the data-fit table (which is the skeleton table updated with water-equivalent CO_2 data) and the final multi-fluid table are small. In these figures, symbols refer to the data-fit table at the grid points for each parameter and solid lines refer to the final smoothened TC LUT. Figure 6.1 shows an example of smoothing in the pressure direction at G = 1000 kg/m^{2}s, ΔT_w = 20 K and H_b = 2150 kJ/kg. Here the variation of HTC in the P direction is shown for the data-fit LUT and the final TC LUT. Similarly, Figures 6.2, 6.3 and 6.4 show respectively the variations of HTC in the G, ΔT_w and H_b directions for the data-fit LUT and the final TC LUT. LUT conditions for these figures are given in the figures captions.

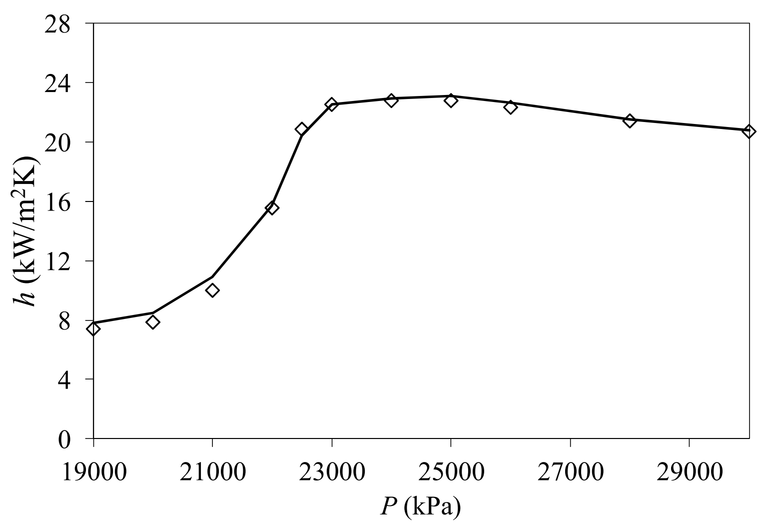

Figure 6.1: Variation of HTC in the P direction in the data-fit LUT (symbols) and final TC LUT (solid lines). G = 1000 kg/m^{2}s, ΔT_w = 20 K and H_b = 2150 kJ/kg.

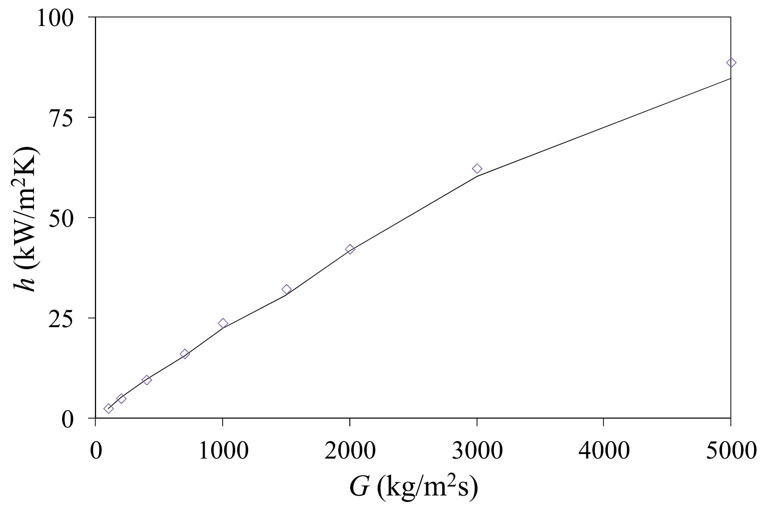

Figure 6.2: Variation of HTC in the G direction in the data-fit LUT (symbols) and final TC LUT (solid lines). P = 25 MPa, ΔT_w = 10 K and H_b = 2400 kJ/kg.

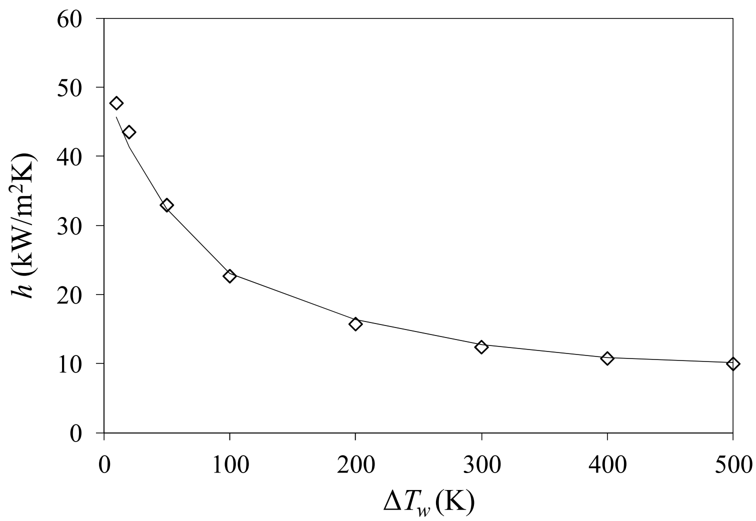

Figure 6.3: Variation of HTC in the ΔT_w in the data-fit LUT (symbols) and final TC LUT (solid lines). P = 21 MPa, G = 3000 kg/m^{2}s and H_b = 2300 kJ/kg.

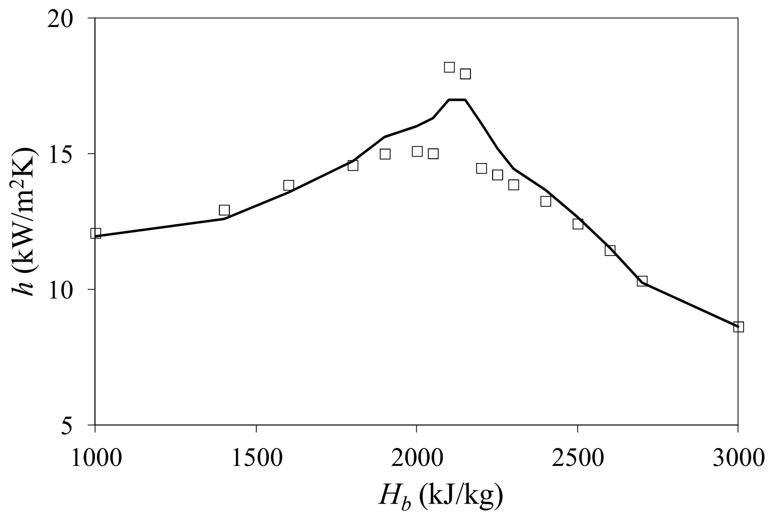

Figure 6.4: Variation of HTC in the H_b direction in the data-fit LUT (symbols) and final TC LUT (solid lines). P = 26 MPa, G = 1000 kg/m^{2}s and ΔT_w = 50.

6.4 Uncertainty analysis of the multi-fluid TC LUT

Evaluation method: The smoothened multi-fluid TC LUT was first applied to scaled data only, namely, all 8 mm tube NHT CO_2 data at water equivalent conditions that fell within the range of parameters of the skeleton table (5006 points - case (i)). Subsequently, the table was applied to the full multi-fluid table database, which includes the original water data and the CO_2 data scaled to water (case (ii)).

In case (i), as discussed earlier, only 2073 of the 5006 NHT data points were used in the data-fit table, while the remaining 2933 data points were rejected, because they corresponded to conditions for which water data existed, so they were not used at all in the table construction. However, all data were used in the current uncertainty assessment of the multi-fluid table. The multi-fluid table was applied to the 5006 scaled data points to water equivalent conditions. The predicted HTCs by the multi-fluid table were *then converted back into their original CO_2 conditions using the alternative scaling method, and compared to the corresponding experimental HTCs in CO_2*. The uncertainty analysis presented in Table 6.1 shows the results of this calculation procedure. In case (ii) the multi-fluid database (18016 data points) was used in this uncertainty analysis. Tables 6.2

– 6.5 show the results based on this multi-fluid database, these two cases will be discussed further in the remainder of this section.

Because the multi-fluid database includes scaled data, the reported error analysis includes also the uncertainty of the used scaling laws, except for the SC gas-like and the subcritical superheated steam regions where water-equivalent CO_2 data did not exist (this is indicated in the footnotes of Tables 6.3 and 6.4). When using water-equivalent CO_2 data, one can anticipate that the uncertainty of the leading correlations discussed in Chapter 3 will increase slightly. This increase is attributed to, firstly, the difference in fluid type between these correlations reference water database (all these correlations were developed based on water data) and the used CO_2 data and, secondly, the uncertainty of the scaling method[8] itself which is included in the scaled data values. It is also expected that, compared to the TC LUT (which was based only on water data), the multi-fluid table would have a slightly larger uncertainty, if applied only to water data; this is because the values of HTCs of the multi-fluid table were subjected to an additional smoothing process described in Section 6.2.

Results: The overall average error e_{avg} and the root mean square error e_{rms} in HTC (defined in Chapter 3), as estimated by the current multi-fluid table, for these two cases are as follows.

Case (i): The uncertainty values are presented in Table 6; although they include the scaling law uncertainty, the e_{rms} values are relatively small and even slightly smaller than those of the scaling laws uncertainty, because a significant portion (40%) of these scaled data were used in the table construction[9] in regions where no water data were available and the original carbon dioxide data are in NHT mode, for which most likely the smoothing process did not affect significantly their corresponding normalized values

[8] Scaling law uncertainty was estimated in Chapter 3 and found, in terms of root mean square error, to be 10% for the subcritical pressure region, 15% for the SC pressure region, and 14% for the entire trans-critical heat transfer region.

[9] Unlike the case when the alternative scaling laws were developed and assessed based on the TC LUT, which is not based on any CO_2 data, the uncertainty of the alternative scaling laws would be expected to be higher than those reported in Table 6.1.

in the table. Therefore, it was expected that the multi-fluid table would agree fairly well with the scaled CO_2 NHT data. This table shows e_{avg} and e_{rms} for the high subcritical and SC pressure region; numbers in square brackets indicate the amount of experimental data in the corresponding region.

Case (ii): This case was based on the entire multi-fluid database with 18016 points, which include 13010 water data points and 5006 scaled water data points. These results are presented in Tables 6.2 – 6.5. Table 6.2 shows a summary of the uncertainty numbers for all data in the high subcritical and the SC pressure regions, while Table 6.3 compares the errors for the leading three SCHT correlations and the current multi-fluid table in the liquid-like, gas-like and close to critical or pseudo-critical point region. In addition, Table 6.4 shows uncertainties for the single-phase, high-subcritical pressure liquid and superheated steam regions, where different correlations were applied. In summary, Tables 6.3 and 6.4 show that the multi-fluid table has the lowest rms error for the three SC regions and the high subcritical pressure regions. Table 6.5 shows percentages of the SC multi-fluid data (16245 data point) as predicted by the most accurate correlations and the smoothened multi-fluid LUT within error bands of +10% (e_{10}), +20% (e_{20}), +30% (e_{30}), and +50% (e_{50}) for the various supercritical subregions. This table shows that larger numbers of data, within the specified error bands, were predicted by the current multi-fluid table than those by the leading correlations in different SCHT regions.

Table 6.1: Overall average and rms error of the multi-fluid LUT (CO_2 NHT database).

Current smoothed multi-fluid LUT	All trans-critical data [5006][10]		SC data [3952]		Subcritical data [1054]	
	e_{avg} (%)	e_{rms} (%)	e_{avg} (%)	e_{rms} (%)	e_{avg} (%)	e_{rms} (%)
Data without scatter removal	0.0	10.4	0.17	10.7	-0.6	9.2

Table 6.2: Overall average and rms error of the multi-fluid LUT (multi-fluid database).

Current smoothed LUT	All trans-critical data [18016]		SC data [16245]		Subcritical data [1771]	
	e_{avg} (%)	e_{rms} (%)	e_{avg} (%)	e_{rms} (%)	e_{avg} (%)	e_{rms} (%)
Data without scatter removal	0.0	15.6	0.6	15.9	-1.0	11.4
Data with scatter removal	0.0	14.4	0.34	14.6	-2.1	11.3

Table 6.3: Average and rms errors in the three supercritical regions (multi-fluid database).

Prediction method	Liquid-like region [2038]		Gas-like Region [3075]*		Close to Cr. or PC point region [11132]	
	e_{avg} (%)	e_{rms} (%)	e_{avg} (%)	e_{rms} (%)	e_{avg} (%)	e_{rms} (%)
Swenson et al. (1965)	2.1	15.3	-14.3	19.6	4.1	22.0
Mokry et al. (2008)	1.7	14.1	-7.3	15.2	-1.3	16.9
Gupta et al. (2010)	-14	19.2	-10.4	18.5	-1.8	17
Current smoothened LUT	1.2	13.1	1.8	13	-1.9	16.8

* Gas-like region does not include scaled data.

[10] Numbers in brackets refer to number of data used.

Table 6.4: Overall average and rms error in the high-pressure sub-critical region (multi-fluid database).

Correlation	Subcritical liquid [1211]		Superheated steam [560]*	
	e_{avg} (%)	e_{rms} (%)	e_{avg} (%)	e_{rms} (%)
Dittus-Boelter (1930)	22	24	73.1	123.1
Sieder and Tate (1936)	37	39	81	132.1
Hadaller and Banerjee (1969)	40.5	42	18.4	32.1
Gnielinski (1976)	8.7	14	79.1	126.3
Mokry et al. (2009)	13.8	15.6	-5.0	17.4
Current smoothened LUT	-0.7	10.5	-1.7	13.1

* Superheated steam region does not include scaled data.

Table 6.5: Error bands for the smoothened multi-fluid table and best correlations.

Error band for 11132 points	Percentage of data predicted by a correlation (%)			
	Mokry et al. (2009)	Gupta et al. (2010)	Swenson et al. (1965)	Current LUT
Near critical. or pseudocritical point region				
e_{10}	46	50	43	46
e_{20}	77	78	70	81
e_{30}	91	93	86	93
e_{50}	100	99	96	100
Error band for 2038 points	Mokry et al. (2009)	Bishop et al. (1965)	Kuang et al. (2008)	Current LUT
High density state region (liquid-like region)				
e_{10}	64	14	45	62
e_{20}	88	68	73	90
e_{30}	95	92	92	96
e_{50}	99	99	99	100
Error band for 3075 points	Mokry et al. (2009)	Gupta et al. (2010)	Bishop et al. (1965)	Current LUT
Low density state region (gas-like region)				
e_{10}	51	36	46	57
e_{20}	82	73	77	88
e_{30}	95	91	90	97
e_{50}	100	99	97	100

6.5 Graphical comparisons of table HTC trends against correlations and experimental data

In the following figures, predictions of the smoothened multi-fluid TC LUT were compared to experimental data in water and CO_2 and to the predictions of several leading correlations. The water data of Shitsman (1963) were plotted in Figure 6.5 ─ these data show local deterioration in HTC as discussed in Chapter 3. This figure compares HTC profiles (top plot) and the corresponding wall temperatures (bottom) of experimental data and those predicted by the Mokry et al. (2009) correlation, the TC LUT and the current multi-fluid table. The predictions of the multi-fluid table in solid black line follow the experimental trend and the predicted profile by the TC LUT. The agreement with data in terms of wall temperatures is obvious for both the multi-fluid and the TC LUT. Similarly, in terms of HTC profiles, the agreement between the predictions of these two tables and the data is also clear, however, the multifluid table shows slightly worse agreement with the data than the TC LUT at the inlet of the heated section and in the proximity of the pseudo-critical enthalpy. In general, the minmum in HTC was overestimated and the maximum was underestimated.

The predictions of the multi-fluid TC LUT were also compared graphically with Jackson's (2009) correlation (which was based on CO_2 data) and the UO CO_2 data. The NHT data compilation of the 8 mm tube is used in Figures 6.6 to 6.9 ─ these figures show pairs of plots: at the top for HTC, while at the bottom the corresponding T_w values. Figures 6.6 and 6.7 show the predictions of the multi-fluid table and Jackson's (2009) correlation in the SC region, while Figures 6.8 and 6.9 show the multi-fluid table predictions in the high-pressure subcritical region. The experimental data of Figure 6.6 were obtained at a pressure close to the Canadian SCWR nominal operating pressuure P/P_c = 1.14. In terms of HTC profiles, this figure and Figure 6.7 show good agreement between the table prediction and the experiment; this agreement is slightly better than that between Jackson's (2009) correlation and experiment. Clearly, the two figures show excellent agreement in T_w as predicted by both the multi-fluid table and Jackson's (2009) correlation and experiment. In Figure 6.8 (high subcritical pressure), the HTC profile of the multi-fluid table and the experiment are in good agreement. Good agreement with the LUT was also observed in Figure 6.9 for the carbon dioxide data at P/P_c = 0.94, although the slightly increasing experimental trend of HTC with H_b was not predicted by the table. Note also the excellent agreement in wall temperature profiles of the multi-fluid table and the experiment shown in Figures 6.8 and 6.9.

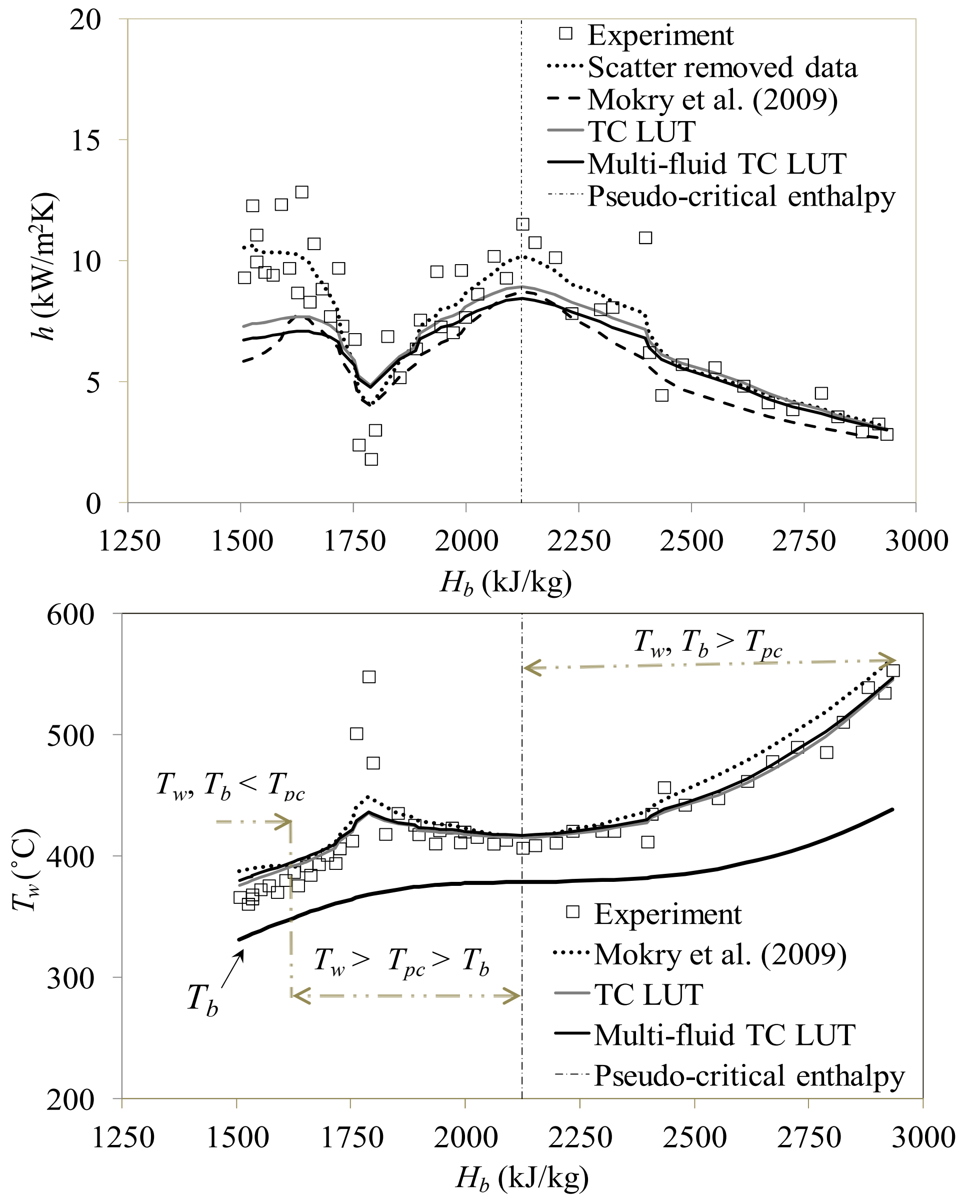

Figure 6.5: Comparison of h (top) and T_w (bottom) as predicted by the current multi-fluid TC LUT, TC LUT, Mokry et al. (2009) correlation and experiment by Shitsman (1963); P = 23300 kPa, G = 430 kg/m^{2}s, q = 326 kW/m^2, d = 10 mm.

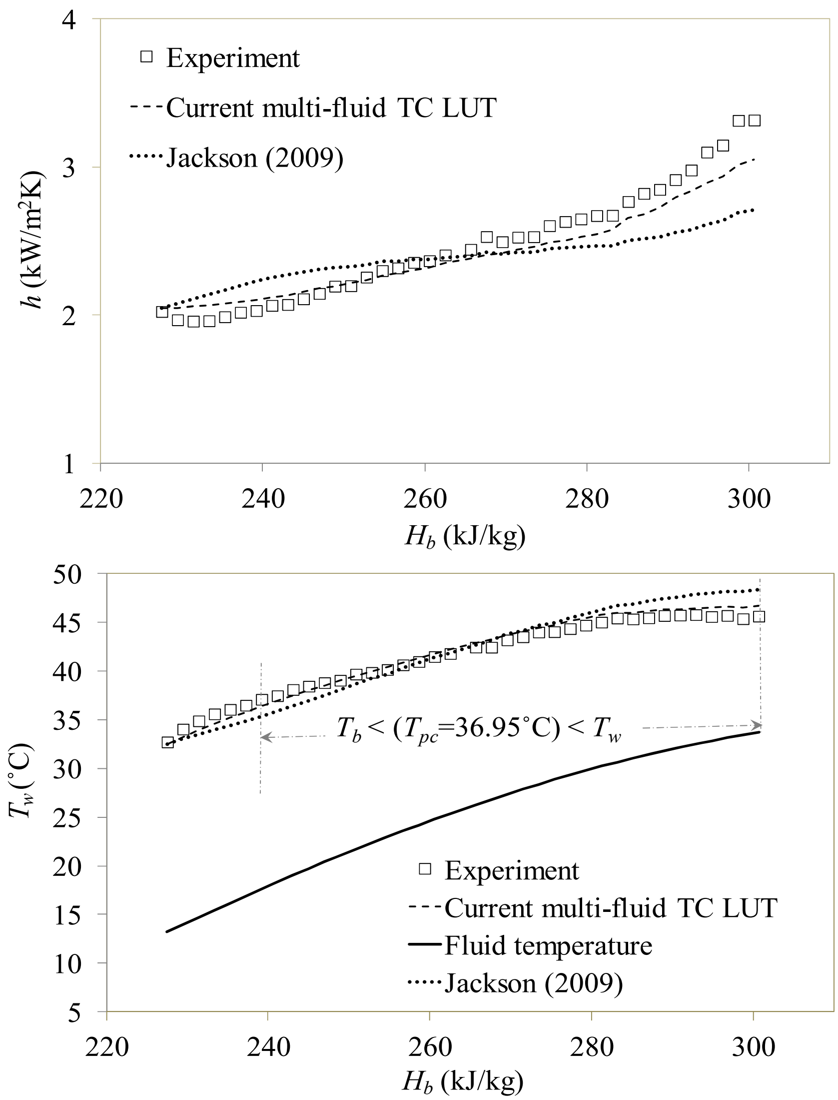

Figure 6.6: Comparison of h (top) and T_w (bottom) as predicted by the current multi-fluid TC LUT, Jackson (2009) correlation and experiment. University of Ottawa carbon dioxide database for NHT; P/P_c = 1.14, G = 508 kg/m^{2}s, q = 39.5 kW/m^2, T_{in} = 12.4˚C, T_{pc} = 36.95˚C.

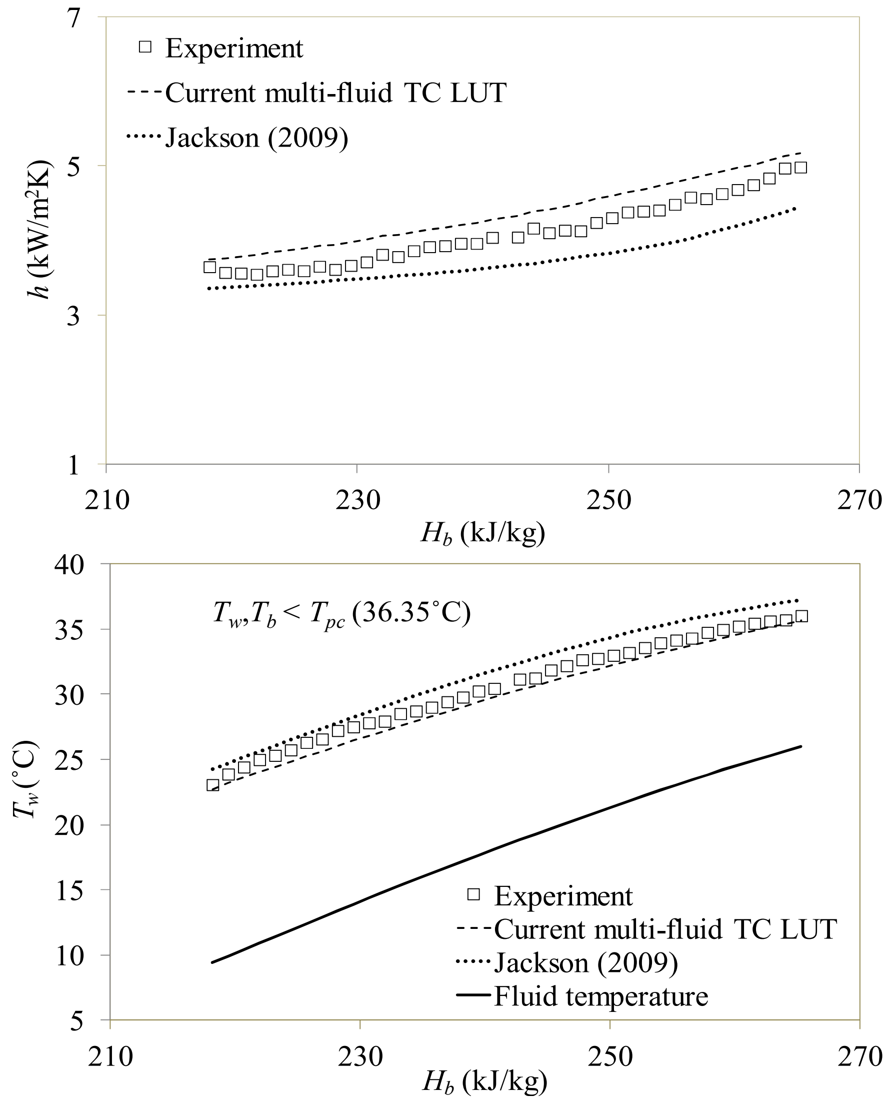

Figure 6.7: Comparison of h (top) and T_w (bottom) as predicted by the current multi-fluid TC LUT, Jackson (2009) correlation and experiment. University of Ottawa carbon dioxide database for NHT; $P/P_c = 1.27$, $G = 995$ kg/m^{2}s, $q = 50$ kW/m^2, $T_{in} = 8.8$˚C, $T_{pc} = 36.35$˚C.

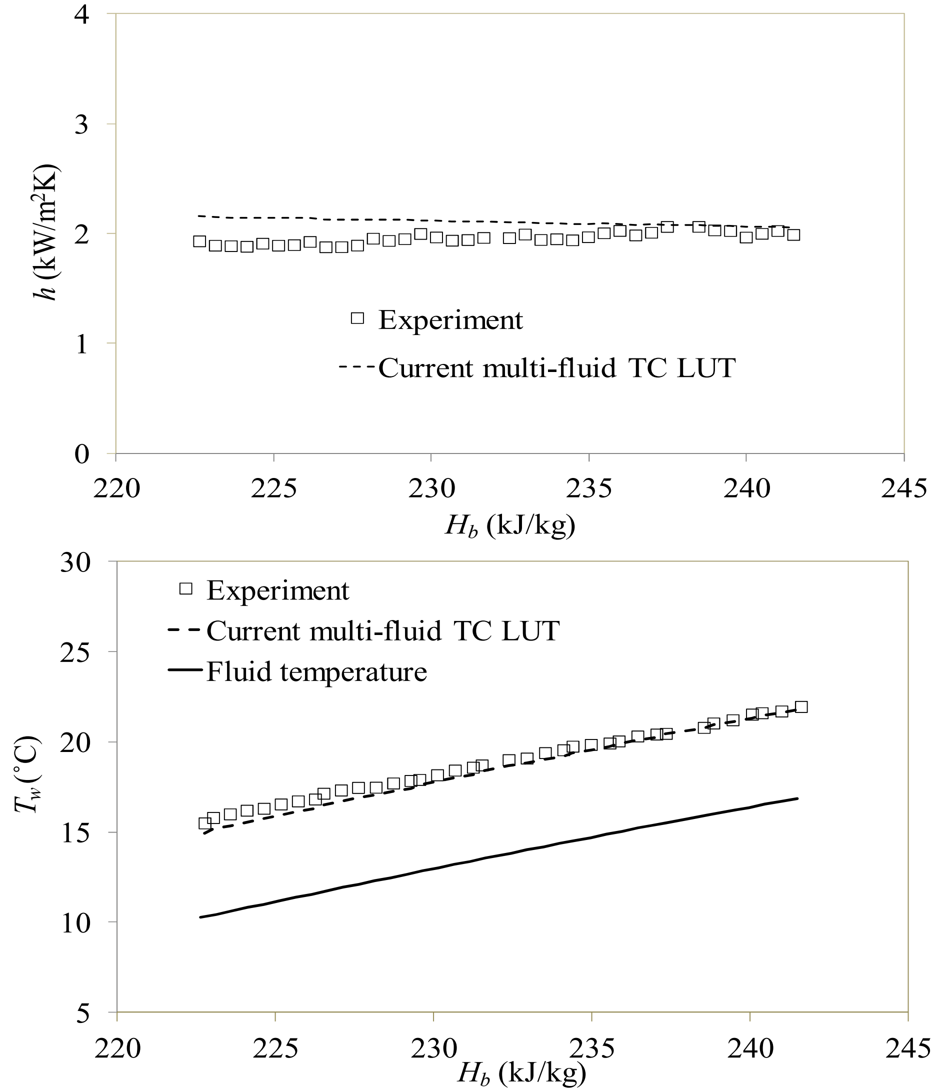

Figure 6.8: Comparison of h (top) and T_w (bottom) as predicted by the current multi-fluid TC LUT and experiment. University of Ottawa carbon dioxide database for NHT; P/P_c = 0.88, G = 506 kg/m^{2}s, q = 10.1 kW/m^2, T_{in} = 10.1˚C, T_{sat} = 25.6˚C.

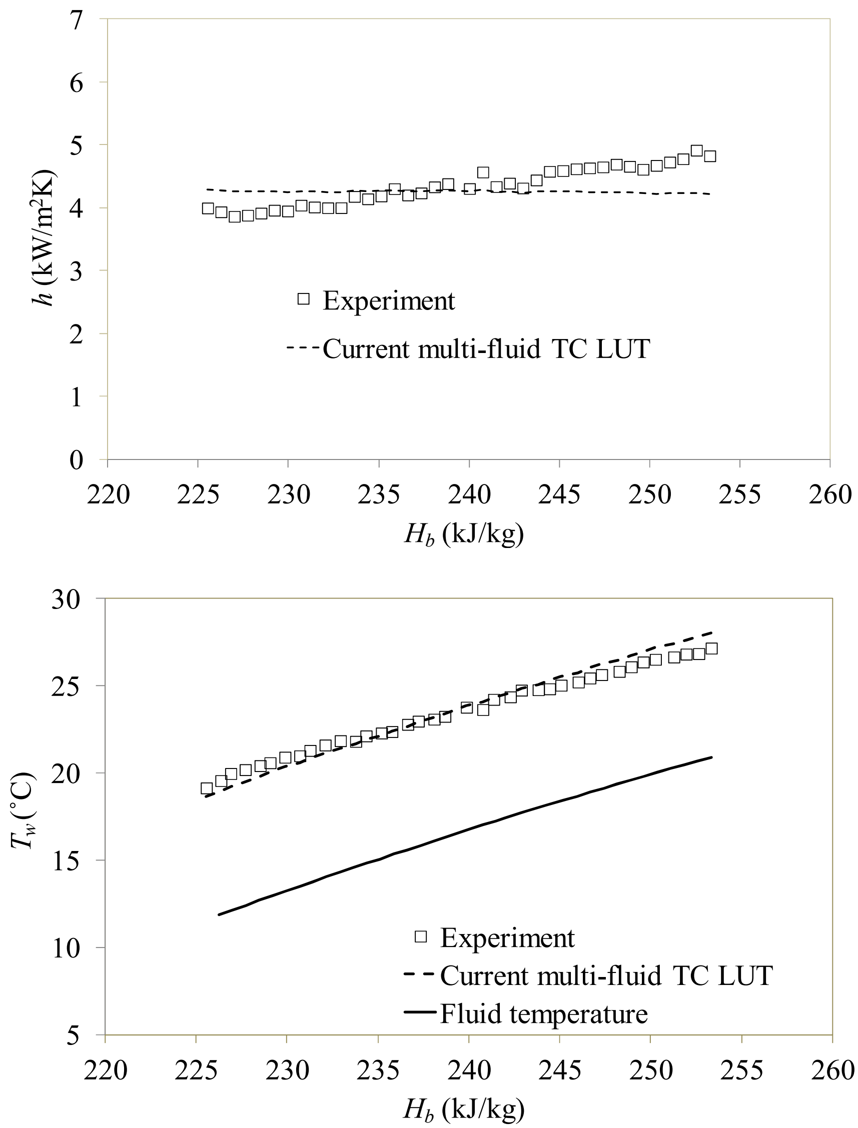

Figure 6.9: Comparison of h (top) and T_w (bottom) as predicted by the current multi-fluid TC LUT and experiment. University of Ottawa carbon dioxide database for NHT; P/P_c = 0.94, G = 1021 kg/m^{2}s, q = 30.2 kW/m^2, T_{in} = 11.3˚C, T_{sat} = 28.2˚C.

6.6 Identification of heat transfer regions according to table uncertainty

Groeneveld et al. (2005), in presenting their critical heat flux LUT, used a colour coding approach to indicate regions of different uncertainties. A similar procedure was used for the multi-fluid LUT: each of the heat transfer coefficient regions in the multi-fluid LUT has been marked with a specific colour according to the source of its HTCs. Three categories have been distinguished: (i) LUT regions based on experimental water data were highlighted in blue, (ii) other regions based on water equivalent CO_2 data were coloured in yellow, and (iii) the remaining regions, which are based on the 'best' prediction methods, were left uncoloured. This categorization implies that the lowest uncertainty should exist in the LUT regions that were based on water data (category i). A slightly larger uncertainty would be present for the category (ii) regions, which were based on water equivalent CO_2 data. The largest uncertainty would correspond to the category (iii) subregions, which were based only on 'best' heat transfer prediction methods (Zahlan et al., 2011; see also Chapter 3, Section 3). Note that, although the uncoloured subregions show estimated HTC values based on 'best' prediction methods, it is expected that the uncoloured subregions directly adjacent to the experimental data-based regions would have a relatively small uncertainty. This is because the LUT value in these transition regions is based on extrapolations from data-based regions. A section of the multi-fluid table is presented in Table 6.6, which shows the three colour-coded uncertainty regions.

Multi-fluid table uses: The developed trans-critical heat transfer look-up table can be used for the prediction of heat transfer coefficient for different fluids. With the application of the alternative scaling method, it provides a useful and easy-to-use method for scaling experimental conditions between different fluids and prediction of heat transfer for a wide range of flow conditions. It can be viewed as a more general heat transfer prediction method compared to existing correlations and tables; the multi-fluid table should be accurate for wide ranges of conditions, including the near critical and supercritical heat transfer regions and different fluids. It is suitable for use in thermal design and safety studies.

Table 6.6: A section of the coloured-coded[11] version of the multi-fluid trans-critical LUT.

P kPa	G kg/m^{2}s	ΔT_w K	H_b, kJ/kg																
			1000	1400	1600	1800	1900	2000	2050	2100	2150	2200	2250	2300	2400	2500	2600	2700	3000
22500	1000	10	15.4	15.1	17.3	20.8	23.1	24	24.4	24.7	25.3	26.1	26.4	25.5	23.2	19.9	16.3	12.8	9.33
		20	14.1	13.5	15	17.4	19	19.6	19.9	20.1	20.5	21	21.4	21.1	19.7	17.6	15	12.2	9.02
		50	11.8	11.9	12.4	13	13.3	13.6	14.1	14.3	14.5	14.5	14.8	14.9	14.6	13.7	12.3	10.6	8.34
		100	8.8	8.86	8.75	8.61	8.55	8.74	9.17	9.43	9.46	9.37	9.51	9.74	9.78	9.59	9.14	8.35	7.16
		200	5.89	5.97	5.86	5.69	5.59	5.63	5.79	5.93	6.05	6.17	6.35	6.52	6.6	6.6	6.48	6.2	5.69
		300	3.73	3.98	4.03	3.99	3.97	4.01	4.13	4.29	4.48	4.68	4.87	4.99	5.03	5.01	4.94	4.81	4.59
		400	2.57	2.76	2.88	2.97	3.08	3.25	3.45	3.66	3.88	4.08	4.24	4.33	4.34	4.31	4.24	4.15	4.02
		500	2.15	2.27	2.39	2.53	2.71	2.93	3.17	3.41	3.63	3.82	3.96	4.03	4.04	4.01	3.96	3.89	3.79
	1500	10	21.4	18.9	22.6	28.6	32	33.2	33.7	34.3	35.3	36.7	37.5	36.4	33.2	28.6	23.9	19.4	15.1
		20	19.7	16.7	19.3	23.7	26.2	27.1	27.8	28.5	29.1	29.6	30.1	29.8	28	25.1	21.7	18.2	14.4
		50	16.3	15.9	16.7	17.8	18.4	19.6	22.1	23.7	23.4	21.7	20.9	21	20.6	19.4	17.6	15.4	12.7
		100	12	12.1	12.1	12	12	13	15.5	17.1	16.6	14.6	13.7	13.8	13.9	13.6	13	12	10.4
		200	7.81	7.92	7.92	7.87	7.88	8.18	8.86	9.39	9.47	9.2	9.17	9.33	9.4	9.34	9.15	8.76	8.04
		300	4.89	5.07	5.19	5.3	5.46	5.7	5.99	6.29	6.57	6.82	7.02	7.12	7.12	7.05	6.94	6.74	6.4
		400	3.48	3.63	3.79	3.98	4.24	4.56	4.91	5.24	5.55	5.82	6.01	6.1	6.09	6.03	5.94	5.8	5.61
		500	2.98	3.11	3.27	3.48	3.76	4.1	4.45	4.79	5.1	5.36	5.55	5.64	5.64	5.59	5.52	5.42	5.29
	2000	10	26.7	26.7	32.4	40.6	45.1	45	45.2	46.7	48.7	50.5	51.2	49.4	45.1	39.7	34.8	30.3	25.1
		20	24.4	23.8	27.8	33.4	36.4	36.2	36.7	38.2	39.5	40.3	40.7	40.1	37.9	34.6	31.1	27.3	22.3
		50	20.3	21.1	22.9	24.6	25.4	26.1	28.9	32.3	32.9	30.5	28.5	28	27.4	25.9	23.8	21.2	17.7
		100	15.1	15.7	16.4	16.7	16.6	17.2	20.2	23.8	24.2	21.3	19.1	18.6	18.4	17.9	16.8	15.3	13.1
		200	9.65	9.98	10.3	10.5	10.6	11	11.9	13.1	13.5	13.1	12.8	12.8	12.7	12.4	11.9	11.1	9.85
		300	6.16	6.39	6.65	6.95	7.31	7.74	8.22	8.7	9.16	9.54	9.81	9.89	9.8	9.61	9.35	8.95	8.32
		400	4.61	4.79	5.03	5.34	5.74	6.22	6.73	7.22	7.67	8.06	8.32	8.43	8.4	8.29	8.13	7.92	7.61
		500	4.05	4.22	4.44	4.75	5.14	5.61	6.1	6.57	7	7.37	7.63	7.75	7.75	7.68	7.58	7.44	7.24
	3000	10	36.6	40.1	51.1	67.4	75.8	69.7	66.4	68.3	70.8	72.4	72.3	69.1	62.7	54.8	47.1	39.7	31.4
		20	33.5	35.9	44.3	56.5	62.9	57.1	53.8	55.1	56.5	57.5	57.9	56.6	53.1	47.9	42.2	36	28.5
		50	28	31.5	37.3	42.5	44.1	41.9	42.1	44.5	43.9	41.8	40.5	39.9	38.6	36.1	32.6	28.5	23.3
		100	20.8	23	26.2	28.2	28	27.4	29.9	33.6	32.7	29.8	27.7	27	26.4	25.3	23.5	21.1	18.1
		200	13.3	14.1	15.1	15.8	16.2	16.5	17.7	19.2	19.5	19.3	19.1	19	18.7	18.1	17.2	16	14.2
		300	8.73	9.08	9.5	9.99	10.6	11.3	12	12.8	13.5	14.1	14.5	14.6	14.4	14.1	13.7	13.1	12.2
		400	6.66	6.92	7.27	7.74	8.34	9.05	9.81	10.5	11.2	11.8	12.2	12.3	12.3	12.1	11.9	11.5	11.1
		500	5.86	6.12	6.45	6.9	7.48	8.16	8.88	9.57	10.2	10.7	11.1	11.3	11.3	11.2	11	10.8	10.5
	5000	10	50.7	57.7	69.8	87.3	98	95	94.2	97.5	99.9	100	98.8	94.2	85.6	73.8	60.4	46.1	30.6
		20	46.9	53.4	62.6	76	84.4	80.8	78.5	80	81.2	81.9	82	79.9	74.4	65.7	55	42.9	29.3
		50	38.8	45.8	54.2	61.6	65.2	63.8	62.3	62.1	59.8	58.8	59.3	58.8	56.1	51.1	44.3	36.3	26.8
		100	27.8	32.3	38.4	42.9	45	45.4	46.6	46.9	42.5	40.3	40.5	40.3	39	36.6	33.2	29	23.6
		200	17.9	19.4	21	22.5	23.7	24.9	26.4	27.6	27.4	27.6	28.1	28.1	27.5	26.4	25	23	20.5
		300	12.4	12.8	13.3	14	15	16.2	17.5	18.7	19.8	20.7	21.4	21.5	21.3	20.8	20.1	19.2	18
		400	9.84	10.2	10.6	11.3	12.2	13.3	14.4	15.5	16.5	17.4	17.9	18.2	18.1	17.9	17.5	17.1	16.4
		500	8.72	9.05	9.52	10.2	11	12.1	13.1	14.1	15.1	15.9	16.4	16.7	16.7	16.5	16.3	16	15.6

[11] Blue corresponds to water data-based regions with the highest prediction accuracy, yellow to regions which are based on scaled water data from CO_2 with slightly lower accuracy and the blank to regions from selected correlations with the smallest accuracy.

CHAPTER 7

CONCLUSION

7.1 Summary

This study proposed two new look-up tables capable of predicting normal and abnormal heat transfer in tubes. The range of application of these two look-up tables covers not only the supercritical pressure region but also the high subcritical and near-critical pressure regions. The two tables predict convective HTC in tubes for water and other fluids flowing vertically upward. The first look up table, the TC LUT, applies to water and can predict different heat transfer modes including enhancement and deterioration. The second table, the multi-fluid look up table, in conjunction with newly proposed scaling laws can predict normal heat transfer for fluids other than water. It can also predict normal and abnormal heat transfer for water directly without the use of scaling laws like the TC LUT. When compared to existing prediction methods, the TC LUT and the multi-fluid table have a much wider range of application, higher prediction accuracy, and a capability to reproduce more closely the experimental trends. In addition, in contrast to previous methods, the tables are capable of predicting deteriorated heat transfer for water. With the application of a correction factor for the tube diameter effect, the tables can be used for flows in tubes having a fairly wide range of diameters.

A large trans-critical heat transfer databank for water-cooled tubes was compiled at University of Ottawa. It included, in addition to the University of Ottawa data compilation, three other compilations from different universities. This is believed to be the world's largest trans-critical databank. The databank was subsequently screened for duplicates, unreliable data and outliers.

The trans-critical databank was used for comprehensive assessment of all promising single phase and supercritical heat transfer correlations; those correlations, which could closely represent the experimental data, were identified and used in the subsequent construction of the TC LUT, which was based on the heat transfer water databank compiled at University of Ottawa.

Careful screening of the trans-critical water databases used for the construction of the TC LUT and the application of data scatter reduction and HTC smoothing procedures were found to improve measurably the accuracy of the look-up table.

A series of original heat transfer experiments in CO_2 flowing vertically upward in 8 and 22 mm tubes were conducted to model water behaviour at conditions equivalent to those of interest for the SCWR and have been reported. The pressure drop measurements for the 8 mm tube are reported as well. The present carbon dioxide data were used to develop and improve fluid-to-fluid scaling methods for high subcritical and supercritical pressure and, after conversion to water-equivalent data, to supplement the water database for conditions for which water data were not available.

The UO supercritical CO_2 heat transfer data showed good agreement with data from previous investigators obtained at similar experimental conditions, thus demonstrating the reproducibility of such measurements. An examination of various parametric trends (pressure, mass flux, heat flux, inlet temperature and diameter) on the HTC and wall temperature *vs.* bulk enthalpy profiles has been made for conditions equivalent to those of interest to SCWR. In general, the friction factor for convective flows at high subcritical and supercritical pressure exceeded that for incompressible flow at low subcritical pressures and seemed to approach the incompressible value with increasing Reynolds number.

In this thesis, two sets of fluid-to-fluid scaling laws for supercritical heat transfer have been reviewed and two new scaling laws, which are based on an empirically adjusted version of the Dittus-Boelter correlation, have been proposed. The four scaling laws were applied to the collected carbon dioxide data in NHT mode to compute a water-equivalent heat transfer coefficient, which was compared to predictions of the trans-critical look-up table. These comparisons have demonstrated that, unlike the two earlier methods, which overestimate the heat transfer coefficient in water, the two proposed scaling methods introduce no bias, and have a precision uncertainty, which is significantly lower than those of the previous scaling methods.

An interesting phenomenon was observed at high subcritical and SC pressures in the 22 mm tube in the single phase liquid and liquid-like regions. Peaks in wall temperature profile were observed near the start of the heated length at very low heat and mass fluxes, where a monotonically increasing temperature profile was expected. This behaviour was attributed to buoyancy effects in the thermal entry region. The observed temperature peaks at subcritical pressures were suppressed by the occurrence of nucleate boiling.

7.2 Main contributions

A significant contribution of this work is the development of the TC LUT, which is applicable to high pressure subcritical and supercritical conditions. The TC LUT is capable of predicting the SCHT in the normal and deteriorated heat transfer regions. Compared to the prediction methods and experimental data, the uncertainty of the TC LUT was lower and the parametric trends of the table represented closely experimental data. It is expected that the TC LUTs will be used in thermal-hydraulic system codes for safety analysis of SCWR and in other applications like heat exchangers design.

This thesis provided high quality and original thermal-hydraulic measurements in CO_2 for wide range of conditions; these measurements were used in the development of new scaling laws and in the expansion of the TC LUT database. The database can be used to better assess the occurrence of heat transfer deterioration and enhancement.

As a result of this thesis investigation, new scaling laws have been proposed, applicable not only for the supercritical region like existing scaling methods, but also, and for the first time, for the high subcritical and near critical pressure region.

This study proposed also the multi-fluid table, which is based on the new scaling laws, and can be used for the prediction of heat transfer in water as well as other fluids for the same range of conditions covered by the TC LUT.

This research study shed light and provided a physical explanation from the literature to some abnormal behaviour of properties and the erroneous increase in thermal conductivities near the critical point.

This thesis has reported the existence of an interesting heat transfer phenomenon, referred to as the non-typical heat transfer phenomenon. This phenomenon was observed to occur during tube heat transfer experiments in CO_2 but only at low flows and very low heat fluxes.

7.3 Recommendations for future work

A further improvement of the table accuracy is possible by the incorporation of additional experimental results, as they become available. This will permit the identification of the regions of the LUT where significant heat transfer deterioration can occur. Identification of TC LUTs regions with severe heat transfer deterioration is recommended; corrections to account for over estimated HTC by the tables can be applied in these regions.

The use of empirical correction factors, which remain to be derived, will permit the extension of the present table to applications involving different channel geometries and flow orientations.

Further study of the non-typical heat transfer region is strongly recommended. This thesis has clearly demonstrated its occurrence but more detailed measurements are required to determine the boundaries over which this phenomenon can occur. Also, the possible existence of this phenomenon in other geometries (bundles, spacer-equipped geometries) should be investigated.

REFERENCES

Ackerman, J.W., “Pseudoboiling heat transfer to supercritical pressure water in smooth and ribbed tubes”, J. Heat Transfer, Trans. ASME, 92(3), pp. 490–498 (Paper No.69–WA/HT-2), 1970.

Alekseev, G.V., V.A. Silin, A.M. Smirnov and V.I. Subottin, “Study of the thermal conditions on the wall of a pipe during the removal of heat by water at a supercritical pressure”, High Temp., Vol. 14, No. 4, pp. 683–687, 1976.

Alferov, N.S., B.F. Balunov and R.A. Rybin, “Calculating heat transfer with mixed convection”, Therm. Eng., Vol. 22, No. 6, pp. 96–100, 1975.

Alferov, N.S., R.A. Rybin, and B.F Balunov, “Heat transfer with turbulent water flow in a vertical tube under conditions of appreciable influence of free convection”, Therm. Eng., Vol. 16, No.12, pp. 90–95, 1969.

Ambrosini, W. and M. De Rosa, “Application of similarity principles for heat transfer and fluid-dynamics to different fluids at supercritical pressure”, Proc. of the 5th Int. Sym. SCWR (ISSCWR-5), Vancouver, British Columbia, Canada, March 13–16, 2011.

Anglart, H., “Heat transfer deterioration in application to HPLWR – mechanisms identification and ranking table”, Proc. of the 4th Int. Sym. on SCWR (ISSCWR-4), March 8–11, 2009, Heidelberg, Germany.

Barulin, Yu. D., Yu.V. Vikhrev, and B.V. Dyadyakin, “Heat transfer during turbulent flow in vertical and horizontal tubes to supercritical water”, J. Eng. Phys., Vol. 20, No. 5, pp. 929–930, 1971.

Bazargan, M., “Forced convection heat transfer to turbulent flow of SCW in a round horizontal tube”, PhD Thesis, University of British Columbia, Canada, 2001.

Becker, K.M., C.H. Ling, , S. Heelberg and G. Strand, “An experimental investigation of post dryout heat transfer”, KTH-NEL-33, 1983.

Bishop, A.A., L.E. Efferding and L.S. Tong, “A review of heat transfer and fluid flow of water in the supercritical region and during “once-through” operation”, Report WCAP-2040, 106 pages, December,1962.

Bishop, A.A., R.O. Sandberg and L.S. Tong, “Forced convection heat transfer to water at near critical temperatures and supercritical pressures”, A.I.Ch.E.-I.Chem.E, Sym. Series No. 2, pp. 77–85, 1965.

Chatharaju, M., “Computational study of critical flow discharge in Supercritical Water Cooled Reactors, Master Thesis, McMaster University, Canada, 2011.

Cheng, X., X.J. Liu and H.Y. Gu, “Fluid-to-fluid scaling of heat transfer in circular tubes cooled with supercritical fluids”, Nucl. Eng. Des, Vol. 241, pp. 498–508, 2011.

Cheng, X. , X.J. Liu and H.Y. Gu, “Fluid-to-fluid scaling of heat transfer in supercritical fluids”, Proc. 2nd Canada-China Joint Workshop on Supercritical Water-Cooled Reactors, Toronto, Canada, April 25–28, 9 pages, 2010.

Cheng, X., Y.H. Yang and S.F. Huang, “A simple heat transfer correlation for SC fluid flow in circular tubes”, NURETH-13, Kanazawa City, Ishikawa Prefecture, Japan, September 27–October 2, 2009.

Cheng, X. and T. Schulenberg, “Heat transfer at supercritical pressures – Literature review and application to an HPLWR”, Tech. report FZKA 6609, Forschungs zentrum Karlsruhe, May 2001.

Chun, S.Y., C.H. Shin, S.D. Hong and C.H. Song, “Heat transfer characteristics near the critical pressure in a rod bundle cooled by R-134a fluid during pressure transient”, 4th Int. Sym. on SCWR, March 8–11, 2009, Heidelberg, Germany, 2009.

Deissler, R.G., “Heat transfer and fluid friction for fully developed turbulent flow of air and supercritical water with variable fluid property”, Transactions of the ASME, pp. 73–85, 1954.

Dickinson, N.L. and C.P. Welch, “Heat transfer to supercritical water”, Trans. ASME 80, pp. 746–752, 1958.

Dittus, F.W. and L. M. K. Boetler, “Heat transfer in automobile radiators of the tubular type”, University of California, Berkeley, Publications on Engineering, Vol. 2 No. 13, pp. 443–461, 1930.

Dyadyakin, B.V. and A.S. Popov, “Heat transfer and thermal resistance of tight seven-rod bundle, cooled with water flow at supercritical pressures”, Trans. VTI (11), pp. 244–253, 1977 (in Russian).

Glushchenko, L.F., S.I. Kalachev, and O.F. Gandzyuk, "Determining the conditions of existence of deteriorated heat transfer at supercritical pressures of the medium", Therm. Eng., Vol.19, No.2, pp. 107–111, 1972.

Gnielinski, V., "New equation for heat and mass transfer in turbulent pipe and channel flow", Intern. Chem. Eng., Vol. 16, No. 2, pp. 359–366, 1976.

Goldmann, K., "Heat transfer to supercritical pressure water at 5000 lb/in2 flowing at high mass flow rates through round tubes", Int. Heat Transfer Conf. Boulder, P66, USA, 1961.

Goldmann, K., "Heat transfer to supercritical water and other fluids with temperature dependent properties", A.I. Chem. Eng. Chemical Engineering Progress Sym. Series, Nuclear Engineering, Part 1, Vol. 50, No. 11, p. 105, 1954.

Grabezhnaya, V.A. and P.L. Kirillov, "Heat transfer in pipes and rod bundles during flow of supercritical-pressure water", Atomic Energy, Vol. 96, No. 5, 2004 (in Russian).

Greer, S.C. and M.R. Moldover, "Thermodynamic anomalies at critical points of fluids", Ann. Rev. Phys. Chem., Vol. 32, pp. 233-265, 1981.

Griem, H., "A new procedure for the at near-and supercritical prediction pressure of forced convection heat transfer", Heat Mass Trans., Vol. 3, 1996, pp. 301–305

Griem, H., "Untersuchungen zur Thermohydraulik innenberippter Verdampferrohre", Dissertation an der Technishen Universität München, February 1995.

Groeneveld, D.C., J.E. Shan, A.Z. Vasic, A. Durmayaz, J. Yang, S.C. Cheng, and A. Tanase, "The 2005 CHF look-up table", log166, NURETH-11, Avignon, France, October 2−6, 2005.

Groeneveld, D.C., L.K, Leung, Vasic, A., Y.J. Guo, and S.C. Cheng, "A look-up table for fully developed film-boiling heat-transfer", NED, Vol. 225, pp. 83–97, 2003.

Groeneveld, D.C. and J.C. Stewart, "The minimum film boiling temperature for water during film boiling collapse", Proc. of the 7th IHTC, Munich, FRG, Vol. 4, pp. 393–398, 1982.

Gupta, S., S. Mokry, A. Farah, K. King, W. Peiman and I. Pioro, "Developing a heat-transfer correlation for supercritical-water flow in bare vertical tubes and its application", UOIT unpublished report, 2010.

Hadaller, G. and S. Banerjee, “Heat transfer to superheated steam in round tubes”, AECL Report, 1969.

Hall, W.B., J.D. Jackson and A. Watson, “A review of forced convection heat transfer to fluids at supercritical pressures”, Proc. I. Mech. E., Vol. 182, Part 3I, Bristol Sym., HTFS 3907, 1968.

Hendricks, R.C., R.J. Simoneau and R.V. Smith, “Survey of heat transfer to near critical fluids”, NASA Technical Memorandum NASA TM X-S 2612 also Adv. Cryog. Eng. Vol. 15, pp. 197–237, HTFS 12278, 1970.

Herkenrath, H., “Heat transfer to water in tube flow at supercritical pressure”, PhD dissertation, Technical University of Aachen, Germany, 1970.

Herkenrath, H., P. Mörk-Mörkenstein, U. Jung, and F. J. Weckermann, Wärmeubergung an Wasser bei Erzwungener Strömung in Drückbereich von 140 bis 250 Bar”, EUR-3658d, 1967.

Huang, X. C. and S. C. Cheng, “Simple method for smoothing multidimensional experimental data with application to the CHF and PDO look-up table, Numer. Heat Trans., Part B, Vol. 26, 1994, pp. 425– 438, 1994.

Ishigai, S., M. Kadgi and M. Nakamoto, “Heat transfer and friction for water flow in tubes at supercritical pressures” Teplomassoobmen (Heat-Mass-Transfer)–V, Proc. of the 5th All-Union Conference on Heat Mass Transfer, Vol.1, No.1, Minsk, Belarus, pp. 261–269 (in Russian), 1976.

Jackson, J.D., “On the deterioration of forced convection heat transfer to fluids at supercritical pressure due to bulk flow acceleration”, ISSCWR6, Shenzhen, China, 2013.

Jackson, J.D., M. Anderson, X. Cheng, H. Zahlan, Y.Y. Bae and K. Yamada, “Review of progress on the development of new empirical correlation equations under the framework of the IAEA Coordinated Research Programme on heat transfer in SCWR’s”, Proc. of ICAPP ’12, Chicago, USA, June 24–28, Paper 12268, 2012.

Jackson, J.D., editor, “Chapter 6 in Heat transfer behaviour and thermohydraulics code testing for SCWRs”, IAEA TECDOC-1746, 2012.

Jackson, J.D., “A model of developing mixed convection heat transfer in vertical tubes to fluids at supercritical pressure”, P104, Proc. of the 5th Int. Sym. SCWR (ISSCWR-5), Vancouver, British Columbia, Canada, March 13–16, 2011a.

Jackson, J. D., “A semi-empirical model of turbulent convective heat transfer to fluids at supercritical pressure,” Proc. 16th Int. Conf. on Nucl. Eng., Orlando, USA, May 11–15, 2008.

Jackson, J.D., “Requirements for similarity in the case of heat transfer to fluids at pressures above the critical value and an approach to the correlation of experimental data”, Paper G3, Proceedings of the 10th UK National Heat Transfer Conference, Edinburgh, September 2007.

Jackson, J. D., “Consideration of the heat transfer properties of supercritical pressure water in connection with the cooling of advanced nuclear reactors”, Proc. of the 13th Pacific Basin Nuclear Conference Shenzhen City, China, 2002.

Jackson, J.D., Cotton, M.A. and B.P. Axcell, “Studies of mixed convection in vertical tubes”, Int. J. of H. and F. Flow, Vol. 10, No. 1, pp 2–15, 1989.

Jackson, J.D. and W.B. Hall, “Forced convection heat transfer to fluids at supercritical pressure”, in “Turbulent Forced Convection in Channels and Bundles”, S. Kakaç and D.B. Spalding (editors), Hemisphere Publishing Corp., Washington, USA, Vol. 2, pp. 563–611, 1979a.

Jackson, J.D. and W.B. Hall, “Influences of buoyancy on heat transfer to fluids flowing in vertical tubes under turbulent conditions”, in “Turbulent Forced Convection in Channels and Bundles”, S. Kakaç and D.B. Spalding (editors), Hemisphere Publishing Corp., Washington, USA, Vol. 2, pp. 613–641, 1979b.

Kaye, G.W.C. and T.H. Laby, “Tables of physical and chemical constants and some mathematical functions”, 14th edition, Longman, London, UK, pp. 183–186, 1973.

Kirillov, P., R. Pometko, A. Smirnov, et al., “Experimental study on heat transfer to supercritical water flowing in 1- and 4-m-long vertical tubes”, Proc. GLOBAL’05, Tsukuba, Japan, Oct. 9–13, P518, 2005.

Krasyakova, L.Yu., I.I. Belyakov and N.D. Fefelova, “Heat transfer with a downward flow of water at SC pressure”, Therm. Eng., Vol. 24, No. 1, pp. 9–14, 1977.

Kraan, M., M.M.W. Peeters, M.V. Fernandez Cid, G.F. Woerlee, W.J.T. Veugelers and G.J. Witkamp, “The influence of variable physical properties and buoyancy on heat exchanger design for near- and supercritical conditions”, J. of Supercritical Fluids 34 (2005) 99–105, 2005.

Krasnoshchekov, E.A. and V.S. Protopopov, "Experimental study of heat exchange in carbon dioxide in the supercritical range at high temperature drops", Teplofizika Vysokikh Temperatur, Vol. 4, No. 3, pp. 389–398, May 1966.

Kuang, B., Y. Zhang and X. Cheng, "A new wide-ranged heat transfer correlation of water at supercritical pressures in vertical upward ducts", NUTHOS-7, Seoul, Korea, October 5–9, 2008.

Kondratiev, N.S., "About regimes of the deteriorated heat transfer at flow of supercritical pressure water in tubes," Trans. IV All-Union Conf. Heat Transfer and Thermal-Hydraulics of Two-Phase Flow in Power Engineering Machines and Apparatuses, Leningrad, Russia, pp. 71–74, 1971.

Koshizuka, S. and Yo. Oka, "Computational analysis of deterioration phenomena and thermal-hydraulic design of SCR," Proc. 1st Int. Sym. on SCWR Design and Technology (SCR-2000), Tokyo, Japan, paper 302, 2000.

Lee, J., "The flow structure under mixed convection in a uniformly heated vertical pipe", Master thesis, MIT, 2006.

Lee, R.A. and K.H. Haller, "Supercritical water heat transfer developments and applications", Proc. of the 5th IHT Conference, IV, Tokyo, Japan, September 3–7, Paper B7.7, pp. 335–339, 1974.

Lemmon, E.W., M.O. M'cLinden and D.G. Friend, "Thermophysical properties of fluid systems", NIST Standard Reference Database Number 69, NIST Reference Fluid Thermodynamic and Transport Properties Database: Version 7.0, 2002.

Leung, L.K.H., "Canada's Super-Critical Water cooled Reactor design", NSERC/NRCan /AECL Generation IV Energy Technologies Program–Wrap-up Workshop, 2011.

Leung, L.K.H., "Canada's Super-Critical Water-cooled Reactor Design Concept", Phase-II NSERC/ NRCan/AECL Gen-IV Energy Technologies Program, Kick-off Meeting, Saskatoon, Canada, June 14, 2012.

Leung, L.K.H., M. Yetisir, W. Diamond, D. Martin, J. Pencer, B. Hyland, H. Hamilton, D. Guzonas and R. Duffey, "A next generation heavy water nuclear reactor with supercritical water as coolant", Int. Conf. Future of HWRs, Paper No. 042, Ottawa, Ontario, Canada, Oct. 02-05, 2011.

Liu, X., B. Kuang, C. Ni and X. Cheng, "Look-up table establishment of supercritical water heat transfer in vertical upward flow and tube-size effect investigation", The 5th Int. Sym. SCWR (ISSCWR-5), Vancouver, Canada, March 13–16, 2011.

Löwenberg, M., J. Starflinger, E. Laurien, A. Class, and T. Schulenberg, "Supercritical heat transfer in vertical tubes, a look-up table". Prog. Nucl. Energy, Vol. 50, pp. 532−538, 2008.

Löwenberg, M., J. Starflinger, E. Laurien and T. Schulenberg, "A look-up table for heat transfer of SC water", Proc. GLOBAL 2005, Paper No. 037, pp. 1–6, 2005.

Mikielewicz, D.P., A.M. Shehata, J.D. Jackson, and D.M. McEligot, "Temperature, velocity and mean turbulence structure in strongly-heated internal gas flows, comparison of numerical predictions with data", Int. J. Heat Mass Transfer 45, 4333–4352. , 2002.

McDonald, M., B. Hyland, H. Hamilton, L. Leung N. Onder, J. Pencer and R. Xu, **"**Pre-conceptual fuel design concepts for the Canadian Super critical Water-Cooled Reactor", the 5th Int. Sym. SCWR (ISSCWR-5), Vancouver, British Columbia, Canada, March 13–16, 2011.

McElligot, D.M. and J.D. Jackson, "Deterioration criteria for convective heat transfer in gas flow through non-circular ducts", Nucl. Eng. Des., Vol. 232, pp. 327–333, 2004.

Miropolsky, Z.L. and M.E. Shitsman, "Heat transfer to water and steam at variable specific heat (in near critical region)", Soviet Physics, Vol. 2, No. 10, pp 2196–2208, 1957.

Mokry, S., Ye. Gospodinov, I. Pioro and P. Kirillov, "Supercritical water heat-transfer correlation for vertical bare tubes", Proceedings of the ICONE-17, Brussels, Belgium, July 12–16, 8 pages, 2009a.

Nakla, M., private communication, 2010.

Ornatskiy, A.P., L.F. Glushchenko, and S.I. Kalachev, "Heat transfer with rising and falling flows of water in tubes of small diameter at supercritical pressures", Therm. Eng., Vol. 18, No. 5, pp. 137–141, 1971.

Petukhov, B.S. and A.F. Polyakov, “Heat transfer in turbulent mixed convection” (edited by B.E. Launder), Published by Hemisphere Publishing Corporation, 1988.

Petukhov, B.S., V.S. Protopopov and V.A. Silin, “Experimental investigation of worsened heat-transfer conditions with the turbulent flow of carbon dioxide at supercritical pressure”, translated from Teplofizica Vysokikh Temperatur, Vol. 10, No. 2, pp. 347–354, 1972.

Petukhov, B.S., “Heat transfer and friction in turbulent pipe flow with variable physical properties” in book ‘Advances in Heat Transfer’, (Editors J. P. Hartnett and T. F., Irvine, Jr.), Academic Press, Volume 6, pp 504–564, 1970.

Petukhov, B.S., “Heat transfer in a single-phase medium under supercritical conditions”, Teplofizika Vysokikh Temperatur, Vol. 6, No. 4, pp. 732–745, HTFS 5050, July–August 1968.

Pioro, I.L. and R.B. Duffey, “Heat transfer and hydraulic resistance at supercritical pressures in power engineering applications”, ASME Press, New York, NY, USA, 334 pages, 2007.

Pioro, I.L. and R.B. Duffey, “Experimental heat transfer in supercritical water flowing inside channels (survey)”, Nucl. Eng. Des., Vol. 235, pp. 2407−2430, 2005.

Pioro, I.L., H.F. Khartabil, and R.B. Duffey, “Heat transfer to supercritical fluids flowing in channels – empirical correlations (survey)”, Nucl. Eng. Des., Vol. 230, No. 1–3, pp. 69–91, 2004.

Pioro, I.L., H.F. Khartabil and R.B. Duffey, “Literature survey devoted to the heat transfer and hydraulic resistance of fluids at supercritical pressures and near critical pressures”, AECL Report, 2002.

Pis’menny, E. N., V. G. Razumovskiy, E. M. Maevskiy, A. E. Koloskov, I. L. Pioro and R. Duffey, “Experimental study on temperature regimes to supercritical water flowing in vertical tubes at significant impact of free convection”, Proc. of GLOBAL 2005, P519, Tsukuba, Japan, Oct 9–13, 2005.

Popov, V.N., “Theoretical calculation of heat transfer and friction for carbon dioxide in the supercritical range”, Proc. 2nd all Soviet Union Conference on Heat and Mass Transfer, Minsk, Published as Rand Report R-451-PR, 1964.

Razumovskiy, V.G., “Experimental study on heat transfer to supercritical water flowing in small diameter vertical tubes at low mass fluxes”, National Technology University of Ukraine “KPI”, Kyiv, Ukraine, 2005.

Richards, G., A.S. Shelegov, P.L. Kirillov, I.L. Pioro and G. Harvel, “Temperature profiles of a vertical bare 7-element bundle cooled with supercritical Freon-12”, Proc. ICONE19, Chiba, Japan, May 16–19, 2011a.

Richards, G., A.S. Shelegov, P.L. Kirillov, I.L. Pioro and G. Harvel, “Heat transfer profiles of a vertical, bare, 7-element bundle cooled with supercritical Freon-12”, Proc. NURETH-14, Toronto, Ontario, Canada, September 25–30, 2011b.

Seider, N. M. and G. E. Tate, “Heat transfer and pressure drop of liquids in tubes”, Ind. Eng. Chem., Vol. 28, No.12, pp. 1429–1435, 1936.

Sengers, J.V. and A.L. Sengers, “The critical region”, Chem. & Engr. News, Vol. 46, No. 25, pp. 104-118, June 1968.

Schmidt,K.R.,“WärmetechnischeUntersuchungen am hochbelasteten Kesselheizflachen”, Mitt. Ver. Grosskesselbesitzer, N. 63, 1959.

Shitsman, M.E.,“Temperature conditions in tubes at supercritical pressures”, Therm. Eng. Vol., 15, No. 5, pp. 72–77, 1968.

Shitsman, M.E.,“Impairment of the heat transmission at supercritical pressures”, Teplofiz. Vysokikh Temperatur, Vol. 1, No. 2, 1963.

Styrikovich, M.A., T.K. Margulova, and Z.L. Miropolskii, “Problems in the development of designs of SC boilers”, Therm. Eng., Vol. 14, No. 6, pp. 5–9, 1967.

Subbotin, V.I., O.V. Remizov and V.A. Vorobiev, “Temperature regimes and heat transfer in the region of degraded heat transfer”, IPPE Institute, J. TVT, Vol. 11, No. 6, pp. 73 (in Russian), 1973.

Swenson, H.S., J.R. Carver, and C.R. Kakarala, “Heat Transfer to Supercritical Water in Smooth-Bore Tubes”, J. of Heat Transfer, Trans. ASME Series C, Vol. 87, No. 4, pp. 477– 484, 1965.

Tanaka, H., S. Maruyama and S. Hatano, “Combined forced convection heat transfer for upward flow in a uniformly heated vertical pipe”, Int. J. Heat Mass Transfer, Vol. 30, No. 1, pp. 165–174, 1987.

Tavoularis, S., “Measurement in fluid mechanics”, Text Book, Cambridge University Press, 2005.

Thom, J.R.S., W.M. Walker, T.A. Fallon and G. Reising, “Boiling in sub-cooled water during flow up heated tubes or annuli”, Proc. Inst. Mech. Eng., Manchester, 1965.

Townsend AA., “The Structure of turbulent shear flow”, Cambridge: Cambridge Univ. Press, 1976.

Vikhrev, Yu.V., Yu. D. Barulin and A.S. Kon’kov, “A study of heat transfer in vertical tubes at supercritical pressures”, Thermal Engineering, Vol. 14, No.9, pp. 116–119, 1967.

Vikhrev, Yu.V., A.S. Kon’kov, V.A. Lokshin et al., “Temperature regime of steam generating tubes at supercritical pressure”, (In Russian), Trans. of the IVth All-Union Conference on heat transfer and hydraulics at movement of two-phase flow inside elements of power engineering machines and apparatuses, Leningrad, Russia, pp. 21–40, 1971.

Wang, J., H. Li , S. Yu and T. Chen, “Comparison of the heat transfer characteristics of supercritical pressure water to that of subcritical pressure water in vertically upward tubes The 2nd CCSC-2010, Toronto, Canada, April 25–28, 2010.

Watts, M. J. and C-T. Chou, “Mixed convection heat transfer to supercritical pressure water”, Proc. 7th IHTC, Munich, Germany, pp. 495–500, 1982.

Yamagata, K., K. Nishikawa, S. Hasegawa, T. Fujii and S. Yoshida, “Forced convective heat transfer to supercritical water flowing in tubes”, Int. J. Heat Mass Transfer, Vol. 15, No.12, pp. 2575–2593, 1972.

Yin, F., T-K Chen and H.-X. Li, “An investigation on heat transfer to SC water in inclined upward smooth tubes, HT Eng., 27 (9), pp. 44–52, 2006.

Yetisir, M., M. Gaudet and D. Rhodes, “Development and integration of Canadian SCWR concept with counter-flow fuel assembly”, ISSCWR6, Shenzhen, Guangdong, China, March 2012.

Yoshida, S. and H. Mori, “Heat transfer to supercritical pressure fluids flowing in tubes,” Proc.1st Int. Symposium on SCWR Design and Technology, University of Tokyo, pp. 72–78, 2000.

Yu, J., Y., W. Songtao and J. Baoshan, "Development of sub-channel analysis code for SC CANDU type reactor", 3rd Int. Sym. on SCWR-Design and technology, Shanghai, China, March l2–15, 2007a.

Yu, J., Y., W. Songtao and J. Baoshan, "Development of sub-channel analysis code for CANDU-SCWR", Prog. Nucl. Ener., Vol. 49, pp. 334–350, 2007b.

Zahlan, H., D.C. Groeneveld and S. Tavoularis, "Measurements of convective heat transfer to vertical upward flows of CO2 in circular tubes at near-critical and supercritical pressures". Nucl. Eng. Des., under review for publication, 2015.

Zahlan, H., S. Tavoularis and D.C. Groeneveld, "A look-up table for trans-critical heat transfer in water-cooled tubes", Nucl. Eng. Des., under publication (revised version was submitted), 2015.

Zahlan, H., D.C. Groeneveld and S. Tavoularis, "Fluid-to-fluid scaling for convective heat transfer in tubes at supercritical and high subcritical pressures", Int. J. Heat Mass Tran.73, Vol. 73, pp. 274–283. 2014.

Zwolinski, S., M. Anderson, M. Corradini and J. Licht, "Evaluation of fluid-to-fluid scaling method for water and carbon dioxide at supercritical pressure, Proc. 5th Int. Sym. SCWR, Vancouver, Canada, 2011.

APPENDIX A

ANOMALOUS BEHAVIOUR OF FLUIDS NEAR THE CRITICAL POINT

A.1 Critical opalescence

This is an interesting physical phenomenon, which explains the turbid appearance of transparent fluids as pressure and temperature approach the critical values. Investigations on fluid properties and related physical phenomena in the vicinity of the critical point are of interest to physicists. For example, Sengers and Sengers (1968) reported that clear fluids show turbid appearance as they approach the critical point, a phenomenon known as critical opalescence. Critical opalescence is attributed to light scattering, because of local fluctuations in refractive index caused by fluctuations of density for one-component fluid; this density fluctuation is caused by large values of isothermal compressibility, which also gives rise to large values of specific heat at constant pressure, which were discussed in Section 1.2. This fluid behaviour can affect significantly flow visualization and optical flow measurement techniques. Greer and Moldover (1981), in their review on thermodynamic anomalies in fluids at the critical point, stated that thermodynamic fluctuations become **macroscopic** and extend from one heat transfer region to other regions; the fluctuations are long-lived as the critical point is approached. A reference size of the fluctuating region is called the correlation length, which shows singularity at the critical point. These fluctuations become large enough to scatter light in fluids which would be transparent at all other thermodynamic states.

A.2 Thermal conductivity

The property tables of the International Association for the Properties of Water and Steam (IAPWS; Cooper, 2008) and by the National Institute of Standards and Technology properties for water (NIST; Lemmon et al., 2002) for the high subcritical pressures of $P/P_c \geq 0.982$ show that the thermal conductivity of the saturated vapour k_g becomes greater than or equal to the thermal conductivity of the saturated liquid k_f. Just before the critical point, *e.g.*, at P_{sat} = 22.052 MPa, the values of saturated vapour and liquid k estimated by the 2002-NIST software are even larger than k at the critical point[12]. One expects that by approaching the critical point, k for different states of water should converge to a single value. The peaks in the value of k at T_c and T_{pc} are shown in Figure A1. This Figure shows erroneous and anomalous variations of k when compared with trends away from the critical point. The anomalous behaviour of k was also found in both water and CO_2 (NIST; Lemmon et al., 2002) at high-subcritical pressures. It is expected that this effect will influence the accuracy of the predicted heat transfer coefficient in the high subcritical pressure region.

As the thermodynamic vapour-liquid saturation curve, in a T vs. v diagram of water, approaches its maximum at the critical point, the saturated liquid and vapour lines become closer and converge at the critical point. In the region close to this critical point, thermodynamic and transport properties of a fluid exhibit significant change within a narrow range of temperatures and a linear approximation of such change in a property code can lead to wrong results. It is known that such jumps in properties with temperature occur at the critical and pseudo-critical points. Surprisingly, this behaviour was found to start at high subcritical pressures (*e.g.,* for k at $P/P_c \approx 0.983$), reaching a maximum change just before the critical point, and extending further to supercritical pressures. A comparison of the slopes of the properties with temperature in the vicinity of the critical and pseudo-critical point shows that these slopes at the pseudo-critical point decrease with increasing supercritical pressure. Table A.1 shows a sample of the thermo-physical properties for water as estimated by NIST (2002) for a range of high subcritical pressures; this table shows also that at P = 22 MPa, k_g becomes greater than k_f.

---

[12]Specific heat c_p and Prandtl number Pr show similar anomalous trend.

Table A. 1: Sample of thermo-physical properties of saturated water (NIST-2002).

P_{sat}	T_{sat}	k_f	k_g	μ_f	μ_g	$\mathrm{Pr_f}$	$\mathrm{Pr_g}$
MPa	˚C	W/mK	W/mK	Pa.s	Pa.s	-	-
19	361.47	0.423	0.192	5.94E-05	2.61E-05	2.30	4.13
20	365.75	0.416	0.234	5.62E-05	2.75E-05	3.11	5.35
21	369.83	0.424	0.318	5.23E-05	2.96E-05	5.33	8.58
21.5	371.79	0.46	0.420	4.95E-05	3.13E-05	9.72	13.84
22	373.71	0.87	1.042	4.68E-05	3.75E-05	67.24	69.61

Figure A.1 compares variations of the k_f, k_g and k (at $P = P_c$) *vs.* T. The temperature range includes the high subcritical and supercritical temperatures. The thermal conductivities of both saturated water vapour and saturated water liquid start to increase as T_{sat} increases showing the expected superior conductivity of k_f over k_g up to T = 372.5˚C, where the two curves intersect; beyond this temperature and up to the critical point, k_g becomes larger than k_f and increases more rapidly than k_f. Furthermore, when approaching T_c, k_g and k_f have sharp and strange increases. They are expected to converge finally at $T = T_c$, where $k_f = k_g = k_c$, however this is not the case: just before T_c, both k_g and k_f become greater than k_c (≈ 1.37 W/mK). This trend of the saturated thermal conductivities at high subcritical pressures is found unrealistic and erroneous and is caused by the application of interpolating (curve fitting) equations for k near the critical point, where divergence of some properties occur at the critical or pseudo-critical point; this will be discussed in detail later. Figure A.2 compares the variations of single-phase thermal conductivity (away from saturation region and pseudo-critical point) with temperature for a range of pressures surrounding the critical value.

It is worth noting that variations of normalized specific heat ($c_p/c_{p,c}$) *versus* temperature for saturated and single phase water show similar erroneous trend near the critical point, however the slopes for specific heat are much sharper (Figure A.3). As expected and shown in Figure A.4, the Prandtl number $\mathrm{Pr} = \mu c_p / k$ also displays an erroneous trend with temperature near the critical point since it is based on k and c_p. This figure shows sharp increases for the saturated liquid and vapour Pr at high subcritical pressures (relatively stronger than the one observed for k); approaching the critical point, the saturated liquid Pr becomes greater than the saturated vapour Pr. This anomalous behaviour is not limited to water: Figure A.5 shows a similar variation of thermal conductivity near the critical point for CO_2.

Differences between property codes: Differences between values of properties, namely *k*, based on different property codes (NIST, ASME steam tables and IAPWS) are expected to some extent, considering that these codes are based on complex curve fits to the experimental data, especially in the near critical region. There are two formulations for properties, one for industrial use and the other for general and scientific application; this will be discussed in detail next.

In 2008, the International Association for the Properties of Water and Steam published a revised release on the IAPWS Formulation 1985 for the thermal conductivity of ordinary water (Cooper, 2008). Thermal conductivity data for water or steam (single-phase) were evaluated critically and tabulated in a uniform grid for a wide range of P = 0.1 to 100 MPa and T = 0 to 800˚C; k values were presented in tables along with the associated uncertainty. k was also presented for extrapolated points outside the range of reliable experimental data. Similarly, tables of saturated liquid and vapour k with the corresponding uncertainty were also provided. The range of P was 0.0006117 to 21.814 MPa and of T was 0.01 to 373˚C. This table shows that values of k_f are always larger than k_g, however, at high subcritical pressures, as P approaches the upper limit of the table at P = 21.814 MPa, the difference between k_f and k_g decreases continuously, and at $P \geq$ 18.666 MPa, there is a sharp increase in k_g which is larger than the increase in k_f. Cooper (2008) also presented an interpolating function for industrial use, "industrial formulation" abbreviated IAPWS-IF97, and a similar one for "general and scientific use" abbreviated IAPWS-95 formulation. The difference between these two formulations is described as follows: IAPWS-IF97 is used in industry because (i) this formulation fits industrial needs in terms of fast computation time, as such property subroutines may be called millions of times during design calculations, and (ii) industry requires a formulation that will not change for many years. IAPWS-IF97 was fitted to match IAPWS-95 formulation, except in two regions, one of which was near the critical point. As a result; the properties of

IAPWS-IF97 may not be entirely up-to-date. In the vicinity of the critical point, IAPWS-IF97 properties are inferior (http://www.iapws.org/faq2/twoform.htm). The industrial formulation has the following interpolating function for thermal conductivity in a non-dimensional form

$$\bar{k}(\bar{T},\bar{\rho}), \text{ where } \bar{k} = k/k^* \text{ , } \bar{T} = T/T^* \text{ and } \bar{\rho} = \rho/\rho^* \qquad \text{(A.1)}$$

where T is temperature on the International Temperature Scale of 1990 and the overbar indicates a non-dimensional property. The reference constants are T^* = 647.26 K, ρ^* = 317.7 kg/m^3, k^* = 1 W/mK; these constants are close but not identical to the critical point values. This function is a complicated curve fit, which considers abnormal trend of k; such trends exist near the critical point. The applicable range of validity for this equation depends on the pressure and temperature ranges as follows:

$P \leq 100$ MPa for $0°C \leq T \leq 500°C$

$P \leq 70$ MPa for $500 < T \leq 650°C$

$P \leq 40$ MPa for $650°C < T \leq 800°C$

The interpolating equation for the "general and scientific use" has similar property dependency to the industrial formulation equation, i.e., $\bar{k}(\bar{T},\bar{\rho})$ but the thermal conductivity dependence on temperature and density are different and contains also a term which includes viscosity and a partial derivative of P with respect to T. This term was introduced to account for enhancement of k near the critical point. The reference constants are T^* = 647.226 K, ρ^* = 317.763 kg/m^3, P^* = 22.115×10^6 Pa and k^* = 0.4945 W/mK; the constants are also close but not identical to the critical point values. The non-dimensional variables, in addition to those mentioned above, are:

$$\bar{P} = P/P^* \text{ and } \bar{\chi}_T = \bar{\rho}(\partial\bar{\rho}/\partial\bar{P})_{\bar{T}} \qquad \text{(A.2)}$$

The applicable range of validity of the scientific formulation is

$P \leq 400$ MPa for $0°C \leq T \leq 125°C$

$P \leq 200$ MPa for $125°C \leq T \leq 250°C$

$P \leq 150$ MPa for $250°C \leq T \leq 400°C$

$P \leq 100$ MPa for $400°C \leq T \leq 800°C$

which is wider than the industrial one. It is worth noting that the application of the interpolating equation for industrial use produced normal trend as reported by Cooper (2008); e.g., at P_{sat} = 21.814, T_{sat} = 373˚C, k_g = 507.03 and k_f = 534.96 W/mK, while the application of the corresponding equation for general and scientific use (Cooper, 2008) produced irregular value at the same P_{sat} mentioned earlier *i.e.*, k_g = 592.2 and k_f = 548.2 W/mK. NIST uses the two interpolating equations recommended by IAPWS.

Based on the previous discussions, it can be noted that IAPWS and NIST properties are similar and use the same complex interpolating functions based on experimental data for evaluation of properties in codes; the trends of the experimental data are not smooth. There are two formulations: the industrial and the scientific application. Because the scope of research at the University of Ottawa includes not only ordinary water but also CO_2 and other fluids, this option of extracting thermo-physical properties for different fluids was made available by NIST [UO, AECL, NIST, and UOIT communication; 2010].

Effect on heat transfer coefficient (HTC) at high subcritical pressures: as described above, thermal conductivity as extracted by the available methods shows anomalous and erroneous behaviour at high subcritical pressures. Generally, heat transfer prediction methods correlate Nu (= $h\ d\ /k$) with other non-dimensional parameters/ properties including Pr (= $c_p\ \mu\ /k$), which is raised to a certain power, n. The predicted Nu number using erroneous estimations of thermal conductivity at very high subcritical pressures will lead to an overestimation of the HTC significantly in the transition and film boiling regions. A tentative remedy for this erroneous prediction of k is to assume $k_f = k_g$ = average (k_g, k_f) for $P/P_c \geq 0.982$, or an average value of k in this region including k_c, or $k = k_c$.

Physical explanation of the anomalous *k* behaviour from literature: water is a highly polar fluid. Because of this characteristic, k for water is generally larger than that for other non-polar fluids. Lee (1990) modeled k (ρ, T) near the critical point in the same way as in the IAPWS model, *i.e.*, he separated k into normal k in the absence of critical fluctuations and a critical enhancement Δk due to critical fluctuations; i.e., $k = k_n + \Delta k_c$. The enhancement of k near the critical point region was also found to exist in carbon dioxide, Helium-3 and other fluids including the simple mono-atomic Argon and Xenon (Lee, 1990). In the textbook of Reid et al. (1987) for fluids other than water, the authors tried to explain the physical grounds of the anomalous behaviour of k; they referred to additional molecular transfer contribution to k (resulted from additional movement of the molecular clusters, when the fluid approaches the critical point) in the region close to the critical point. Kawasaki (1976) considered that the mobility of clusters of molecules is a pure diffusion process. He also assumed direct analogy between the diffusion coefficient and the thermal diffusivity. Based on this assumption, the enhancement in k near the critical point is calculated. This enhancement for water (ordinary and heavy) in the critical region is associated with the strong polar and hydrogen bonding. From the above discussions one may conclude that k_f is always greater than k_g and therefore the NIST prediction that at high subcritical pressures k_g can be greater than k_f is erroneous.

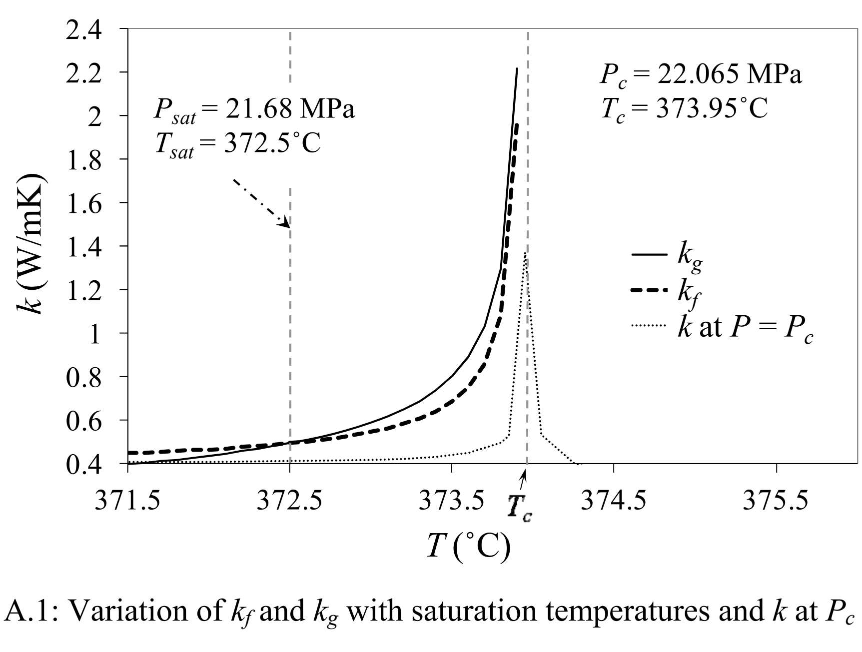

Figure A.1: Variation of k_f and k_g with saturation temperatures and k at P_c (NIST-2002).

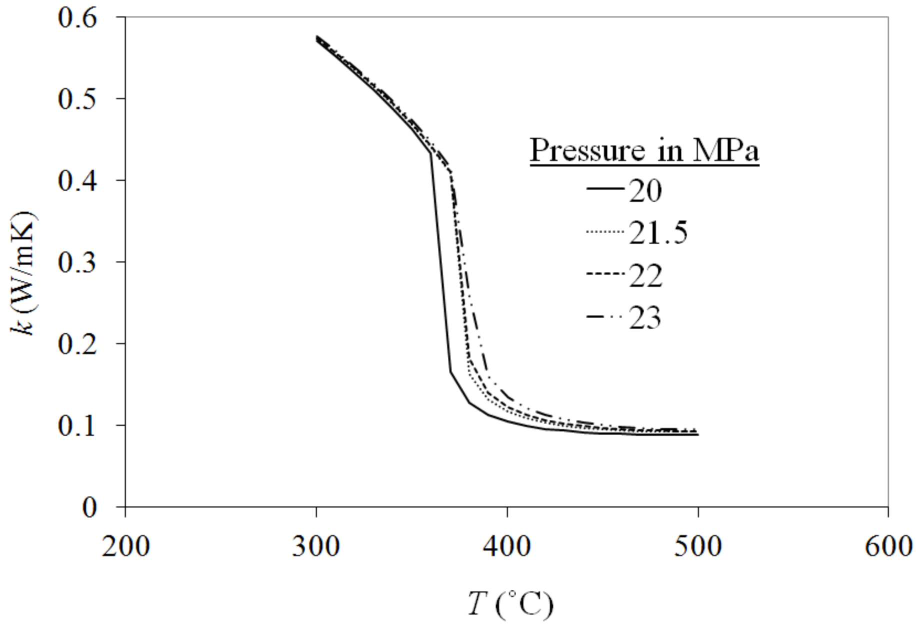

Figure A.2: Effect of temperature on thermal conductivity for several near-critical pressures

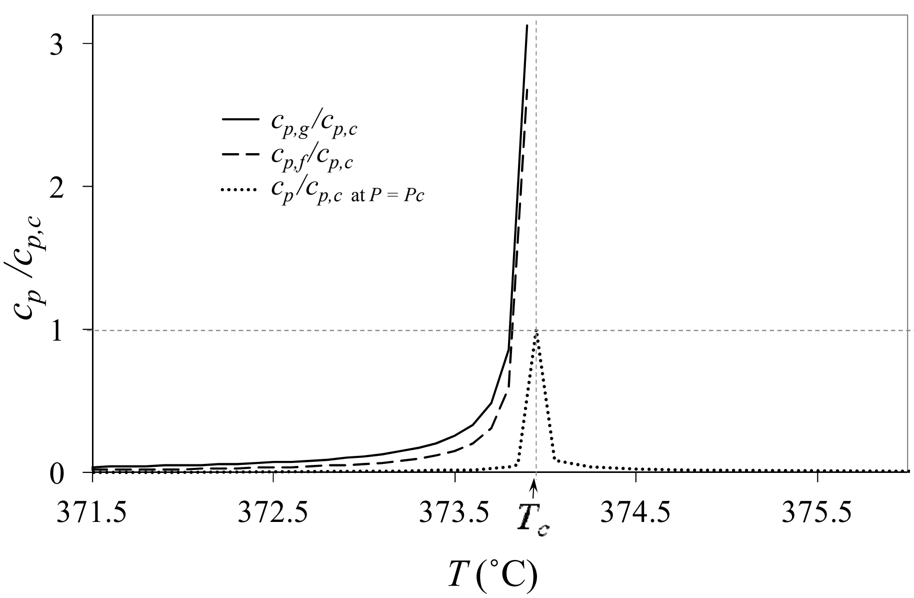

Figure A.3 Variation of $c_{p,f} / c_{p,c}$ and $c_{p,g} / c_{p,c}$ with T_{sat} and $c_p / c_{p,c}$ *vs*. T at P_c.

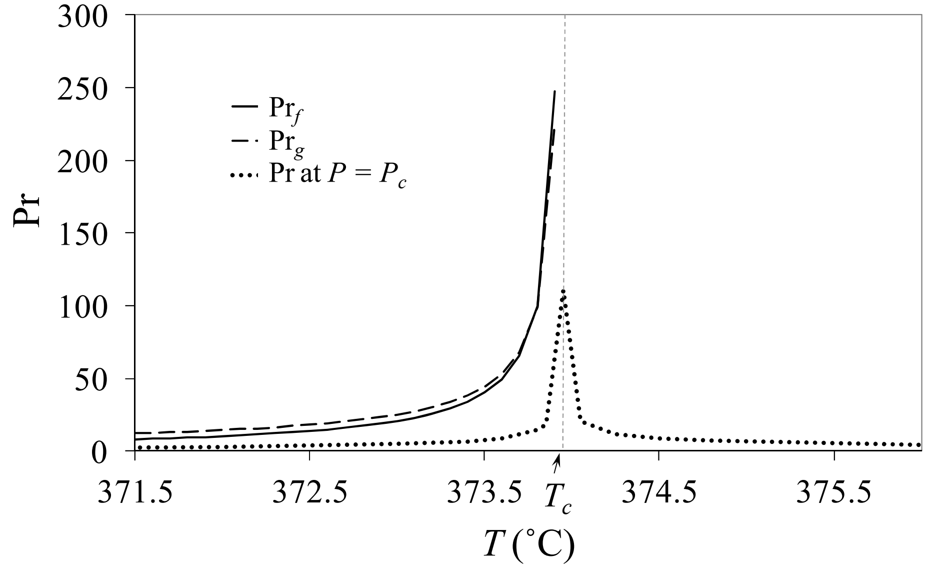

Figure A.4 Variation of saturated Pr numbers with temperature at high subcritical pressures and Pr variations at P_c.

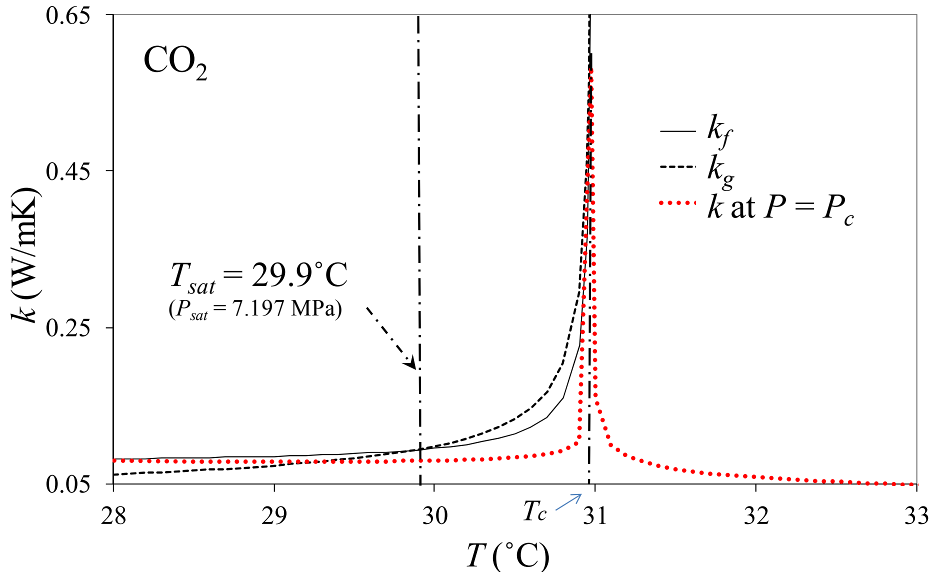

Figure A.5: Variations of k_f and k_g at different saturation temperatures and k at P_c (NIST-2002) for a range of temperatures for CO_2.

References

Cooper, J. R., “Revised Release on the IAPS Formulation 1985 for the thermal conductivity of ordinary water substance”, the International Association for the Properties of Water and Steam, Berlin, Germany, September 2008.

Kawasaki, K., “Mode coupling & critical dynamics”; in Phase transition & critical phenomena, Domb, C. & M. Green, Eds.; Academic press, Vol. 5a. New York, 1976.

Lee, H., “Generalized treatment of thermal conductivity enhancement in the critical region”, Ind. Eng. Chem. Res. 1990, Vol. 29, pp. 488-494, 1990 American Chemical Society, 1990.

Lemmon, E.W., M.O. M’cLinden and D.G. Friend, “Thermophysical Properties of Fluid Systems”, NIST Standard Reference Database Number 69, NIST Reference Fluid Thermodynamic and Transport Properties Database, Version 7.0, 2002.

Private communication [UO, AECL, NIST, and UOIT; 2010].

Reid R.C., J. M. Prausnitz and B. E. Poling, text book, “The properties of gases and liquids”, 4th edition, McGrow-Hill, 1987.

APPENDIX B

ASSESSMENT OF SUPERCRITICAL HEAT TRANSFER PREDICTION METHODS

This appendix shows results of assessment of supercritical heat transfer prediction methods. The results are presented in the form of a paper entitled:

Zahlan, H., D.C. Groeneveld and S. Tavoularis, S. Mokry and I. Pioro "Assessment of supercritical heat transfer prediction methods", the 5th Int. Sym. SCWR (ISSCWR-5), Vancouver, British Columbia, Canada, March 13-16, 2011, 20 pages,

which was presented at the 5th International Symposium of SCWR, March 11-16, 2011. This study included leading single phase and SCHT correlations, which were applied to a large trans-critical water databank compiled at University of Ottawa. The databank was screened for duplicates and outliers before its use in this assessment.

ASSESSMENT OF SUPERCRITICAL HEAT TRANSFER PREDICTION METHODS

H. Zahlan[1], D.C. Groeneveld[1], S. Tavoularis[1],
S. Mokry[2] and I. Pioro[2]
[1]University of Ottawa, Ottawa, Ontario, Canada
[2]University of Ontario Institute of Technology, Oshawa, Ontario, Canada

Abstract

A large supercritical water databank has been compiled at the University of Ottawa (UO). This databank originally contained 36,030 tube data points. After a thorough screening process, during which duplicate and unreliable data and obvious outliers were removed, a final databank was assembled, containing more than 24,000 screened data points. This databank is the result of the combination of four different databases, the more recent one being the University of Ontario Institute of Technology database. The UO combined databank covers a wide range of near-critical and supercritical heat transfer (SCHT) conditions and is used for the assessment of existing SCHT correlations and the derivation of the transcritical heat transfer look-up table. Twelve SCHT correlations and four single-phase heat transfer correlations have been applied to the combined UO databank. The assessed SCHT prediction methods include four correlations that were developed recently, with one of these correlations published in 2010. An error analysis and an examination of the parametric trends were performed for the most promising correlations. The result of the assessment showed that the heat transfer coefficient was predicted more accurately by the recent correlations in the three supercritical heat transfer regions: (i) close to the critical or pseudo-critical point, (ii) the high-density or liquid-like state and (iii) the low-density or gas-like state. The most accurate correlations will be used in the construction of the skeleton look-up table that is currently under development at UO.

Keywords: SCHT, Supercritical heat transfer, Water data, Prediction methods

Introduction

Thermo-physical properties of fluids at near-critical conditions exhibit sharp changes within a narrow range of temperature, resulting in significant variations in fluid properties within a cross-section of a tube. This will lead to significant prediction errors when using SCHT correlations based on average property values (assuming a linear profile). Away from the critical point, such property changes become smaller at supercritical pressures but remain evident near the pseudo-critical temperature. Because of these abnormal changes in the properties, the near-critical heat transfer coefficient is difficult to predict, especially in the range of relatively low mass velocities and high heat fluxes.

More than twenty correlations are available in the literature for predicting the heat transfer in the near-critical and supercritical region; most of the available correlations are modified versions of the Dittus-Boelter (1930) equation. Although these correlations account for the changes in properties in the near critical region, they usually do not account for heat transfer enhancement or deterioration in the vicinity of the pseudo-critical temperature T_{pc}. Some prediction methods considered the enhancement and deterioration in heat transfer when $T_b < T_w < T_{pc}$, where T_w is the wall temperature and T_b is the bulk temperature. The objectives of the current study are (i) to find the best SCHT correlations which will be used in the construction of a trans-critical heat transfer look-up table (LUT), covering a wide range of flow conditions, in contrast to current correlations, each of which is bounded by a much narrower validity range and (ii) to analyse the predicted SCHT trends and to compare these trends with the experimental data.

Super-critical heat transfer database

The UO team has compiled a large subcritical and supercritical database (Groeneveld and Zahlan, 2009; Zahlan et al., 2010). The database includes data for water and other fluids and different geometries. Additional water data sets, tabulated and/or identified by Lowenberg et al. (2005, 2008; University of Stuttgart), and by Cheng (2009; Shanghai JiaoTong University) have been included in the expanded UO trans-critical heat transfer database. Recently, UO received an additional SCHT water database compiled at the University of Ontario Institute of Technology (UOIT) containing 10479 SCHT data points (Pioro, 2010). The main contributor to the UOIT data base for vertical upflow in circular tubes is Kirillov (2005), although their database also includes data from other authors. The UOIT database was subject to careful review, heat balance test and screening for duplicates and obvious outliers. The intention of the authors is to make all data publicly available, unless they are subjected to proprietary restrictions.

Table 1 shows a summary of the SCHT water data compilations from different sources and Table 2 describes all data sets from all sources and the range of their parameters. Figure 1 presents the numbers of data points for different tube diameter ranges for the combined SCHT water database. Some of these data sets were extracted from graphs using data digitization software (as were some of the data included in the original UO database), which introduces additional uncertainties (Zahlan et al., 2010). Frequently, more than one set of SCHT data set covers the same flow conditions; this will enhance the reliability of the LUT.

Supercritical sub-regions

At an earlier stage of this research, the SCHT data were classified into three distinctive supercritical sub-regions: (i) a high density state (liquid-like) region (T_w, $T_b < T_{pc}$), (ii) a near-critical or near-pseudo-critical region ($T_{pc} < T_w$ and $T_b < T_{pc}$), and (iii) a low density state (gas-like) region ($T_{pc} < T_w$, T_b). This classification was meant to take into consideration the distinct heat transfer mechanisms that apply within each sub-region. However, this approach would be complicated by the fact that the thermo-physical properties change significantly within a range of temperatures near the pseudo-critical value. Therefore, it was deemed to be preferable to redefine the boundaries of the near-critical/pseudo-critical region by introducing a narrow range of temperatures $T_{pc} - \Delta T < T < T_{pc} + \Delta T$, within which the thermo-physical properties change significantly. It was found that this range was described fairly well for different pressures by the empirical relationship $\Delta T/T_{pc} = 3.1\times10^{-3}(P/P_c)$, where the numerical values of all temperatures are in degrees K. Figure 2 shows the variation of C_p vs. temperature near the pseudo-critical value for different pressures and also illustrates the magnitude of ΔT for each pressure. In the current work, each SCW data point was classified in one of these three redefined sub-regions: (i) high density state (liquid-like) region ($T_w, T_b < T_{pc} - \Delta T$), (ii) near-critical or near-pseudo-critical region ($T_{pc} - \Delta T < T_w$ and $T_b < T_{pc} + \Delta T$), and (iii) low density state (gas-like) region ($T_{pc} + \Delta T < T_w, T_b$).

Data screening for duplicates

The method for screening the data for (i) duplicates (runs and points between different datasets and within a dataset), (ii) data that did not agree with a simple heat balance, and (iii) obvious outliers was presented by Zahlan et al. (2010). The results are summarized in Table 3. This updated table shows the number of data before and after screening for all datasets for the four combined databases.

Prediction methods

Several reviews of SCHT correlations have been published previously. Hall et al. (1968), Jackson and Hall (1979a, 1979b) and Cheng and Schulenberg (2001) have presented overviews of SCHT correlations and assessments of SC heat transfer correlations against both SC water and SC CO_2 data. Pioro et al. (2004) recently presented a more up-to-date review of such correlations that have been applied to SC conditions. The UO assessment covers more correlations and compares them against a much larger database: four single-phase correlations and twelve SCHT correlations have been assessed against the UO combined database.

Single-phase correlations

The single-phase correlations have a form similar to the Dittus-Boelter (1930) equation, but with different exponents. The Dittus-Boelter equation was originally based on water data only and evaluates the fluid properties at the bulk fluid temperature, whereas the Sieder-Tate (1936) equation includes a viscosity ratio term to account for the difference in fluid viscosity at the wall and in the bulk flow. The Hadaller and Banerjee (1969) equation is based on high-pressure superheated steam data. The most recent single-phase heat transfer equation is that of Gnielinski (1976) for fully developed turbulent flows, which includes a friction factor term to account for the increasing heat transfer with an increase in friction factor. The Gnielinski (1976) correlation includes also a factor to account for the developing boundary layer effect on heat transfer coefficient enhancement. These correlations are described below.

SCHT correlations

One of the earliest SCHT correlations is that of Bishop et al. (1965) who modified the Dittus-Boelter (1930) equation by including a density ratio (ratio of the density at wall temperature and the density at bulk fluid temperature) and replacing the specific heat in the Prandtl number by the effective integrated specific heat capacity. The Swenson et al.

(1965) correlation has similar parameters to those in the Bishop et al. (1965) correlation, except that T_w was used as the reference temperature for Nu, Re, and averaged Pr number. Krasnoscheckov et al. (1967) proposed a modified version of a SCHT correlation previously derived in 1959 and 1960. This correlation showed errors within 15% (for their database) and was recommended for the following ranges:

$2\times10^4 < Re_b < 8.6\times10^5$, $0.85 < \bar{Pr}_b < 65$, $0.9 < \frac{\mu_b}{\mu_w} < 3.6$, $1.0 < k_b/k_w < 6.0$ and $0.07 < \bar{C_p}/C_{p,b} < 4.5$ Jackson's (2002) correlation is basically a modified form of the Krasnoscheckov et al. (1967) equation, the exponent n of the specific heat ratio is (with T in K):

$$n = 0.4, \text{ for } T_b < T_w < T_{pc} \text{ and } 1.2T_{pc} < T_b < T_w$$

$$n = 0.4 + 0.2(T_w/T_{pc} - 1), \text{for } T_b < T_{pc} < T_w$$

$$n = 0.4 + 0.2(T_w/T_{pc} - 1)(1 - 5(T_b/T_{pc} - 1)), \text{ for } T_{pc} < T_b < 1.2T_{pc}$$

Yamagata et al. (1972) introduced a correction factor to the Dittus-Boelter equation, which is a function of the Eckert number E (= $(T_{pc}-T_b)/(T_w-T_b)$) and the Prandtl number at the pseudo-critical temperature or the effective integrated specific heat capacity ratio. Watts and Chou (1982) correlated mixed convection (forced and natural) water and CO_2 data for upwards and downwards flows; they used the deterioration criterion of Jackson and Hall (1979b) in the development of their correlations for normal and deteriorated heat transfer. Griem (1996) modified the Dittus-Boelter equation by considering C_p at five reference temperatures from T_b to T_w; the selected $C_{p,sel}$ is based on excluding the largest two C_p values and averaging the other three; $C_{p,sel} = (\sum_{i=1}^{i=5} C_{p,i} - C_{p,1^{st}\max} - C_{p,2^{nd}\max})/3$. Griem (1996) also introduced a correction factor to cover the entire enthalpy range; this factor is a function of H_b. The correlation of Koshizuka and Oka (2000) is based on their earlier numerical study of SC water flow in a 10 mm tube (Cheng and Schulenberg, 2001); they proposed an empirical correlation, in which the pseudo-CHF is equal to $200G^{1.2}$; this parameter indicates the deteriorated heat transfer occurrence. Kuang et al. (2008) used their SCHT databank for water in vertical upwards flow in tubes to develop their correlation. They investigated the enhanced and deteriorated heat transfer region based on the normal heat transfer coefficient predicted by Dittus-Boelter (1930). Kuang et al. used the modified Grashof number term Gr^* (there is a negative correlation between HTC and Gr^*), first introduced by Jackson et al. (1989) to account for buoyancy effects (strong variations in density causing mixed instead of pure forced convection). In addition they used the McEligot et al. (2004) non-dimensional heat-flux number q^+ to consider the streamwise thermal acceleration effect from heating on the HTC. Mokry et al. (2008) used the SCHT water data of Kirillov et al. (2005; 89 runs with 81 data points per run) in deriving their correlation. In the development of their correlation, Mokry et al. (2008) excluded the data with both enhanced and deteriorated heat transfer. Cheng et al. (2009) derived a simple SCHT correlation to predict the deviation from the normal heat transfer predicted by the Dittus-Boelter (1930) equation. This correlation is a function of the dimensionless acceleration number π_A, this number is the non-dimensional heat flux number and is the same as q^+ in the Kuang et al. (2008) correlation. Recently, Gupta et al. (2010) modified the Swenson et al. (1965) correlation which considers properties for Nu, Re and average Pr at wall temperature. Gupta et al. (2010) added a viscosity ratio term, to account for viscosity variations between wall and bulk fluid. They included also a correction factor to account for the developing boundary layer effects at the entry region: this was a function decreasing exponentially with an increase of the ratio of the distance from the entrance of the test section and diameter (*L/D*). The correlations are listed in Table 5.

Assessment of the heat transfer prediction methods

Error analysis was performed using the 2009-UO combined database (Zahlan et al., 2010). In the current assessment, two new correlations were added to the study: the correlations of Gupta et al. (2010) and Koshizuka and Oka (2000). Twelve SCHT correlations and four single-phase correlations have been applied to the expanded UO database, including the new compilation from UOIT. The overall average error (e_A) and the root mean square error (e_S) were calculated for all correlations. The average and root mean square error are defined as

$$\begin{aligned} error &= \frac{HTC_{pred}}{HTC_{exe}} - 1 \\ e_A = avg_{error} &= \frac{\sum_{i=1}^{l} error_i}{l} \times 100 \qquad (1) \\ e_S = rms_{error} &= \sqrt{\frac{\sum_{i=1}^{l} error_i^2}{l}} \times 100 \end{aligned}$$

Table 4 compares the average and rms errors for all correlations in the three supercritical regions. This table shows that the Mokry et al. (2008) correlation has the least rms error in the three SCHT regions. The distributions of average and rms errors for the best correlations, including the one by Mokry et al. (2008), with respect to Re_b, $Pr_{avg,b}$, and P/P_c were presented by Zahlan et al. (2010) in the form of plots for the three supercritical regions for the combined UO, SJTU, and U of S database. Table 6 shows percentages of all combined data predicted by the most promising correlations within an error band of ±10% (e_{10}), ±20% (e_{20}), ±30% (e_{30}), and ±50% (e_{50}). Figure 3 and 4 show the distribution of e_A and e_S vs. D for the near-critical region.

Prediction of entry region effect on SC heat transfer coefficient

The correlations of Bishop et al. (1965), Gupta et al. (2010) and Mokry et al. (2008) were applied to 5668 data points (of which 1314 points have $L/D < 50$) in the three SCHT regions. Table 7 compares percentages of error predicted by the best two correlations in the three SCHT regions.

Error analysis for each dataset

An error analysis has been performed on each dataset in the three supercritical regions. The average, rms and percentage errors for the four error bands were calculated for each dataset. Note that datasets having fewer than 20 data points were ignored in this analysis. Tables 8–10 list these calculations for the near-critical, gas-like and liquid-like regions.

Summary and concluding remarks

A detailed error analysis has been performed on the 2010 version of the UO combined data bank.

In the supercritical region, the correlation of Mokry et al. (2008) showed the best agreement with the data for all three sub-regions.

Correlations that account for the *L/D* effect were applied to part of the compiled data; these correlations are compared to the Mokry et al. (2008) correlation. This correlation showed better agreement than other correlations, even though it does not include an *L/D* effect factor.

Nomenclature

D	tube inside diameter	(mm, m)
G	mass flux	(kg m^{-2} s^{-1})
H	enthalpy	(kJ kg^{-1})
P	pressure	(kPa)
q	heat flux	(kW m^{-2})
T	temperature	(˚C or K)
e	error	(%)

Subscripts

b	bulk
c	critical
pc	pseudo-critical
w	wall
A, S	average error, root mean square

Dimensionless numbers

Re	Reynolds number	$(= G\,D\,\mu^{-1})$
Gr^*	modified Grashof number based on q	$(= g\beta q D_{hy}{}^4 / k\upsilon^2)$
q^+	non-dimensional heat flux number	$(= (q/G)\,(\beta/Cp))$
Pr	Prandtl number	$(=\mu C_p/k)$
Pr_{avg}, $\overline{Pr}$	averaged or modified Prandtl number	$(= (H_w - H_b)\mu_b / (k_b \times (T_w - T_b)))$

Abbreviations

CP	critical point
SCW	supercritical water
SCHT	supercritical heat transfer
HTC	heat transfer coefficient

5. References

Bishop, A.A., Sandberg, R.O., and Tong, L.S., "Forced convection heat transfer to water at near-critical temperatures and supercritical pressures", *A.I.Ch.E.-I.Chem.E Symposium Series No*. 2, 1965, pp. 77−85

Bourke, P.J., and Denton, W.H., "An unusual phenomenon of heat transfer near the critical point", Memorandum AERE-M 1946, Chemical Engineering and Process

Technology Division, U.K.A.E.A. Research Group, Atomic Energy Research Establishment, Harwell, Berkshire, August, 1967, 9 pages

Chalfant, A.I., "Heat transfer and fluid friction experiments for the supercritical water reactor", Report PWAC-109, 1954

Cheng, X., 2009, Private communication

Cheng, X., Yang, Y.H., and Huang, S.F., "A simple heat transfer correlation for SC fluid flow in circular tubes", NURETH-13, Kanazawa City, Ishikawa Prefecture, Japan, September 27-October 2, 2009

Cheng, X., and Schulenberg, T., "Heat transfer at supercritical pressures–literature review and application to an HPLWR", Wissenschaftliche Berichte (Tech. Report) FZKA6609, Forschungszentrum Karlsruhe, Mai, 2001

Dittus, F.W., and Boelter, L.M.K., University of California, Berkeley, Publications on Engineering, Vol. 2, 1930, pp. 443–461

Gnielinski, V., "New equation for heat and mass transfer in turbulent pipe and channel flow", *Intern. Chem. Eng.*, Vol. 16, No. 2, 1976, pp. 359–366

Griem, H., A new procedure for the at near-and supercritical prediction pressure of forced convection heat transfer, *Heat Mass Trans.*, Vol. 3, 1996, pp. 301–305

Groeneveld, D.C., and Zahlan, H.Z., SCWR data compilation and LUT, Progress Report to AECL, December 31, 2009

Gupta, S., Mokry, S., Farah, A., King, K., Peiman, W., and Pioro, I., "Developing a heat-transfer correlation for supercritical-water flow in bare vertical tubes and its application", 2010 UOIT unpublished report

Hadaller, G., and Banerjee, S., "Heat transfer to superheated steam in round tubes", AECL Report, 1969

Hall, W.B., Jackson, J.D. and Watson, A., "A review of forced convection heat transfer to fluids at supercritical pressures", *Proc. I. Mech. E.*, Vol. 182, Part 31, Bristol Symposium, HTFS 3907, 1968

Harrison, G.S., and Watson, A., "A experimental investigation of forced convection to supercritical pressure water in heated small bore tubes", Proceedings of the Institute of Mechanical Engineers, 190 (40/76), 1976b, pp. 429–435

Herkenrath, H., Mörk-Mörkenstein, P., Jung, U., and Weckermann, F. J., "Wärmeubergung an wasser bei erzwungener strömung in drückbereich von 140 bis 250 Bar", EUR-3658d, 1967

Jackson, J. D., "Consideration of the heat transfer properties of supercritical pressure water in connection with the cooling of advanced nuclear reactors", Proc. of the 13th Pacific Basin Nuclear Conference Shenzhen City, China, 2002

Jackson, J. D., Cotton, M. A., and Axcell, B. P., "Studies of mixed convection in vertical tubes", *Int. J. Heat Fluid Flow*, Vol.10, No. 1, 1989

Jackson, J.D. and Hall, W.B., "Forced convection heat transfer to fluids at supercritical pressure", in "Turbulent forced convection in channels and bundles, S. Kakaç and D.B. Spalding (editors), Hemisphere Publishing Corp., Washington, USA, Vol. 2, 1979a, pp. 563−611

Jackson, J.D., and Hall, W.B., "Influences of buoyancy on heat transfer to fluids flowing in vertical tubes under turbulent conditions, in "Turbulent forced convection in channels and bundles", S. Kakaç and D.B. Spalding (editors), Hemisphere Publishing Corp., Washington, USA, Vol. 2, 1979b, pp. 613−641

Kirillov, P., Pometko, R., Smirnov, A. et al., "Experimental study on heat transfer to supercritical water flowing in 1- and 4-m-Long Vertical Tubes", Proc. GLOBAL'05, Tsukuba, Japan, Oct. 9–13, Paper No. 518, 2005

Koshizuka, S., and Oka, Yo., "Computational analysis of deterioration phenomena and thermal-hydraulic design of SCR, Proceedings of the 1st International Symposium on Supercritical Water-Cooled Reactor Design and Technology (SCR-2000), Paper No. 302, 2000

Krasnoshchekov, E. A., and Protopopov, V. S., "Experimental study of heat exchange in carbon dioxide in the supercritical range at high temperature drops", *Teplofizika Vysokikh Tempraturi* (High Temp.), Vol. 4, No. 3, 1966

Kuang, B., Zhang, Y., and Cheng, X., "A new, wide-ranged heat transfer correlation of water at supercritical pressures in vertical upward ducts, NUTHOS-7, Seoul, Korea, 2008

Löwenberg, M., Starflinger, J., Laurien, E., and Schulenberg, T., "A look-up table for heat transfer of supercritical water", Proc. GLOBAL 2005, Paper No. 037, 2005, pp. 1–6

Löwenberg, M., Starflinger, J., Laurien, E., Class, A., and Schulenberg, T., "Supercritical heat transfer in vertical tubes": A Look-up table, *Progress in Nuclear Energy*, Vol. 50, 2008, pp. 532−538

McEligot, D. M., and Jackson, J. D., "Deterioration criteria for convective heat transfer in gas flow through non-circular ducts", *Nucl. Eng. Des.,* 2004, pp. 327−333

Mokry, S., Gospodinov, Ye., Pioro, I., and Kirillov, P., "Supercritical water heat-transfer correlation for vertical bare tubes", Proceedings of the 17th International Conference on Nuclear Engineering ICONE-17, Brussels, Belgium, July 12-16, Paper # 76010, 2009a, 8 pages

Petukhov, B.S., and Polyakov, A.F., "Heat transfer in turbulent mixed convection", Hemisphere Publishing Corp., New York, NY, USA, Chapter 7.1, Heat Transfer at Supercritical Pressures, 1988, pp. 183–201

Pioro, I.L., and Duffey, R.B., "Experimental heat transfer in supercritical water flowing inside channels (survey)", *Nucl. Eng. Des.,* Vol. 235, 2005, pp. 2407−2430

Pioro, I.L., Khartabil, H.F., and Duffey, R.B., Heat transfer to supercritical fluids flowing in channels – empirical correlations (survey), *Nucl. Eng. Des.*, Vol. 230, No. 1–3, 2004, pp. 69–91

Pioro, I.L. 2010, Private communication

Pis'mennyy, E.N., Razumovskiy, V.G., Maevskiy E.M. et al., "Experimental study on temperature regimes to supercritical water flowing in vertical tubes at low mass fluxes, Proceedings of the International Conference GLOBAL-2005, Tsukuba, Japan, October 9–13, Paper No. 519, 2005, 9 pages

Polyakov, A.F., "Mechanism and limits on the formation of conditions for impaired heat transfer at a supercritical coolant pressure", High Temperatures (Теплофизика Высоких Температур, стр. 1210–1219), 13 (6), 1975, pp. 1119–1126

Randall, D.G., "Some heat transfer and fluid friction experiments with supercritical water", Report NDA 2051, November (also TID-7529, Part 3, November, 1957

Seider, N. M., and Tate, G. E., "Heat transfer and pressure drop of liquids in tubes", *Ind. Eng. Chem.* 28 (12), 1936, pp. 1429–1435

Shiralkar, B.S. and Griffith, P., "Deterioration in heat transfer to fluids at supercritical pressures and high heat fluxes", *Journal of Heat Transfer*, Transactions of the ASME, 91(1), February, 1969, pp. 27–36

Shiralkar, B. and Griffith, P., "The deterioration in heat transfer to fluids at SCP and high heat fluxes, Report, Engineering Projects Laboratory, MIT, Cambridge, MA, USA, June, 1968, 185 pages

Swenson, H.S., Carver, J.R., and Kakarala, C.R., Heat transfer to supercritical water in smooth-bore tubes, *J. of Heat Transfer*, *Trans. ASME Series C*, 87 (4), 1965, pp. 477–484

Thompson, W.R. and Geery, E.L., 1960, "Heat transfer to cryogenic hydrogen at supercritical pressures", Cryogenic Engineering Conference (US), 1960, pp. 391–40

Watts, M. J., and Chou, C-T., "Mixed convection heat transfer to supercritical pressure water", Proc. 7th, IHTC, Munich, Germany, 1982, pp. 495–500

Yamagata, K., Nishikawa, K., Hasegawa, S., Fujii, T., and Yoshida, S., "Forced convective heat transfer to supercritical water flowing in tubes", *Int. J. Heat Mass Transfer*, Vol. 15 (12), 1972, pp. 2575–2593

Zahlan, H., Groeneveld, D.C., Tavoularis, S., "Look-up table for trans-critical heat transfer", the 2nd Canada-China Joint Workshop on Supercritical Water-Cooled Reactors (CCSC-2010), Toronto, Canada, April 25-28, 2010, 18 pages

Table 1 SCHT water data compilation

Database source	Number of references	Number of data after screening	Data availability
UO	28	6024	Tables and graphs
SJTU	11	7168	Tables and graphs
Stuttgart U	15	2936	Tables and graphs
UOIT	20	8125	Tables and graphs
Combined compilation for all databases			
Number of data before screening	36030	Number of data after screening	24253

Table 2: All combined SCHT water data sets

Reference	P (MPa)	T_b (˚C)	q (kW/m^2)	G (kg/m^{2}s)	Tube ID (mm)	Number of data
Ackerman (1970)	22.75−31.03	90.7−405	158− 1260	407−1221	9.4−24.4	409
Alekseev et al. (1976)	24.5	101−341	270−580	380	10.4	99
Alferov et al. (1969)	24.5−30.4	55-261	473−521	342	20	179
Alferov et al. (1975)	26.5	76−248	480	447	20	63
Barulin et al. (1971)	24.5	320−381	480−490	467	3	45
Bishop et al. (1965)	22.47−27.8	271−524	309−3526	663−3607	2.5−5.1	809
Belyakov data of Cheng (xx)*	25	115−489	174−1161	300−2000	20	85
Bourke and Denton (1967)	23−25..4	310−348	1230−2240	1207−2713	4	52
Chalfant (1954)	34.5	96−223	3533−5457	2034, 2712	1.4, 1.6	93
Dickenson and Welch (1958)	24.2−31.1	102−536	748−1844	2170−3418	7.6	123
Domin (xx)*	22.7−25	338−398	1254−2264	1210−2720	4	43
Dyadyakin and Koblyakov (1971)	22.5	391−418	3910	5000	3 mm	10
Glushchenko et al. (1972)	22.54	19−402	1050−1770	750, 1000	4, 6, 8	104
Goldmann (1961)	34.5	222−363	3533−3659	2034	1.6	26
Griem (1996)	22.08−25	332−424	300−600	500−2500	14	666
Harrison and Watson (1976b)	22.5, 24.5	86−370	490−2323	467−2250	1.64−20	174
Herkenrath et al. (1967)	22.5−25	302−446	200−2000	700−3500	10, 20	4580
Ishigai et al. (1976)	25.3	207−531	151−698	500	3.92	169
Jackson (2002)	22.8−26.5	54−348	221−820	407−686	2−20.4	334
Jacopo (xx)*	24.5	104−360	329, 698	376, 1180	10, 16	151
Kirillov et al. (2005)	23.9−25	299−516	72 −1308	201−1506	10	7871
Koshizuka and Oka (2000)	31	351−356	473	540	9.4	11
Krasyakova et al. (1977)	24.5	202−393	81−900	90−1000	20	216
Lee et al. (1974)	24.1	243−382	252−1577	542−2441	38.	1330

Continued

Table 2: All combined SCHT water data sets

Reference	P (MPa)	T_b (˚C)	q (kW/m^2)	G (kg/m^{2}s)	Tube ID (mm)	Number of data
Ornatsky et al. (1971)	25.5	24−384	395−1810	850−1530	3	116
Petukhov and Polyakov (1988)	22.6−29.4	186−380	379−2400	424−2000	3, 5, 8	115
Pis'Menny et al. (2005)	23.5	18−304	76−496	248−509	6.3, 9.5	395
Polyakov (1975)	24.5−29.4	124−319	490−1810	424−1500	3, 8	90
Randall (1956)	24.5	201−218.6	570	595	8	17
Razumovskiy (2005)	23.5	17−325	76−496	248,249	6.28, 9.5	380
Schmidt (1959)	22.3−30.4	192−564	291– 815	700	5	369
Shiralkar and Griffith (1969)	22.8	312.5−375	252−426	461	10	165
Shitsman (1963)	23−25.3	202−434	190−1083	323−1500	6, 8, 10	1211
Shitsman (1968)	24.5−34.3	74−403	238−700	103−608	8, 16	580
Swenson et al. (1965)	22.75−31	127–516	787−1741	2150	9.4	439
Thompson and Geery (1960)	23	333−368	280−340	430	8	47
Vikhrev et al. (1967)	24.6, 26.5	60−407	362−1160	493−1400	7.8−20.4	668
Watts and Chou (1982)	25	149−177	250	493	32.2	20
Yamagata et al. (1972)	24.5	294−488	233−930	1200−1830	7.5, 10	1472
Yin et al. (2006)	26	286−434	200	600	29	34
Yoshida and Mori (2000)	24.5, 25.3	78−466	230−698	376−1180	10, 16, 18	493

* These datasets have unknown full reference.

Table 3 Number of SCW data by dataset before and after screening (all databases)

Reference	Before	After	Reference	Before	After
Ackerman (1970)	1038	409	Shitsman (1968)	732	580
Alekseev et al. (1976)	99	99	Styrikovich et al. (1967)	119	0
Alferov et al. (1969)	211	179	*Swenson et al. (1965)*	647	439
Alferov et al. (1975)	63	63	Vikhrev et al. (1967)	1069	668
Barulin et al. (1971)	45	45	Watts and Chou (1982)	20	20
Bishop et al. (1965)	1218	809	*Yamagata et al. (1972)*	1899	1472
Belyakov (xx)	85	85	Yin et al. (2006)	34	34
Dickenson and Welch (1958)	123	123	*Yoshida and Mori (2000)*	494	493
Dyadyakin & Koblyakov (1971)	10	10	Zhu (xx)*	87	0
Domin (xx)	43	43	*Bourke and Denton (1967)*	52	52
Glushchenko et al. (1972)	132	104	*Chalfant (1954)*	93	93
Goldmann (1961)	26	26	*Harrison and Watson (1976b)*	174	174
Griem (1996)	1201	666	*Jacopo (xx)*	151	151
Herkenrath et al. (1967)	8745	4580	*Jackson (2002)*	334	334
Ishigai et al. (1976)	169	169	*Koshizuka and Oka (2000)*	11	11
Kirillov et al. (2005)	11421	7871	*Petukhov and Polyakov (1988)*	187	115
Krasyakova et al. (1977)	216	216	*Pis'Menny et al. (2005)*	411	395
Lee et al. (1974)	2062	1330	*Polyakov (1975)*	90	90
Ornatsky et al. (1971)	210	116	*Randall (1956)*	17	17
Razumovskiy (2005)	380	380	*Shiralkar and Griffith (1969)*	165	165
Schmidt (1959)	369	369	*Thompson and Geery (1960)*	47	47
Shitsman (1963)	1331	1211	**Total**	**36030**	**24253**

References in italics were updated recently by UOIT database.
* This dataset has an unknown full reference.

Table 4 Overall average and rms errors in the three supercritical sub-regions

Correlation	Liquid-like region		Gas-like region		Close to CP or PC point	
	e_A, %	e_S, %	e_A, %	e_S, %	e_A, %	e_S, %
Bishop et al. (1965)	5	28	5	20	23	31
Swenson et al. (1965)	1	31	-16	21	4	23
Krasnochekov et al. (1967)	18	40	-30	32	24	65
Watts and Chou (1982), Normal	6	30	-6	21	11	28
Watts and Chou (1982), Deter.	2	26	9	24	17	30
Griem (1996)	2	28	11	28	9	35
Jackson (2002)	15	36	15	32	30	49
Mokry et al. (2008)	-5	26	-9	18	-1	17
Kuang et al. (2008)	-6	27	10	24	-3	26
Cheng et al. (2009)	4	30	2	28	21	85
Gupta et al. (2010)	-26	33	-12	20	-1	18
Koshizuka and Oka (2000)	26	47	27	54	39	83
Hadaller and Banerjee (1969)	34	53	14	24	-	-
Sieder and Tate (1936)	46	65	97	132	-	-
Dittus-Boelter (1930)	24	44	90	127	-	-
Gnielinski (1976)	10	36	99	139	-	-

Table 5 Single-phase and supercritical prediction methods used for the application of the compiled water data

Reference	Prediction method
Dittus-Boelter (1930)†	$\mathrm{Nu_b} = 0.0243\mathrm{Re_b^{0.8}}\,\mathrm{Pr_b^{0.4}}$
Sieder and Tate (1936)†	$\mathrm{Nu_b} = 0.027\,\mathrm{Re_b^{0.8}}\,\mathrm{Pr_b^{1/3}}(\mu/\mu_w)^{0.14}$
Hadaller and Banerjee (1969)†	$\mathrm{Nu_f} = 0.0101\,\mathrm{Re}_f^{0.8774}\,\mathrm{Pr}_f^{0.6112}(L/D)^{0.0328}$
Gnielinski (1976)†	$\mathrm{Nu} = \frac{(f/8)(\mathrm{Re_b}-1000)\mathrm{Pr_b}}{1+12.7(f/8)^{1/2}(\mathrm{Pr}^{2/3}-1)}\left(\frac{\mathrm{Pr_b}}{\mathrm{Pr_w}}\right)^{0.11}(1+(D/L)^{2/3})$ where $f = 1/(1.82\,log_{10}(\mathrm{Re})-1.64)^2$ $(T_b/T_w)^{0.45}$ replaces $(\mathrm{Pr_b}/\mathrm{Pr_w})^{0.11}$ when $T_b > T_{pc}$
Bishop et al. (1965)	$\mathrm{Nu_b} = 0.0069\mathrm{Re}_b^{0.9}\,\overline{\mathrm{Pr}}_b^{0.66}\left(\frac{\rho_w}{\rho_b}\right)^{0.43}(1+2.4\frac{D}{L})$
Swenson et al. (1965)	$\mathrm{Nu_w} = 0.00459\mathrm{Re_w^{0.923}}\,\overline{\mathrm{Pr}}_w^{0.613}(\rho_w/\rho_b)^{0.231}$
Krasnoscheckov et al. (1967)	$\mathrm{Nu_b} = \mathrm{Nu_0}(\rho_w/\rho_b)^{0.3}(C_{p,avg}/C_{p,b})^n$, $\mathrm{Nu_0} = \frac{(\xi/8)\mathrm{Re_b}\overline{\mathrm{Pr}}}{12.7(\xi/8)^{0.5}(\overline{\mathrm{Pr}}^{2/3}-1)+1.07}$ and $\xi = 1/(1.82Log_{10}\mathrm{Re}_b - 1.64)^2$, $n = 0.4$ for $(T_w/T_{pc}) \le 1$ or $(T_b/T_{pc}) \ge 1.2$, $n = n_1 = 0.22 + 0.18(T_w/T_{pc})$ for $1 \le (T_w/T_{pc}) < 2.5$ and $n = n_1 + (5n_1-2)(1-(T_b/T_{pc}))$ for $1 \le (T_b/T_{pc}) \le 1.2$, T in K
Yamagata et al. (1972)	$\mathrm{Nu_b} = 0.0135\mathrm{Re_b^{0.85}}\mathrm{Pr_b^{0.8}}F_c$, $F_c = 1$ for $\mathrm{E} \succ 1$, $F_c = 0.67\overline{Pr}_{pc}^{(\ 0.05)}(\overline{Cp}/Cp_b)^{n1}$ for $0 < \mathrm{E} < 1$ and $F_c = (\overline{Cp}/Cp_b)^{n2}$ for $\mathrm{E} \prec 0$, $\mathrm{E} = (T_{pc} - T_b)/(T_w - T_b)$ $n_1 = 0.77(1+1/\mathrm{Pr_{pc}}) + 1.49$ and $n_2 = 1.44(1+1/\mathrm{Pr_{pc}}) - 0.53$
Koshizuka and Oka (2000)	$\mathrm{Nu_b} = 0.015\,\mathrm{Re_b^{0.85}}\,\mathrm{Pr_b}^{(0.69-81000/CHF+1000f_cq)}$, $q(\mathrm{W/m^2})$, $fc = 2.9\times10^{-8} + 0.11/CHF$, for $H < 1.5$ MJ/kg $fc = -8.7\times10^{-8} - 0.65/CHF$, for $1.5 \le H \le 3.3$ MJ/kg and $fc = -9.7\times10^{-7} + 1.3/CHF$, for $3.3 < H \le 4$ MJ/kg, $CHF = 200G^{1.2}$

Continued, † single-phase correlation

The 5th Int. Sym. SCWR (ISSCWR-5)
Vancouver, British Columbia, Canada, March 13-16, 2011

Table 5 Single-phase and supercritical prediction methods used for the application of the compiled water data

Reference	Prediction method
Watts and Chou (1982)	$Nu_b = 0.021 Re_b^{0.8} Pr_b^{0.55} (\frac{\rho_w}{\rho_b})^{0.35} f(\frac{Gr_b}{Re_b^{2.7} Pr_b^{0.5}})$, where for normal heat transfer: $f(\frac{Gr_b}{Re_b^{2.7} Pr_b^{-0.5}}) = (1 - 3000\frac{Gr_b}{Re_b^{2.7} Pr_b^{0.5}})^{0.295}$ if $\frac{Gr_b}{Re_b^{2.7} Pr_b^{0.5}} \le 10^{-4}$, or $f(\frac{Gr_b}{Re_b^{2.7} Pr_b^{-0.5}}) = (7000\frac{Gr_b}{Re_b^{2.7} Pr_b^{0.5}})^{0.295}$ if $\frac{Gr_b}{Re_b^{2.7} Pr_b^{0.5}} \succ 10^{-4}$ where $Gr_b = (\rho_b - \rho_{avg}) D_{hy}^3 g/\rho_b \nu_b^2$
Griem (1996)	$Nu_b = 0.0169 Re_b^{0.8356} Pr_{sel}^{0.432} \omega, \; \bar{k} = 0.5(k_b + k_w), \mu = \mu_b, Pr_{sel} = Cp_{sel}\, \mu_b / \bar{k}$ and $\omega = \min(1.0, \max(0.82; 0.82 + 9.7\times10^{-7}(H_b - 1.54\times10^{6})))$, H_b in kJ/kg
Jackson (2002)	$Nu_b = 0.0183 Re_b^{0.82} Pr_b^{0.5} (\frac{\rho_w}{\rho_b})^{0.3} (\frac{\bar{Cp}}{Cp_b})^{n}$
Kuang et al. (2008)	$Nu = 0.0239 Re_b^{0.759} \bar{Pr}^{0.833} (\frac{k_w}{k_b})^{0.0863} (\frac{\mu_w}{\mu_b})^{0.832} (\frac{\rho_w}{\rho_b})^{0.31} (\overset{*}{Gr})^{0.014} (\overset{+}{q})^{-0.021}$ This correlation is valid for: P = 22.75–31.03 MPa, G = 380–3600 kg/m^2 s, q = 233–3474 kW/m2, ID = 7.5–26 mm. P = 22.75–31.03 MPa, G = 380–3600 kg/m^2 s, q = 233–3474 kW/m^2, ID = 7.5–26 mm
Mokry et al. (2008)	$Nu = 0.0061 Re_b^{0.904} \bar{Pr}_b^{0.684} (\frac{\rho_w}{\rho_b})^{0.564}$
Cheng, Xu et al. (2009)	$F = Nu/Nu_0 = Nu/0.023 Re_b^{0.8} Pr_b^{1/3} = \min(F_1, F_2), \; F_1 = 0.85 + 0.776(\pi_A \times 10^3)^{2.4}$ and $F_2 = 0.48/(\pi_{A,pc} \times 10^3)^{1.55} + 1.21(1 - \pi_A/\pi_{A,pc})$
Gupta et al. (2010)	$Nu_w = 0.0033 Re_w^{0.941} Pr_{avg,w}^{0.764} (\frac{\rho_w}{\rho_b})^{0.156} (\frac{\mu_w}{\mu_b})^{0.398}$; $Nu_{w,entrance} = Nu_w (1 + exp(-\frac{L}{24D}))^{0.3}$

Table 6 Error bands for the best correlations for the combined databases at the three SCHT regions

Error band for 15283 data points	Percentage of data predicted by a correlation, %		
	Mokry et al. (2008)	Gupta et al. (2010)	Swenson et al. (1965)
Near CP region			
e_{10}	46	50	44
e_{20}	79	78	71
e_{30}	92	91	86
e_{50}	99	98	95
Error band for 4386 data points	Mokry et al. (2008)	Watts & Chou (1982), DHT	Kuang et al. (2008)
High density state region (liquid-like region)			
e_{10}	41	28	33
e_{20}	64	57	59
e_{30}	79	79	79
e_{50}	94	95	94
Error band for 4584 data points	Mokry et al. (2008)	Gupta et al. (2010)	Bishop et al. (1965)
Low density state region (gas-like region)			
e_{10}	47	35	45
e_{20}	79	71	75
e_{30}	92	88	89
e_{50}	99	98	97

DHT deteriorated heat transfer

Table 7 Error bands for the best correlations including the entry region effect for the three SCHT regions

Error band for 3441 data points	Percentage of data predicted by a correlation, %	
	Mokry et al. (2008)	Gupta et al. (2010)
	Near CP region:	
e_{10}	54	54
e_{20}	80	77
e_{30}	90	89
e_{50}	99	98
Error band for 1674 data points	High density state region (liquid-like region)	
e_{10}	33	15
e_{20}	56	36
e_{30}	69	61
e_{50}	89	88
Error band for 553 data points	Low density state region (gas-like region)	
e_{10}	38	27
e_{20}	71	63
e_{30}	84	79
e_{50}	97	95

Table 8 Average error, rms error and error band percentage for the best correlations by dataset (close to critical point region)

Data set	# Points	Kuang et al. (2008)						Gupta et al. (2010)						Mokry et al. (2008)					
		e_A	e_S	e_{10}	e_{20}	e_{30}	e_{50}	e_A	e_S	e_{10}	e_{20}	e_{30}	e_{50}	e_A	e_S	e_{10}	e_{20}	e_{30}	e_{50}
Ackerman (1970)	245	-4	17	42	76	96	100	2	15	59	82	97	99	2	14	61	81	96	100
Alekseev et al. (1976)	41	-32	34	2	7	37	93	-20	22	10	39	90	100	-16	18	22	61	100	100
Barulin et al. (1971)	44	0	18	30	68	91	100	-12	19	18	55	100	100	-11	15	41	84	100	100
Bishop et al. (1965)	429	-20	25	18	43	76	100	-15	17	31	73	100	100	-15	17	24	69	99	100
Belyakov data of Cheng	22	-25	29	5	23	50	100	-22	27	32	50	59	96	-23	28	14	46	68	91
Bourke and Denton (1967)	46	12	39	30	41	63	78	21	40	11	33	54	80	14	32	17	41	65	87
Chalfant (1954)	50	-46	46	0	0	2	68	-39	39	0	0	16	94	-31	32	0	2	36	100
Domin	34	8	40	21	38	59	85	14	39	9	38	59	82	9	33	18	47	62	88
Glushchenko et al. (1972)	47	-40	46	2	17	21	51	-35	37	9	13	30	96	-34	37	6	11	23	98
Griem (1996)	511	14	18	32	67	95	100	20	28	37	54	70	92	17	22	34	63	81	98
Harrison and Watson (1976b)	143	-12	23	29	60	80	99	-6	15	46	88	94	100	-6	15	59	80	95	100
Herkenrath et al. (1967)	3687	-14	21	29	59	84	100	-2	14	55	86	95	100	-3	14	48	86	97	100
Ishigai et al. (1976)	61	7	23	36	66	79	95	-5	19	53	67	82	100	-7	14	57	85	97	100
Jacopo (xx)	82	-11	17	35	62	100	100	-2	15	56	78	94	100	-3	13	68	83	100	100
Jackson (2002)	151	-11	23	36	62	80	97	-13	24	24	54	74	99	-12	21	38	62	76	100
Kirillov et al. (2005)	5678	9	28	37	61	78	91	0	14	60	86	96	100	2	15	55	84	94	100
Krasyakova et al. (1977)	111	-31	34	9	23	33	100	-24	25	6	23	87	100	-24	25	7	27	74	100
Lee et al. (1974)	1093	-26	30	11	32	59	98	-4	18	43	77	92	99	-10	17	34	75	95	100
Ornatsky et al. (1971)	27	2	47	22	41	59	89	15	43	33	56	74	89	7	28	33	74	85	89
Petukhov and Polyakov	71	-4	26	20	44	76	96	-12	20	28	63	87	100	-11	18	47	70	87	100
Pis'Menny et al. (2005)	35	-26	40	9	23	40	71	-22	38	9	26	34	94	-18	30	20	37	51	100
Polyakov (1975)	52	1	31	15	33	46	96	-3	15	40	85	100	100	0	10	62	96	100	100
Razumovskiy (2005)	25	-42	43	0	8	20	68	-36	37	0	8	20	100	-27	30	20	28	52	100
Schmidt (1959)	139	3	25	32	60	77	95	-1	24	24	56	84	97	-2	21	33	68	90	97
Shiralkar and Griffith (1969)	131	7	22	55	70	79	96	1	25	26	53	80	95	0	16	47	79	92	100
Shitsman (1963)	777	3	23	38	67	85	96	-2	23	38	72	89	95	-2	19	40	75	92	98
Shitsman (1968)	206	-11	29	20	49	70	89	-7	21	41	68	87	98	-5	19	45	74	88	99
Swenson et al. (1965)	99	-8	16	64	77	86	100	0	15	62	85	94	100	1	12	66	90	98	100
Thompson and Geery (1960)	42	2	18	36	74	95	98	0	16	43	86	93	98	-2	12	48	95	98	100
Vikhrev et al. (1967)	279	-24	28	18	36	53	100	-6	13	46	89	100	100	-8	13	47	88	100	100
Yamagata et al. (1972)	645	11	33	34	64	75	88	5	24	38	68	85	93	4	22	41	74	86	95
Yoshida and Mori (2000)	223	1	25	33	60	87	93	18	35	19	31	47	87	21	38	17	26	41	83

Table 9 Average error, rms error and error band percentage for the leading correlations by dataset (gas-like region)

Data set	# Points	Bishop et al. (1965)						Mokry et al. (2008)						Gupta et al. (2010)					
		e_A	e_S	e_{10}	e_{20}	e_{30}	e_{50}	e_A	e_S	e_{10}	e_{20}	e_{30}	e_{50}	e_A	e_S	e_{10}	e_{20}	e_{30}	e_{50}
Bishop et al. (1965)	335	4	12	60	92	97	100	-11	14	50	88	97	100	-12	15	42	82	97	100
Belyakov data of Cheng	25	-7	22	20	56	80	100	-18	25	20	48	80	100	-19	26	28	48	72	96
Dickenson and Welch (1958)	66	-4	21	88	94	97	97	-13	22	29	96	97	99	-16	24	11	82	97	99
Griem (1996)	143	8	11	58	97	100	100	-4	8	78	99	100	100	-9	11	62	94	100	100
Herkenrath et al. (1967)	811	3	15	51	82	96	100	-11	15	42	77	97	100	-12	17	40	71	94	100
Ishigai et al. (1976)	60	-11	19	27	73	90	98	-22	25	12	37	83	98	-26	30	13	32	58	97
Jackson (2002)	21	-33	33	0	0	29	100	-42	42	0	0	0	100	-47	47	0	0	0	95
Kirillov et al. (2005)	1799	13	21	44	75	87	96	-4	13	57	87	98	100	-7	17	36	80	94	100
Krasyakova et al. (1977)	34	3	11	62	94	100	100	-14	16	27	79	100	100	-16	20	29	53	91	100
Polyakov (1975)	32	-24	34	41	53	56	78	-33	39	6	38	53	72	-34	42	19	41	53	66
Schmidt (1959)	159	-25	28	11	25	62	99	-33	35	2	11	28	98	-38	39	1	3	13	97
Shiralkar and Griffith (1969)	29	-6	15	66	79	93	100	-18	21	38	66	83	100	-25	27	0	41	69	100
Shitsman (1963)	131	1	22	37	65	82	97	-13	22	30	64	86	99	-18	25	24	49	81	96
Shitsman (1968)	25	39	42	0	20	32	64	14	18	32	60	100	100	14	21	44	64	72	100
Swenson et al. (1965)	166	-2	21	21	73	87	96	-12	22	51	70	86	95	-14	23	50	63	81	93
Vikhrev et al. (1967)	49	15	19	37	69	94	100	-3	7	86	100	100	100	-1	10	67	98	100	100
Yamagata et al. (1972)	527	7	14	58	83	96	100	-4	12	53	95	99	100	-10	15	39	81	98	100
Yoshida and Mori (2000)	99	-36	41	0	14	55	80	-41	44	0	5	27	76	-45	48	0	0	8	70

Table 10 Average error, rms error and error band percentage for the leading correlations by dataset (liquid-like region)

Data set	# Points	Watts & Chou (1982), DHT						Mokry et al. (2008)						Kuang et al. (2008)					
		e_A	e_S	e_{10}	e_{20}	e_{30}	e_{50}	e_A	e_S	e_{10}	e_{20}	e_{30}	e_{50}	e_A	e_S	e_{10}	e_{20}	e_{30}	e_{50}
Ackerman (1970)	160	6	18	28	61	98	100	-3	12	60	92	99	100	-1	16	44	74	97	100
Alekseev et al. (1976)	58	-10	23	29	50	81	100	4	30	28	52	72	90	-9	19	36	66	90	100
Alferov et al. (1969)	174	-27	28	2	11	69	99	-5	8	75	98	99	100	-23	24	0	40	87	99
Alferov et al. (1975)	63	-10	14	46	86	100	100	-7	23	16	46	91	98	-21	24	27	43	76	100
Bishop et al. (1965)	45	15	17	29	80	93	100	-10	12	49	96	100	100	-14	17	20	73	100	100
Belyakov data of Cheng	38	-21	32	11	21	40	97	-19	31	24	42	58	90	-15	28	16	45	63	100
Chalfant (1954)	43	7	14	49	77	100	100	-27	29	0	23	72	100	-38	38	0	0	14	95
Dickenson and Welch (1958)	50	23	25	4	38	84	98	4	10	82	98	98	100	-3	10	68	98	98	100
Glushchenko et al. (1972)	52	9	16	33	75	96	100	-17	21	29	65	77	100	-40	42	0	0	25	79
Harrison and Watson (1976b)	24	-18	20	21	54	96	100	-44	44	0	0	0	79	-42	43	0	0	0	96
Herkenrath et al. (1967)	82	22	26	11	37	74	99	5	16	51	84	94	100	3	11	74	94	98	100
Ishigai et al. (1976)	48	3	27	46	67	81	88	-26	33	8	17	63	94	-8	28	25	54	75	92
Jacopo (xx)	54	-11	20	20	61	91	100	3	25	28	70	80	94	-2	16	43	80	91	100
Jackson (2002)	162	-12	20	44	74	89	96	-10	27	56	72	75	88	-19	24	27	61	78	96
Kirillov et al. (2005)	394	-1	29	21	47	72	90	-7	23	41	70	83	95	6	27	39	66	80	90
Krasyakova et al. (1977)	71	-4	12	62	87	99	100	-26	31	18	34	65	90	-28	29	0	10	73	97
Lee et al. (1974)	237	5	12	51	93	99	100	2	11	65	94	99	100	-6	13	68	88	95	100
Ornatsky et al. (1971)	89	9	20	44	70	87	98	-9	19	37	74	90	100	-8	20	27	60	92	100
Pis'Menny et al. (2005)	360	-5	29	24	50	71	91	0	32	25	50	68	89	0	34	24	46	65	86
Polyakov (1975)	34	17	24	18	44	74	100	-8	15	62	82	91	100	-7	15	74	82	91	100
Razumovskiy (2005)	355	2	28	22	54	73	92	3	38	17	36	52	86	3	44	18	36	56	83
Schmidt (1959)	71	13	18	24	75	94	100	-18	20	14	69	92	100	-8	14	42	87	100	100
Shitsman (1963)	303	-10	26	33	59	78	94	-27	33	18	36	60	90	-21	27	24	50	78	94
Shitsman (1968)	349	-11	23	35	62	81	97	-12	27	31	51	77	93	-16	24	30	60	83	95
Swenson et al. (1965)	174	19	20	9	60	99	100	1	5	95	100	100	100	-4	8	86	95	99	100
Vikhrev et al. (1967)	340	14	21	36	66	84	98	3	13	73	92	97	99	-10	17	29	75	96	100
Watts, M.J., and Chou (1982)	20	3	10	55	95	100	100	-5	11	75	90	95	100	-3	9	80	95	100	100
Yamagata et al. (1972)	300	31	39	16	31	50	82	13	21	44	69	80	99	22	30	32	50	67	91
Yoshida and Mori (2000)	171	4	37	32	52	71	90	-3	40	14	37	55	77	-4	26	29	52	74	98

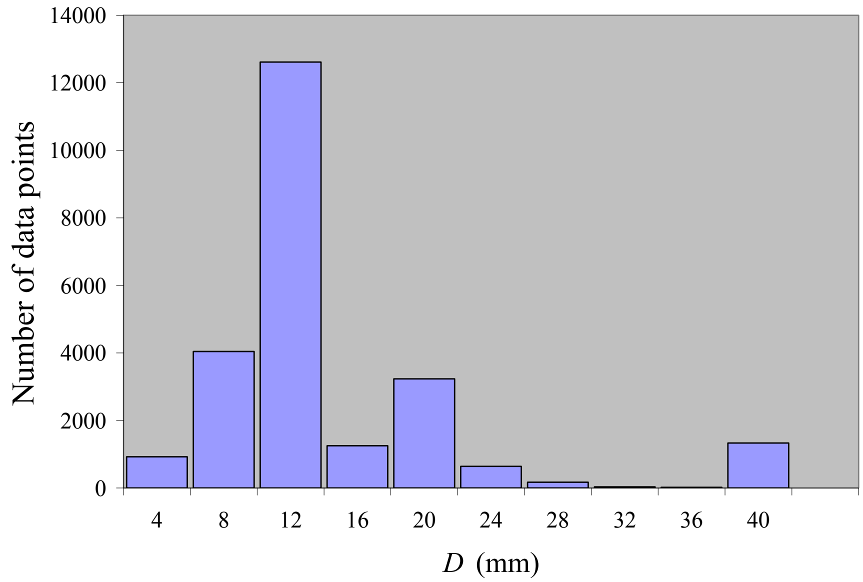

Figure 1 Numbers of data points for different *D* ranges for the combined SCW database.

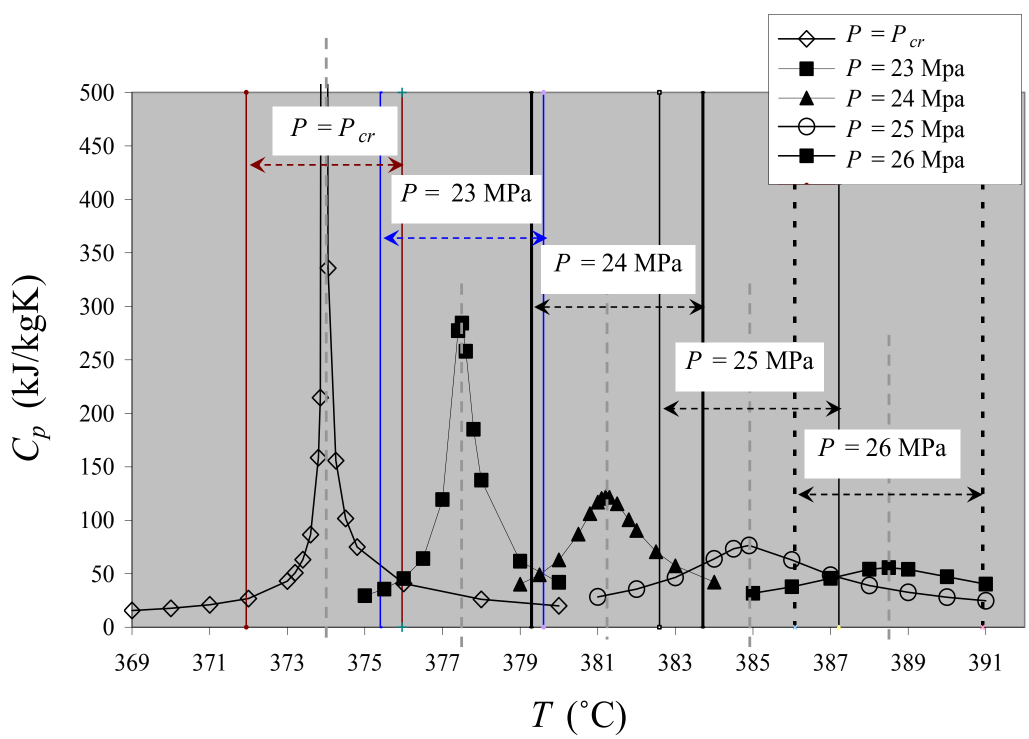

Figure 2 Variation of C_p for different pressures; horizontal lines mark the near-critical/ pseudo-critical ranges, each having a width of 2Δ*T*.

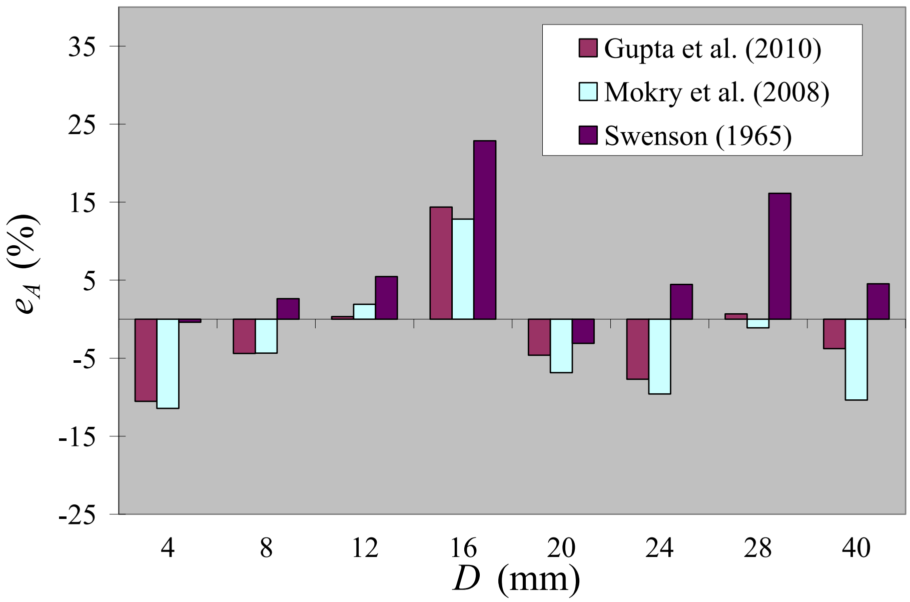

Figure 3 Distribution of e_A vs. D for the leading correlations in the near-critical/pseudo-critical sub-region.

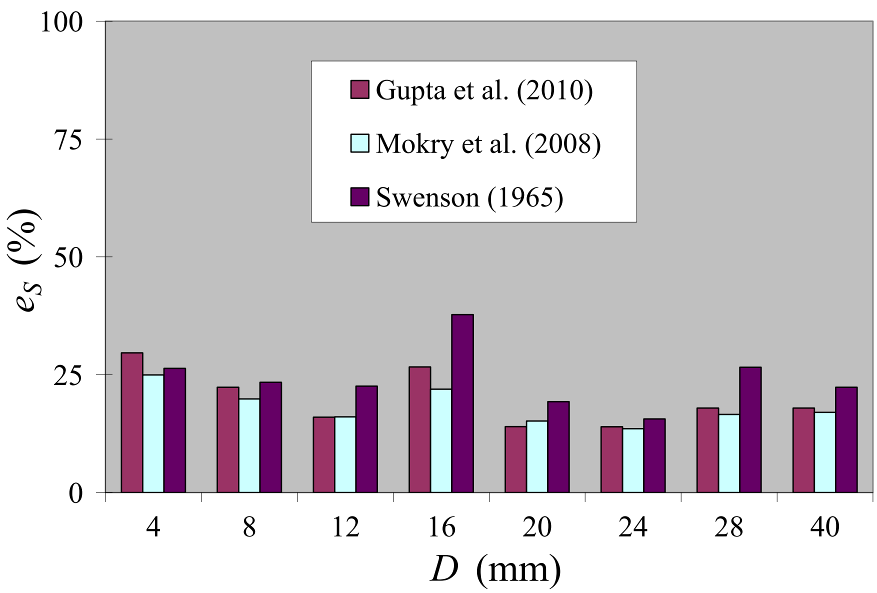

Figure 4 Distribution of e_S vs. D for the leading correlations in the near-critical/pseudo-critical sub-region.

APPENDIX C

TABULATED HEAT TRANSFER COEFFICIENTS OF THE TRANS-CRITICAL HEAT TRANSFER LOOK-UP TABLE

Guidelines for using the trans-critical heat transfer look-up table (TC LUT)

The table is designed for water flowing vertically upward inside heated tubes.

TC LUT flow conditions: pressure, mass flux, wall temperature difference and fluid enthalpy

The first row starting with the number1000 lists all TC LUT grid points for fluid enthalpy in kJ/kg, the first column from left starting with the number 19000 corresponds to all table grid points for pressure in kPa, the second column starting with the number100 presents all table grid points of mass flux in kg/m^{2}s and the third, column which starts with the number10 lists all table grid points for wall temperature difference in Kelvin.

TC LUT heat transfer coefficients

Numbers bounded by the third column from left and the first row from top to the end, correspond to the heat transfer coefficients h_{ref} in kW/m^{2}K of the TC LUT for a reference tube diameter of 8 mm; for a different diameter use the correction factor:

$$h = h_{ref} \left(\frac{d}{d_{ref}} \right)^{-0.2} .$$

			1000	1400	1600	1800	1900	2000	2050	2100	2150	2200	2250	2300	2400	2500	2600	2700	3000
19000	100	10	2.2	1.6	1.2	0.9	0.7	0.6	0.6	0.6	0.6	0.6	0.7	0.7	0.8	0.9	1.0	1.1	1.0
19000	100	20	2.1	1.5	1.1	0.8	0.6	0.6	0.5	0.6	0.6	0.6	0.6	0.7	0.8	0.9	1.0	1.1	1.0
19000	100	50	1.9	1.4	1.0	0.7	0.6	0.5	0.5	0.5	0.5	0.5	0.6	0.6	0.7	0.8	0.9	1.0	0.9
19000	100	100	1.5	1.2	0.9	0.7	0.5	0.5	0.4	0.5	0.5	0.5	0.5	0.6	0.6	0.7	0.8	0.9	0.8
19000	100	200	1.1	0.9	0.8	0.6	0.5	0.4	0.4	0.4	0.4	0.4	0.5	0.5	0.6	0.7	0.8	0.8	0.8
19000	100	300	0.9	0.9	0.7	0.6	0.4	0.4	0.4	0.4	0.4	0.4	0.4	0.5	0.5	0.6	0.7	0.8	0.8
19000	100	400	0.9	0.9	0.7	0.6	0.4	0.4	0.4	0.4	0.4	0.4	0.4	0.4	0.5	0.6	0.7	0.8	0.7
19000	100	500	0.9	0.9	0.7	0.6	0.4	0.4	0.3	0.3	0.4	0.4	0.4	0.4	0.5	0.6	0.7	0.7	0.7
19000	200	10	4.0	3.1	2.4	1.8	1.5	1.4	1.5	1.5	1.6	1.7	1.8	1.9	2.0	2.2	2.3	2.3	1.9
19000	200	20	3.8	2.9	2.2	1.7	1.4	1.3	1.4	1.5	1.5	1.6	1.7	1.8	2.0	2.1	2.2	2.2	1.9
19000	200	50	3.4	2.5	1.9	1.5	1.3	1.2	1.3	1.4	1.4	1.5	1.6	1.7	1.8	1.9	2.0	1.9	1.7
19000	200	100	2.6	2.0	1.6	1.3	1.1	1.1	1.2	1.2	1.3	1.3	1.4	1.5	1.6	1.6	1.6	1.5	1.4
19000	200	200	1.7	1.5	1.3	1.1	1.0	1.0	1.0	1.1	1.1	1.1	1.2	1.2	1.3	1.3	1.3	1.2	1.2
19000	200	300	1.4	1.4	1.2	1.0	0.9	0.8	0.9	0.9	0.9	0.9	1.0	1.0	1.1	1.1	1.2	1.2	1.2
19000	200	400	1.4	1.4	1.2	0.9	0.8	0.7	0.7	0.7	0.8	0.8	0.8	0.9	1.0	1.1	1.2	1.2	1.2
19000	200	500	1.4	1.4	1.1	0.9	0.8	0.7	0.7	0.7	0.7	0.7	0.8	0.8	0.9	1.1	1.2	1.3	1.2
19000	400	10	6.6	5.2	3.9	3.0	2.5	2.4	2.6	2.8	2.9	3.1	3.3	3.6	3.8	4.1	4.2	4.1	3.6
19000	400	20	6.2	4.9	3.7	2.8	2.4	2.3	2.5	2.6	2.8	3.0	3.2	3.4	3.7	4.0	4.2	4.1	3.6
19000	400	50	5.5	4.3	3.2	2.5	2.1	2.1	2.2	2.4	2.5	2.6	2.8	3.0	3.3	3.5	3.6	3.6	3.1
19000	400	100	4.3	3.4	2.6	2.1	1.8	1.8	1.9	2.0	2.1	2.2	2.3	2.5	2.6	2.7	2.8	2.7	2.5
19000	400	200	2.9	2.5	2.1	1.7	1.5	1.5	1.6	1.6	1.7	1.7	1.8	1.9	2.0	2.1	2.2	2.2	2.2
19000	400	300	2.3	2.2	1.8	1.6	1.4	1.3	1.3	1.3	1.4	1.4	1.5	1.6	1.7	1.9	2.0	2.1	2.1
19000	400	400	2.2	2.1	1.8	1.5	1.3	1.2	1.2	1.2	1.2	1.3	1.3	1.5	1.6	1.9	2.1	2.2	2.1
19000	400	500	2.2	2.1	1.8	1.5	1.2	1.1	1.1	1.1	1.2	1.2	1.3	1.4	1.6	1.9	2.1	2.2	2.1
19000	700	10	10.7	8.7	6.9	5.4	4.5	4.3	4.4	4.7	4.9	5.3	5.7	6.1	6.5	6.7	6.7	6.4	5.6
19000	700	20	10.1	8.3	6.5	5.1	4.2	4.0	4.2	4.4	4.7	5.0	5.4	5.9	6.4	6.7	6.6	6.3	5.5
19000	700	50	8.8	7.2	5.6	4.4	3.7	3.6	3.7	3.9	4.2	4.5	4.9	5.4	5.8	6.1	6.0	5.7	5.0
19000	700	100	6.8	5.4	4.3	3.4	3.0	2.9	3.0	3.2	3.3	3.5	3.8	4.1	4.5	4.7	4.8	4.7	4.3
19000	700	200	4.4	3.9	3.2	2.7	2.4	2.3	2.3	2.4	2.5	2.6	2.8	3.0	3.3	3.5	3.7	3.8	3.7
19000	700	300	3.4	3.3	2.8	2.4	2.0	1.9	1.9	1.9	2.0	2.1	2.2	2.5	2.8	3.1	3.4	3.6	3.5
19000	700	400	3.3	3.2	2.8	2.3	1.9	1.7	1.7	1.7	1.8	1.9	2.1	2.3	2.6	3.0	3.3	3.5	3.4
19000	700	500	3.3	3.2	2.7	2.2	1.8	1.7	1.7	1.7	1.8	1.9	2.0	2.3	2.6	3.0	3.3	3.5	3.4
19000	1000	10	14.6	12.3	10.5	8.8	7.4	6.8	6.9	7.3	7.7	8.3	9.0	9.8	10.4	10.7	10.6	9.9	8.3
19000	1000	20	13.6	11.4	9.6	8.0	6.8	6.4	6.6	6.9	7.4	8.0	8.8	9.6	10.3	10.6	10.5	9.7	8.3
19000	1000	50	11.9	9.8	8.0	6.6	5.8	5.6	5.8	6.2	6.6	7.3	8.1	9.1	9.7	9.9	9.6	8.9	7.6
19000	1000	100	9.3	7.5	6.1	5.1	4.6	4.5	4.6	4.8	5.2	5.7	6.4	7.2	7.8	8.0	7.9	7.4	6.5
19000	1000	200	6.4	5.5	4.7	3.9	3.4	3.3	3.3	3.4	3.6	3.9	4.3	4.8	5.4	5.8	6.1	6.1	5.6
19000	1000	300	4.9	4.7	4.0	3.4	2.9	2.7	2.6	2.7	2.8	3.0	3.3	3.7	4.3	4.8	5.3	5.4	5.1
19000	1000	400	4.6	4.5	3.9	3.2	2.7	2.4	2.4	2.5	2.6	2.8	3.0	3.4	4.0	4.5	5.0	5.2	4.9
19000	1000	500	4.6	4.5	3.8	3.1	2.6	2.4	2.4	2.4	2.6	2.7	3.0	3.4	3.9	4.5	4.9	5.1	4.8
19000	1500	10	19.2	16.5	14.4	12.5	11.2	10.9	11.4	12.2	13.1	14.1	15.2	16.3	17.0	17.0	16.4	15.0	12.4
19000	1500	20	18.0	15.6	13.4	11.5	10.4	10.3	10.8	11.6	12.5	13.5	14.6	15.7	16.5	16.7	16.2	14.9	12.6
19000	1500	50	15.6	13.4	11.1	9.4	8.7	8.8	9.5	10.2	11.0	12.0	13.3	14.5	15.4	15.6	15.2	14.2	11.9
19000	1500	100	11.9	10.1	8.4	7.2	6.7	6.9	7.3	7.9	8.5	9.4	10.5	11.8	12.7	13.1	13.0	12.3	10.3
19000	1500	200	8.2	7.5	6.5	5.6	5.1	5.0	5.2	5.5	5.9	6.5	7.3	8.2	9.2	10.0	10.3	10.1	8.6
19000	1500	300	6.8	6.6	5.7	4.9	4.3	4.0	4.1	4.3	4.6	5.0	5.6	6.4	7.4	8.2	8.7	8.7	7.7

19000	1500	400	6.5	6.3	5.4	4.6	3.9	3.7	3.8	3.9	4.2	4.6	5.1	5.8	6.6	7.4	7.9	8.0	7.2
19000	1500	500	6.4	6.2	5.3	4.4	3.8	3.6	3.6	3.8	4.1	4.4	4.9	5.5	6.2	7.0	7.6	7.8	7.0
19000	2000	10	25.3	21.5	17.9	15.3	14.2	14.6	15.9	17.2	18.6	19.9	21.1	22.0	22.5	22.3	21.2	19.2	15.3
19000	2000	20	23.5	20.4	16.9	14.4	13.4	13.9	15.2	16.5	17.9	19.2	20.5	21.6	22.2	22.1	20.9	18.7	14.8
19000	2000	50	20.3	17.2	14.2	12.2	11.6	12.3	13.5	14.7	16.0	17.3	18.6	19.8	20.7	20.7	19.9	18.0	14.2
19000	2000	100	15.7	13.2	11.0	9.7	9.3	9.8	10.6	11.6	12.6	13.7	15.0	16.3	17.4	17.9	17.5	16.2	13.3
19000	2000	200	11.0	10.0	8.7	7.6	7.2	7.3	7.8	8.5	9.2	10.1	11.1	12.3	13.4	14.2	14.4	13.8	11.8
19000	2000	300	9.1	8.8	7.6	6.6	6.0	6.0	6.3	6.8	7.4	8.1	9.0	9.9	11.0	11.8	12.3	12.1	10.6
19000	2000	400	8.5	8.4	7.2	6.2	5.5	5.4	5.7	6.1	6.6	7.1	7.8	8.6	9.6	10.5	11.0	11.1	9.8
19000	2000	500	8.4	8.2	7.1	6.0	5.2	5.1	5.3	5.7	6.2	6.7	7.3	8.1	9.0	9.9	10.5	10.6	9.5
19000	3000	10	36.6	30.7	24.7	20.3	18.2	18.7	20.3	22.3	24.2	26.1	27.7	29.1	30.0	30.0	28.8	26.2	20.2
19000	3000	20	33.8	28.7	23.2	19.1	17.3	18.0	19.6	21.5	23.4	25.3	27.1	28.7	29.7	29.8	28.6	25.9	20.0
19000	3000	50	29.0	24.4	19.8	16.6	15.5	16.3	17.9	19.7	21.5	23.2	25.0	26.6	27.9	28.3	27.4	24.9	19.4
19000	3000	100	22.3	19.0	15.7	13.5	12.8	13.5	14.9	16.3	17.9	19.4	20.9	22.5	24.0	24.7	24.3	22.5	17.7
19000	3000	200	15.4	14.2	12.3	10.9	10.4	10.9	11.9	13.0	14.3	15.5	16.7	18.0	19.3	20.1	20.2	19.2	15.8
19000	3000	300	12.6	12.2	10.7	9.5	8.9	9.2	10.0	10.9	11.8	12.8	13.9	15.0	16.1	17.1	17.5	17.0	14.6
19000	3000	400	11.9	11.6	10.1	8.7	8.0	8.1	8.6	9.3	10.1	11.0	11.9	12.9	14.1	15.2	15.8	15.7	13.8
19000	3000	500	11.6	11.3	9.8	8.4	7.5	7.5	7.9	8.6	9.3	10.1	11.0	12.0	13.3	14.4	15.1	15.1	13.5
19000	5000	10	51.8	42.1	32.3	24.9	20.7	20.1	21.3	23.1	25.1	27.2	29.5	31.8	33.8	34.8	34.4	32.4	27.6
19000	5000	20	47.9	39.7	30.5	23.4	19.7	19.3	20.6	22.3	24.2	26.3	28.7	31.2	33.2	34.1	33.6	31.7	26.9
19000	5000	50	40.9	33.8	26.1	20.5	17.9	18.0	19.3	20.9	22.6	24.4	26.5	28.7	30.6	31.6	31.4	29.8	25.6
19000	5000	100	31.0	26.0	20.8	17.1	15.5	15.8	17.0	18.4	19.8	21.3	23.0	24.9	26.9	28.2	28.5	27.4	23.8
19000	5000	200	21.7	19.7	16.7	14.4	13.2	13.5	14.4	15.6	16.9	18.2	19.7	21.5	23.3	24.9	25.5	24.9	22.0
19000	5000	300	17.7	16.9	14.7	12.8	11.8	11.9	12.7	13.7	14.9	16.2	17.6	19.2	21.1	22.6	23.4	23.1	20.7
19000	5000	400	16.6	16.0	14.0	12.1	11.0	11.1	11.8	12.7	13.8	15.0	16.4	18.0	19.8	21.3	22.2	22.0	19.8
19000	5000	500	16.3	15.8	13.8	11.8	10.7	10.7	11.3	12.3	13.3	14.5	15.8	17.4	19.1	20.7	21.6	21.4	19.3
20000	100	10	2.2	1.8	1.4	1.0	0.8	0.7	0.7	0.7	0.8	0.8	0.9	1.0	1.1	1.2	1.2	1.2	0.9
20000	100	20	2.0	1.7	1.3	0.9	0.7	0.6	0.6	0.6	0.7	0.7	0.8	0.9	1.0	1.1	1.1	1.1	0.9
20000	100	50	1.7	1.4	1.0	0.7	0.6	0.5	0.5	0.5	0.6	0.6	0.7	0.7	0.8	0.9	1.0	1.0	0.8
20000	100	100	1.3	1.0	0.8	0.6	0.5	0.4	0.4	0.4	0.5	0.5	0.5	0.6	0.7	0.8	0.9	0.9	0.7
20000	100	200	0.9	0.8	0.6	0.5	0.4	0.4	0.4	0.4	0.4	0.4	0.5	0.5	0.6	0.7	0.7	0.8	0.7
20000	100	300	0.7	0.7	0.6	0.5	0.4	0.3	0.3	0.3	0.3	0.4	0.4	0.5	0.5	0.6	0.7	0.7	0.6
20000	100	400	0.7	0.7	0.6	0.5	0.4	0.3	0.3	0.3	0.3	0.3	0.4	0.4	0.5	0.6	0.6	0.7	0.6
20000	100	500	0.7	0.7	0.6	0.5	0.4	0.3	0.3	0.3	0.3	0.3	0.4	0.4	0.5	0.6	0.6	0.7	0.6
20000	200	10	4.2	3.5	2.7	2.1	1.7	1.6	1.6	1.7	1.9	2.0	2.2	2.3	2.5	2.6	2.7	2.5	1.9
20000	200	20	3.9	3.2	2.5	1.9	1.5	1.4	1.4	1.5	1.6	1.8	1.9	2.1	2.3	2.4	2.5	2.4	1.8
20000	200	50	3.2	2.6	2.0	1.5	1.2	1.2	1.2	1.3	1.4	1.5	1.6	1.7	1.9	2.0	2.1	2.0	1.6
20000	200	100	2.3	1.9	1.5	1.2	1.0	1.0	1.0	1.1	1.2	1.3	1.4	1.5	1.6	1.6	1.6	1.6	1.4
20000	200	200	1.4	1.3	1.1	1.0	0.9	0.9	0.9	0.9	1.0	1.0	1.1	1.2	1.3	1.3	1.3	1.3	1.2
20000	200	300	1.1	1.1	1.0	0.8	0.7	0.7	0.7	0.8	0.8	0.8	0.9	0.9	1.0	1.1	1.2	1.2	1.1
20000	200	400	1.1	1.1	0.9	0.8	0.7	0.6	0.6	0.6	0.7	0.7	0.8	0.8	0.9	1.0	1.1	1.2	1.1
20000	200	500	1.1	1.1	0.9	0.8	0.6	0.6	0.6	0.6	0.6	0.7	0.7	0.8	0.9	1.0	1.1	1.1	1.0
20000	400	10	7.1	6.1	4.9	3.7	3.0	2.8	2.9	3.2	3.4	3.8	4.1	4.5	4.8	4.9	4.8	4.5	3.6
20000	400	20	6.6	5.7	4.4	3.4	2.7	2.5	2.6	2.8	3.1	3.3	3.7	4.0	4.4	4.6	4.6	4.3	3.5
20000	400	50	5.5	4.6	3.5	2.7	2.1	2.0	2.1	2.3	2.5	2.7	2.9	3.3	3.6	3.8	3.9	3.6	3.0
20000	400	100	4.0	3.3	2.5	2.0	1.7	1.6	1.7	1.8	2.0	2.1	2.3	2.5	2.7	2.9	2.9	2.8	2.5

20000	400	200	2.4	2.2	1.8	1.5	1.4	1.3	1.4	1.4	1.5	1.6	1.7	1.9	2.1	2.2	2.3	2.3	2.2
20000	400	300	1.8	1.8	1.6	1.3	1.2	1.1	1.1	1.2	1.2	1.3	1.4	1.6	1.8	1.9	2.1	2.1	2.0
20000	400	400	1.8	1.7	1.5	1.3	1.1	1.0	1.0	1.1	1.1	1.2	1.3	1.4	1.6	1.8	2.0	2.1	1.9
20000	400	500	1.7	1.7	1.5	1.2	1.0	1.0	1.0	1.0	1.1	1.1	1.2	1.4	1.6	1.8	2.0	2.0	1.8

20000	700	10	11.7	10.4	8.7	7.0	5.6	4.9	4.9	5.3	5.7	6.4	7.2	8.0	8.4	8.3	7.8	7.0	5.6
20000	700	20	10.8	9.9	8.2	6.4	5.0	4.4	4.4	4.7	5.1	5.7	6.5	7.3	7.8	7.8	7.5	6.7	5.4
20000	700	50	8.9	8.1	6.6	5.1	4.0	3.6	3.6	3.9	4.2	4.6	5.2	5.9	6.5	6.7	6.5	6.0	4.9
20000	700	100	6.2	5.3	4.2	3.4	2.8	2.7	2.8	2.9	3.1	3.4	3.8	4.3	4.8	5.0	5.1	4.8	4.2
20000	700	200	3.7	3.3	2.8	2.4	2.1	2.0	2.1	2.2	2.3	2.5	2.7	3.0	3.4	3.7	3.9	3.9	3.6
20000	700	300	2.8	2.7	2.4	2.1	1.8	1.7	1.7	1.7	1.8	2.0	2.2	2.4	2.8	3.2	3.4	3.5	3.2
20000	700	400	2.7	2.6	2.3	1.9	1.7	1.5	1.5	1.6	1.7	1.8	2.0	2.2	2.6	3.0	3.3	3.3	3.0
20000	700	500	2.6	2.6	2.3	1.9	1.6	1.5	1.5	1.5	1.6	1.7	1.9	2.2	2.5	2.9	3.2	3.3	2.9

20000	1000	10	15.9	14.7	13.3	11.3	9.1	7.8	7.6	7.9	8.7	9.7	11.2	12.5	13.3	13.2	12.3	10.8	8.3
20000	1000	20	14.6	13.6	12.0	10.0	8.1	7.1	6.9	7.2	7.9	8.9	10.3	11.8	12.7	12.8	12.0	10.7	8.3
20000	1000	50	12.1	11.1	9.4	7.8	6.4	5.7	5.7	6.0	6.5	7.4	8.7	10.0	11.0	11.1	10.6	9.5	7.6
20000	1000	100	8.6	7.4	6.1	5.1	4.4	4.1	4.2	4.5	4.8	5.4	6.2	7.2	8.0	8.3	8.1	7.6	6.4
20000	1000	200	5.3	4.8	4.1	3.5	3.1	2.9	3.0	3.1	3.3	3.6	4.1	4.7	5.4	5.9	6.1	5.9	5.2
20000	1000	300	4.0	3.9	3.4	2.9	2.5	2.4	2.3	2.4	2.6	2.8	3.1	3.6	4.2	4.8	5.2	5.2	4.6
20000	1000	400	3.7	3.7	3.2	2.7	2.3	2.2	2.2	2.2	2.4	2.6	2.9	3.3	3.9	4.5	4.8	4.8	4.3
20000	1000	500	3.7	3.6	3.2	2.7	2.3	2.1	2.1	2.2	2.3	2.5	2.8	3.2	3.8	4.3	4.7	4.7	4.1

20000	1500	10	20.8	19.6	18.0	15.5	13.0	11.8	11.9	12.7	14.0	15.8	18.2	20.7	21.7	20.9	18.8	16.0	12.3
20000	1500	20	19.0	18.3	16.4	13.9	11.6	10.6	10.7	11.5	12.6	14.2	16.4	18.7	20.0	19.8	18.5	16.4	13.0
20000	1500	50	15.5	15.0	12.9	10.6	8.9	8.4	8.8	9.5	10.4	11.7	13.6	15.6	16.9	17.1	16.5	15.2	12.4
20000	1500	100	10.8	9.8	8.3	7.0	6.2	6.2	6.6	7.1	7.8	8.7	10.1	11.6	12.8	13.4	13.3	12.6	10.3
20000	1500	200	7.0	6.5	5.6	4.9	4.5	4.4	4.6	4.9	5.4	6.0	6.8	7.8	8.9	9.7	10.0	9.6	7.9
20000	1500	300	5.6	5.4	4.8	4.2	3.7	3.6	3.6	3.8	4.2	4.6	5.3	6.1	7.0	7.8	8.2	8.0	6.7
20000	1500	400	5.2	5.2	4.6	3.9	3.4	3.3	3.3	3.5	3.8	4.2	4.7	5.4	6.2	7.0	7.4	7.3	6.2
20000	1500	500	5.1	5.1	4.5	3.8	3.3	3.1	3.2	3.4	3.7	4.0	4.5	5.1	5.9	6.6	7.0	7.0	5.9

20000	2000	10	27.3	25.3	22.0	18.5	15.9	15.3	16.1	17.6	19.3	21.2	23.2	24.9	25.7	25.2	23.4	20.3	14.6
20000	2000	20	24.6	23.7	20.3	16.8	14.3	13.8	14.6	16.0	17.5	19.4	21.7	23.9	25.2	25.1	23.6	20.6	14.5
20000	2000	50	20.0	18.9	15.9	13.2	11.5	11.4	12.2	13.4	14.7	16.3	18.3	20.4	21.9	22.2	21.3	19.1	14.4
20000	2000	100	14.2	12.7	10.7	9.2	8.5	8.7	9.4	10.3	11.3	12.5	14.0	15.8	17.4	18.1	17.7	16.3	12.8
20000	2000	200	9.5	8.7	7.6	6.7	6.3	6.4	6.8	7.5	8.2	9.1	10.2	11.5	12.7	13.6	13.7	13.0	10.4
20000	2000	300	7.5	7.3	6.4	5.7	5.2	5.2	5.5	6.0	6.6	7.3	8.1	9.1	10.2	11.1	11.4	11.0	9.0
20000	2000	400	6.9	6.8	6.1	5.3	4.7	4.7	4.9	5.3	5.8	6.4	7.1	7.9	8.9	9.8	10.2	10.0	8.3
20000	2000	500	6.7	6.7	5.9	5.1	4.5	4.4	4.6	5.0	5.4	6.0	6.6	7.4	8.3	9.2	9.7	9.5	7.9

20000	3000	10	39.4	35.9	30.0	24.5	20.7	19.9	21.2	23.2	25.7	28.3	30.9	33.2	34.4	34.1	32.1	28.1	20.1
20000	3000	20	35.8	33.5	27.9	22.4	18.8	18.1	19.2	21.1	23.4	26.1	29.3	32.4	34.2	34.1	32.2	28.2	20.2
20000	3000	50	29.2	27.2	22.5	18.2	15.5	15.3	16.4	18.1	19.9	22.2	24.9	27.9	30.2	30.8	29.6	26.5	20.0
20000	3000	100	20.6	18.6	15.5	13.0	11.8	12.1	13.1	14.4	15.9	17.6	19.6	22.0	24.3	25.6	25.2	22.8	17.5
20000	3000	200	13.3	12.4	10.8	9.6	9.1	9.5	10.3	11.3	12.4	13.7	15.0	16.6	18.3	19.5	19.6	18.3	14.5
20000	3000	300	10.4	10.2	9.1	8.1	7.6	7.9	8.6	9.4	10.3	11.3	12.3	13.5	14.8	15.9	16.3	15.6	12.8
20000	3000	400	9.7	9.5	8.5	7.4	6.8	6.9	7.4	8.0	8.8	9.6	10.6	11.7	13.0	14.1	14.6	14.2	11.9
20000	3000	500	9.4	9.3	8.2	7.1	6.5	6.4	6.8	7.4	8.1	8.9	9.8	10.9	12.2	13.3	13.9	13.6	11.4

20000	5000	10	55.2	48.7	38.7	29.9	24.5	23.2	24.5	27.0	29.9	33.5	37.4	41.2	43.6	43.7	41.5	37.0	29.0
20000	5000	20	50.4	46.2	36.3	27.4	21.9	20.7	22.0	24.1	26.8	30.5	35.4	40.4	43.2	43.1	40.5	36.0	28.0

20000	5000	50	41.0	37.8	29.7	22.4	18.1	17.5	18.6	20.4	22.5	25.4	29.5	33.8	36.8	37.4	36.0	32.5	26.0
20000	5000	100	28.6	25.5	20.6	16.6	14.4	14.4	15.4	16.8	18.5	20.4	22.8	25.7	28.6	30.6	30.7	28.4	23.4
20000	5000	200	19.1	17.5	15.0	12.8	11.7	11.9	12.7	13.8	15.2	16.7	18.4	20.5	22.9	24.8	25.4	24.4	20.8
20000	5000	300	14.9	14.3	12.6	11.1	10.3	10.4	11.0	12.0	13.2	14.5	16.0	17.8	19.9	21.6	22.4	21.8	18.9
20000	5000	400	13.7	13.2	11.8	10.4	9.5	9.6	10.2	11.1	12.1	13.4	14.8	16.5	18.4	20.1	20.8	20.4	17.6
20000	5000	500	13.3	12.9	11.5	10.1	9.2	9.2	9.8	10.6	11.7	12.8	14.2	15.8	17.7	19.3	20.1	19.6	16.9
21000	100	10	2.2	2.0	1.6	1.4	1.2	1.1	1.1	1.2	1.3	1.5	1.6	1.7	1.7	1.6	1.5	1.3	0.9
21000	100	20	1.9	1.7	1.4	1.1	0.9	0.9	0.9	0.9	1.1	1.2	1.3	1.4	1.4	1.4	1.3	1.2	0.9
21000	100	50	1.5	1.2	0.9	0.7	0.6	0.6	0.6	0.6	0.7	0.8	0.9	1.0	1.1	1.1	1.1	1.0	0.8
21000	100	100	0.9	0.7	0.6	0.5	0.4	0.4	0.4	0.4	0.5	0.6	0.7	0.7	0.8	0.9	0.9	0.8	0.7
21000	100	200	0.5	0.4	0.4	0.3	0.3	0.3	0.3	0.3	0.4	0.4	0.5	0.6	0.6	0.7	0.7	0.7	0.6
21000	100	300	0.4	0.4	0.3	0.3	0.3	0.3	0.3	0.3	0.3	0.4	0.4	0.5	0.5	0.6	0.6	0.6	0.5
21000	100	400	0.4	0.4	0.3	0.3	0.2	0.2	0.2	0.3	0.3	0.3	0.4	0.4	0.5	0.5	0.6	0.6	0.5
21000	100	500	0.3	0.4	0.3	0.3	0.2	0.2	0.2	0.2	0.3	0.3	0.3	0.4	0.4	0.5	0.5	0.5	0.5
21000	200	10	4.2	3.8	3.2	2.7	2.3	2.2	2.3	2.5	2.8	3.2	3.4	3.6	3.5	3.4	3.1	2.7	1.8
21000	200	20	3.7	3.3	2.7	2.2	1.8	1.7	1.8	2.0	2.2	2.5	2.8	2.9	3.0	3.0	2.8	2.4	1.7
21000	200	50	2.8	2.4	1.8	1.4	1.2	1.2	1.2	1.4	1.5	1.7	1.9	2.1	2.2	2.3	2.2	2.0	1.6
21000	200	100	1.7	1.4	1.1	0.9	0.8	0.8	0.9	1.0	1.1	1.3	1.4	1.6	1.7	1.7	1.7	1.6	1.4
21000	200	200	0.9	0.8	0.7	0.7	0.6	0.6	0.7	0.7	0.8	0.9	1.1	1.2	1.3	1.3	1.3	1.3	1.2
21000	200	300	0.6	0.6	0.6	0.5	0.5	0.5	0.5	0.6	0.7	0.7	0.8	0.9	1.0	1.1	1.1	1.1	1.0
21000	200	400	0.6	0.6	0.5	0.5	0.5	0.5	0.5	0.5	0.6	0.6	0.7	0.8	0.9	1.0	1.0	1.0	1.0
21000	200	500	0.6	0.6	0.5	0.5	0.4	0.4	0.4	0.5	0.5	0.6	0.7	0.7	0.8	0.9	1.0	1.0	0.9
21000	400	10	7.5	7.0	6.1	5.1	4.4	4.1	4.2	4.6	5.2	5.9	6.5	6.9	6.8	6.4	5.8	4.9	3.4
21000	400	20	6.6	6.1	5.1	4.2	3.5	3.2	3.3	3.6	4.0	4.6	5.3	5.7	5.8	5.6	5.2	4.5	3.2
21000	400	50	5.1	4.4	3.5	2.8	2.3	2.1	2.2	2.4	2.8	3.2	3.6	4.0	4.3	4.3	4.2	3.8	2.9
21000	400	100	3.3	2.6	2.1	1.7	1.5	1.5	1.6	1.7	1.9	2.2	2.5	2.8	3.1	3.2	3.2	3.0	2.5
21000	400	200	1.6	1.4	1.2	1.1	1.1	1.1	1.1	1.3	1.4	1.6	1.8	2.0	2.2	2.4	2.4	2.3	2.1
21000	400	300	1.0	1.0	1.0	0.9	0.9	0.9	0.9	1.0	1.1	1.3	1.4	1.6	1.8	2.0	2.0	2.0	1.9
21000	400	400	0.9	0.9	0.9	0.8	0.8	0.8	0.8	0.9	1.0	1.1	1.3	1.4	1.6	1.8	1.9	1.9	1.7
21000	400	500	0.9	0.9	0.8	0.8	0.7	0.7	0.8	0.8	0.9	1.0	1.2	1.3	1.5	1.7	1.8	1.8	1.6
21000	700	10	12.5	11.8	10.9	9.5	7.9	7.0	6.9	7.3	8.3	9.6	11.1	12.1	12.1	11.1	9.5	7.7	5.4
21000	700	20	11.3	10.8	9.7	8.2	6.6	5.7	5.6	5.9	6.6	7.8	9.2	10.3	10.6	9.9	8.8	7.3	5.2
21000	700	50	8.7	8.2	7.1	5.8	4.5	3.9	3.9	4.1	4.6	5.4	6.3	7.2	7.8	7.8	7.3	6.3	4.7
21000	700	100	5.2	4.5	3.7	3.0	2.6	2.5	2.6	2.8	3.1	3.6	4.2	4.8	5.3	5.6	5.5	5.0	4.1
21000	700	200	2.5	2.3	2.0	1.8	1.7	1.7	1.8	1.9	2.2	2.5	2.9	3.3	3.7	3.9	4.0	3.9	3.5
21000	700	300	1.6	1.6	1.5	1.4	1.4	1.4	1.4	1.5	1.7	2.0	2.3	2.6	2.9	3.2	3.3	3.3	3.0
21000	700	400	1.4	1.5	1.4	1.3	1.2	1.2	1.3	1.4	1.5	1.8	2.0	2.3	2.6	2.9	3.0	3.0	2.8
21000	700	500	1.3	1.4	1.3	1.2	1.1	1.1	1.2	1.3	1.5	1.7	1.9	2.1	2.4	2.7	2.9	2.9	2.6
21000	1000	10	17.2	16.7	16.0	14.4	12.2	10.8	10.5	10.9	12.1	14.2	16.6	18.3	18.4	17.0	14.7	11.8	8.0
21000	1000	20	15.4	15.0	14.0	12.4	10.5	9.3	8.9	9.1	10.0	11.8	14.0	16.0	16.7	16.0	14.2	11.7	8.2
21000	1000	50	11.9	11.4	10.2	8.7	7.3	6.5	6.3	6.4	7.1	8.4	10.2	11.9	12.9	12.9	11.9	10.3	7.6
21000	1000	100	7.0	6.1	5.3	4.6	4.0	3.8	3.9	4.1	4.6	5.4	6.5	7.5	8.3	8.7	8.5	7.8	6.4
21000	1000	200	3.5	3.2	2.9	2.6	2.5	2.5	2.5	2.7	3.1	3.6	4.2	4.8	5.4	5.8	6.0	5.8	5.1
21000	1000	300	2.3	2.3	2.2	2.1	1.9	1.9	2.0	2.1	2.4	2.8	3.2	3.7	4.2	4.6	4.9	4.8	4.3
21000	1000	400	2.0	2.1	2.0	1.8	1.7	1.7	1.8	1.9	2.2	2.5	2.9	3.3	3.7	4.1	4.4	4.3	3.9
21000	1000	500	1.9	2.0	1.9	1.7	1.6	1.6	1.7	1.9	2.1	2.4	2.7	3.1	3.5	3.9	4.1	4.1	3.7

21000	1500	10	23.1	22.9	22.1	20.1	17.5	15.7	15.3	15.9	17.8	21.2	25.7	29.6	30.2	27.3	22.6	17.5	12.3
21000	1500	20	20.3	20.3	19.1	16.9	14.4	12.7	12.2	12.7	14.3	17.1	21.1	24.7	26.1	24.9	22.2	18.6	14.1
21000	1500	50	15.3	15.3	13.8	11.7	9.6	8.4	8.3	8.9	10.1	12.2	15.1	18.1	19.8	19.8	18.7	16.9	13.8
21000	1500	100	8.8	8.2	7.2	6.2	5.5	5.3	5.5	6.0	6.8	8.1	9.8	11.7	13.2	13.9	13.9	13.3	11.3
21000	1500	200	4.6	4.3	3.9	3.6	3.5	3.6	3.8	4.1	4.7	5.4	6.4	7.4	8.4	9.1	9.3	9.0	7.7
21000	1500	300	3.1	3.2	3.0	2.9	2.8	2.8	3.0	3.2	3.7	4.3	4.9	5.6	6.4	7.0	7.2	7.0	6.1
21000	1500	400	2.7	2.9	2.7	2.6	2.5	2.5	2.6	2.9	3.3	3.8	4.3	4.9	5.5	6.1	6.4	6.3	5.5
21000	1500	500	2.6	2.7	2.6	2.5	2.3	2.4	2.5	2.7	3.1	3.5	4.0	4.6	5.2	5.7	6.0	5.9	5.2
21000	2000	10	29.3	29.3	27.6	24.4	20.9	19.2	19.4	21.0	23.7	27.2	30.9	33.3	33.3	31.3	27.8	23.0	15.1
21000	2000	20	25.5	25.9	23.7	20.3	17.0	15.3	15.5	16.8	19.0	22.4	26.5	30.1	31.6	30.9	28.4	24.1	15.5
21000	2000	50	18.8	19.0	16.8	14.0	11.7	10.7	11.0	11.9	13.6	16.1	19.4	22.7	24.8	25.1	23.9	21.3	16.1
21000	2000	100	11.3	10.6	9.3	8.2	7.5	7.3	7.7	8.3	9.4	11.0	13.1	15.6	17.5	18.4	18.0	16.7	13.5
21000	2000	200	6.1	5.7	5.3	5.0	4.8	5.0	5.4	5.9	6.7	7.7	9.0	10.4	11.6	12.4	12.5	11.8	9.8
21000	2000	300	4.2	4.2	4.0	3.8	3.8	3.9	4.2	4.7	5.3	6.1	7.0	7.9	8.8	9.5	9.8	9.5	8.1
21000	2000	400	3.6	3.8	3.6	3.4	3.3	3.5	3.7	4.1	4.7	5.3	6.1	6.9	7.7	8.3	8.6	8.4	7.4
21000	2000	500	3.5	3.6	3.5	3.3	3.2	3.2	3.5	3.8	4.3	5.0	5.6	6.3	7.1	7.8	8.1	7.9	7.0
21000	3000	10	40.7	39.9	36.6	32.0	27.8	26.1	27.0	29.6	33.5	38.3	42.9	45.7	45.6	43.0	38.3	31.8	21.0
21000	3000	20	36.0	36.4	32.4	27.2	22.8	20.9	21.5	23.5	26.8	31.6	37.3	42.3	44.2	42.7	38.7	32.4	21.1
21000	3000	50	27.2	27.7	24.1	19.8	16.4	15.1	15.5	16.9	19.2	22.7	27.3	32.1	35.0	35.3	33.1	29.0	21.5
21000	3000	100	16.1	15.5	13.7	11.9	10.7	10.5	11.0	12.0	13.6	15.8	18.7	22.1	25.1	26.5	25.8	23.3	18.4
21000	3000	200	8.5	8.2	7.6	7.1	7.0	7.3	7.9	8.8	9.9	11.4	13.1	15.0	16.9	18.1	18.2	17.0	14.1
21000	3000	300	5.9	5.9	5.7	5.5	5.5	5.8	6.3	7.0	8.0	9.2	10.4	11.6	12.9	13.9	14.2	13.7	11.8
21000	3000	400	5.1	5.3	5.1	4.9	4.8	5.0	5.5	6.1	6.9	7.9	8.9	10.0	11.1	12.1	12.5	12.2	10.8
21000	3000	500	4.9	5.1	4.9	4.6	4.5	4.7	5.1	5.6	6.4	7.3	8.3	9.3	10.4	11.3	11.7	11.5	10.2
21000	5000	10	58.0	55.0	47.7	40.7	36.1	35.1	37.1	41.0	46.6	53.4	60.3	64.9	65.2	61.2	54.0	44.3	30.1
21000	5000	20	52.5	51.5	43.0	34.7	29.2	28.0	29.5	32.5	37.2	44.2	53.1	60.8	63.1	59.7	52.5	42.8	28.8
21000	5000	50	39.9	39.9	32.4	25.1	20.5	19.7	20.8	23.0	26.3	31.5	38.7	45.7	49.0	48.0	43.6	36.6	26.3
21000	5000	100	23.0	21.7	18.1	15.0	13.3	13.4	14.5	16.2	18.5	21.6	25.4	29.3	32.6	34.4	33.5	29.8	23.2
21000	5000	200	12.4	11.7	10.6	9.7	9.4	9.8	10.7	11.9	13.6	15.7	18.0	20.3	22.7	24.6	25.0	23.6	20.1
21000	5000	300	8.6	8.6	8.2	7.9	7.8	8.1	8.8	9.8	11.1	12.9	14.7	16.6	18.4	19.9	20.5	20.0	17.9
21000	5000	400	7.5	7.6	7.4	7.1	7.0	7.3	7.9	8.8	10.0	11.5	13.1	14.7	16.4	17.8	18.4	18.1	16.3
21000	5000	500	7.1	7.2	7.0	6.8	6.7	6.9	7.5	8.3	9.4	10.8	12.3	13.8	15.4	16.7	17.4	17.1	15.5
22000	100	10	2.1	2.0	2.0	2.0	2.1	2.1	2.2	2.3	2.5	2.6	2.7	2.6	2.4	2.1	1.7	1.4	0.9
22000	100	20	1.8	1.7	1.6	1.5	1.5	1.6	1.7	1.7	1.9	2.0	2.1	2.1	1.9	1.7	1.5	1.2	0.9
22000	100	50	1.3	1.2	1.0	1.0	0.9	1.0	1.0	1.1	1.2	1.3	1.4	1.4	1.4	1.3	1.2	1.0	0.8
22000	100	100	0.8	0.7	0.6	0.6	0.6	0.6	0.6	0.7	0.8	0.9	0.9	1.0	1.0	1.0	0.9	0.8	0.7
22000	100	200	0.4	0.4	0.4	0.4	0.4	0.4	0.4	0.5	0.5	0.6	0.7	0.7	0.7	0.7	0.7	0.7	0.6
22000	100	300	0.2	0.2	0.3	0.3	0.3	0.3	0.3	0.4	0.4	0.5	0.5	0.6	0.6	0.6	0.6	0.6	0.5
22000	100	400	0.2	0.2	0.2	0.2	0.2	0.3	0.3	0.3	0.4	0.4	0.4	0.5	0.5	0.5	0.5	0.5	0.5
22000	100	500	0.2	0.2	0.2	0.2	0.2	0.2	0.3	0.3	0.3	0.4	0.4	0.4	0.5	0.5	0.5	0.5	0.4
22000	200	10	3.9	3.9	4.0	4.1	4.1	4.3	4.4	4.7	5.0	5.3	5.5	5.3	4.8	4.2	3.5	2.8	1.8
22000	200	20	3.4	3.3	3.2	3.1	3.0	3.1	3.2	3.4	3.7	4.1	4.3	4.3	4.0	3.6	3.1	2.6	1.7
22000	200	50	2.5	2.3	2.1	1.9	1.9	1.9	2.0	2.2	2.4	2.6	2.8	2.9	2.8	2.7	2.4	2.1	1.6
22000	200	100	1.5	1.3	1.2	1.1	1.1	1.2	1.3	1.4	1.5	1.7	1.9	2.0	2.0	1.9	1.8	1.7	1.4
22000	200	200	0.8	0.7	0.7	0.7	0.7	0.8	0.9	0.9	1.1	1.2	1.3	1.4	1.4	1.4	1.4	1.3	1.2
22000	200	300	0.5	0.5	0.5	0.5	0.6	0.6	0.7	0.7	0.8	0.9	1.0	1.1	1.1	1.1	1.1	1.1	1.0
22000	200	400	0.4	0.4	0.4	0.4	0.5	0.5	0.6	0.6	0.7	0.8	0.9	0.9	1.0	1.0	1.0	1.0	0.9
22000	200	500	0.3	0.4	0.4	0.4	0.4	0.5	0.5	0.6	0.6	0.7	0.8	0.9	0.9	0.9	0.9	0.9	0.9

22000	400	10	7.2	7.7	8.0	8.1	7.9	7.9	8.0	8.4	9.0	9.8	10.2	10.0	9.2	8.1	6.8	5.5	3.5
22000	400	20	6.2	6.3	6.3	6.1	5.8	5.7	5.8	6.1	6.7	7.4	8.0	8.2	7.7	7.0	6.1	5.0	3.3
22000	400	50	4.6	4.3	4.0	3.7	3.5	3.5	3.6	3.8	4.2	4.8	5.3	5.5	5.5	5.2	4.7	4.1	2.9
22000	400	100	2.9	2.5	2.3	2.1	2.1	2.2	2.3	2.5	2.8	3.1	3.5	3.7	3.7	3.7	3.5	3.1	2.5
22000	400	200	1.4	1.4	1.3	1.3	1.3	1.4	1.6	1.7	1.9	2.2	2.4	2.5	2.6	2.6	2.5	2.4	2.1
22000	400	300	0.8	0.9	0.9	1.0	1.0	1.1	1.2	1.3	1.5	1.7	1.9	2.0	2.0	2.1	2.1	2.0	1.9
22000	400	400	0.7	0.7	0.8	0.8	0.9	0.9	1.0	1.1	1.3	1.4	1.6	1.7	1.8	1.8	1.8	1.8	1.7
22000	400	500	0.6	0.6	0.7	0.7	0.8	0.9	0.9	1.0	1.2	1.3	1.5	1.6	1.6	1.7	1.7	1.7	1.6
22000	700	10	12.1	12.5	12.9	12.8	12.3	11.9	11.9	12.4	13.4	15.0	16.3	16.6	15.5	13.4	11.0	8.6	5.5
22000	700	20	10.8	11.1	11.1	10.6	9.8	9.3	9.2	9.5	10.4	11.7	13.1	13.7	13.2	11.7	10.0	8.1	5.3
22000	700	50	8.3	8.4	7.9	7.1	6.4	6.0	6.0	6.2	6.8	7.8	8.7	9.3	9.3	8.8	7.9	6.7	4.9
22000	700	100	5.2	4.7	4.2	3.8	3.6	3.7	3.8	4.1	4.5	5.1	5.7	6.1	6.3	6.2	5.8	5.3	4.3
22000	700	200	2.7	2.5	2.3	2.2	2.3	2.4	2.6	2.7	3.0	3.5	3.9	4.1	4.3	4.3	4.2	4.0	3.6
22000	700	300	1.5	1.6	1.7	1.7	1.7	1.8	1.9	2.1	2.3	2.7	3.0	3.2	3.3	3.3	3.3	3.2	3.0
22000	700	400	1.1	1.2	1.2	1.3	1.4	1.5	1.6	1.8	2.0	2.3	2.6	2.7	2.8	2.9	2.9	2.9	2.7
22000	700	500	0.9	1.0	1.1	1.2	1.3	1.4	1.5	1.7	1.9	2.1	2.3	2.5	2.6	2.7	2.7	2.7	2.6
22000	1000	10	17.0	17.4	18.4	18.8	18.5	18.2	18.1	18.4	19.7	22.0	24.1	24.6	23.0	19.9	16.1	12.4	8.1
22000	1000	20	15.3	15.4	15.7	15.6	15.3	15.1	14.8	14.7	15.6	17.4	19.3	20.3	19.8	18.1	15.4	12.3	8.2
22000	1000	50	11.9	11.8	11.3	10.8	10.3	10.0	9.8	9.7	10.3	11.7	13.2	14.3	14.6	14.0	12.7	10.7	7.8
22000	1000	100	7.1	6.6	6.1	5.8	5.6	5.6	5.6	5.7	6.2	7.1	8.0	8.8	9.2	9.3	9.0	8.2	6.8
22000	1000	200	3.8	3.7	3.5	3.4	3.4	3.4	3.5	3.7	4.1	4.7	5.3	5.7	6.0	6.1	6.1	5.8	5.2
22000	1000	300	2.1	2.4	2.5	2.5	2.5	2.5	2.6	2.8	3.1	3.6	4.1	4.4	4.7	4.8	4.7	4.6	4.3
22000	1000	400	1.5	1.7	1.8	1.9	2.0	2.1	2.3	2.5	2.8	3.2	3.6	3.9	4.0	4.1	4.1	4.1	3.9
22000	1000	500	1.3	1.4	1.5	1.7	1.8	2.0	2.1	2.4	2.6	3.0	3.3	3.6	3.7	3.8	3.8	3.8	3.7
22000	1500	10	24.4	25.3	26.7	27.3	26.9	26.1	25.4	25.8	27.8	31.5	35.7	37.9	36.0	30.9	24.5	18.4	12.9
22000	1500	20	21.5	21.6	22.1	21.9	21.1	20.1	19.4	19.6	21.2	24.2	27.9	30.3	30.1	27.4	23.6	19.3	14.5
22000	1500	50	16.3	16.1	15.5	14.6	13.4	12.5	12.2	12.5	13.7	16.0	18.8	21.1	21.9	21.2	19.5	17.2	14.1
22000	1500	100	9.6	9.0	8.5	8.0	7.6	7.4	7.5	7.9	8.7	10.1	11.7	13.2	14.1	14.4	14.1	13.3	11.7
22000	1500	200	5.0	4.9	4.8	4.8	4.8	4.9	5.2	5.5	6.1	6.9	7.7	8.4	8.9	9.1	9.1	8.9	8.0
22000	1500	300	2.8	3.0	3.1	3.2	3.4	3.6	3.9	4.3	4.7	5.4	6.0	6.4	6.7	6.8	6.8	6.6	6.1
22000	1500	400	2.1	2.2	2.4	2.6	2.8	3.0	3.3	3.6	4.1	4.6	5.1	5.5	5.7	5.8	5.9	5.7	5.5
22000	1500	500	1.8	2.0	2.2	2.3	2.5	2.8	3.0	3.3	3.8	4.3	4.7	5.0	5.2	5.4	5.4	5.4	5.1
22000	2000	10	29.5	32.1	33.9	33.8	32.5	31.6	31.9	33.6	36.9	41.4	45.2	45.7	42.4	37.3	32.2	27.3	19.8
22000	2000	20	25.6	27.3	27.5	26.4	24.8	23.7	23.7	24.8	27.4	31.4	35.7	38.3	37.8	35.2	31.6	27.1	18.9
22000	2000	50	19.0	19.9	19.0	17.5	16.1	15.4	15.3	16.0	17.6	20.4	23.9	26.7	27.8	26.9	24.8	22.0	17.1
22000	2000	100	11.6	11.6	11.1	10.6	10.2	10.0	10.0	10.5	11.5	13.2	15.3	17.3	18.4	18.4	17.5	16.1	13.4
22000	2000	200	5.9	5.8	5.9	6.0	6.2	6.5	6.8	7.3	8.1	9.3	10.4	11.3	11.8	11.8	11.6	10.9	9.4
22000	2000	300	3.4	3.6	3.8	4.1	4.4	4.8	5.2	5.7	6.4	7.3	8.1	8.6	8.9	9.0	8.9	8.6	7.9
22000	2000	400	2.7	2.9	3.2	3.4	3.7	4.0	4.4	4.9	5.5	6.3	7.0	7.4	7.7	7.8	7.9	7.7	7.3
22000	2000	500	2.4	2.7	2.9	3.1	3.4	3.7	4.1	4.5	5.1	5.7	6.4	6.8	7.1	7.2	7.3	7.2	6.9
22000	3000	10	40.3	43.1	45.1	45.4	44.9	44.9	46.5	49.8	54.5	60.0	64.3	64.2	59.0	51.6	44.1	36.8	26.1
22000	3000	20	35.5	38.2	37.7	36.0	34.1	33.4	34.2	36.3	39.9	45.3	51.0	54.2	53.1	48.8	42.9	36.0	24.9
22000	3000	50	27.1	28.9	27.2	25.0	23.3	22.7	22.9	23.9	26.0	29.6	34.1	37.8	38.9	37.3	34.0	29.5	22.9
22000	3000	100	16.3	16.7	16.1	15.4	15.0	14.9	15.1	15.9	17.3	19.5	22.1	24.6	26.0	26.0	24.7	22.4	18.6
22000	3000	200	8.2	8.3	8.5	8.7	9.0	9.5	10.0	10.9	12.1	13.7	15.3	16.5	17.3	17.5	17.1	16.0	14.0
22000	3000	300	5.0	5.2	5.5	5.9	6.4	6.9	7.6	8.4	9.4	10.7	11.9	12.7	13.1	13.3	13.1	12.7	11.7

22000	3000	400	3.9	4.3	4.6	4.9	5.3	5.9	6.4	7.1	8.0	9.1	10.1	10.8	11.2	11.4	11.4	11.2	10.6
22000	3000	500	3.5	3.9	4.2	4.5	4.9	5.4	5.9	6.5	7.4	8.4	9.3	9.9	10.3	10.5	10.6	10.4	10.0

22000	5000	10	57.4	58.8	59.3	59.6	60.3	62.0	65.8	71.5	78.1	84.8	90.2	90.9	84.9	74.1	61.4	47.7	30.6
22000	5000	20	52.0	54.8	52.3	49.8	48.7	49.6	51.9	55.3	60.4	67.4	74.9	79.2	76.9	69.0	58.2	45.6	29.2
22000	5000	50	39.8	42.7	39.0	35.5	34.1	35.0	36.6	38.5	41.5	46.4	52.5	57.0	57.2	53.2	46.6	38.1	26.6
22000	5000	100	22.8	23.4	21.6	20.3	20.2	21.3	22.9	24.7	27.2	30.4	33.8	36.2	37.0	36.2	33.7	29.6	23.4
22000	5000	200	11.4	11.7	11.7	11.9	12.5	13.5	14.8	16.3	18.3	20.8	23.0	24.4	25.0	25.1	24.5	22.9	20.2
22000	5000	300	7.4	7.8	8.2	8.8	9.5	10.4	11.4	12.6	14.2	16.1	17.9	19.1	19.7	19.9	19.7	19.1	17.8
22000	5000	400	6.0	6.4	6.9	7.4	8.1	8.9	9.8	10.8	12.2	13.8	15.4	16.4	17.0	17.3	17.3	17.0	16.2
22000	5000	500	5.3	5.8	6.3	6.8	7.4	8.2	9.0	9.9	11.2	12.7	14.1	15.0	15.6	16.0	16.0	15.9	15.3

22500	100	10	1.8	1.9	2.3	2.8	3.1	3.4	3.5	3.6	3.6	3.6	3.4	3.1	2.7	2.2	1.8	1.4	0.9
22500	100	20	1.6	1.6	1.9	2.1	2.4	2.5	2.6	2.7	2.7	2.7	2.7	2.5	2.2	1.9	1.5	1.2	0.9
22500	100	50	1.3	1.3	1.3	1.4	1.5	1.6	1.6	1.7	1.8	1.8	1.8	1.7	1.5	1.4	1.2	1.0	0.8
22500	100	100	0.9	0.9	0.9	0.9	0.9	1.0	1.0	1.1	1.1	1.2	1.2	1.2	1.1	1.0	0.9	0.8	0.7
22500	100	200	0.5	0.5	0.5	0.6	0.6	0.6	0.7	0.7	0.8	0.8	0.8	0.8	0.8	0.8	0.7	0.7	0.6
22500	100	300	0.4	0.4	0.4	0.4	0.4	0.5	0.5	0.6	0.6	0.6	0.6	0.6	0.6	0.6	0.6	0.6	0.5
22500	100	400	0.3	0.3	0.3	0.3	0.4	0.4	0.4	0.5	0.5	0.5	0.5	0.5	0.5	0.5	0.5	0.5	0.5
22500	100	500	0.3	0.3	0.3	0.3	0.3	0.4	0.4	0.4	0.4	0.5	0.5	0.5	0.5	0.5	0.5	0.5	0.4

22500	200	10	3.5	4.1	5.0	5.8	6.5	6.9	7.1	7.2	7.2	7.2	6.9	6.4	5.5	4.7	3.9	3.0	2.0
22500	200	20	3.1	3.6	4.0	4.5	4.8	5.0	5.2	5.3	5.4	5.4	5.4	5.1	4.6	4.1	3.4	2.8	1.9
22500	200	50	2.5	2.7	2.8	2.9	3.0	3.1	3.2	3.3	3.4	3.5	3.5	3.4	3.2	2.9	2.6	2.2	1.6
22500	200	100	1.8	1.8	1.8	1.8	1.9	2.0	2.1	2.2	2.2	2.3	2.4	2.4	2.3	2.1	1.9	1.7	1.4
22500	200	200	1.1	1.2	1.2	1.2	1.2	1.3	1.3	1.4	1.5	1.6	1.6	1.7	1.6	1.5	1.4	1.3	1.2
22500	200	300	0.7	0.8	0.8	0.8	0.9	0.9	1.0	1.1	1.1	1.2	1.2	1.3	1.2	1.2	1.1	1.1	1.0
22500	200	400	0.6	0.6	0.6	0.7	0.7	0.8	0.8	0.9	1.0	1.0	1.1	1.1	1.0	1.0	1.0	1.0	0.9
22500	200	500	0.5	0.5	0.5	0.6	0.6	0.7	0.8	0.8	0.9	0.9	1.0	1.0	1.0	0.9	0.9	0.9	0.9

22500	400	10	6.7	8.8	10.6	11.8	12.4	12.6	12.7	12.8	13.0	13.1	12.8	11.9	10.7	9.3	8.1	6.7	4.3
22500	400	20	5.7	7.1	8.0	8.7	9.0	9.1	9.3	9.4	9.7	9.9	10.0	9.7	9.0	8.2	7.2	6.1	3.9
22500	400	50	4.5	5.1	5.3	5.4	5.5	5.6	5.7	5.8	6.0	6.3	6.5	6.5	6.3	5.9	5.3	4.6	3.3
22500	400	100	3.3	3.3	3.3	3.2	3.3	3.5	3.6	3.8	4.0	4.1	4.2	4.3	4.2	4.0	3.7	3.3	2.6
22500	400	200	2.1	2.1	2.1	2.1	2.1	2.2	2.4	2.5	2.6	2.7	2.8	2.9	2.9	2.8	2.6	2.5	2.2
22500	400	300	1.3	1.4	1.5	1.5	1.6	1.7	1.8	1.9	2.0	2.1	2.2	2.2	2.2	2.1	2.1	2.0	1.9
22500	400	400	1.0	1.1	1.1	1.2	1.3	1.4	1.5	1.7	1.8	1.8	1.9	1.9	1.9	1.9	1.8	1.8	1.7
22500	400	500	0.9	0.9	1.0	1.1	1.2	1.3	1.4	1.5	1.6	1.7	1.7	1.7	1.7	1.7	1.7	1.6	1.6

22500	700	10	10.8	13.1	15.1	16.5	17.3	17.7	17.9	18.1	18.5	19.1	19.3	18.6	16.8	14.5	12.2	9.9	6.7
22500	700	20	9.7	11.4	12.5	13.1	13.4	13.6	13.7	13.8	14.2	14.8	15.3	15.1	14.1	12.6	11.0	9.2	6.3
22500	700	50	8.1	9.0	9.1	9.0	8.8	8.8	8.9	9.1	9.3	9.8	10.2	10.3	10.0	9.3	8.5	7.3	5.5
22500	700	100	6.4	6.3	5.8	5.5	5.5	5.7	6.0	6.1	6.4	6.6	6.8	6.9	6.8	6.5	6.2	5.6	4.6
22500	700	200	4.2	4.1	3.8	3.6	3.6	3.8	4.0	4.1	4.3	4.5	4.6	4.7	4.6	4.5	4.4	4.2	3.8
22500	700	300	2.5	2.7	2.7	2.7	2.7	2.8	2.9	3.1	3.2	3.4	3.5	3.6	3.5	3.5	3.4	3.3	3.1
22500	700	400	1.7	1.8	1.9	2.0	2.1	2.3	2.5	2.6	2.8	2.9	3.0	3.1	3.0	3.0	2.9	2.8	2.7
22500	700	500	1.5	1.5	1.6	1.7	1.9	2.1	2.2	2.4	2.6	2.7	2.8	2.8	2.8	2.7	2.7	2.7	2.6

22500	1000	10	15.1	17.0	20.2	23.1	25.0	26.1	26.5	26.6	27.2	28.2	28.6	27.4	24.3	20.1	16.1	12.5	8.8
22500	1000	20	13.8	15.3	17.1	18.7	19.9	20.5	20.7	20.5	20.9	21.7	22.2	21.8	20.3	17.9	15.2	12.2	8.5
22500	1000	50	11.6	12.5	12.9	13.2	13.4	13.5	13.5	13.4	13.6	14.2	14.7	14.9	14.6	13.8	12.5	10.7	8.2
22500	1000	100	8.8	8.9	8.6	8.3	8.2	8.3	8.2	8.2	8.3	8.6	9.0	9.2	9.3	9.3	9.1	8.4	7.1

22500	1000	200	5.9	6.2	5.9	5.6	5.4	5.4	5.4	5.5	5.5	5.7	5.9	6.1	6.2	6.2	6.2	6.0	5.5
22500	1000	300	3.7	4.2	4.3	4.1	3.9	3.9	3.9	4.1	4.2	4.5	4.7	4.9	4.9	4.8	4.7	4.6	4.4
22500	1000	400	2.5	2.7	2.8	2.9	3.0	3.2	3.4	3.6	3.9	4.1	4.2	4.3	4.3	4.2	4.1	4.0	3.9
22500	1000	500	2.1	2.2	2.3	2.4	2.6	2.9	3.2	3.4	3.6	3.8	3.9	4.0	3.9	3.9	3.8	3.8	3.7

22500	1500	10	22.3	25.4	29.7	33.3	35.7	36.6	36.7	37.0	38.1	39.9	41.1	40.0	35.6	29.4	23.5	18.6	14.3
22500	1500	20	20.5	22.0	24.5	26.6	28.0	28.4	28.2	28.1	28.8	30.1	31.3	31.1	29.0	25.5	21.7	18.1	14.1
22500	1500	50	17.2	17.6	18.1	18.5	18.6	18.5	18.2	18.2	18.6	19.6	20.8	21.4	21.0	19.7	17.8	15.6	12.8
22500	1500	100	12.4	12.3	12.2	12.0	11.7	11.6	11.5	11.5	11.8	12.4	13.1	13.6	13.8	13.6	13.1	12.4	10.9
22500	1500	200	7.9	8.1	8.0	7.9	7.9	7.9	8.0	8.2	8.4	8.7	8.9	9.1	9.1	9.1	9.0	8.9	8.2
22500	1500	300	4.7	4.9	5.0	5.2	5.4	5.7	6.0	6.4	6.6	6.9	7.0	7.1	7.0	6.9	6.8	6.6	6.3
22500	1500	400	3.4	3.5	3.6	3.9	4.2	4.5	5.0	5.3	5.6	5.9	6.1	6.1	6.0	5.9	5.8	5.7	5.5
22500	1500	500	2.9	3.0	3.2	3.4	3.7	4.1	4.5	4.8	5.1	5.4	5.6	5.6	5.5	5.5	5.4	5.3	5.2

22500	2000	10	26.4	32.0	38.4	42.9	45.3	46.4	47.6	49.5	51.9	54.4	55.7	53.1	46.8	40.2	35.6	32.8	28.0
22500	2000	20	23.9	27.2	30.5	32.7	34.0	34.6	35.1	35.9	37.3	39.3	41.1	40.9	38.3	34.9	31.9	29.3	23.9
22500	2000	50	19.7	21.4	22.2	22.6	22.8	22.9	22.9	23.1	23.6	24.7	26.2	27.1	26.7	25.1	23.1	20.9	17.3
22500	2000	100	14.9	15.4	15.4	15.4	15.2	15.0	15.0	15.2	15.5	16.1	16.9	17.5	17.4	16.8	15.8	14.5	12.0
22500	2000	200	8.9	9.2	9.5	9.7	9.9	10.2	10.5	10.8	11.2	11.7	12.0	12.0	11.7	11.3	10.9	10.3	8.7
22500	2000	300	5.6	5.8	6.1	6.4	6.9	7.4	8.0	8.5	8.9	9.3	9.6	9.6	9.3	9.1	8.8	8.5	7.8
22500	2000	400	4.4	4.6	4.8	5.1	5.5	6.1	6.6	7.1	7.6	8.0	8.2	8.2	8.1	8.0	7.8	7.6	7.3
22500	2000	500	3.9	4.0	4.2	4.5	5.0	5.5	6.0	6.5	6.9	7.2	7.4	7.5	7.4	7.3	7.2	7.1	6.9

22500	3000	10	36.7	43.9	52.6	59.8	64.9	68.3	71.4	74.8	77.6	79.6	79.8	75.2	65.7	55.7	48.0	42.6	34.9
22500	3000	20	33.3	38.4	42.6	45.9	48.4	50.2	51.7	53.1	54.8	57.0	58.7	57.9	53.9	48.5	43.4	38.7	31.0
22500	3000	50	28.0	30.8	31.7	32.4	33.3	34.1	34.6	34.9	35.3	36.3	37.5	38.1	37.1	34.6	31.5	28.2	23.8
22500	3000	100	21.2	22.2	22.3	22.3	22.5	22.8	23.2	23.6	24.1	24.5	25.0	25.2	24.8	23.8	22.2	20.3	17.5
22500	3000	200	12.8	13.3	13.8	14.3	14.7	15.3	15.9	16.5	17.2	17.8	18.2	18.1	17.6	16.9	16.2	15.2	13.4
22500	3000	300	8.2	8.5	8.9	9.4	10.1	10.9	11.7	12.5	13.2	13.8	14.2	14.2	13.8	13.4	13.0	12.5	11.6
22500	3000	400	6.4	6.6	6.9	7.4	8.0	8.8	9.6	10.4	11.0	11.6	11.9	12.0	11.8	11.6	11.4	11.1	10.7
22500	3000	500	5.6	5.8	6.2	6.6	7.2	7.9	8.7	9.4	10.0	10.5	10.8	10.9	10.8	10.7	10.5	10.3	10.1

22500	5000	10	51.5	58.5	69.8	80.8	89.6	95.8	101.7	107.3	109.8	109.1	106.9	101.7	91.0	76.8	62.0	47.5	30.9
22500	5000	20	47.5	55.4	61.9	68.0	73.3	77.3	80.2	82.5	84.0	84.9	85.3	83.5	77.5	67.8	56.5	44.2	29.6
22500	5000	50	39.7	46.2	48.6	51.0	53.9	56.7	58.5	59.0	59.1	59.3	59.9	59.4	56.5	51.1	44.4	36.8	26.9
22500	5000	100	28.0	31.0	31.3	31.7	32.9	34.8	36.8	38.2	39.2	40.0	40.4	39.9	38.2	35.7	32.6	28.9	23.6
22500	5000	200	17.1	18.2	18.5	19.0	20.0	21.6	23.3	24.9	26.2	27.3	27.9	27.7	26.8	25.6	24.3	22.7	20.3
22500	5000	300	12.2	12.5	12.9	13.6	14.7	16.1	17.5	18.8	19.9	20.9	21.5	21.5	21.1	20.5	19.8	19.0	17.9
22500	5000	400	9.9	10.1	10.5	11.2	12.2	13.4	14.7	15.8	16.8	17.6	18.2	18.3	18.0	17.7	17.3	16.9	16.3
22500	5000	500	8.6	8.9	9.4	10.1	11.0	12.1	13.3	14.3	15.2	16.0	16.5	16.6	16.5	16.2	16.0	15.7	15.4

23000	100	10	1.5	1.8	2.4	3.0	3.6	3.9	4.0	4.0	4.0	3.8	3.5	3.1	2.7	2.2	1.8	1.4	0.9
23000	100	20	1.4	1.6	2.0	2.4	2.7	2.9	3.0	3.1	3.0	2.9	2.8	2.5	2.2	1.9	1.5	1.2	0.9
23000	100	50	1.2	1.3	1.4	1.6	1.7	1.8	1.9	2.0	2.0	1.9	1.9	1.7	1.6	1.4	1.2	1.0	0.8
23000	100	100	1.0	1.0	1.0	1.0	1.1	1.1	1.2	1.3	1.3	1.3	1.3	1.2	1.2	1.1	1.0	0.8	0.7
23000	100	200	0.6	0.6	0.6	0.7	0.7	0.7	0.8	0.9	0.9	0.9	0.9	0.9	0.9	0.9	0.8	0.7	0.6
23000	100	300	0.5	0.5	0.5	0.5	0.5	0.6	0.6	0.6	0.7	0.7	0.7	0.7	0.7	0.7	0.6	0.6	0.5
23000	100	400	0.4	0.4	0.4	0.4	0.4	0.5	0.5	0.5	0.5	0.6	0.6	0.6	0.6	0.5	0.5	0.5	0.5
23000	100	500	0.3	0.3	0.3	0.4	0.4	0.4	0.4	0.5	0.5	0.5	0.5	0.5	0.5	0.5	0.5	0.5	0.5

23000	200	10	3.4	4.2	5.3	6.4	7.2	7.7	7.8	7.8	7.7	7.5	7.1	6.5	5.8	5.0	4.2	3.3	2.3
23000	200	20	3.1	3.8	4.5	5.1	5.5	5.7	5.7	5.7	5.7	5.6	5.5	5.2	4.9	4.4	3.8	3.0	2.1

23000	200	50	2.7	3.1	3.2	3.4	3.5	3.6	3.7	3.7	3.7	3.6	3.6	3.5	3.3	3.1	2.8	2.4	1.8
23000	200	100	2.1	2.3	2.3	2.3	2.3	2.3	2.4	2.4	2.4	2.4	2.4	2.4	2.4	2.2	2.0	1.8	1.5
23000	200	200	1.4	1.6	1.6	1.6	1.5	1.5	1.5	1.6	1.6	1.6	1.7	1.7	1.7	1.6	1.4	1.3	1.2
23000	200	300	0.9	1.0	1.1	1.1	1.1	1.1	1.1	1.2	1.3	1.3	1.3	1.3	1.3	1.2	1.1	1.1	1.0
23000	200	400	0.7	0.7	0.8	0.8	0.8	0.9	1.0	1.0	1.1	1.1	1.1	1.1	1.1	1.0	1.0	1.0	0.9
23000	200	500	0.6	0.6	0.7	0.7	0.7	0.8	0.9	0.9	1.0	1.0	1.0	1.0	1.0	0.9	0.9	0.9	0.9

23000	400	10	6.7	9.3	11.3	12.8	13.8	14.3	14.3	14.2	14.1	13.8	13.3	12.3	11.2	10.1	9.2	8.0	5.8
23000	400	20	5.7	7.5	8.7	9.6	10.2	10.5	10.6	10.6	10.6	10.5	10.3	9.9	9.3	8.6	8.0	7.1	5.1
23000	400	50	4.8	5.6	6.0	6.2	6.3	6.4	6.5	6.5	6.5	6.6	6.6	6.5	6.3	6.0	5.6	5.1	3.8
23000	400	100	3.8	4.0	3.9	3.9	3.9	4.0	4.1	4.2	4.2	4.2	4.2	4.2	4.1	4.0	3.7	3.4	2.8
23000	400	200	2.6	2.7	2.7	2.6	2.5	2.5	2.6	2.7	2.7	2.7	2.7	2.8	2.8	2.7	2.6	2.4	2.2
23000	400	300	1.6	1.7	1.8	1.8	1.8	1.9	2.0	2.1	2.1	2.2	2.2	2.2	2.2	2.1	2.0	2.0	1.9
23000	400	400	1.2	1.3	1.4	1.4	1.5	1.6	1.7	1.8	1.9	2.0	2.0	1.9	1.9	1.9	1.8	1.8	1.7
23000	400	500	1.1	1.2	1.2	1.3	1.4	1.5	1.6	1.7	1.8	1.8	1.8	1.8	1.7	1.7	1.7	1.7	1.6

23000	700	10	10.3	13.2	15.8	17.9	19.5	20.4	20.7	20.7	20.7	20.6	20.2	19.1	17.2	15.0	13.0	11.2	8.6
23000	700	20	9.4	11.4	12.9	14.1	14.9	15.4	15.7	15.7	15.7	15.7	15.6	15.0	14.0	12.8	11.5	10.2	7.9
23000	700	50	8.4	9.3	9.6	9.7	9.8	9.9	10.1	10.1	10.1	10.1	10.1	10.0	9.7	9.2	8.6	7.7	6.1
23000	700	100	7.1	7.0	6.6	6.3	6.3	6.5	6.7	6.8	6.8	6.8	6.8	6.7	6.6	6.4	6.1	5.6	4.8
23000	700	200	4.8	4.7	4.5	4.3	4.2	4.4	4.5	4.6	4.6	4.6	4.6	4.6	4.5	4.4	4.3	4.2	3.8
23000	700	300	3.0	3.2	3.2	3.2	3.1	3.2	3.3	3.4	3.5	3.6	3.6	3.6	3.5	3.4	3.3	3.3	3.1
23000	700	400	2.1	2.2	2.3	2.4	2.5	2.6	2.8	3.0	3.1	3.1	3.1	3.1	3.0	3.0	2.9	2.8	2.8
23000	700	500	1.8	1.9	1.9	2.0	2.2	2.4	2.6	2.7	2.8	2.9	2.9	2.8	2.8	2.8	2.7	2.7	2.6

23000	1000	10	14.3	16.3	20.4	24.2	27.2	29.0	29.9	30.2	30.3	30.4	29.8	27.6	23.7	19.2	15.4	12.6	10.1
23000	1000	20	13.1	15.0	17.5	19.7	21.4	22.4	22.7	22.6	22.5	22.5	22.2	21.1	19.2	16.7	14.3	11.9	9.1
23000	1000	50	11.5	12.8	13.5	14.1	14.4	14.6	14.6	14.4	14.3	14.3	14.3	14.0	13.5	12.7	11.6	10.3	8.3
23000	1000	100	9.4	9.8	9.7	9.5	9.3	9.2	9.2	9.0	8.9	8.8	8.8	8.8	8.8	8.7	8.6	8.1	7.1
23000	1000	200	6.7	7.1	6.9	6.5	6.2	6.1	6.1	6.1	6.0	5.9	5.8	5.8	5.8	5.8	5.8	5.9	5.6
23000	1000	300	4.4	5.0	5.0	4.8	4.5	4.4	4.5	4.6	4.6	4.6	4.7	4.6	4.5	4.5	4.4	4.5	4.4
23000	1000	400	3.1	3.3	3.4	3.4	3.5	3.7	3.9	4.1	4.2	4.3	4.3	4.3	4.2	4.1	4.0	4.0	3.9
23000	1000	500	2.6	2.7	2.7	2.9	3.1	3.4	3.6	3.8	4.0	4.1	4.1	4.0	4.0	3.9	3.8	3.8	3.7

23000	1500	10	20.5	23.8	29.4	34.6	38.5	40.6	41.4	41.8	42.2	42.5	41.9	39.0	33.5	27.2	22.1	18.6	15.4
23000	1500	20	19.1	21.3	24.7	27.9	30.4	31.6	31.8	31.6	31.5	31.5	31.1	29.6	26.8	23.2	19.8	17.0	13.7
23000	1500	50	16.9	18.1	19.3	20.2	20.7	20.8	20.6	20.3	20.1	20.1	20.2	19.9	19.1	17.7	16.1	14.2	11.9
23000	1500	100	13.6	14.1	14.1	13.9	13.6	13.3	13.1	12.9	12.7	12.7	12.8	12.8	12.6	12.4	12.0	11.4	10.2
23000	1500	200	9.3	9.6	9.6	9.4	9.3	9.2	9.1	9.1	9.1	8.9	8.8	8.6	8.5	8.4	8.4	8.5	8.1
23000	1500	300	5.8	6.0	6.1	6.2	6.3	6.6	6.9	7.2	7.2	7.2	7.0	6.8	6.6	6.5	6.4	6.4	6.3
23000	1500	400	4.2	4.3	4.4	4.6	4.9	5.3	5.7	6.0	6.2	6.3	6.2	6.1	6.0	5.9	5.7	5.6	5.5
23000	1500	500	3.7	3.7	3.8	4.0	4.3	4.7	5.1	5.4	5.6	5.7	5.7	5.7	5.6	5.5	5.4	5.3	5.2

23000	2000	10	23.4	29.3	38.1	45.4	50.3	52.9	54.9	57.0	58.6	59.3	58.5	54.7	48.2	41.8	37.2	34.2	29.3
23000	2000	20	22.0	25.7	30.6	34.8	37.8	39.4	40.3	40.9	41.4	41.7	41.5	40.1	37.3	34.2	31.8	29.8	24.7
23000	2000	50	19.9	21.9	23.6	24.9	25.7	26.1	26.1	26.0	25.8	25.7	25.8	25.6	24.8	23.5	22.1	20.5	17.5
23000	2000	100	16.9	17.7	18.0	18.0	17.8	17.5	17.3	17.3	17.1	17.0	16.9	16.8	16.3	15.7	14.9	13.8	11.7
23000	2000	200	11.0	11.5	12.0	12.2	12.2	12.2	12.2	12.3	12.4	12.3	12.2	11.9	11.4	11.0	10.6	10.2	8.8
23000	2000	300	7.1	7.4	7.7	8.0	8.3	8.8	9.2	9.6	9.8	9.9	9.8	9.6	9.3	9.0	8.8	8.5	7.9
23000	2000	400	5.6	5.7	5.8	6.1	6.5	7.1	7.6	8.1	8.3	8.5	8.5	8.3	8.2	8.0	7.8	7.6	7.4
23000	2000	500	4.9	5.0	5.1	5.4	5.8	6.3	6.8	7.3	7.5	7.7	7.7	7.6	7.5	7.4	7.2	7.1	7.0

23000	3000	10	33.0	40.8	53.0	64.2	72.8	78.2	82.1	85.1	86.6	86.5	84.3	78.1	68.0	57.8	49.9	44.1	36.8
23000	3000	20	30.9	36.7	43.6	49.9	54.7	57.7	59.4	60.4	60.8	60.9	60.1	57.7	53.3	48.3	43.7	39.5	32.6
23000	3000	50	28.1	31.4	33.9	36.0	37.6	38.6	39.1	39.0	38.7	38.2	37.8	37.1	35.7	33.4	30.8	28.0	24.6
23000	3000	100	23.9	25.3	26.0	26.3	26.4	26.5	26.7	26.9	26.7	26.3	25.7	25.0	24.0	22.8	21.3	19.6	17.4
23000	3000	200	15.7	16.8	18.0	18.6	18.8	19.0	19.2	19.4	19.5	19.5	19.2	18.5	17.6	16.7	15.9	15.0	13.4
23000	3000	300	10.4	10.8	11.4	11.9	12.5	13.2	13.8	14.4	14.7	14.9	14.8	14.5	14.0	13.5	13.0	12.5	11.7
23000	3000	400	8.1	8.2	8.5	8.9	9.5	10.3	11.1	11.7	12.2	12.3	12.3	12.2	11.9	11.7	11.4	11.1	10.7
23000	3000	500	7.0	7.2	7.5	7.9	8.5	9.2	9.9	10.6	11.0	11.2	11.2	11.1	10.9	10.7	10.5	10.3	10.1

23000	5000	10	46.9	56.9	74.5	91.8	105.8	115.2	121.9	125.9	125.2	120.4	113.6	104.4	91.7	76.8	61.8	47.3	31.3
23000	5000	20	43.9	54.8	66.5	76.8	84.6	89.3	91.9	93.0	92.3	90.2	87.6	83.7	77.2	67.5	55.9	43.3	29.9
23000	5000	50	39.1	47.7	53.3	57.7	60.9	62.9	63.9	63.9	62.9	61.7	60.7	59.4	56.5	51.2	44.2	36.3	27.2
23000	5000	100	31.0	35.5	36.9	37.7	38.5	39.9	41.4	42.4	42.8	42.5	41.8	40.6	38.6	35.9	32.6	28.9	23.8
23000	5000	200	20.8	22.3	22.7	23.2	24.0	25.4	27.0	28.3	29.1	29.3	29.0	28.2	27.1	25.8	24.4	22.8	20.4
23000	5000	300	15.1	15.5	15.8	16.5	17.5	18.8	20.2	21.4	22.1	22.3	22.2	21.8	21.2	20.6	19.9	19.1	18.0
23000	5000	400	12.3	12.5	12.8	13.5	14.4	15.6	16.9	17.9	18.5	18.8	18.8	18.6	18.2	17.8	17.4	16.9	16.4
23000	5000	500	10.8	11.0	11.4	12.0	12.9	14.0	15.2	16.1	16.7	17.0	17.0	16.9	16.6	16.3	16.0	15.8	15.4

24000	100	10	1.4	1.7	2.3	2.9	3.5	3.8	3.9	3.9	3.8	3.7	3.4	3.1	2.6	2.2	1.8	1.4	0.9
24000	100	20	1.3	1.5	1.9	2.4	2.7	2.9	3.0	3.0	3.0	2.9	2.7	2.4	2.2	1.9	1.6	1.3	0.9
24000	100	50	1.2	1.3	1.5	1.6	1.8	1.9	1.9	2.0	2.0	2.0	1.9	1.7	1.6	1.4	1.3	1.1	0.8
24000	100	100	1.0	1.0	1.0	1.1	1.1	1.2	1.3	1.4	1.4	1.4	1.3	1.3	1.3	1.2	1.1	0.9	0.7
24000	100	200	0.7	0.7	0.7	0.7	0.7	0.8	0.9	1.0	1.0	1.1	1.1	1.1	1.1	1.0	0.9	0.7	0.6
24000	100	300	0.5	0.5	0.5	0.5	0.5	0.6	0.6	0.7	0.7	0.8	0.8	0.9	0.8	0.8	0.7	0.6	0.5
24000	100	400	0.4	0.4	0.4	0.4	0.4	0.5	0.5	0.5	0.5	0.6	0.6	0.6	0.6	0.6	0.5	0.5	0.5
24000	100	500	0.3	0.3	0.3	0.4	0.4	0.4	0.4	0.5	0.5	0.5	0.5	0.5	0.5	0.5	0.5	0.5	0.5

24000	200	10	3.2	3.8	4.8	5.8	6.6	7.1	7.2	7.1	7.0	6.7	6.4	6.1	5.6	5.0	4.3	3.5	2.4
24000	200	20	3.1	3.6	4.2	4.8	5.2	5.3	5.3	5.3	5.2	5.2	5.1	5.0	4.8	4.4	3.9	3.2	2.3
24000	200	50	2.8	3.1	3.3	3.4	3.5	3.5	3.4	3.4	3.4	3.4	3.4	3.3	3.3	3.1	2.9	2.6	2.1
24000	200	100	2.2	2.4	2.4	2.4	2.3	2.3	2.3	2.3	2.3	2.3	2.3	2.3	2.3	2.2	2.1	1.9	1.6
24000	200	200	1.5	1.7	1.7	1.6	1.5	1.5	1.5	1.6	1.6	1.6	1.6	1.6	1.6	1.5	1.4	1.3	1.2
24000	200	300	0.9	1.1	1.2	1.2	1.1	1.1	1.1	1.2	1.3	1.3	1.3	1.3	1.3	1.2	1.1	1.0	1.0
24000	200	400	0.7	0.8	0.8	0.9	0.9	0.9	1.0	1.0	1.1	1.1	1.1	1.1	1.1	1.0	1.0	1.0	0.9
24000	200	500	0.7	0.7	0.7	0.7	0.8	0.8	0.9	0.9	0.9	1.0	1.0	1.0	1.0	0.9	0.9	0.9	0.9

24000	400	10	6.4	8.3	10.0	11.5	12.8	13.5	13.7	13.5	13.2	12.8	12.4	11.7	10.9	10.1	9.2	8.1	6.3
24000	400	20	5.8	7.1	8.2	9.1	9.8	10.2	10.3	10.2	10.1	10.0	9.8	9.5	9.1	8.6	8.0	7.1	5.6
24000	400	50	5.2	5.8	6.1	6.2	6.4	6.4	6.4	6.4	6.4	6.4	6.4	6.4	6.3	6.0	5.7	5.2	4.3
24000	400	100	4.0	4.2	4.1	4.1	4.0	4.1	4.1	4.1	4.1	4.1	4.1	4.1	4.0	3.9	3.8	3.6	3.1
24000	400	200	2.7	2.8	2.8	2.7	2.6	2.6	2.6	2.7	2.7	2.6	2.6	2.7	2.6	2.6	2.5	2.4	2.2
24000	400	300	1.7	1.8	1.9	1.9	1.9	1.8	1.9	2.0	2.1	2.1	2.2	2.2	2.1	2.1	2.0	1.9	1.9
24000	400	400	1.3	1.4	1.4	1.5	1.5	1.6	1.7	1.8	1.9	1.9	1.9	1.9	1.9	1.9	1.8	1.8	1.7
24000	400	500	1.2	1.2	1.3	1.3	1.4	1.5	1.6	1.6	1.7	1.7	1.8	1.7	1.7	1.7	1.7	1.7	1.6

24000	700	10	9.8	12.2	14.6	17.1	19.3	20.6	21.1	21.1	20.9	20.7	20.3	19.3	17.4	15.2	13.1	11.4	9.4
24000	700	20	9.3	10.9	12.4	13.8	15.0	15.7	15.9	15.9	15.8	15.7	15.4	14.8	13.8	12.6	11.4	10.3	8.7
24000	700	50	8.7	9.3	9.7	9.9	10.0	10.2	10.3	10.3	10.2	10.1	10.0	9.8	9.5	9.1	8.5	7.8	6.7
24000	700	100	7.0	7.0	6.8	6.7	6.6	6.7	6.8	6.8	6.8	6.7	6.6	6.5	6.4	6.2	6.0	5.7	5.0
24000	700	200	4.6	4.6	4.6	4.5	4.5	4.5	4.6	4.6	4.6	4.5	4.5	4.4	4.3	4.2	4.2	4.1	3.8
24000	700	300	3.0	3.1	3.3	3.3	3.2	3.2	3.3	3.4	3.5	3.5	3.5	3.4	3.3	3.3	3.2	3.2	3.1
24000	700	400	2.2	2.3	2.4	2.5	2.5	2.6	2.8	2.9	3.0	3.1	3.1	3.0	3.0	2.9	2.9	2.8	2.8
24000	700	500	1.9	2.0	2.0	2.1	2.2	2.4	2.5	2.7	2.7	2.8	2.8	2.8	2.8	2.7	2.7	2.7	2.6

24000	1000	10	14.9	16.1	19.6	23.6	27.1	29.2	30.2	30.6	30.8	30.9	30.4	28.2	24.2	19.8	16.3	14.1	11.7
24000	1000	20	13.7	14.9	17.3	19.7	21.6	22.7	23.0	22.9	22.8	22.6	22.2	21.1	19.1	16.8	14.5	12.5	10.1
24000	1000	50	11.9	12.8	13.6	14.3	14.6	14.8	14.7	14.5	14.4	14.2	14.0	13.7	13.2	12.4	11.4	10.3	8.7
24000	1000	100	9.2	9.7	9.8	9.7	9.6	9.5	9.4	9.2	9.1	9.0	8.9	8.8	8.6	8.5	8.3	8.0	7.2
24000	1000	200	6.4	6.7	6.7	6.5	6.4	6.3	6.2	6.2	6.2	6.1	5.9	5.7	5.6	5.5	5.5	5.7	5.6
24000	1000	300	4.3	4.6	4.6	4.6	4.5	4.5	4.5	4.6	4.7	4.7	4.5	4.3	4.1	4.0	4.0	4.2	4.4
24000	1000	400	3.2	3.3	3.4	3.4	3.6	3.7	3.9	4.1	4.2	4.2	4.2	4.1	4.0	4.0	3.9	3.9	3.9
24000	1000	500	2.7	2.8	2.9	3.0	3.2	3.4	3.6	3.8	3.9	4.0	4.0	4.0	3.9	3.9	3.8	3.8	3.7
24000	1500	10	20.7	22.6	27.8	33.3	38.0	40.6	41.7	42.0	42.2	42.2	41.4	38.6	33.3	27.3	22.5	19.3	15.7
24000	1500	20	19.0	20.7	24.2	27.7	30.4	31.7	32.0	31.9	31.6	31.4	30.8	29.3	26.5	23.1	19.9	17.1	13.6
24000	1500	50	16.9	18.1	19.4	20.5	21.0	21.1	20.9	20.6	20.3	20.1	19.9	19.5	18.6	17.3	15.7	14.1	11.8
24000	1500	100	13.5	14.2	14.4	14.3	14.1	13.8	13.5	13.2	13.0	12.8	12.7	12.5	12.2	11.8	11.4	10.9	9.9
24000	1500	200	9.1	9.4	9.6	9.6	9.5	9.3	9.1	9.0	8.9	8.8	8.6	8.3	8.1	7.9	7.9	7.9	7.7
24000	1500	300	5.9	6.0	6.1	6.3	6.4	6.6	6.8	7.0	7.0	7.0	6.8	6.4	6.1	6.0	6.0	6.1	6.2
24000	1500	400	4.4	4.5	4.6	4.7	5.0	5.3	5.6	5.9	6.0	6.1	6.1	5.9	5.8	5.7	5.6	5.6	5.5
24000	1500	500	3.9	3.9	4.0	4.2	4.4	4.7	5.0	5.3	5.5	5.6	5.6	5.6	5.5	5.5	5.4	5.3	5.2
24000	2000	10	23.0	27.2	36.0	44.2	50.2	53.4	55.1	56.2	56.6	56.3	55.1	52.3	47.5	41.6	35.7	30.2	22.7
24000	2000	20	21.8	24.8	30.0	34.7	38.1	39.6	40.2	40.5	40.6	40.5	40.3	39.4	37.3	34.3	31.1	27.6	20.5
24000	2000	50	20.9	22.6	24.3	25.6	26.3	26.4	26.3	26.1	25.9	25.8	25.8	25.6	25.0	23.8	22.4	20.6	17.2
24000	2000	100	17.6	18.5	18.9	18.9	18.5	18.0	17.7	17.5	17.4	17.2	17.1	16.8	16.5	15.9	15.3	14.4	12.6
24000	2000	200	11.3	12.2	12.8	13.0	12.8	12.5	12.3	12.2	12.2	12.1	12.0	11.8	11.5	11.2	11.0	10.6	9.5
24000	2000	300	7.5	7.8	8.1	8.4	8.6	8.9	9.2	9.4	9.6	9.7	9.6	9.4	9.2	9.0	8.8	8.6	8.1
24000	2000	400	5.9	6.0	6.1	6.3	6.7	7.1	7.5	7.9	8.1	8.3	8.3	8.2	8.1	8.0	7.8	7.7	7.4
24000	2000	500	5.1	5.2	5.4	5.6	5.9	6.3	6.8	7.1	7.4	7.5	7.5	7.5	7.4	7.4	7.3	7.1	7.0
24000	3000	10	32.1	38.2	50.3	62.3	71.9	77.9	81.3	83.3	84.0	83.5	81.3	76.2	67.8	57.9	48.4	39.9	30.3
24000	3000	20	30.6	36.0	43.4	50.3	55.4	58.2	59.6	60.3	60.7	60.8	60.1	58.1	54.1	48.8	43.0	37.1	28.5
24000	3000	50	28.8	32.0	34.9	37.0	38.1	38.5	38.6	38.6	38.5	38.4	38.2	37.7	36.3	34.1	31.4	28.4	24.4
24000	3000	100	24.6	26.1	27.1	27.4	27.1	26.7	26.6	26.5	26.4	26.1	25.8	25.2	24.4	23.2	22.0	20.5	18.2
24000	3000	200	16.4	17.9	19.4	20.0	19.9	19.7	19.5	19.5	19.5	19.4	19.0	18.5	17.8	17.1	16.4	15.6	14.1
24000	3000	300	11.0	11.5	12.2	12.7	13.0	13.4	13.9	14.3	14.5	14.6	14.6	14.3	14.0	13.6	13.2	12.8	12.0
24000	3000	400	8.5	8.7	8.9	9.3	9.7	10.4	11.0	11.5	11.9	12.1	12.1	12.0	11.9	11.7	11.4	11.2	10.8
24000	3000	500	7.4	7.6	7.8	8.2	8.6	9.2	9.8	10.3	10.7	10.9	11.0	10.9	10.8	10.7	10.6	10.4	10.2
24000	5000	10	45.1	55.9	73.4	90.6	105.1	115.6	122.8	126.1	125.0	120.6	113.6	103.7	90.6	76.0	61.5	47.5	32.0
24000	5000	20	42.9	54.6	66.9	77.4	85.0	89.5	91.9	92.5	91.5	89.5	86.9	82.9	76.3	66.8	55.5	43.4	30.3
24000	5000	50	39.0	48.1	54.3	58.4	60.5	61.3	61.6	61.4	60.8	60.2	59.9	59.0	56.2	51.0	44.2	36.6	27.5
24000	5000	100	31.7	36.5	38.4	39.0	39.0	39.4	40.2	41.0	41.5	41.6	41.3	40.4	38.6	36.0	32.9	29.3	24.0
24000	5000	200	21.7	23.3	23.8	24.1	24.6	25.6	26.7	27.8	28.5	28.8	28.6	28.0	27.0	25.9	24.6	23.0	20.6
24000	5000	300	15.5	16.1	16.5	17.1	17.9	18.9	20.0	20.9	21.6	21.9	21.8	21.6	21.1	20.6	20.0	19.2	18.1
24000	5000	400	12.7	13.0	13.4	14.0	14.7	15.7	16.7	17.5	18.1	18.4	18.4	18.3	18.1	17.8	17.4	17.0	16.5
24000	5000	500	11.4	11.6	11.9	12.4	13.2	14.1	15.0	15.7	16.3	16.6	16.7	16.6	16.5	16.3	16.1	15.9	15.5
25000	100	10	1.3	1.6	2.1	2.7	3.3	3.6	3.7	3.7	3.6	3.5	3.3	3.0	2.6	2.2	1.8	1.4	0.9
25000	100	20	1.3	1.5	1.9	2.3	2.6	2.8	2.9	2.9	2.8	2.8	2.6	2.4	2.1	1.8	1.5	1.3	0.9
25000	100	50	1.2	1.3	1.4	1.6	1.8	1.9	1.9	2.0	2.0	1.9	1.8	1.7	1.6	1.4	1.3	1.1	0.8
25000	100	100	1.0	1.0	1.0	1.1	1.1	1.2	1.3	1.3	1.4	1.4	1.3	1.3	1.3	1.2	1.1	0.9	0.7
25000	100	200	0.7	0.7	0.7	0.7	0.7	0.8	0.8	0.9	1.0	1.0	1.0	1.1	1.1	1.0	0.9	0.7	0.6
25000	100	300	0.5	0.5	0.5	0.5	0.5	0.6	0.6	0.7	0.7	0.8	0.8	0.8	0.8	0.8	0.7	0.6	0.5

25000	100	400	0.4	0.4	0.4	0.4	0.4	0.5	0.5	0.5	0.5	0.6	0.6	0.6	0.6	0.6	0.5	0.5	0.5
25000	100	500	0.3	0.3	0.4	0.4	0.4	0.4	0.4	0.4	0.5	0.5	0.5	0.5	0.5	0.5	0.5	0.5	0.5
25000	200	10	2.9	3.4	4.3	5.3	6.2	6.7	6.8	6.7	6.4	6.1	5.8	5.4	5.1	4.6	4.1	3.3	2.3
25000	200	20	2.9	3.2	3.9	4.5	5.0	5.2	5.1	5.1	5.0	4.9	4.8	4.6	4.5	4.2	3.7	3.1	2.3
25000	200	50	2.8	3.0	3.2	3.4	3.4	3.4	3.4	3.4	3.3	3.3	3.3	3.3	3.3	3.2	3.0	2.7	2.2
25000	200	100	2.2	2.3	2.4	2.4	2.3	2.3	2.3	2.3	2.3	2.3	2.3	2.3	2.3	2.2	2.1	2.0	1.7
25000	200	200	1.4	1.6	1.6	1.6	1.6	1.6	1.6	1.6	1.6	1.6	1.6	1.6	1.6	1.5	1.4	1.3	1.2
25000	200	300	0.9	1.1	1.2	1.2	1.2	1.1	1.2	1.2	1.3	1.3	1.3	1.4	1.3	1.3	1.1	1.1	1.0
25000	200	400	0.7	0.8	0.9	0.9	0.9	0.9	0.9	1.0	1.0	1.1	1.1	1.1	1.1	1.1	1.0	1.0	1.0
25000	200	500	0.7	0.7	0.7	0.7	0.8	0.8	0.8	0.9	0.9	0.9	0.9	1.0	1.0	0.9	0.9	0.9	0.9
25000	400	10	5.9	7.1	8.7	10.4	11.9	12.8	13.1	12.8	12.3	11.7	11.0	10.4	9.7	9.0	8.1	7.0	5.6
25000	400	20	5.5	6.5	7.7	8.8	9.6	10.0	10.1	10.0	9.8	9.6	9.3	9.0	8.6	8.1	7.4	6.5	5.3
25000	400	50	5.1	5.7	6.1	6.4	6.5	6.6	6.6	6.6	6.6	6.7	6.7	6.7	6.6	6.4	6.1	5.7	4.8
25000	400	100	4.0	4.2	4.3	4.3	4.4	4.4	4.5	4.5	4.5	4.5	4.5	4.4	4.4	4.4	4.3	4.1	3.5
25000	400	200	2.6	2.8	2.9	2.9	2.9	3.0	3.0	3.0	3.0	2.9	2.9	2.8	2.8	2.7	2.6	2.5	2.3
25000	400	300	1.8	1.9	2.0	2.1	2.0	2.0	2.0	2.1	2.1	2.2	2.2	2.2	2.2	2.1	2.0	2.0	1.9
25000	400	400	1.4	1.4	1.5	1.5	1.6	1.6	1.7	1.7	1.8	1.9	1.9	1.9	1.9	1.9	1.8	1.8	1.7
25000	400	500	1.2	1.2	1.3	1.3	1.4	1.5	1.5	1.6	1.7	1.7	1.7	1.7	1.7	1.7	1.7	1.7	1.6
25000	700	10	9.2	10.8	13.2	16.0	18.5	20.1	20.7	20.6	20.2	19.7	19.1	18.0	16.2	14.0	12.0	10.3	8.4
25000	700	20	8.9	10.3	11.9	13.5	14.9	15.6	15.9	15.8	15.6	15.3	14.9	14.3	13.2	12.0	10.7	9.6	8.2
25000	700	50	8.6	9.3	9.8	10.1	10.3	10.4	10.4	10.4	10.4	10.3	10.2	10.0	9.7	9.3	8.7	8.1	7.1
25000	700	100	6.9	7.1	7.2	7.1	7.1	7.1	7.2	7.1	7.1	7.0	6.9	6.8	6.7	6.5	6.3	6.0	5.3
25000	700	200	4.6	4.7	4.8	4.9	4.9	5.0	5.0	5.0	4.9	4.8	4.6	4.5	4.4	4.3	4.2	4.1	3.9
25000	700	300	3.1	3.2	3.4	3.4	3.4	3.4	3.4	3.5	3.6	3.5	3.5	3.4	3.4	3.3	3.2	3.2	3.1
25000	700	400	2.3	2.4	2.4	2.5	2.6	2.6	2.7	2.9	3.0	3.0	3.0	3.0	3.0	2.9	2.9	2.9	2.8
25000	700	500	2.0	2.0	2.1	2.1	2.2	2.4	2.5	2.6	2.7	2.7	2.8	2.8	2.8	2.8	2.7	2.7	2.6
25000	1000	10	14.7	15.6	18.8	22.8	26.4	28.6	29.5	29.8	30.0	30.0	29.5	27.5	23.8	19.8	16.7	14.4	11.5
25000	1000	20	13.6	14.7	17.0	19.5	21.6	22.7	23.0	22.9	22.8	22.5	22.0	20.9	19.0	16.8	14.6	12.6	10.0
25000	1000	50	12.1	12.9	13.8	14.6	15.0	15.1	15.0	14.9	14.7	14.5	14.2	13.9	13.3	12.4	11.4	10.3	8.6
25000	1000	100	9.1	9.7	9.9	9.9	9.9	9.8	9.6	9.6	9.5	9.3	9.2	9.0	8.8	8.5	8.2	7.9	7.1
25000	1000	200	6.1	6.4	6.5	6.5	6.5	6.5	6.4	6.4	6.5	6.4	6.3	6.1	5.8	5.6	5.5	5.6	5.6
25000	1000	300	4.2	4.3	4.4	4.4	4.5	4.6	4.6	4.7	4.8	4.8	4.6	4.4	4.2	4.0	4.0	4.2	4.5
25000	1000	400	3.2	3.3	3.3	3.4	3.6	3.7	3.9	4.0	4.1	4.2	4.2	4.1	4.0	4.0	3.9	3.9	4.0
25000	1000	500	2.8	2.8	2.9	3.0	3.2	3.3	3.5	3.7	3.8	3.9	3.9	3.9	3.9	3.9	3.8	3.8	3.7
25000	1500	10	20.6	22.3	27.0	32.4	36.9	39.6	40.6	40.9	40.8	40.4	39.5	36.9	32.3	27.0	22.5	19.0	14.6
25000	1500	20	19.0	20.6	24.2	27.8	30.5	31.8	32.1	32.0	31.6	31.1	30.4	29.0	26.3	23.0	19.8	16.8	12.9
25000	1500	50	16.8	18.2	19.8	21.1	21.8	22.0	21.9	21.6	21.2	20.8	20.5	20.0	18.9	17.4	15.8	14.0	11.4
25000	1500	100	13.2	14.0	14.4	14.6	14.5	14.2	14.0	13.8	13.5	13.4	13.2	12.9	12.5	12.0	11.4	10.7	9.5
25000	1500	200	8.5	8.9	9.2	9.4	9.5	9.3	9.2	9.1	9.0	9.0	8.9	8.6	8.4	8.1	8.0	7.8	7.4
25000	1500	300	5.7	5.8	6.0	6.2	6.4	6.5	6.7	6.8	6.9	6.9	6.8	6.5	6.2	6.1	6.0	6.0	6.1
25000	1500	400	4.5	4.5	4.6	4.8	5.0	5.2	5.5	5.7	5.9	6.0	6.0	5.9	5.8	5.7	5.6	5.6	5.6
25000	1500	500	3.9	4.0	4.1	4.2	4.5	4.7	4.9	5.2	5.3	5.4	5.5	5.5	5.5	5.5	5.4	5.4	5.3
25000	2000	10	22.7	26.3	34.6	42.7	48.8	51.8	52.9	52.9	51.8	50.0	48.1	45.9	42.3	37.0	31.1	24.9	17.2
25000	2000	20	21.8	24.6	30.1	35.1	38.4	39.5	39.7	39.5	39.1	38.5	38.0	37.2	35.2	31.8	27.8	23.3	16.7
25000	2000	50	21.4	23.0	25.0	26.5	27.1	27.1	26.8	26.5	26.3	26.2	26.1	25.9	25.1	23.7	21.9	19.6	16.0
25000	2000	100	17.4	18.4	18.9	19.0	18.7	18.3	17.9	17.6	17.4	17.3	17.2	17.1	16.9	16.4	15.8	14.8	12.9

25000	2000	200	11.2	12.0	12.6	12.8	12.6	12.4	12.2	12.1	12.0	12.0	12.0	11.9	11.8	11.7	11.4	11.0	9.9
25000	2000	300	7.5	7.9	8.2	8.4	8.6	8.7	9.0	9.2	9.4	9.5	9.5	9.4	9.3	9.2	9.0	8.8	8.3
25000	2000	400	6.0	6.1	6.2	6.4	6.7	7.0	7.4	7.7	7.9	8.1	8.1	8.1	8.1	8.0	7.9	7.7	7.5
25000	2000	500	5.3	5.3	5.5	5.7	6.0	6.3	6.6	6.9	7.1	7.3	7.4	7.4	7.4	7.4	7.3	7.2	7.1
25000	3000	10	31.6	37.2	48.4	60.0	69.7	75.5	78.2	79.1	78.7	77.3	74.6	69.9	62.3	53.0	43.5	34.4	24.2
25000	3000	20	30.6	36.1	43.6	50.6	55.7	58.2	59.1	59.6	59.9	59.8	59.0	56.8	52.2	45.9	39.1	32.4	24.0
25000	3000	50	29.4	32.5	35.6	37.8	39.0	39.2	39.0	38.9	38.9	39.1	39.1	38.4	36.5	33.7	30.4	27.1	22.7
25000	3000	100	24.5	26.0	27.1	27.4	27.2	26.7	26.4	26.2	26.0	25.9	25.8	25.5	24.7	23.7	22.4	20.9	18.5
25000	3000	200	16.4	17.8	19.0	19.5	19.3	18.9	18.8	18.7	18.7	18.7	18.5	18.2	17.9	17.4	16.9	16.2	14.7
25000	3000	300	11.2	11.7	12.3	12.6	12.8	13.1	13.4	13.8	14.0	14.2	14.2	14.1	13.9	13.7	13.4	13.0	12.2
25000	3000	400	8.7	8.9	9.1	9.4	9.8	10.3	10.7	11.2	11.5	11.8	11.9	11.9	11.8	11.7	11.5	11.3	10.9
25000	3000	500	7.6	7.8	8.0	8.3	8.7	9.2	9.6	10.1	10.4	10.6	10.8	10.8	10.8	10.7	10.6	10.5	10.3
25000	5000	10	45.1	55.6	72.3	89.8	105.1	115.8	121.8	123.4	121.7	117.5	110.9	101.4	88.7	74.7	60.9	47.7	32.7
25000	5000	20	43.7	54.7	67.0	77.9	86.2	90.8	92.7	92.7	91.5	89.7	87.0	82.5	75.0	65.1	54.3	43.5	30.8
25000	5000	50	40.3	48.6	54.7	58.8	60.9	61.7	61.8	61.6	61.1	60.7	60.2	58.7	55.2	49.6	43.2	36.4	27.8
25000	5000	100	32.3	36.5	38.2	38.7	38.8	39.1	39.6	40.2	40.6	40.8	40.6	39.8	38.0	35.5	32.6	29.2	24.3
25000	5000	200	22.1	23.4	23.9	24.2	24.6	25.3	26.2	27.0	27.6	28.0	27.9	27.5	26.8	25.8	24.6	23.1	20.8
25000	5000	300	15.9	16.5	16.8	17.3	18.0	18.8	19.6	20.4	20.9	21.3	21.4	21.3	21.0	20.6	20.0	19.4	18.2
25000	5000	400	13.1	13.4	13.7	14.2	14.8	15.6	16.3	17.0	17.5	17.9	18.1	18.1	18.0	17.8	17.5	17.2	16.6
25000	5000	500	11.7	11.8	12.1	12.6	13.2	14.0	14.7	15.3	15.8	16.2	16.4	16.5	16.4	16.3	16.2	16.0	15.7
26000	100	10	1.3	1.6	2.0	2.6	3.1	3.4	3.5	3.5	3.5	3.3	3.1	2.9	2.5	2.1	1.8	1.4	0.9
26000	100	20	1.3	1.5	1.8	2.2	2.5	2.7	2.8	2.8	2.7	2.6	2.5	2.3	2.1	1.8	1.5	1.3	0.9
26000	100	50	1.2	1.3	1.5	1.6	1.7	1.8	1.8	1.9	1.9	1.8	1.7	1.6	1.5	1.4	1.2	1.1	0.8
26000	100	100	1.0	1.0	1.0	1.1	1.1	1.2	1.2	1.2	1.2	1.2	1.2	1.2	1.2	1.1	1.0	0.9	0.7
26000	100	200	0.7	0.7	0.7	0.7	0.7	0.8	0.8	0.8	0.9	0.9	0.9	0.9	0.9	0.9	0.8	0.7	0.6
26000	100	300	0.5	0.5	0.5	0.5	0.5	0.6	0.6	0.6	0.6	0.7	0.7	0.7	0.7	0.7	0.6	0.6	0.5
26000	100	400	0.4	0.4	0.4	0.4	0.4	0.5	0.5	0.5	0.5	0.5	0.5	0.6	0.6	0.5	0.5	0.5	0.5
26000	100	500	0.3	0.4	0.4	0.4	0.4	0.4	0.4	0.4	0.5	0.5	0.5	0.5	0.5	0.5	0.5	0.5	0.5
26000	200	10	2.8	3.2	4.1	5.1	6.0	6.6	6.8	6.7	6.5	6.2	5.8	5.3	4.8	4.3	3.7	3.0	2.1
26000	200	20	2.7	3.1	3.8	4.5	5.0	5.3	5.3	5.3	5.2	5.0	4.8	4.5	4.2	3.9	3.4	2.8	2.1
26000	200	50	2.6	2.8	3.1	3.3	3.5	3.5	3.5	3.5	3.5	3.5	3.5	3.4	3.3	3.1	2.9	2.6	2.1
26000	200	100	2.0	2.1	2.2	2.3	2.3	2.4	2.4	2.4	2.4	2.4	2.4	2.4	2.3	2.2	2.1	2.0	1.7
26000	200	200	1.4	1.4	1.5	1.5	1.6	1.6	1.6	1.7	1.7	1.7	1.6	1.6	1.6	1.5	1.5	1.4	1.2
26000	200	300	1.0	1.0	1.1	1.1	1.1	1.1	1.2	1.2	1.2	1.3	1.3	1.3	1.3	1.2	1.2	1.1	1.1
26000	200	400	0.8	0.8	0.8	0.9	0.9	0.9	0.9	1.0	1.0	1.0	1.1	1.1	1.1	1.0	1.0	1.0	1.0
26000	200	500	0.7	0.7	0.7	0.7	0.8	0.8	0.8	0.9	0.9	0.9	0.9	0.9	0.9	0.9	0.9	0.9	0.9
26000	400	10	5.4	6.5	8.1	9.8	11.3	12.3	12.7	12.6	12.1	11.5	10.8	9.9	9.0	8.0	6.9	5.8	4.5
26000	400	20	5.2	6.3	7.6	8.7	9.6	10.1	10.3	10.2	9.9	9.5	9.2	8.7	8.1	7.4	6.6	5.7	4.7
26000	400	50	4.7	5.5	6.1	6.5	6.8	6.9	7.0	7.0	7.0	7.0	7.0	6.9	6.8	6.6	6.3	5.8	5.0
26000	400	100	3.8	4.0	4.3	4.5	4.7	4.8	4.9	4.9	4.9	4.9	4.8	4.8	4.8	4.7	4.6	4.3	3.7
26000	400	200	2.6	2.7	2.9	3.0	3.2	3.3	3.4	3.4	3.2	3.1	3.1	3.0	3.0	2.9	2.8	2.7	2.4
26000	400	300	2.0	1.9	2.0	2.1	2.1	2.1	2.2	2.2	2.2	2.2	2.2	2.2	2.2	2.1	2.1	2.0	1.9
26000	400	400	1.5	1.5	1.5	1.6	1.6	1.6	1.7	1.8	1.8	1.8	1.9	1.9	1.9	1.9	1.8	1.8	1.8
26000	400	500	1.2	1.3	1.3	1.4	1.4	1.5	1.5	1.6	1.6	1.7	1.7	1.7	1.7	1.7	1.7	1.7	1.7
26000	700	10	8.6	10.1	12.5	15.2	17.7	19.4	20.1	20.0	19.6	18.9	18.0	16.7	14.8	12.7	10.7	8.9	6.7
26000	700	20	8.3	9.8	11.6	13.2	14.6	15.4	15.6	15.6	15.4	15.0	14.5	13.7	12.6	11.2	9.9	8.5	6.8

26000	700	50	8.0	8.9	9.6	10.1	10.4	10.5	10.5	10.5	10.5	10.4	10.3	10.1	9.8	9.3	8.7	8.0	6.8
26000	700	100	6.6	6.9	7.2	7.3	7.4	7.4	7.4	7.4	7.3	7.2	7.1	7.0	6.9	6.7	6.4	6.0	5.3
26000	700	200	4.7	4.7	4.9	5.1	5.2	5.3	5.3	5.2	5.1	4.9	4.8	4.7	4.6	4.4	4.3	4.1	3.8
26000	700	300	3.4	3.3	3.4	3.5	3.5	3.5	3.6	3.6	3.6	3.6	3.6	3.5	3.5	3.4	3.3	3.3	3.1
26000	700	400	2.4	2.4	2.5	2.5	2.6	2.7	2.7	2.8	2.9	3.0	3.0	3.0	3.0	3.0	3.0	2.9	2.8
26000	700	500	2.0	2.0	2.1	2.2	2.3	2.4	2.5	2.5	2.6	2.7	2.7	2.8	2.8	2.8	2.7	2.7	2.7

26000	1000	10	13.5	14.8	18.0	21.7	25.2	27.5	28.5	28.7	28.5	28.0	26.9	24.8	21.7	18.4	15.4	12.8	9.3
26000	1000	20	12.9	14.2	16.6	19.1	21.2	22.3	22.6	22.6	22.3	21.8	21.1	19.8	18.0	15.8	13.6	11.5	8.6
26000	1000	50	12.1	13.1	14.0	14.7	15.1	15.2	15.1	15.0	14.8	14.5	14.1	13.7	13.0	12.0	10.9	9.7	7.7
26000	1000	100	9.4	9.9	10.0	10.0	9.9	9.7	9.6	9.6	9.5	9.3	9.2	9.1	8.9	8.6	8.1	7.6	6.5
26000	1000	200	6.1	6.3	6.3	6.4	6.4	6.4	6.4	6.5	6.5	6.5	6.4	6.3	6.2	6.0	5.8	5.6	5.3
26000	1000	300	4.2	4.2	4.3	4.4	4.5	4.6	4.7	4.8	4.9	4.9	4.9	4.8	4.7	4.6	4.5	4.5	4.5
26000	1000	400	3.3	3.3	3.4	3.5	3.6	3.7	3.9	4.0	4.1	4.2	4.2	4.2	4.2	4.1	4.1	4.1	4.0
26000	1000	500	2.9	2.9	3.0	3.1	3.2	3.3	3.5	3.6	3.7	3.8	3.9	3.9	3.9	3.9	3.9	3.8	3.8

26000	1500	10	19.6	21.8	26.4	31.5	36.0	38.8	40.0	40.2	39.7	38.6	36.9	34.2	30.1	25.5	21.3	17.4	12.5
26000	1500	20	18.4	20.4	24.3	28.1	30.9	32.4	32.8	32.6	32.0	31.1	29.9	28.1	25.4	22.2	19.1	15.9	11.6
26000	1500	50	16.8	18.4	20.2	21.7	22.5	22.8	22.8	22.5	22.0	21.5	21.0	20.2	19.0	17.3	15.6	13.6	10.7
26000	1500	100	13.3	14.1	14.5	14.6	14.6	14.4	14.2	14.1	13.9	13.8	13.7	13.4	13.0	12.4	11.7	10.8	9.0
26000	1500	200	8.4	8.7	8.9	9.1	9.1	9.1	9.1	9.1	9.2	9.2	9.3	9.2	9.1	8.9	8.6	8.1	7.2
26000	1500	300	5.7	5.8	5.9	6.1	6.3	6.4	6.6	6.8	6.9	7.0	7.0	6.9	6.8	6.7	6.6	6.4	6.2
26000	1500	400	4.6	4.6	4.7	4.9	5.0	5.3	5.5	5.6	5.8	5.9	6.0	6.0	5.9	5.9	5.8	5.7	5.6
26000	1500	500	4.0	4.1	4.2	4.3	4.5	4.7	4.9	5.1	5.2	5.4	5.4	5.5	5.5	5.5	5.5	5.4	5.3

26000	2000	10	21.8	25.8	34.2	42.5	48.8	52.1	53.2	52.9	51.3	48.9	46.3	43.1	38.8	33.5	27.9	22.3	15.5
26000	2000	20	21.3	24.6	31.2	37.2	41.2	42.5	42.7	42.1	40.9	39.4	37.9	36.1	33.2	29.5	25.5	21.3	15.8
26000	2000	50	20.8	22.8	25.5	27.7	28.9	29.1	28.7	28.2	27.7	27.2	26.9	26.3	25.2	23.7	21.7	19.4	16.1
26000	2000	100	16.7	17.6	18.3	18.8	18.9	18.6	18.2	17.8	17.6	17.6	17.6	17.5	17.4	17.0	16.4	15.2	13.1
26000	2000	200	11.0	11.5	12.0	12.3	12.4	12.3	12.2	12.1	12.1	12.2	12.2	12.3	12.3	12.2	12.0	11.4	9.8
26000	2000	300	7.7	7.9	8.1	8.3	8.5	8.7	8.9	9.1	9.3	9.4	9.5	9.5	9.5	9.4	9.2	9.0	8.3
26000	2000	400	6.2	6.2	6.4	6.5	6.8	7.0	7.3	7.6	7.8	7.9	8.0	8.1	8.1	8.0	7.9	7.8	7.6
26000	2000	500	5.4	5.5	5.6	5.8	6.0	6.3	6.6	6.8	7.0	7.2	7.3	7.4	7.4	7.4	7.3	7.3	7.1

26000	3000	10	31.0	36.2	47.0	58.6	68.5	74.5	77.1	77.4	76.2	73.8	70.1	64.8	57.3	48.7	40.2	31.9	22.2
26000	3000	20	30.5	35.3	43.5	51.2	57.0	59.7	60.5	60.4	59.9	58.9	57.1	53.9	48.9	42.7	36.3	30.0	22.4
26000	3000	50	29.2	32.2	35.7	38.6	40.3	40.9	40.7	40.4	40.2	40.0	39.5	38.3	36.1	33.2	30.0	26.6	22.2
26000	3000	100	23.9	25.1	26.2	26.9	27.2	27.1	26.8	26.6	26.5	26.4	26.2	25.9	25.2	24.1	22.8	21.3	18.8
26000	3000	200	16.2	16.9	17.7	18.1	18.1	18.0	18.0	18.1	18.2	18.2	18.2	18.1	17.9	17.6	17.1	16.4	14.9
26000	3000	300	11.4	11.6	11.9	12.2	12.4	12.7	13.0	13.4	13.6	13.8	13.9	13.9	13.9	13.7	13.5	13.1	12.3
26000	3000	400	9.0	9.1	9.3	9.5	9.9	10.3	10.7	11.0	11.3	11.6	11.7	11.8	11.8	11.7	11.6	11.4	11.0
26000	3000	500	7.9	8.0	8.2	8.4	8.8	9.2	9.6	9.9	10.2	10.5	10.6	10.7	10.8	10.7	10.7	10.6	10.4

26000	5000	10	45.6	53.9	69.6	87.2	103.3	114.2	119.3	120.0	117.8	113.6	107.2	98.1	86.2	73.1	60.3	47.8	32.8
26000	5000	20	44.6	52.8	64.7	76.3	85.5	90.8	92.8	92.6	91.3	89.1	85.8	80.5	72.7	63.2	53.4	43.5	31.1
26000	5000	50	41.6	47.7	53.0	57.0	59.6	60.8	61.3	61.3	60.9	60.3	59.2	57.1	53.2	48.1	42.4	36.4	28.1
26000	5000	100	33.4	35.9	37.1	37.7	38.0	38.5	39.1	39.6	39.9	40.0	39.7	38.8	37.2	35.0	32.3	29.3	24.6
26000	5000	200	23.3	23.7	23.9	24.2	24.6	25.3	26.0	26.6	27.1	27.4	27.5	27.2	26.6	25.8	24.7	23.3	21.0
26000	5000	300	16.8	17.0	17.2	17.6	18.1	18.8	19.5	20.1	20.6	20.9	21.1	21.1	21.0	20.6	20.2	19.5	18.4
26000	5000	400	13.7	13.8	14.0	14.4	15.0	15.6	16.2	16.8	17.3	17.6	17.9	18.0	18.0	17.8	17.6	17.3	16.8
26000	5000	500	12.1	12.2	12.4	12.8	13.4	14.0	14.6	15.1	15.6	15.9	16.2	16.3	16.4	16.4	16.3	16.1	15.8

28000	100	10	1.3	1.5	1.9	2.4	2.8	3.1	3.3	3.3	3.3	3.2	3.0	2.7	2.4	2.1	1.7	1.4	1.0
28000	100	20	1.2	1.5	1.8	2.1	2.4	2.6	2.6	2.6	2.6	2.5	2.4	2.3	2.0	1.8	1.5	1.3	0.9
28000	100	50	1.2	1.3	1.5	1.6	1.7	1.7	1.8	1.8	1.8	1.7	1.7	1.6	1.5	1.4	1.2	1.1	0.8
28000	100	100	1.0	1.0	1.1	1.1	1.1	1.1	1.1	1.1	1.2	1.2	1.1	1.1	1.1	1.0	1.0	0.9	0.7
28000	100	200	0.7	0.7	0.7	0.7	0.7	0.7	0.8	0.8	0.8	0.8	0.8	0.8	0.8	0.8	0.7	0.7	0.6
28000	100	300	0.5	0.5	0.5	0.5	0.5	0.6	0.6	0.6	0.6	0.6	0.6	0.6	0.6	0.6	0.6	0.6	0.5
28000	100	400	0.4	0.4	0.4	0.4	0.4	0.5	0.5	0.5	0.5	0.5	0.5	0.5	0.5	0.5	0.5	0.5	0.5
28000	100	500	0.4	0.4	0.4	0.4	0.4	0.4	0.4	0.4	0.5	0.5	0.5	0.5	0.5	0.5	0.5	0.5	0.5

28000	200	10	2.8	3.2	4.0	4.9	5.7	6.3	6.5	6.6	6.4	6.2	5.8	5.4	4.8	4.1	3.5	2.8	2.0
28000	200	20	2.7	3.1	3.8	4.4	4.9	5.2	5.3	5.3	5.2	5.0	4.8	4.5	4.1	3.6	3.1	2.6	1.9
28000	200	50	2.5	2.8	3.1	3.3	3.5	3.5	3.6	3.6	3.5	3.5	3.4	3.3	3.1	2.9	2.6	2.3	1.9
28000	200	100	2.0	2.1	2.2	2.2	2.3	2.3	2.3	2.3	2.3	2.3	2.3	2.3	2.2	2.1	2.0	1.8	1.6
28000	200	200	1.4	1.4	1.4	1.5	1.5	1.5	1.6	1.6	1.6	1.6	1.6	1.6	1.6	1.5	1.4	1.4	1.2
28000	200	300	1.0	1.0	1.0	1.1	1.1	1.1	1.1	1.2	1.2	1.2	1.2	1.2	1.2	1.2	1.2	1.1	1.1
28000	200	400	0.8	0.8	0.8	0.9	0.9	0.9	0.9	1.0	1.0	1.0	1.0	1.0	1.0	1.0	1.0	1.0	1.0
28000	200	500	0.7	0.7	0.7	0.8	0.8	0.8	0.8	0.9	0.9	0.9	0.9	0.9	0.9	0.9	0.9	0.9	0.9

28000	400	10	5.2	6.4	7.9	9.4	10.7	11.6	12.0	12.0	11.7	11.3	10.7	9.8	8.7	7.6	6.4	5.2	3.8
28000	400	20	5.0	6.2	7.5	8.6	9.4	9.8	10.0	9.9	9.6	9.3	8.9	8.3	7.6	6.8	5.9	5.0	3.9
28000	400	50	4.6	5.3	5.9	6.4	6.6	6.8	6.8	6.8	6.7	6.6	6.5	6.3	6.1	5.8	5.4	4.8	4.0
28000	400	100	3.8	3.9	4.1	4.3	4.4	4.5	4.6	4.6	4.6	4.5	4.5	4.4	4.3	4.2	4.0	3.8	3.2
28000	400	200	2.8	2.6	2.7	2.8	3.0	3.1	3.2	3.1	3.1	3.0	2.9	2.9	2.9	2.8	2.7	2.5	2.3
28000	400	300	2.1	1.9	1.9	2.0	2.0	2.1	2.2	2.2	2.2	2.2	2.2	2.2	2.2	2.1	2.1	2.0	1.9
28000	400	400	1.5	1.5	1.5	1.6	1.6	1.6	1.7	1.8	1.8	1.8	1.9	1.9	1.9	1.9	1.9	1.8	1.8
28000	400	500	1.3	1.3	1.3	1.4	1.4	1.5	1.5	1.6	1.6	1.7	1.7	1.7	1.7	1.7	1.7	1.7	1.7

28000	700	10	8.4	9.8	12.0	14.4	16.7	18.2	19.0	19.1	18.8	18.2	17.2	15.9	14.1	12.1	10.2	8.2	5.8
28000	700	20	8.2	9.5	11.2	12.7	14.0	14.8	15.2	15.2	15.0	14.6	14.0	13.2	12.0	10.7	9.2	7.8	5.8
28000	700	50	7.7	8.5	9.2	9.7	10.0	10.2	10.2	10.3	10.2	10.0	9.8	9.6	9.1	8.6	7.9	7.0	5.8
28000	700	100	6.5	6.6	6.7	6.8	6.9	7.0	7.0	7.0	6.9	6.8	6.7	6.7	6.5	6.3	5.9	5.5	4.8
28000	700	200	4.7	4.5	4.6	4.7	4.8	4.9	4.9	4.9	4.8	4.7	4.7	4.6	4.6	4.4	4.2	4.0	3.7
28000	700	300	3.4	3.3	3.3	3.3	3.4	3.4	3.5	3.5	3.5	3.5	3.6	3.6	3.5	3.5	3.4	3.3	3.1
28000	700	400	2.5	2.5	2.5	2.5	2.6	2.7	2.7	2.8	2.9	2.9	3.0	3.0	3.0	3.0	3.0	2.9	2.9
28000	700	500	2.1	2.1	2.2	2.2	2.3	2.4	2.5	2.5	2.6	2.7	2.7	2.7	2.8	2.8	2.8	2.7	2.7

28000	1000	10	12.7	14.1	17.0	20.3	23.5	25.8	27.0	27.2	26.8	26.0	24.7	22.8	20.2	17.3	14.5	11.7	8.1
28000	1000	20	12.4	13.7	15.9	18.2	20.1	21.3	21.7	21.7	21.4	20.8	20.0	18.7	17.0	15.0	12.9	10.7	7.8
28000	1000	50	12.0	12.9	13.7	14.2	14.6	14.6	14.6	14.5	14.3	14.0	13.6	13.2	12.5	11.5	10.4	9.1	7.1
28000	1000	100	9.7	10.0	9.9	9.7	9.5	9.3	9.2	9.2	9.2	9.0	8.9	9.0	8.8	8.5	8.0	7.3	6.1
28000	1000	200	6.3	6.3	6.2	6.2	6.2	6.2	6.3	6.3	6.4	6.4	6.4	6.4	6.4	6.2	6.0	5.7	5.1
28000	1000	300	4.4	4.3	4.3	4.4	4.5	4.6	4.7	4.8	4.9	5.0	5.0	5.0	5.0	4.9	4.8	4.7	4.5
28000	1000	400	3.4	3.4	3.5	3.5	3.6	3.8	3.9	4.0	4.1	4.2	4.2	4.3	4.3	4.3	4.2	4.2	4.1
28000	1000	500	3.0	3.0	3.1	3.1	3.3	3.4	3.5	3.6	3.7	3.8	3.8	3.9	3.9	3.9	3.9	3.9	3.8

28000	1500	10	18.0	20.2	24.5	29.2	33.7	36.7	38.3	38.6	37.9	36.6	34.7	32.0	28.4	24.4	20.4	16.4	11.4
28000	1500	20	17.4	19.4	23.0	26.6	29.5	31.1	31.6	31.5	30.9	29.9	28.5	26.7	24.2	21.3	18.3	15.2	11.0
28000	1500	50	16.6	18.0	19.5	20.8	21.5	21.8	21.7	21.5	21.2	20.7	20.1	19.4	18.2	16.7	15.0	13.1	10.2
28000	1500	100	13.6	14.1	14.2	14.2	14.1	13.9	13.7	13.6	13.6	13.5	13.4	13.2	12.9	12.4	11.6	10.6	8.7
28000	1500	200	8.8	8.8	8.8	8.8	8.9	8.9	8.9	9.0	9.1	9.2	9.3	9.4	9.3	9.2	8.8	8.2	7.2
28000	1500	300	5.9	5.9	6.0	6.1	6.3	6.4	6.6	6.7	6.9	7.0	7.1	7.1	7.1	7.1	6.9	6.7	6.3
28000	1500	400	4.8	4.8	4.9	5.0	5.1	5.3	5.5	5.6	5.8	5.9	6.0	6.0	6.0	6.0	6.0	5.9	5.7
28000	1500	500	4.2	4.2	4.3	4.4	4.6	4.7	4.9	5.1	5.2	5.3	5.4	5.5	5.5	5.5	5.5	5.5	5.4

28000	2000	10	21.3	25.2	32.8	40.6	46.8	50.5	52.0	52.0	50.7	48.6	45.9	42.3	37.6	32.4	27.1	21.9	15.5
28000	2000	20	21.0	24.4	31.0	37.0	41.2	43.0	43.4	42.8	41.4	39.7	37.8	35.4	32.2	28.6	24.8	20.9	15.9
28000	2000	50	20.4	22.4	25.3	27.6	29.1	29.4	29.1	28.6	28.0	27.4	26.8	25.9	24.8	23.2	21.3	19.1	15.9
28000	2000	100	16.6	17.3	18.0	18.6	18.8	18.7	18.2	17.8	17.6	17.6	17.6	17.6	17.4	17.0	16.3	15.1	12.9
28000	2000	200	11.4	11.5	11.8	12.1	12.2	12.2	12.2	12.1	12.2	12.2	12.3	12.4	12.4	12.4	12.1	11.4	9.8
28000	2000	300	8.1	8.1	8.2	8.4	8.6	8.8	8.9	9.1	9.3	9.4	9.5	9.6	9.6	9.5	9.4	9.1	8.4
28000	2000	400	6.4	6.4	6.5	6.7	6.9	7.1	7.3	7.5	7.7	7.9	8.0	8.1	8.1	8.1	8.0	7.9	7.6
28000	2000	500	5.6	5.7	5.8	5.9	6.1	6.4	6.6	6.8	7.0	7.1	7.2	7.3	7.4	7.4	7.4	7.3	7.2
28000	3000	10	30.3	35.1	45.0	55.7	65.3	71.6	74.5	74.8	73.5	70.9	67.2	61.8	54.9	47.1	39.3	31.6	22.1
28000	3000	20	30.0	34.3	42.4	50.2	56.1	59.2	60.1	59.9	58.9	57.3	55.0	51.5	46.7	41.2	35.5	29.6	22.1
28000	3000	50	28.8	31.7	35.3	38.4	40.4	41.1	41.0	40.6	40.2	39.7	38.9	37.5	35.3	32.6	29.6	26.3	21.8
28000	3000	100	24.0	24.9	25.8	26.5	26.9	27.0	26.8	26.6	26.5	26.4	26.2	25.8	25.1	24.1	22.8	21.2	18.6
28000	3000	200	16.7	16.7	17.0	17.3	17.4	17.5	17.6	17.8	17.9	18.0	18.0	18.0	17.8	17.5	17.1	16.4	14.8
28000	3000	300	11.9	11.8	11.9	12.1	12.3	12.6	12.9	13.2	13.4	13.7	13.8	13.9	13.8	13.7	13.5	13.2	12.4
28000	3000	400	9.4	9.4	9.5	9.7	10.0	10.3	10.7	11.0	11.2	11.5	11.6	11.7	11.8	11.7	11.6	11.5	11.1
28000	3000	500	8.2	8.2	8.4	8.6	8.9	9.2	9.6	9.9	10.1	10.4	10.5	10.7	10.7	10.8	10.7	10.6	10.5
28000	5000	10	44.3	51.7	65.6	81.6	96.7	107.6	113.0	113.9	112.1	108.2	102.4	94.2	83.5	71.6	59.8	47.9	33.0
28000	5000	20	43.7	50.9	61.9	73.1	82.4	88.0	90.2	90.2	88.9	86.6	83.0	77.6	70.3	61.9	53.0	43.7	31.5
28000	5000	50	41.8	47.0	51.7	55.6	58.2	59.5	60.1	60.1	59.8	59.0	57.6	55.2	51.7	47.2	42.3	36.6	28.5
28000	5000	100	35.5	36.6	37.1	37.5	37.8	38.2	38.7	39.1	39.3	39.3	39.0	38.1	36.7	34.8	32.4	29.5	24.9
28000	5000	200	25.6	24.9	24.6	24.6	24.9	25.4	25.9	26.4	26.8	27.1	27.2	27.0	26.6	25.8	24.8	23.5	21.3
28000	5000	300	18.2	17.8	17.8	18.0	18.4	19.0	19.5	20.0	20.4	20.8	21.0	21.0	21.0	20.7	20.3	19.7	18.6
28000	5000	400	14.3	14.3	14.4	14.8	15.2	15.7	16.2	16.7	17.1	17.5	17.7	17.9	17.9	17.9	17.7	17.5	16.9
28000	5000	500	12.5	12.6	12.8	13.1	13.6	14.1	14.6	15.0	15.4	15.8	16.1	16.3	16.4	16.4	16.4	16.2	16.0
30000	100	10	1.3	1.5	1.8	2.2	2.7	3.0	3.1	3.2	3.1	3.0	2.9	2.7	2.4	2.1	1.7	1.4	1.0
30000	100	20	1.2	1.5	1.8	2.1	2.3	2.5	2.6	2.6	2.5	2.5	2.4	2.2	2.0	1.8	1.5	1.3	0.9
30000	100	50	1.2	1.3	1.5	1.6	1.7	1.7	1.7	1.7	1.7	1.7	1.7	1.6	1.5	1.4	1.2	1.1	0.8
30000	100	100	1.0	1.1	1.1	1.1	1.1	1.1	1.1	1.1	1.1	1.1	1.1	1.1	1.1	1.0	0.9	0.9	0.7
30000	100	200	0.7	0.7	0.7	0.7	0.7	0.7	0.8	0.8	0.8	0.8	0.8	0.8	0.8	0.8	0.7	0.7	0.6
30000	100	300	0.5	0.5	0.5	0.5	0.5	0.6	0.6	0.6	0.6	0.6	0.6	0.6	0.6	0.6	0.6	0.6	0.6
30000	100	400	0.4	0.4	0.4	0.4	0.4	0.5	0.5	0.5	0.5	0.5	0.5	0.5	0.5	0.5	0.5	0.5	0.5
30000	100	500	0.4	0.4	0.4	0.4	0.4	0.4	0.4	0.4	0.4	0.5	0.5	0.5	0.5	0.5	0.5	0.5	0.5
30000	200	10	2.7	3.1	3.9	4.7	5.4	5.9	6.2	6.3	6.2	6.0	5.7	5.3	4.7	4.1	3.4	2.8	1.9
30000	200	20	2.6	3.1	3.7	4.3	4.7	5.0	5.1	5.1	5.0	4.9	4.7	4.4	4.0	3.5	3.1	2.6	1.9
30000	200	50	2.5	2.8	3.1	3.3	3.4	3.5	3.5	3.5	3.4	3.4	3.3	3.2	3.0	2.7	2.5	2.2	1.7
30000	200	100	2.1	2.1	2.1	2.2	2.2	2.2	2.3	2.3	2.3	2.3	2.2	2.2	2.1	2.0	1.9	1.7	1.5
30000	200	200	1.5	1.4	1.4	1.4	1.5	1.5	1.5	1.5	1.6	1.6	1.6	1.6	1.5	1.5	1.4	1.4	1.2
30000	200	300	1.1	1.0	1.0	1.0	1.1	1.1	1.1	1.2	1.2	1.2	1.2	1.2	1.2	1.2	1.2	1.1	1.1
30000	200	400	0.9	0.8	0.8	0.9	0.9	0.9	0.9	1.0	1.0	1.0	1.0	1.0	1.0	1.0	1.0	1.0	1.0
30000	200	500	0.7	0.7	0.8	0.8	0.8	0.8	0.8	0.9	0.9	0.9	0.9	0.9	0.9	1.0	1.0	0.9	0.9
30000	400	10	5.1	6.2	7.8	9.1	10.2	10.9	11.3	11.3	11.2	10.8	10.3	9.6	8.6	7.4	6.3	5.1	3.6
30000	400	20	5.0	6.1	7.4	8.3	9.0	9.3	9.5	9.4	9.2	8.9	8.5	8.0	7.3	6.5	5.6	4.7	3.5
30000	400	50	4.7	5.2	5.7	6.1	6.3	6.4	6.5	6.4	6.3	6.2	6.0	5.8	5.5	5.1	4.6	4.1	3.3
30000	400	100	3.9	3.7	3.7	3.8	3.9	4.1	4.2	4.2	4.2	4.1	4.1	4.0	3.9	3.8	3.6	3.3	2.8
30000	400	200	2.8	2.5	2.4	2.5	2.6	2.7	2.8	2.9	2.9	2.8	2.8	2.8	2.8	2.7	2.6	2.5	2.3
30000	400	300	2.0	1.8	1.8	1.8	1.9	2.0	2.1	2.1	2.1	2.2	2.2	2.2	2.2	2.2	2.1	2.1	2.0

30000	400	400	1.6	1.5	1.5	1.6	1.6	1.7	1.7	1.8	1.8	1.8	1.9	1.9	1.9	1.9	1.9	1.8	1.8
30000	400	500	1.3	1.3	1.4	1.4	1.4	1.5	1.5	1.6	1.6	1.7	1.7	1.7	1.7	1.7	1.7	1.7	1.7
30000	700	10	8.2	9.5	11.6	13.9	15.9	17.3	18.1	18.3	18.0	17.5	16.7	15.4	13.8	11.9	10.0	8.1	5.6
30000	700	20	8.1	9.2	10.6	12.1	13.4	14.3	14.7	14.8	14.6	14.2	13.6	12.8	11.7	10.4	9.0	7.5	5.5
30000	700	50	7.7	8.1	8.5	8.9	9.3	9.7	9.9	10.0	9.9	9.7	9.5	9.2	8.7	8.0	7.3	6.4	5.1
30000	700	100	6.4	6.2	6.0	6.0	6.1	6.4	6.6	6.7	6.6	6.6	6.5	6.4	6.2	5.9	5.6	5.1	4.4
30000	700	200	4.6	4.2	4.1	4.1	4.3	4.4	4.5	4.6	4.6	4.6	4.6	4.6	4.5	4.4	4.2	4.0	3.6
30000	700	300	3.4	3.1	3.1	3.1	3.2	3.3	3.3	3.4	3.5	3.5	3.5	3.5	3.5	3.5	3.4	3.3	3.2
30000	700	400	2.6	2.5	2.5	2.5	2.6	2.7	2.8	2.8	2.9	2.9	3.0	3.0	3.0	3.0	3.0	3.0	2.9
30000	700	500	2.2	2.2	2.2	2.3	2.3	2.4	2.5	2.5	2.6	2.7	2.7	2.7	2.8	2.8	2.8	2.8	2.7
30000	1000	10	11.8	13.2	15.9	19.0	22.1	24.4	25.6	26.0	25.6	24.9	23.6	21.9	19.5	16.9	14.2	11.5	8.0
30000	1000	20	11.6	12.9	15.0	17.3	19.2	20.4	21.0	21.0	20.7	20.1	19.3	18.1	16.5	14.7	12.7	10.5	7.6
30000	1000	50	11.3	12.2	12.9	13.5	14.0	14.2	14.2	14.1	14.0	13.7	13.4	12.9	12.2	11.3	10.2	8.9	7.0
30000	1000	100	9.5	9.6	9.5	9.3	9.2	9.1	9.1	9.1	9.1	9.0	8.9	8.9	8.8	8.4	7.9	7.2	6.1
30000	1000	200	6.5	6.3	6.1	6.1	6.1	6.1	6.2	6.3	6.3	6.4	6.4	6.4	6.4	6.2	6.0	5.7	5.1
30000	1000	300	4.5	4.4	4.4	4.4	4.5	4.6	4.7	4.8	4.9	4.9	5.0	5.0	5.0	5.0	4.9	4.7	4.5
30000	1000	400	3.5	3.5	3.5	3.6	3.7	3.8	3.9	4.0	4.1	4.2	4.2	4.3	4.3	4.3	4.3	4.2	4.1
30000	1000	500	3.1	3.1	3.1	3.2	3.3	3.4	3.5	3.6	3.7	3.8	3.8	3.9	3.9	3.9	3.9	3.9	3.9
30000	1500	10	16.3	18.4	22.4	26.9	31.2	34.5	36.3	36.7	36.2	35.0	33.3	30.8	27.5	23.8	20.1	16.2	11.3
30000	1500	20	16.0	18.1	21.4	24.7	27.5	29.3	30.0	30.0	29.4	28.6	27.4	25.7	23.4	20.7	17.9	14.9	10.9
30000	1500	50	15.6	17.0	18.4	19.5	20.2	20.5	20.5	20.4	20.1	19.8	19.3	18.5	17.5	16.1	14.6	12.7	10.0
30000	1500	100	13.4	13.6	13.6	13.5	13.4	13.3	13.3	13.2	13.2	13.1	13.1	12.9	12.6	12.0	11.3	10.3	8.6
30000	1500	200	9.2	8.9	8.8	8.7	8.7	8.8	8.8	8.9	9.0	9.1	9.2	9.2	9.2	9.0	8.7	8.1	7.2
30000	1500	300	6.3	6.1	6.1	6.2	6.3	6.5	6.6	6.7	6.9	7.0	7.1	7.1	7.1	7.1	6.9	6.7	6.3
30000	1500	400	4.9	4.9	5.0	5.1	5.2	5.3	5.5	5.6	5.7	5.9	5.9	6.0	6.0	6.0	6.0	5.9	5.7
30000	1500	500	4.3	4.3	4.4	4.5	4.6	4.8	4.9	5.1	5.2	5.3	5.4	5.5	5.5	5.5	5.5	5.5	5.4
30000	2000	10	20.5	24.1	30.4	37.1	43.1	47.2	49.2	49.6	48.7	47.0	44.6	41.2	36.8	31.9	26.9	21.8	15.5
30000	2000	20	20.3	23.6	29.1	34.3	38.3	40.4	41.2	40.9	39.9	38.6	36.8	34.5	31.5	28.0	24.3	20.5	15.3
30000	2000	50	19.8	21.9	24.4	26.4	27.6	28.1	28.0	27.7	27.2	26.7	26.1	25.1	23.8	22.2	20.3	18.0	14.7
30000	2000	100	16.9	17.3	17.7	18.1	18.2	18.1	17.9	17.7	17.6	17.5	17.5	17.3	17.0	16.4	15.6	14.4	12.3
30000	2000	200	12.1	11.7	11.7	11.8	11.9	12.0	12.0	12.0	12.1	12.2	12.3	12.3	12.2	12.1	11.8	11.1	9.8
30000	2000	300	8.5	8.3	8.3	8.4	8.5	8.7	8.9	9.1	9.2	9.4	9.5	9.5	9.5	9.5	9.3	9.1	8.5
30000	2000	400	6.7	6.6	6.7	6.8	7.0	7.2	7.4	7.5	7.7	7.9	8.0	8.1	8.1	8.1	8.0	7.9	7.7
30000	2000	500	5.8	5.8	5.9	6.0	6.2	6.4	6.6	6.8	7.0	7.1	7.2	7.3	7.4	7.4	7.4	7.4	7.3
30000	3000	10	29.3	34.0	42.6	52.1	61.0	67.5	70.8	71.5	70.5	68.2	64.8	59.9	53.5	46.4	39.1	31.6	22.1
30000	3000	20	29.0	33.5	40.7	47.8	53.5	56.9	58.2	58.1	57.2	55.6	53.4	50.0	45.6	40.5	35.0	29.3	21.6
30000	3000	50	28.2	31.3	34.6	37.3	39.2	39.9	40.0	39.7	39.3	38.8	37.9	36.4	34.3	31.7	28.8	25.4	20.5
30000	3000	100	24.5	25.1	25.5	25.9	26.1	26.2	26.2	26.1	26.0	26.0	25.8	25.3	24.6	23.5	22.2	20.5	17.7
30000	3000	200	17.6	17.1	16.9	17.0	17.1	17.2	17.4	17.5	17.7	17.8	17.9	17.8	17.6	17.3	16.8	16.0	14.5
30000	3000	300	12.4	12.1	12.0	12.1	12.4	12.6	12.9	13.2	13.4	13.6	13.7	13.8	13.8	13.7	13.5	13.1	12.4
30000	3000	400	9.7	9.6	9.7	9.9	10.1	10.4	10.7	11.0	11.2	11.4	11.6	11.7	11.8	11.8	11.7	11.5	11.2
30000	3000	500	8.4	8.4	8.6	8.8	9.0	9.3	9.6	9.9	10.1	10.3	10.5	10.6	10.8	10.8	10.8	10.7	10.6
30000	5000	10	43.1	50.6	63.0	77.3	91.2	101.8	107.4	108.7	107.3	103.9	98.7	91.3	81.6	70.6	59.4	48.0	33.3
30000	5000	20	42.8	50.0	60.4	70.8	79.7	85.3	87.7	87.8	86.6	84.3	80.9	75.9	69.1	61.2	52.9	43.9	31.8
30000	5000	50	41.6	46.9	51.6	55.2	57.7	59.0	59.4	59.4	58.9	58.1	56.7	54.4	51.1	47.0	42.3	36.9	28.9
30000	5000	100	37.1	37.6	37.8	38.0	38.1	38.3	38.6	38.9	39.0	39.0	38.7	37.9	36.6	34.8	32.5	29.7	25.2

30000	5000	200	27.3	25.9	25.3	25.1	25.2	25.6	26.0	26.4	26.8	27.0	27.1	26.9	26.6	25.9	25.0	23.7	21.5
30000	5000	300	19.1	18.4	18.2	18.3	18.7	19.1	19.6	20.0	20.4	20.7	20.9	21.0	21.0	20.8	20.4	19.8	18.8
30000	5000	400	14.8	14.6	14.7	15.0	15.4	15.9	16.3	16.7	17.1	17.4	17.7	17.9	18.0	18.0	17.8	17.6	17.1
30000	5000	500	12.8	12.8	13.0	13.4	13.8	14.2	14.6	15.0	15.4	15.7	16.0	16.2	16.4	16.5	16.4	16.3	16.1

APPENDIX D

TABLE OF EXPERIMENTAL DATA OF THE CO_2 TESTS

An example of the CO_2 data is presented here (Table D.1), however the complete database is provided in electronic form (file name: UO Heat Transfer Database) because of its large size.

Table D.1: A sample of the CO_2 heat transfer data.

d, m	z_h, m	P_{in}, kPa	G, kg/m^{2}s	q, kW/m^2	T_{in}, ˚C	T_{out}, ˚C	T_b, ˚C	H_b, kJ/kg	$T_{w,in}$, ˚C
0.008	0.053	6745.4	1962	201.1	8.4	26.3	9.4	220.2	28.6
0.008	0.103	6745.4	1962	201.1	8.4	26.3	10.4	222.7	28.5
0.008	0.153	6745.4	1962	201.1	8.4	26.3	11.4	225.3	28.2
0.008	0.203	6745.4	1962	201.1	8.4	26.3	12.3	227.9	28.7
0.008	0.253	6745.4	1962	201.1	8.4	26.3	13.3	230.4	29.0
0.008	0.303	6745.4	1962	201.1	8.4	26.3	14.2	233.0	28.4
0.008	0.353	6745.4	1962	201.1	8.4	26.3	15.1	235.6	28.4
0.008	0.403	6745.4	1962	201.1	8.4	26.3	16.0	238.1	27.9
0.008	0.453	6745.4	1962	201.1	8.4	26.3	16.8	240.7	28.0
0.008	0.503	6745.4	1962	201.1	8.4	26.3	17.6	243.2	28.4
0.008	0.553	6745.4	1962	201.1	8.4	26.3	18.5	245.8	28.6
0.008	0.603	6745.4	1962	201.1	8.4	26.3	19.2	248.4	28.2
0.008	0.653	6745.4	1962	201.1	8.4	26.3	20.0	250.9	28.2
0.008	0.703	6745.4	1962	201.1	8.4	26.3	20.7	253.5	28.3
0.008	0.753	6745.4	1962	201.1	8.4	26.3	21.4	256.1	27.4
0.008	0.803	6745.4	1962	201.1	8.4	26.3	22.1	258.6	28.4
0.008	0.853	6745.4	1962	201.1	8.4	26.3	22.8	261.2	28.3
0.008	0.903	6745.4	1962	201.1	8.4	26.3	23.4	263.7	28.1
0.008	0.953	6745.4	1962	201.1	8.4	26.3	24.0	266.3	28.1
0.008	1.034	6745.4	1962	201.1	8.4	26.3	24.8	270.5	28.2
0.008	1.084	6745.4	1962	201.1	8.4	26.3	25.3	273.0	27.6
0.008	1.134	6745.4	1962	201.1	8.4	26.3	25.8	275.6	28.3
0.008	1.184	6745.4	1962	201.1	8.4	26.3	26.2	278.1	28.2
0.008	1.234	6745.4	1962	201.1	8.4	26.3	26.5	280.7	28.5
0.008	1.284	6745.4	1962	201.1	8.4	26.3	26.9	283.3	28.1
0.008	1.334	6745.4	1962	201.1	8.4	26.3	26.9	285.8	28.1

APPENDIX E

AN EXAMPLE OF APPLICATION OF THE MULTI-FLUID TABLE FOR THE PREDICTION OF THE HEAT TRANSFER COEFFICIENT IN CARBON DIOXIDE

Problem statement: estimate the HTC for CO_2 flowing vertically upward inside a uniformly heated tube (0.008 mm ID) at the conditions of Table 1 and 2. This is an experimental data point from the University of Ottawa CO_2 database for the 8 mm tube.

Table 1

P	G
Pa	kg/m^{2}s
8310×10^3	995

Table 2

T	˚C	K
T_b	12.4	285.6
T_w	26.3	299.4

Since the multi-fluid table provides HTC values at water conditions of the table, the flow conditions in CO_2 corresponding to the input parameters of the multi-fluid table namely P, G, T_b, T_w-T_b should be first scaled to water-equivalent conditions. Based on water equivalent values of pressure and bulk fluid temperature, then the corresponding water equivalent enthalpy will be estimated from NIST tables. It is noted that tube ID in the current problem and the reference tube ID for the multi-fluid table are the same.

Scaling starts with converting pressure and bulk fluid temperature to their water equivalent values, these two properties are also required for extraction of other thermo-physical properties in the two fluids: using the alternative scaling method described in Chapter 5. The water equivalent value of pressure is determined using

$$P_{\mathrm{H_2O}} = P_{c,\mathrm{H_2O}} \left(\frac{P}{P_c}\right)_{\mathrm{CO_2}} = 22064 \times 10^3 \, \frac{8310\times10^3}{7377\times10^3} = 24854.5 \times 10^3 \text{ Pa} \quad \text{(E1)}$$

Bulk fluid temperature T_b is scaled with pseudo-critical temperature: T_{pc} is estimated for the given carbon dioxide pressure of 8310×10^3 Pa based on the definition of the pseudo-critical temperature. Similarly, for the scaled water pressure resulted from Equation (E1), the pseudo-critical temperature in water is estimated, $T_{pc,\mathrm{CO_2}}$=309.5 K and $T_{pc,\mathrm{H_2O}}$= 657.5 K. The water equivalent bulk temperature $T_{b,\mathrm{H_2O}}$ is then calculated as

$$T_{b,\mathrm{H_2O}} = T_{pc,\mathrm{H_2O}} \left(\frac{T_b}{T_{pc}}\right)_{\mathrm{CO_2}} = 657.5 \frac{285.6}{309.5} = 606.7 \text{ K.} \tag{E2}$$

Similarly, the water equivalent wall temperature $T_{w,\mathrm{H_2O}}$ is calculated as

$$T_{w,\mathrm{H_2O}} = T_{pc,\mathrm{H_2O}} \left(\frac{T_w}{T_{pc}}\right)_{\mathrm{CO_2}} = 657.5 \frac{299.4}{309.5} = 636.2 \text{ K}, \tag{E3}$$

subtracting Equation (E2) from (E3) gives $(T_w - T_b)_{\mathrm{H_2O}} = 29.5$ K. Note that all temperatures in Kelvin.

Next, we evaluate three CO_2 properties at the given P and T_b: Prandtl number Pr_b evaluated at bulk fluid temperature, bulk fluid thermal conductivity k_b and bulk fluid viscosity μ_b from the NIST thermo-physical properties tables; they are presented in Table E3.

Table E3: Values of Pr_b, μ_b and k_b
at CO_2 pressure and temperature.

Pr_b –	μ_b Pa.s	k_b W/mK
2.18	8.9×10^{-5}	0.10

Similarly, based on the water equivalent values of P and T_b (Equations; E1, E2), find from NIST tables, for water, the corresponding values of Pr, μ_b, H_b and k_b (see Table 4). Next evaluate $G_{\mathrm{H_2O}}$ from

$$G_{H_2O} = \left(\frac{\mu_b}{d\mathrm{Pr}_b^{\gamma}}\right)_{H_2O}\left(\frac{Gd\mathrm{Pr}_b^{\gamma}}{\mu_b}\right)_{CO_2} = \left(\frac{7.9\times10^{-5}}{0.93^{0.66}}\right)\left(\frac{995\times2.18^{0.66}}{8.9\times10^{-5}}\right) = 1550\,\frac{\mathrm{kg}}{\mathrm{m^2 s}}\ , \quad \text{(E4)}$$

Note in the above equation $\gamma = 0.66$ for the supercritical region as determined in Chapter 5, Section 4.2 and d is canceled out.

Table E4: Values of water properties at the equivalent conditions.

Pr_b –	μ_b Pa.s	H_b J/kg	k_b W/mK
0.93	7.9×10^{-5}	1518×10^{3}	0.52

Now, all input parameters of the multi-fluid table in terms of water equivalent conditions were identified, since the multi-fluid table uses the kPa for the pressure and the kJ/kg for the enthalpy, the reported values should be converted into these units. Thus, the multi-fluid table input parameters are

P = 24854.5 kPa

G = 1550 kg/m2s

$T_w - T_b$ = 29.5 K

H_b = 1518 kJ/kg (corresponds to T_b = 606.7 K)

Since the tube diameter is identical to the multi-fluid table reference diameter, there is no need for the application of the diameter correction factor. To find the multi-fluid table value at these parameters, linear interpolation was performed and the value of HTC from the multi-fluid table h_{Table} = 19.4 kW/m^{2}K. Finally, the water equivalent value of h is scaled to the CO_2 conditions using

$$h_{CO_2} = \left(\frac{k_b}{d}\right)_{CO_2}\left(\frac{h\,d}{k_b}\right)_{H_2O} = 0.1\left(\frac{19.4\times10^{3}}{0.52}\right)_{H_2O} = 3.7\times10^{3}\ \frac{\mathrm{W}}{\mathrm{m^2K}} \quad \text{(E5)}$$

Note the measured h_{CO_2} = 3.6×10^{3} W/m^{2}K.

APPENDIX F

TABULATED HEAT TRANSFER COEFFICIENTS OF THE MULTI-FLUID TRANS-CRITICAL HEAT TRANSFER LOOK-UP TABLE

Guidelines for using the multi-fluid trans-critical heat transfer look-up table

The table is designed for vertical upward flow inside an 8 mm ID heated tubes at constant heat flux. The first three columns list respectively table grid points of pressure in kPa, mass flux in kg/m^{2}s and wall temperature difference in K. Multi-fluid table grid points of specific fluid enthalpy (H_b in kJ/kg) are listed horizontally under the heading H_b starting with the value of 1000 to 3000 kJ/kg. These headings are repeated on each page of the LUT.

Multi-fluid TC LUT heat transfer coefficients: numbers bounded by the third column from left and the second row from top in each page, correspond to the heat transfer coefficients h_{ref} in kW/m^{2}K for a reference tube diameter of 8 mm; for a different diameter use the correction factor:

$$h = h_{ref}\left(\frac{d}{d_{ref}}\right)^{-0.2}.$$

Colour code: HTCs of the multi-fluid TC LUT are marked with different colours indicating different uncertainty levels. Blue corresponds to water data-based regions with the highest prediction accuracy, yellow to regions which are based on scaled water data from CO_2 with slightly lower accuracy and the blank to regions from selected correlations with the least accuracy.

P	G	ΔT_w	H_b, kJ/kg																
kPa	Kg/m^{2}s	K	1000	1400	1600	1800	1900	2000	2050	2100	2150	2200	2250	2300	2400	2500	2600	2700	3000
19000	100	10	2.14	1.67	1.27	0.95	0.74	0.63	0.6	0.61	0.63	0.67	0.72	0.79	0.88	0.97	1.05	1.06	0.97
19000	100	20	2.03	1.57	1.19	0.89	0.69	0.59	0.56	0.57	0.59	0.63	0.68	0.74	0.83	0.93	1	1.02	0.95
19000	100	50	1.8	1.39	1.05	0.78	0.61	0.53	0.51	0.51	0.53	0.56	0.6	0.67	0.75	0.84	0.92	0.95	0.89
19000	100	100	1.44	1.14	0.88	0.68	0.54	0.47	0.45	0.45	0.47	0.49	0.53	0.58	0.66	0.75	0.82	0.86	0.82
19000	100	200	1.08	0.93	0.76	0.6	0.48	0.42	0.4	0.41	0.42	0.44	0.47	0.52	0.59	0.67	0.74	0.78	0.76
19000	100	300	0.91	0.83	0.7	0.57	0.45	0.39	0.37	0.37	0.38	0.4	0.43	0.47	0.54	0.62	0.69	0.74	0.72
19000	100	400	0.87	0.82	0.69	0.56	0.44	0.38	0.35	0.35	0.36	0.38	0.4	0.45	0.51	0.59	0.67	0.71	0.7
19000	100	500	0.87	0.81	0.69	0.55	0.44	0.37	0.34	0.34	0.35	0.37	0.39	0.44	0.5	0.58	0.65	0.7	0.68
19000	200	10	4.12	3.28	2.54	1.97	1.63	1.51	1.53	1.61	1.7	1.81	1.93	2.06	2.22	2.35	2.41	2.33	2.01
19000	200	20	3.88	3.07	2.37	1.83	1.52	1.42	1.45	1.52	1.61	1.7	1.81	1.95	2.1	2.24	2.31	2.23	1.94
19000	200	50	3.37	2.65	2.04	1.6	1.35	1.28	1.31	1.37	1.44	1.53	1.62	1.74	1.87	1.98	2.03	1.97	1.75
19000	200	100	2.6	2.09	1.66	1.34	1.16	1.12	1.15	1.2	1.26	1.32	1.41	1.49	1.57	1.63	1.65	1.62	1.52
19000	200	200	1.84	1.59	1.34	1.13	1	0.97	0.98	1.02	1.06	1.11	1.17	1.23	1.29	1.34	1.36	1.36	1.32
19000	200	300	1.46	1.35	1.18	1.01	0.89	0.84	0.84	0.86	0.88	0.92	0.97	1.03	1.1	1.18	1.23	1.26	1.25
19000	200	400	1.38	1.3	1.13	0.95	0.82	0.75	0.73	0.74	0.77	0.8	0.85	0.92	1.01	1.12	1.21	1.26	1.24
19000	200	500	1.37	1.3	1.13	0.94	0.79	0.71	0.68	0.69	0.72	0.75	0.8	0.87	0.98	1.1	1.2	1.26	1.24
19000	400	10	6.85	5.52	4.45	3.59	2.95	2.7	2.76	2.92	3.12	3.35	3.6	3.88	4.14	4.32	4.34	4.14	3.62
19000	400	20	6.44	5.19	4.15	3.33	2.75	2.54	2.59	2.75	2.93	3.14	3.39	3.67	3.95	4.15	4.19	4	3.5
19000	400	50	5.58	4.48	3.53	2.8	2.36	2.23	2.29	2.42	2.57	2.75	2.96	3.21	3.46	3.63	3.67	3.52	3.12
19000	400	100	4.32	3.5	2.78	2.25	1.95	1.87	1.92	2.02	2.13	2.26	2.41	2.59	2.76	2.89	2.93	2.87	2.67
19000	400	200	3.01	2.59	2.17	1.82	1.62	1.55	1.57	1.63	1.7	1.79	1.9	2.03	2.17	2.28	2.36	2.37	2.32
19000	400	300	2.31	2.13	1.86	1.6	1.41	1.32	1.32	1.35	1.4	1.47	1.56	1.68	1.84	2	2.12	2.18	2.16
19000	400	400	2.14	2.02	1.77	1.5	1.3	1.19	1.17	1.2	1.24	1.3	1.4	1.53	1.71	1.91	2.07	2.16	2.12
19000	400	500	2.12	2	1.76	1.47	1.25	1.14	1.11	1.14	1.18	1.25	1.34	1.48	1.67	1.89	2.07	2.16	2.1
19000	700	10	10.8	8.86	7.81	6.84	5.45	4.68	4.64	4.86	5.2	5.62	6.11	6.61	7	7.16	7.02	6.55	5.68
19000	700	20	10.1	8.37	7.26	6.23	5	4.36	4.34	4.56	4.88	5.29	5.79	6.31	6.73	6.93	6.81	6.36	5.52
19000	700	50	8.65	7.23	5.95	4.86	4.07	3.75	3.79	3.99	4.26	4.62	5.07	5.56	5.98	6.18	6.1	5.73	5.04
19000	700	100	6.61	5.49	4.46	3.65	3.17	3.01	3.06	3.2	3.4	3.66	3.99	4.38	4.73	4.94	4.96	4.79	4.38
19000	700	200	4.56	3.96	3.35	2.83	2.49	2.36	2.36	2.44	2.57	2.74	2.97	3.26	3.56	3.81	3.97	3.98	3.81
19000	700	300	3.49	3.23	2.83	2.42	2.11	1.96	1.93	1.97	2.05	2.18	2.36	2.62	2.93	3.25	3.49	3.58	3.48
19000	700	400	3.2	3.03	2.67	2.26	1.94	1.78	1.74	1.77	1.84	1.96	2.14	2.39	2.72	3.06	3.33	3.45	3.34
19000	700	500	3.16	3	2.63	2.22	1.89	1.72	1.68	1.71	1.79	1.91	2.08	2.33	2.66	3.02	3.3	3.42	3.29
19000	1000	10	14.8	12.9	11.8	10.5	8.57	7.47	7.38	7.73	8.29	9.02	9.87	10.7	11.3	11.4	11	10.1	8.52
19000	1000	20	13.8	12.2	11	9.59	7.85	6.95	6.92	7.28	7.83	8.55	9.42	10.3	10.9	11.1	10.8	9.87	8.39
19000	1000	50	11.8	10.5	8.94	7.43	6.33	5.91	6	6.34	6.84	7.51	8.36	9.23	9.87	10.1	9.8	9.04	7.76
19000	1000	100	9.11	7.78	6.5	5.44	4.82	4.63	4.72	4.98	5.36	5.89	6.57	7.32	7.91	8.19	8.1	7.63	6.71
19000	1000	200	6.43	5.63	4.82	4.12	3.67	3.49	3.51	3.65	3.89	4.24	4.71	5.28	5.83	6.26	6.43	6.3	5.75
19000	1000	300	4.97	4.61	4.05	3.47	3.04	2.82	2.79	2.86	3.02	3.27	3.62	4.09	4.64	5.14	5.47	5.52	5.17
19000	1000	400	4.54	4.3	3.79	3.23	2.79	2.56	2.51	2.58	2.72	2.94	3.24	3.67	4.18	4.7	5.07	5.17	4.88
19000	1000	500	4.45	4.22	3.72	3.15	2.7	2.47	2.44	2.51	2.66	2.86	3.15	3.55	4.05	4.57	4.95	5.06	4.78
19000	1500	10	19.5	17.9	16.6	14.9	12.5	11.3	11.5	12.3	13.2	14.4	15.6	16.8	17.4	17.3	16.4	14.8	12.2
19000	1500	20	18.1	16.9	15.6	13.7	11.5	10.5	10.8	11.5	12.5	13.6	14.8	16	16.8	16.8	16.1	14.6	12.2
19000	1500	50	15.5	14.5	12.8	10.8	9.28	8.91	9.3	10	10.9	11.9	13.1	14.3	15.1	15.4	14.9	13.6	11.5
19000	1500	100	11.8	10.5	9.01	7.72	7.01	6.95	7.29	7.83	8.52	9.39	10.4	11.5	12.4	12.8	12.7	11.8	10.1
19000	1500	200	8.5	7.63	6.66	5.82	5.33	5.22	5.39	5.73	6.21	6.84	7.64	8.56	9.43	10	10.2	9.81	8.6
19000	1500	300	6.78	6.36	5.65	4.92	4.42	4.22	4.28	4.5	4.85	5.32	5.95	6.71	7.53	8.23	8.6	8.45	7.6
19000	1500	400	6.26	5.95	5.28	4.56	4.03	3.8	3.83	4.02	4.32	4.72	5.23	5.89	6.63	7.32	7.75	7.73	7.07

P kPa	G Kg/m^2s	ΔT_w K	H_b, kJ/kg																
			1000	1400	1600	1800	1900	2000	2050	2100	2150	2200	2250	2300	2400	2500	2600	2700	3000
19000	1500	500	6.13	5.83	5.16	4.43	3.88	3.65	3.67	3.86	4.14	4.51	4.99	5.59	6.29	6.97	7.42	7.45	6.85
19000	2000	10	26.1	23.7	21.6	19.2	16.2	15.1	15.9	17.2	18.6	20.1	21.5	22.7	23.2	23	21.7	19.3	15.4
19000	2000	20	24.2	22.4	20.3	17.7	15	14.2	15	16.2	17.7	19.1	20.6	21.9	22.6	22.5	21.4	19	15.2
19000	2000	50	20.6	19.3	17	14.4	12.5	12.3	13.1	14.3	15.6	17	18.4	19.8	20.7	20.8	20	18	14.6
19000	2000	100	15.8	14	12.1	10.5	9.71	9.85	10.5	11.5	12.5	13.7	15	16.3	17.4	17.8	17.4	16	13.3
19000	2000	200	11.4	10.3	9.04	8.03	7.55	7.62	8.09	8.75	9.55	10.5	11.5	12.7	13.7	14.4	14.4	13.6	11.7
19000	2000	300	9.16	8.6	7.69	6.82	6.3	6.25	6.55	7.05	7.67	8.4	9.24	10.2	11.2	11.9	12.3	11.9	10.5
19000	2000	400	8.41	8	7.16	6.27	5.69	5.56	5.77	6.18	6.69	7.3	8.01	8.85	9.77	10.6	11	10.8	9.76
19000	2000	500	8.21	7.82	6.97	6.05	5.44	5.26	5.43	5.8	6.27	6.83	7.49	8.29	9.18	10	10.5	10.4	9.42
19000	3000	10	37.1	33.7	29.1	23.8	19.9	19	20	21.8	23.7	25.7	27.6	29.2	30.2	30.1	28.8	25.7	20.5
19000	3000	20	34.3	31.2	26.9	22.2	18.7	18	19	20.7	22.6	24.6	26.6	28.4	29.5	29.6	28.3	25.3	20.2
19000	3000	50	29.1	25.7	22.1	18.6	16.2	16	17	18.6	20.3	22.1	24	25.8	27.1	27.5	26.6	24	19.4
19000	3000	100	22.3	19.3	16.5	14.2	13.1	13.3	14.3	15.6	17	18.5	20.2	21.8	23.2	23.9	23.5	21.6	17.9
19000	3000	200	16	14.4	12.6	11.2	10.6	10.8	11.6	12.6	13.8	15	16.3	17.7	19	19.8	19.9	18.7	16
19000	3000	300	12.7	11.9	10.7	9.59	9.02	9.12	9.71	10.5	11.5	12.5	13.6	14.8	16	16.9	17.2	16.6	14.6
19000	3000	400	11.7	11.1	9.95	8.81	8.15	8.11	8.54	9.22	10	10.9	11.9	13	14.2	15.2	15.7	15.3	13.8
19000	3000	500	11.4	10.8	9.66	8.49	7.75	7.63	7.99	8.6	9.34	10.2	11.1	12.2	13.4	14.4	15	14.7	13.4
19000	5000	10	51.6	47.7	40.2	30.6	23.6	21.4	22.1	23.9	26	28.5	31.1	33.7	35.5	36.2	35.2	32.6	27.7
19000	5000	20	47.8	43.8	36.6	28.1	22.1	20.3	21.1	22.7	24.8	27.2	30	32.6	34.5	35.2	34.3	31.7	27
19000	5000	50	40.4	34.7	28.3	22.5	19	18.3	19.2	20.7	22.5	24.6	27	29.5	31.4	32.3	31.8	29.7	25.6
19000	5000	100	30.7	26.1	21.5	17.9	16	15.8	16.7	18.1	19.6	21.3	23.2	25.3	27.2	28.4	28.4	27	23.7
19000	5000	200	22.1	19.7	17	14.7	13.5	13.5	14.3	15.4	16.7	18.1	19.8	21.6	23.4	24.8	25.2	24.3	21.8
19000	5000	300	17.6	16.4	14.6	12.9	12	11.9	12.6	13.6	14.7	16	17.5	19.2	20.9	22.3	22.9	22.4	20.3
19000	5000	400	16.1	15.2	13.6	12	11.1	11	11.6	12.5	13.6	14.8	16.2	17.8	19.5	20.9	21.6	21.2	19.4
19000	5000	500	15.6	14.8	13.3	11.7	10.8	10.7	11.2	12	13.1	14.3	15.6	17.2	18.9	20.3	21	20.6	18.9
20000	100	10	2.14	1.76	1.39	1.08	0.87	0.77	0.75	0.77	0.83	0.9	0.98	1.06	1.13	1.18	1.19	1.12	0.93
20000	100	20	1.98	1.61	1.26	0.97	0.77	0.68	0.66	0.68	0.73	0.79	0.87	0.94	1.02	1.09	1.11	1.06	0.89
20000	100	50	1.67	1.33	1.03	0.78	0.62	0.55	0.54	0.55	0.59	0.64	0.7	0.78	0.86	0.94	0.98	0.96	0.83
20000	100	100	1.25	1.01	0.79	0.62	0.5	0.45	0.44	0.45	0.48	0.52	0.57	0.63	0.71	0.79	0.84	0.84	0.75
20000	100	200	0.89	0.77	0.64	0.52	0.43	0.38	0.37	0.38	0.4	0.43	0.47	0.53	0.6	0.68	0.73	0.74	0.68
20000	100	300	0.73	0.67	0.58	0.48	0.39	0.34	0.33	0.34	0.36	0.38	0.42	0.47	0.53	0.61	0.66	0.68	0.63
20000	100	400	0.69	0.65	0.57	0.46	0.38	0.33	0.31	0.32	0.33	0.35	0.39	0.43	0.5	0.57	0.63	0.64	0.59
20000	100	500	0.69	0.65	0.57	0.46	0.37	0.32	0.3	0.31	0.32	0.34	0.37	0.42	0.48	0.55	0.61	0.63	0.57
20000	200	10	4.21	3.54	2.85	2.26	1.88	1.74	1.76	1.87	2.02	2.2	2.38	2.54	2.67	2.74	2.69	2.46	1.95
20000	200	20	3.89	3.23	2.57	2.02	1.68	1.55	1.57	1.66	1.8	1.95	2.12	2.28	2.43	2.52	2.5	2.32	1.88
20000	200	50	3.22	2.63	2.08	1.63	1.36	1.27	1.3	1.38	1.48	1.6	1.74	1.89	2.03	2.13	2.13	2.01	1.7
20000	200	100	2.35	1.93	1.55	1.26	1.09	1.04	1.07	1.13	1.21	1.3	1.41	1.53	1.63	1.7	1.71	1.64	1.48
20000	200	200	1.56	1.37	1.17	1	0.89	0.86	0.88	0.92	0.98	1.05	1.13	1.22	1.3	1.36	1.38	1.36	1.28
20000	200	300	1.19	1.11	0.99	0.86	0.77	0.73	0.74	0.77	0.81	0.86	0.92	1	1.09	1.17	1.22	1.23	1.18
20000	200	400	1.11	1.05	0.94	0.8	0.7	0.65	0.65	0.67	0.7	0.74	0.81	0.89	0.99	1.09	1.16	1.18	1.12
20000	200	500	1.1	1.05	0.92	0.78	0.67	0.61	0.6	0.62	0.65	0.7	0.76	0.84	0.94	1.05	1.14	1.16	1.09
20000	400	10	7.18	6.17	5.17	4.25	3.5	3.16	3.19	3.4	3.7	4.07	4.47	4.81	5.03	5.05	4.85	4.38	3.56
20000	400	20	6.63	5.67	4.7	3.81	3.11	2.81	2.83	3.02	3.29	3.62	3.99	4.34	4.59	4.68	4.56	4.16	3.42
20000	400	50	5.52	4.63	3.74	2.97	2.47	2.27	2.31	2.46	2.66	2.92	3.22	3.53	3.79	3.93	3.89	3.62	3.06
20000	400	100	4.02	3.33	2.69	2.17	1.87	1.77	1.82	1.93	2.08	2.25	2.47	2.7	2.91	3.05	3.06	2.93	2.62
20000	400	200	2.61	2.27	1.92	1.63	1.46	1.41	1.44	1.51	1.61	1.73	1.88	2.05	2.23	2.36	2.42	2.4	2.27
20000	400	300	1.91	1.78	1.58	1.38	1.24	1.18	1.19	1.23	1.31	1.4	1.52	1.67	1.85	2.01	2.12	2.14	2.06
20000	400	400	1.73	1.65	1.48	1.28	1.13	1.05	1.05	1.09	1.15	1.23	1.35	1.5	1.69	1.88	2.02	2.05	1.95

P	G	ΔT_w	H_b, kJ/kg																
kPa	Kg/m^{2}s	K	1000	1400	1600	1800	1900	2000	2050	2100	2150	2200	2250	2300	2400	2500	2600	2700	3000
20000	400	500	1.7	1.63	1.45	1.24	1.08	1	0.99	1.03	1.09	1.17	1.29	1.44	1.63	1.83	1.98	2.02	1.89
20000	700	10	11.4	9.98	9.04	7.98	6.41	5.45	5.31	5.58	6.08	6.78	7.57	8.26	8.6	8.48	7.93	7	5.62
20000	700	20	10.5	9.29	8.28	7.14	5.71	4.88	4.76	5	5.44	6.08	6.84	7.54	7.96	7.96	7.53	6.71	5.45
20000	700	50	8.66	7.64	6.47	5.3	4.36	3.9	3.87	4.06	4.41	4.91	5.53	6.17	6.64	6.78	6.55	5.96	4.97
20000	700	100	6.19	5.31	4.4	3.61	3.1	2.9	2.93	3.08	3.33	3.67	4.1	4.58	4.99	5.22	5.19	4.89	4.3
20000	700	200	3.96	3.5	3	2.56	2.27	2.16	2.19	2.29	2.45	2.67	2.96	3.3	3.65	3.92	4.04	3.97	3.69
20000	700	300	2.88	2.7	2.41	2.1	1.87	1.76	1.76	1.83	1.94	2.11	2.33	2.62	2.95	3.26	3.46	3.48	3.29
20000	700	400	2.59	2.49	2.23	1.94	1.7	1.58	1.57	1.63	1.73	1.88	2.08	2.36	2.69	3.01	3.23	3.27	3.07
20000	700	500	2.54	2.44	2.19	1.88	1.64	1.52	1.51	1.57	1.67	1.81	2.01	2.27	2.6	2.93	3.15	3.2	2.97
20000	1000	10	15.7	14	13	11.9	9.91	8.55	8.27	8.62	9.41	10.6	12	13.2	13.7	13.5	12.5	10.8	8.48
20000	1000	20	14.4	13.2	12	10.7	8.84	7.69	7.47	7.79	8.5	9.58	10.9	12.2	12.9	12.8	12	10.6	8.43
20000	1000	50	11.9	11	9.58	7.97	6.73	6.12	6.07	6.37	6.95	7.84	8.99	10.1	10.9	11.1	10.6	9.51	7.82
20000	1000	100	8.5	7.52	6.41	5.37	4.7	4.44	4.49	4.74	5.17	5.8	6.63	7.5	8.19	8.5	8.37	7.78	6.67
20000	1000	200	5.55	4.96	4.31	3.74	3.35	3.2	3.23	3.4	3.68	4.08	4.61	5.23	5.83	6.26	6.4	6.19	5.52
20000	1000	300	4.1	3.86	3.45	3.02	2.7	2.55	2.54	2.65	2.85	3.14	3.53	4.02	4.57	5.05	5.32	5.27	4.8
20000	1000	400	3.67	3.53	3.18	2.77	2.45	2.29	2.28	2.37	2.55	2.8	3.13	3.56	4.07	4.55	4.85	4.85	4.44
20000	1000	500	3.58	3.45	3.1	2.69	2.36	2.2	2.19	2.29	2.46	2.7	3.01	3.42	3.91	4.38	4.68	4.69	4.29
20000	1500	10	20.7	19.1	18	16.4	14	12.5	12.4	13.1	14.4	16.2	18.3	20.1	20.8	20.2	18.5	15.8	12.2
20000	1500	20	18.9	17.9	16.8	15	12.5	11.1	11.1	11.8	13	14.6	16.6	18.4	19.4	19.2	17.9	15.7	12.5
20000	1500	50	15.4	15	13.7	11.8	9.78	8.89	9.02	9.66	10.6	12	13.7	15.4	16.5	16.7	16	14.4	11.9
20000	1500	100	11	10.1	8.88	7.66	6.77	6.51	6.75	7.27	8.01	9.01	10.3	11.6	12.7	13.1	13	12	10.2
20000	1500	200	7.36	6.7	5.93	5.24	4.81	4.72	4.9	5.25	5.75	6.43	7.3	8.28	9.2	9.83	9.97	9.49	8.17
20000	1500	300	5.61	5.31	4.8	4.26	3.89	3.77	3.86	4.1	4.48	4.98	5.62	6.39	7.19	7.85	8.14	7.89	6.92
20000	1500	400	5.07	4.88	4.42	3.9	3.52	3.37	3.43	3.64	3.96	4.39	4.92	5.56	6.28	6.91	7.25	7.11	6.33
20000	1500	500	4.93	4.76	4.3	3.77	3.37	3.22	3.28	3.48	3.78	4.17	4.66	5.26	5.93	6.54	6.89	6.8	6.08
20000	2000	10	27.5	25.5	23.6	21.3	18	16.4	16.8	18.1	19.9	22	24.2	25.9	26.6	26	24	20.5	15.3
20000	2000	20	25	23.8	22.2	19.6	16.2	14.7	15.1	16.4	18	20.1	22.3	24.3	25.4	25.2	23.5	20.4	15.3
20000	2000	50	20.3	20	18.6	16	13.1	12	12.5	13.6	15	16.8	18.8	20.7	22.1	22.3	21.3	18.9	14.9
20000	2000	100	14.6	13.5	12	10.4	9.31	9.12	9.65	10.5	11.6	12.9	14.5	16.2	17.5	18.1	17.7	16.2	13.2
20000	2000	200	9.93	9.04	8.04	7.2	6.76	6.82	7.24	7.87	8.67	9.64	10.8	12	13.2	13.9	14	13.1	11
20000	2000	300	7.59	7.19	6.53	5.88	5.51	5.51	5.8	6.29	6.91	7.66	8.53	9.51	10.5	11.2	11.5	11	9.51
20000	2000	400	6.82	6.58	5.99	5.35	4.94	4.87	5.09	5.49	6.01	6.64	7.37	8.21	9.1	9.86	10.2	9.91	8.71
20000	2000	500	6.62	6.39	5.81	5.15	4.7	4.6	4.78	5.15	5.63	6.2	6.88	7.67	8.53	9.29	9.67	9.44	8.35
20000	3000	10	38.9	36.5	33.4	29.1	23.6	21.1	21.8	23.7	26.2	29	31.8	34.1	35.1	34.5	32.1	27.7	20.7
20000	3000	20	35.4	33.7	31.1	26.8	21.4	19.1	19.7	21.4	23.8	26.6	29.6	32.3	33.8	33.6	31.5	27.3	20.6
20000	3000	50	28.8	27.4	25.4	21.8	17.5	15.9	16.5	18	20	22.3	25.1	27.8	29.6	30	28.6	25.4	19.8
20000	3000	100	20.7	18.8	16.6	14.4	12.7	12.4	13.2	14.4	15.9	17.6	19.7	21.9	23.8	24.7	24.1	21.9	17.8
20000	3000	200	13.9	12.7	11.3	10.1	9.51	9.66	10.3	11.3	12.5	13.8	15.3	16.9	18.4	19.4	19.4	18.1	15.2
20000	3000	300	10.6	10	9.14	8.29	7.87	8	8.54	9.32	10.2	11.3	12.5	13.7	15	16	16.2	15.5	13.4
20000	3000	400	9.5	9.13	8.34	7.53	7.06	7.08	7.49	8.14	8.93	9.83	10.8	12	13.2	14.2	14.6	14.1	12.4
20000	3000	500	9.19	8.85	8.07	7.23	6.7	6.65	7	7.59	8.32	9.17	10.1	11.2	12.4	13.4	13.9	13.5	12
20000	5000	10	53.9	51.6	46.8	39.1	29.7	25.5	26.1	28.4	31.6	35.5	39.5	43	44.8	44.4	41.5	36.4	28.7
20000	5000	20	49.4	47	42.2	34.9	26.5	22.9	23.4	25.5	28.5	32.3	36.7	40.7	42.9	42.7	40	35.1	27.8
20000	5000	50	40.2	36.4	30.8	24.8	20.3	18.8	19.6	21.4	23.7	26.8	30.6	34.4	36.8	37.3	35.7	31.9	25.9
20000	5000	100	28.6	25.3	21.2	17.5	15.4	15.1	16	17.4	19.1	21.3	24	26.8	29.2	30.5	30.1	27.8	23.4
20000	5000	200	19.4	17.5	15.3	13.3	12.3	12.3	13	14.2	15.6	17.2	19.1	21.2	23.3	24.9	25.2	24	21
20000	5000	300	14.8	13.9	12.5	11.3	10.6	10.6	11.2	12.2	13.4	14.8	16.4	18.2	20	21.5	22	21.4	19.1
20000	5000	400	13.2	12.6	11.5	10.4	9.71	9.71	10.3	11.1	12.2	13.5	15	16.6	18.4	19.8	20.4	19.9	17.9

P	G	ΔT_w	H_b, kJ/kg																
kPa	Kg/m^2s	K	1000	1400	1600	1800	1900	2000	2050	2100	2150	2200	2250	2300	2400	2500	2600	2700	3000
20000	5000	500	12.8	12.2	11.1	10	9.36	9.33	9.85	10.7	11.7	13	14.4	16	17.6	19	19.6	19.1	17.2
21000	100	10	2.11	1.87	1.61	1.39	1.25	1.19	1.21	1.28	1.38	1.51	1.61	1.66	1.64	1.56	1.43	1.21	0.89
21000	100	20	1.89	1.64	1.38	1.17	1.02	0.97	0.98	1.04	1.13	1.25	1.34	1.4	1.42	1.38	1.29	1.13	0.86
21000	100	50	1.47	1.23	1	0.82	0.72	0.68	0.69	0.74	0.81	0.9	0.98	1.05	1.1	1.11	1.08	0.98	0.79
21000	100	100	0.97	0.8	0.66	0.55	0.49	0.47	0.48	0.51	0.57	0.63	0.7	0.77	0.83	0.87	0.87	0.82	0.7
21000	100	200	0.6	0.53	0.46	0.4	0.36	0.35	0.36	0.39	0.43	0.48	0.53	0.59	0.65	0.69	0.71	0.69	0.61
21000	100	300	0.44	0.42	0.38	0.34	0.3	0.29	0.3	0.32	0.35	0.39	0.44	0.49	0.54	0.59	0.61	0.61	0.55
21000	100	400	0.4	0.39	0.35	0.31	0.28	0.26	0.27	0.28	0.31	0.35	0.39	0.43	0.48	0.53	0.56	0.56	0.51
21000	100	500	0.39	0.38	0.35	0.3	0.27	0.25	0.25	0.27	0.3	0.33	0.36	0.41	0.45	0.5	0.53	0.53	0.48
21000	200	10	4.22	3.81	3.35	2.93	2.64	2.54	2.6	2.78	3.04	3.32	3.56	3.66	3.62	3.44	3.13	2.64	1.9
21000	200	20	3.77	3.34	2.86	2.44	2.16	2.07	2.12	2.27	2.49	2.75	2.97	3.11	3.14	3.05	2.83	2.44	1.82
21000	200	50	2.92	2.5	2.08	1.73	1.52	1.46	1.51	1.62	1.79	1.99	2.19	2.34	2.43	2.43	2.32	2.08	1.65
21000	200	100	1.93	1.63	1.36	1.15	1.04	1.02	1.07	1.16	1.28	1.43	1.58	1.71	1.81	1.85	1.81	1.68	1.44
21000	200	200	1.14	1.01	0.9	0.8	0.76	0.76	0.8	0.86	0.95	1.06	1.17	1.28	1.37	1.42	1.42	1.37	1.25
21000	200	300	0.77	0.74	0.69	0.64	0.61	0.61	0.64	0.69	0.76	0.84	0.93	1.02	1.11	1.17	1.2	1.18	1.11
21000	200	400	0.67	0.66	0.62	0.57	0.54	0.53	0.55	0.59	0.65	0.72	0.8	0.88	0.97	1.05	1.09	1.09	1.03
21000	200	500	0.64	0.64	0.6	0.54	0.51	0.5	0.52	0.55	0.6	0.67	0.75	0.83	0.91	0.99	1.04	1.04	0.98
21000	400	10	7.41	6.84	6.18	5.5	4.91	4.61	4.66	4.95	5.44	6.03	6.57	6.87	6.8	6.4	5.72	4.78	3.46
21000	400	20	6.65	6.03	5.33	4.63	4.06	3.78	3.81	4.06	4.48	5.01	5.53	5.87	5.94	5.71	5.22	4.45	3.31
21000	400	50	5.2	4.58	3.91	3.29	2.85	2.67	2.71	2.9	3.21	3.61	4.03	4.37	4.55	4.53	4.28	3.79	2.98
21000	400	100	3.46	2.95	2.48	2.09	1.87	1.81	1.88	2.03	2.25	2.53	2.82	3.09	3.29	3.37	3.29	3.04	2.59
21000	400	200	1.99	1.76	1.55	1.38	1.3	1.3	1.36	1.47	1.63	1.82	2.03	2.24	2.41	2.52	2.54	2.44	2.23
21000	400	300	1.27	1.23	1.15	1.07	1.03	1.03	1.08	1.16	1.28	1.43	1.59	1.76	1.93	2.05	2.12	2.09	1.97
21000	400	400	1.07	1.06	1.01	0.94	0.9	0.9	0.94	1.01	1.11	1.24	1.38	1.54	1.7	1.84	1.92	1.92	1.81
21000	400	500	1.02	1.02	0.96	0.89	0.85	0.84	0.88	0.95	1.04	1.16	1.3	1.45	1.6	1.75	1.83	1.84	1.72
21000	700	10	11.9	10.7	10	9.35	8.37	7.64	7.5	7.86	8.64	9.75	10.9	11.6	11.6	10.7	9.4	7.67	5.51
21000	700	20	10.8	9.68	8.86	8.07	7.11	6.44	6.29	6.57	7.23	8.21	9.28	10.1	10.2	9.73	8.71	7.26	5.33
21000	700	50	8.47	7.71	6.8	5.86	5.07	4.62	4.54	4.77	5.25	5.98	6.82	7.54	7.91	7.81	7.27	6.31	4.89
21000	700	100	5.53	4.89	4.21	3.6	3.19	3.02	3.06	3.26	3.61	4.09	4.65	5.19	5.58	5.72	5.55	5.08	4.25
21000	700	200	3.13	2.81	2.5	2.23	2.08	2.05	2.13	2.29	2.53	2.85	3.22	3.59	3.92	4.13	4.17	4	3.6
21000	700	300	1.98	1.92	1.8	1.68	1.6	1.59	1.65	1.77	1.96	2.2	2.48	2.78	3.06	3.29	3.4	3.36	3.13
21000	700	400	1.63	1.63	1.56	1.46	1.39	1.38	1.44	1.55	1.71	1.92	2.16	2.42	2.69	2.92	3.06	3.04	2.85
21000	700	500	1.54	1.55	1.48	1.38	1.31	1.31	1.36	1.47	1.62	1.81	2.04	2.29	2.54	2.77	2.91	2.91	2.72
21000	1000	10	16.7	14.3	13.6	13.6	12.7	11.7	11.4	11.8	12.9	14.7	16.6	18	18	16.8	14.6	11.8	8.4
21000	1000	20	15	13.1	12.3	11.7	10.8	9.98	9.68	9.98	10.9	12.5	14.3	15.7	16.2	15.5	13.8	11.5	8.47
21000	1000	50	11.8	10.9	9.81	8.69	7.77	7.2	7.03	7.28	8	9.19	10.7	12	12.7	12.6	11.7	10.2	7.97
21000	1000	100	7.58	6.9	6.11	5.36	4.83	4.6	4.63	4.88	5.4	6.19	7.16	8.12	8.8	9.05	8.8	8.07	6.78
21000	1000	200	4.35	3.99	3.61	3.28	3.07	3.02	3.11	3.32	3.68	4.19	4.8	5.42	5.96	6.31	6.38	6.1	5.42
21000	1000	300	2.81	2.75	2.6	2.43	2.31	2.29	2.37	2.55	2.82	3.2	3.64	4.1	4.56	4.91	5.06	4.96	4.53
21000	1000	400	2.31	2.33	2.24	2.1	2.01	1.99	2.07	2.23	2.48	2.8	3.16	3.56	3.96	4.3	4.48	4.43	4.09
21000	1000	500	2.18	2.2	2.11	1.98	1.89	1.88	1.96	2.12	2.36	2.65	2.99	3.35	3.73	4.06	4.24	4.21	3.9
21000	1500	10	22.3	20.4	19.7	19.2	17.7	16.4	16.1	16.8	18.6	21.3	24.4	26.6	26.9	25	21.6	17.4	12.5
21000	1500	20	19.8	18.6	18	17	15.1	13.8	13.5	14.1	15.6	18	20.8	23.2	24	23	20.7	17.4	13.1
21000	1500	50	15.3	15	14.3	12.8	10.9	9.88	9.91	10.5	11.7	13.4	15.6	17.6	18.8	18.8	17.7	15.7	12.7
21000	1500	100	9.8	9.26	8.5	7.58	6.76	6.49	6.76	7.32	8.14	9.23	10.6	12.1	13.3	13.7	13.5	12.5	10.6
21000	1500	200	5.72	5.35	4.93	4.55	4.33	4.34	4.57	4.96	5.53	6.28	7.19	8.16	9	9.53	9.61	9.16	8.03
21000	1500	300	3.81	3.74	3.55	3.36	3.26	3.3	3.48	3.78	4.22	4.79	5.45	6.13	6.78	7.26	7.43	7.19	6.43
21000	1500	400	3.18	3.2	3.08	2.92	2.83	2.86	3.02	3.29	3.67	4.15	4.69	5.26	5.82	6.26	6.47	6.33	5.75

P kPa	G Kg/m^2s	ΔT_w K	H_b, kJ/kg																
			1000	1400	1600	1800	1900	2000	2050	2100	2150	2200	2250	2300	2400	2500	2600	2700	3000
21000	1500	500	3.01	3.04	2.92	2.77	2.67	2.69	2.84	3.1	3.46	3.9	4.39	4.91	5.43	5.86	6.08	5.98	5.47
21000	2000	10	28.9	27.6	26.9	25.5	22.8	21.1	21.2	22.7	25.1	28.3	31.5	33.5	33.6	31.6	28.1	23.1	16.3
21000	2000	20	25.6	25.2	24.6	22.7	19.5	17.7	17.9	19.3	21.4	24.3	27.4	30	30.9	29.9	27.2	22.9	16.5
21000	2000	50	19.6	19.9	19.5	17.4	14.4	13.2	14.1	15.7	17.2	18.9	21	23.3	24.8	24.9	23.4	20.5	15.9
21000	2000	100	12.7	12.2	11.5	10.3	9.19	9.13	10.2	11.5	12.6	13.5	14.8	16.6	18	18.6	18.1	16.5	13.6
21000	2000	200	7.54	7.12	6.62	6.19	5.99	6.15	6.69	7.41	8.23	9.15	10.3	11.5	12.6	13.2	13.2	12.3	10.5
21000	2000	300	5.09	4.99	4.78	4.58	4.52	4.67	5.01	5.51	6.17	6.98	7.87	8.77	9.59	10.2	10.3	9.88	8.71
21000	2000	400	4.28	4.31	4.16	3.98	3.92	4.03	4.32	4.75	5.32	5.99	6.73	7.48	8.2	8.76	8.98	8.73	7.87
21000	2000	500	4.05	4.1	3.96	3.77	3.68	3.77	4.03	4.43	4.95	5.57	6.25	6.95	7.63	8.18	8.43	8.25	7.5
21000	3000	10	40.1	39.8	39.3	36.7	31.3	28.5	29.1	31.5	35	39.3	43.2	45.6	45.5	42.8	38.2	31.4	22.1
21000	3000	20	35.9	36.3	35.8	32.6	26.8	23.9	24.4	26.6	29.7	33.6	37.9	41.3	42.3	40.8	36.8	30.7	21.8
21000	3000	50	27.7	28	27.4	24.3	19.7	17.8	19	21.3	23.4	25.8	29.1	32.4	34.3	34.1	31.8	27.5	20.9
21000	3000	100	17.9	17.3	16.1	14.3	12.8	12.5	13.7	15.8	17.3	18.7	20.6	23.1	25.1	25.8	24.9	22.4	18.1
21000	3000	200	10.6	10	9.35	8.74	8.47	8.71	9.48	10.6	11.8	13.1	14.7	16.4	17.9	18.7	18.6	17.3	14.8
21000	3000	300	7.15	7.03	6.75	6.5	6.48	6.76	7.31	8.08	9.06	10.2	11.5	12.7	13.8	14.6	14.8	14.2	12.6
21000	3000	400	6.02	6.04	5.86	5.66	5.62	5.84	6.31	6.97	7.81	8.79	9.84	10.9	11.9	12.7	12.9	12.6	11.4
21000	3000	500	5.69	5.74	5.56	5.35	5.28	5.46	5.87	6.48	7.25	8.17	9.14	10.1	11.1	11.8	12.2	11.9	10.9
21000	5000	10	56.1	56.3	54.8	49.6	41.3	37.7	39.1	42.6	47.6	53.4	59	62.6	62.6	58.7	51.7	42.1	29.7
21000	5000	20	50.7	51	48.7	43.2	35.3	32	33.1	36.1	40.1	45.7	52.1	56.9	58.2	55.3	49.1	40.2	28.5
21000	5000	50	39.3	38	34	29	25.1	24.5	26.2	28.5	30.5	34.3	39.6	44.3	46.6	45.6	41.6	35.1	26.2
21000	5000	100	25.1	23.5	20.6	17.9	16.7	17.4	19.3	20.9	21.9	24.2	27.6	30.9	33.2	33.9	32.5	29	23.3
21000	5000	200	14.8	13.9	12.7	11.7	11.4	11.9	13	14.3	15.7	17.6	19.8	22	24	25.2	25.1	23.6	20.4
21000	5000	300	10.1	9.88	9.43	9.05	8.98	9.34	10.1	11.1	12.5	14.2	15.9	17.7	19.3	20.4	20.8	20.1	18.2
21000	5000	400	8.54	8.5	8.25	7.99	7.96	8.28	8.92	9.85	11.1	12.5	14	15.6	17	18.1	18.6	18.1	16.7
21000	5000	500	8.04	8.05	7.82	7.58	7.54	7.83	8.44	9.31	10.4	11.8	13.2	14.7	16	17.1	17.6	17.2	15.9
22000	100	10	1.99	1.92	1.9	1.93	1.98	2.05	2.12	2.21	2.32	2.42	2.46	2.38	2.18	1.92	1.62	1.29	0.89
22000	100	20	1.76	1.65	1.59	1.56	1.58	1.62	1.68	1.76	1.86	1.96	2.01	1.97	1.85	1.66	1.44	1.18	0.85
22000	100	50	1.33	1.2	1.1	1.05	1.04	1.06	1.11	1.17	1.26	1.35	1.41	1.42	1.38	1.29	1.16	1	0.78
22000	100	100	0.85	0.75	0.69	0.65	0.64	0.66	0.7	0.76	0.83	0.9	0.96	0.99	0.99	0.96	0.91	0.82	0.69
22000	100	200	0.48	0.45	0.43	0.42	0.43	0.45	0.48	0.52	0.57	0.63	0.68	0.72	0.73	0.73	0.71	0.67	0.6
22000	100	300	0.31	0.31	0.31	0.31	0.32	0.34	0.37	0.4	0.44	0.49	0.53	0.56	0.58	0.59	0.59	0.57	0.53
22000	100	400	0.25	0.26	0.26	0.26	0.27	0.29	0.31	0.34	0.38	0.41	0.45	0.48	0.5	0.52	0.52	0.51	0.48
22000	100	500	0.23	0.24	0.24	0.25	0.25	0.27	0.29	0.31	0.35	0.38	0.42	0.44	0.46	0.48	0.49	0.48	0.46
22000	200	10	3.99	4.06	4.12	4.18	4.24	4.32	4.46	4.66	4.92	5.16	5.27	5.13	4.75	4.22	3.6	2.87	1.94
22000	200	20	3.51	3.47	3.4	3.34	3.33	3.38	3.49	3.66	3.9	4.14	4.3	4.27	4.04	3.68	3.21	2.63	1.84
22000	200	50	2.66	2.51	2.36	2.23	2.18	2.21	2.3	2.44	2.63	2.84	3	3.06	2.99	2.82	2.56	2.19	1.66
22000	200	100	1.74	1.59	1.47	1.39	1.37	1.41	1.48	1.59	1.73	1.89	2.03	2.12	2.13	2.07	1.94	1.74	1.44
22000	200	200	0.99	0.95	0.91	0.89	0.9	0.94	1.01	1.09	1.2	1.32	1.43	1.51	1.54	1.53	1.48	1.39	1.24
22000	200	300	0.61	0.62	0.63	0.64	0.67	0.71	0.76	0.83	0.92	1.01	1.1	1.17	1.2	1.22	1.21	1.17	1.09
22000	200	400	0.48	0.5	0.51	0.53	0.56	0.6	0.65	0.7	0.78	0.86	0.93	0.99	1.03	1.05	1.06	1.04	1
22000	200	500	0.43	0.45	0.47	0.49	0.51	0.55	0.59	0.65	0.72	0.79	0.86	0.91	0.95	0.98	0.99	0.98	0.95
22000	400	10	7.16	7.32	7.55	7.72	7.71	7.69	7.8	8.11	8.6	9.15	9.51	9.42	8.83	7.88	6.74	5.37	3.61
22000	400	20	6.31	6.24	6.23	6.22	6.11	6.05	6.13	6.4	6.84	7.38	7.8	7.88	7.56	6.92	6.05	4.94	3.42
22000	400	50	4.85	4.66	4.44	4.21	4.04	3.99	4.07	4.28	4.63	5.06	5.44	5.64	5.58	5.29	4.81	4.09	3.05
22000	400	100	3.22	2.97	2.74	2.56	2.48	2.52	2.63	2.81	3.06	3.36	3.64	3.83	3.89	3.8	3.58	3.21	2.63
22000	400	200	1.84	1.75	1.65	1.6	1.6	1.67	1.78	1.92	2.1	2.32	2.52	2.67	2.75	2.75	2.67	2.51	2.24
22000	400	300	1.1	1.13	1.14	1.15	1.19	1.25	1.34	1.46	1.6	1.77	1.93	2.05	2.13	2.16	2.15	2.08	1.95
22000	400	400	0.82	0.87	0.9	0.94	0.98	1.05	1.13	1.24	1.36	1.51	1.64	1.75	1.82	1.87	1.88	1.85	1.77

P	G	ΔT_w	H_b, kJ/kg																
kPa	Kg/m^2s	K	1000	1400	1600	1800	1900	2000	2050	2100	2150	2200	2250	2300	2400	2500	2600	2700	3000
22000	400	500	0.74	0.78	0.81	0.85	0.9	0.96	1.05	1.14	1.26	1.39	1.52	1.62	1.69	1.74	1.76	1.74	1.68
22000	700	10	11.6	10.6	10.9	11.8	12.1	11.9	11.9	12.3	13.1	14.2	15.1	15.3	14.4	12.8	10.8	8.46	5.72
22000	700	20	10.4	9.31	9.38	9.91	9.93	9.69	9.67	9.96	10.6	11.6	12.5	12.9	12.5	11.4	9.83	7.92	5.52
22000	700	50	8.22	7.79	7.47	7.18	6.85	6.63	6.62	6.84	7.35	8.08	8.82	9.28	9.28	8.82	7.97	6.74	5.06
22000	700	100	5.49	5.14	4.75	4.4	4.2	4.16	4.26	4.48	4.84	5.34	5.84	6.21	6.37	6.28	5.94	5.32	4.39
22000	700	200	3.18	3.01	2.83	2.69	2.65	2.71	2.84	3.02	3.29	3.63	3.97	4.24	4.4	4.44	4.35	4.1	3.67
22000	700	300	1.86	1.92	1.92	1.91	1.93	2	2.11	2.27	2.49	2.75	3.02	3.22	3.36	3.43	3.43	3.33	3.12
22000	700	400	1.32	1.41	1.47	1.51	1.57	1.66	1.78	1.93	2.13	2.36	2.58	2.75	2.88	2.95	2.97	2.92	2.79
22000	700	500	1.15	1.23	1.28	1.34	1.42	1.52	1.64	1.8	1.98	2.19	2.39	2.55	2.67	2.75	2.78	2.75	2.65
22000	1000	10	16.6	14.9	15.6	17.2	17.9	17.8	17.7	18.1	19.2	20.9	22.5	22.9	21.8	19.3	16.1	12.5	8.61
22000	1000	20	15	13.3	13.6	14.6	14.9	14.7	14.6	14.8	15.7	17.2	18.6	19.4	19	17.4	15	12.1	8.63
22000	1000	50	11.8	11.2	10.9	10.7	10.4	10.2	10.2	10.4	11	12	13.2	14.1	14.3	13.7	12.4	10.6	8.16
22000	1000	100	7.73	7.38	6.97	6.59	6.33	6.27	6.4	6.66	7.09	7.73	8.51	9.19	9.58	9.58	9.16	8.32	7
22000	1000	200	4.49	4.37	4.19	4.02	3.94	3.97	4.1	4.32	4.66	5.12	5.64	6.09	6.4	6.54	6.47	6.15	5.53
22000	1000	300	2.67	2.8	2.82	2.8	2.8	2.86	3	3.2	3.51	3.89	4.28	4.61	4.84	4.97	4.97	4.83	4.51
22000	1000	400	1.9	2.04	2.12	2.18	2.25	2.37	2.53	2.75	3.03	3.37	3.69	3.95	4.14	4.26	4.28	4.21	4.01
22000	1000	500	1.64	1.76	1.84	1.92	2.03	2.17	2.35	2.57	2.84	3.15	3.44	3.67	3.84	3.96	4	3.95	3.79
22000	1500	10	22.8	22	23.1	24.7	25	24.6	24.5	25.2	26.9	29.6	32.2	33.3	31.9	28.3	23.7	18.7	13.6
22000	1500	20	20.4	19.4	19.9	20.7	20.5	20	20.1	20.7	22.1	24.2	26.5	27.9	27.6	25.4	22.2	18.3	13.9
22000	1500	50	15.8	15.5	15.3	14.8	14.1	14.1	15	16	16.8	17.6	18.8	20.2	20.7	20	18.4	16.1	13.1
22000	1500	100	10.2	9.95	9.57	9.11	8.74	9.01	10.1	11.1	11.6	11.7	12.3	13.3	14	14.1	13.6	12.5	10.8
22000	1500	200	5.9	5.78	5.64	5.53	5.5	5.68	6.1	6.59	7.07	7.56	8.18	8.82	9.3	9.5	9.41	8.97	8.08
22000	1500	300	3.53	3.63	3.69	3.75	3.86	4.05	4.32	4.66	5.11	5.64	6.17	6.61	6.91	7.07	7.06	6.84	6.34
22000	1500	400	2.57	2.72	2.84	2.95	3.11	3.33	3.6	3.94	4.35	4.81	5.26	5.61	5.86	6.01	6.03	5.9	5.59
22000	1500	500	2.27	2.41	2.53	2.66	2.82	3.04	3.31	3.64	4.03	4.45	4.86	5.18	5.42	5.57	5.61	5.53	5.29
22000	2000	10	28.9	29.7	31.8	33.4	33	32	32.2	33.8	36.5	39.9	42.6	43.2	41	37	32.2	26.8	20.1
22000	2000	20	25.6	26.1	27.2	27.8	26.8	26	26.7	28.5	30.7	33	35.3	36.7	36.1	33.7	30.1	25.5	19.2
22000	2000	50	19.7	20.2	20.4	19.7	18.6	19.1	22.5	25.8	27.1	26.2	25.8	26.8	27.3	26.5	24.5	21.4	17
22000	2000	100	12.9	12.9	12.7	12.3	11.8	12.8	16.2	19.4	20.1	18.5	17.4	18	18.8	18.7	17.9	16.2	13.6
22000	2000	200	7.39	7.39	7.36	7.35	7.42	7.88	8.94	10.1	10.8	11.1	11.5	12.2	12.7	12.8	12.5	11.7	10.2
22000	2000	300	4.51	4.65	4.78	4.94	5.18	5.52	5.97	6.51	7.17	7.91	8.61	9.17	9.52	9.67	9.59	9.2	8.42
22000	2000	400	3.43	3.62	3.78	3.97	4.23	4.57	4.98	5.47	6.05	6.7	7.3	7.77	8.09	8.27	8.28	8.08	7.62
22000	2000	500	3.08	3.27	3.44	3.62	3.87	4.18	4.57	5.03	5.57	6.17	6.72	7.16	7.47	7.67	7.72	7.59	7.25
22000	3000	10	39.5	42.4	47.5	50.8	49.2	46	46.1	48.8	52.6	56.7	59.8	59.9	56.6	50.7	43.8	35.9	26.1
22000	3000	20	35.3	37.6	40.9	42.6	40.4	37.5	37.8	40.5	43.4	46.5	49.7	51.4	50.2	46.4	40.9	33.9	24.8
22000	3000	50	27.5	29	30.1	29.8	28	27.2	30.3	34.9	35.9	35.4	36.2	37.7	38.2	36.6	33.3	28.6	22.2
22000	3000	100	17.9	18.4	18.7	18.4	17.7	18	21.5	26.3	26.8	25.3	24.7	25.6	26.4	26.2	24.7	22.1	18.3
22000	3000	200	10.2	10.4	10.5	10.6	10.8	11.3	12.6	14.4	15.3	15.9	16.7	17.6	18.3	18.4	17.8	16.6	14.5
22000	3000	300	6.37	6.58	6.79	7.07	7.46	8	8.68	9.51	10.5	11.6	12.6	13.4	13.9	14.1	13.9	13.4	12.3
22000	3000	400	4.92	5.18	5.43	5.72	6.11	6.63	7.25	7.97	8.84	9.78	10.7	11.3	11.8	12	12	11.7	11.1
22000	3000	500	4.42	4.7	4.95	5.23	5.6	6.07	6.65	7.33	8.13	8.99	9.8	10.4	10.9	11.1	11.2	11	10.5
22000	5000	10	55.1	58.8	64.2	67.3	65.2	62.8	64.5	68.9	74	79.1	82.8	83.2	78.7	70	58.7	45.6	30.2
22000	5000	20	50	53.2	56.2	57.5	55.4	53.5	54.9	58.1	61.3	65.7	70.4	72.7	70.5	64	54.6	42.9	29
22000	5000	50	38.9	41	41.4	41	41	42.9	46.4	48.5	46.6	47.6	51.5	54.3	54.1	50.7	44.7	36.7	26.5
22000	5000	100	24.8	25.6	25.8	25.8	27	30.4	34.5	36.2	32.9	32.3	34.6	36.7	37.3	36.2	33.5	29.3	23.4
22000	5000	200	14.1	14.3	14.5	14.7	15.5	17	18.9	20.4	20.9	22.1	23.9	25.2	25.9	25.9	25	23.2	20.3
22000	5000	300	9.11	9.38	9.65	10	10.6	11.5	12.6	13.8	15.2	16.8	18.3	19.4	20.1	20.4	20.1	19.4	18
22000	5000	400	7.21	7.54	7.89	8.33	8.93	9.69	10.6	11.7	12.9	14.3	15.6	16.6	17.3	17.6	17.6	17.2	16.4

P kPa	G Kg/m^2s	ΔT_w K	H_b, kJ/kg																
			1000	1400	1600	1800	1900	2000	2050	2100	2150	2200	2250	2300	2400	2500	2600	2700	3000
22000	5000	500	6.48	6.85	7.21	7.65	8.21	8.93	9.78	10.8	11.9	13.2	14.4	15.3	16	16.4	16.5	16.2	15.6
22500	100	10	1.74	1.89	2.18	2.51	2.81	3.02	3.15	3.21	3.23	3.2	3.07	2.83	2.48	2.1	1.71	1.32	0.89
22500	100	20	1.58	1.65	1.82	2.03	2.23	2.38	2.49	2.55	2.58	2.58	2.5	2.34	2.09	1.81	1.51	1.2	0.85
22500	100	50	1.27	1.27	1.31	1.39	1.47	1.56	1.64	1.7	1.75	1.77	1.75	1.67	1.55	1.39	1.21	1.02	0.78
22500	100	100	0.89	0.87	0.87	0.88	0.92	0.98	1.03	1.09	1.14	1.18	1.19	1.17	1.11	1.04	0.94	0.83	0.69
22500	100	200	0.56	0.55	0.56	0.57	0.6	0.64	0.69	0.74	0.79	0.82	0.84	0.84	0.82	0.79	0.73	0.67	0.6
22500	100	300	0.38	0.38	0.39	0.41	0.44	0.47	0.51	0.55	0.59	0.62	0.64	0.65	0.64	0.63	0.6	0.57	0.53
22500	100	400	0.3	0.3	0.31	0.33	0.36	0.39	0.42	0.46	0.49	0.51	0.53	0.54	0.54	0.53	0.52	0.5	0.48
22500	100	500	0.26	0.27	0.28	0.3	0.32	0.35	0.38	0.41	0.44	0.46	0.48	0.49	0.49	0.48	0.48	0.47	0.46
22500	200	10	3.68	4.32	5	5.61	6.07	6.37	6.55	6.67	6.75	6.74	6.56	6.14	5.52	4.8	4.03	3.19	2.17
22500	200	20	3.27	3.72	4.13	4.49	4.77	4.97	5.11	5.22	5.32	5.38	5.32	5.08	4.68	4.17	3.59	2.9	2.02
22500	200	50	2.62	2.8	2.93	3.04	3.14	3.25	3.35	3.45	3.55	3.64	3.67	3.59	3.41	3.14	2.79	2.36	1.77
22500	200	100	1.89	1.93	1.94	1.95	1.98	2.05	2.14	2.23	2.31	2.4	2.45	2.46	2.39	2.25	2.06	1.82	1.49
22500	200	200	1.22	1.25	1.26	1.27	1.29	1.34	1.41	1.49	1.57	1.64	1.7	1.72	1.7	1.64	1.54	1.41	1.25
22500	200	300	0.79	0.83	0.86	0.89	0.93	0.98	1.04	1.11	1.18	1.24	1.29	1.31	1.31	1.27	1.22	1.16	1.09
22500	200	400	0.6	0.63	0.66	0.7	0.75	0.81	0.87	0.93	1	1.05	1.09	1.1	1.1	1.08	1.06	1.03	0.99
22500	200	500	0.53	0.55	0.58	0.62	0.67	0.73	0.79	0.85	0.91	0.96	0.99	1.01	1.01	1	0.99	0.97	0.94
22500	400	10	6.71	8.02	9.24	10.3	10.9	11.2	11.3	11.5	11.7	11.8	11.7	11.1	10.2	9.02	7.76	6.29	4.35
22500	400	20	5.94	6.79	7.55	8.18	8.55	8.74	8.87	9.03	9.25	9.46	9.52	9.25	8.66	7.86	6.9	5.69	3.99
22500	400	50	4.79	5.17	5.4	5.54	5.63	5.72	5.83	5.98	6.18	6.4	6.55	6.53	6.3	5.89	5.32	4.54	3.39
22500	400	100	3.52	3.56	3.53	3.49	3.51	3.6	3.73	3.87	4.03	4.2	4.33	4.37	4.3	4.12	3.82	3.4	2.78
22500	400	200	2.29	2.31	2.28	2.25	2.28	2.36	2.48	2.6	2.72	2.85	2.95	3	2.99	2.9	2.77	2.57	2.29
22500	400	300	1.44	1.52	1.57	1.61	1.65	1.73	1.83	1.95	2.06	2.16	2.25	2.29	2.28	2.24	2.17	2.08	1.96
22500	400	400	1.06	1.13	1.19	1.26	1.33	1.43	1.54	1.65	1.75	1.85	1.91	1.94	1.94	1.92	1.88	1.83	1.77
22500	400	500	0.94	0.98	1.04	1.11	1.19	1.3	1.41	1.52	1.61	1.7	1.76	1.79	1.79	1.77	1.75	1.72	1.68
22500	700	10	10.7	11.3	12.8	14.8	16	16.5	16.8	17	17.4	17.9	18	17.4	15.9	14	11.8	9.44	6.67
22500	700	20	9.73	9.94	10.9	12.2	13	13.3	13.4	13.6	14	14.4	14.7	14.5	13.6	12.2	10.6	8.72	6.28
22500	700	50	8.13	8.41	8.65	8.87	8.97	9.03	9.13	9.28	9.55	9.92	10.2	10.3	9.97	9.33	8.43	7.21	5.55
22500	700	100	6.17	6.13	5.95	5.78	5.72	5.8	5.94	6.09	6.3	6.55	6.77	6.88	6.82	6.59	6.19	5.57	4.67
22500	700	200	4.11	4.06	3.91	3.79	3.76	3.85	3.98	4.12	4.27	4.45	4.61	4.7	4.71	4.63	4.47	4.22	3.82
22500	700	300	2.55	2.68	2.71	2.7	2.72	2.8	2.92	3.06	3.21	3.37	3.5	3.57	3.58	3.54	3.46	3.35	3.17
22500	700	400	1.77	1.89	1.98	2.06	2.15	2.27	2.42	2.58	2.74	2.89	3	3.05	3.05	3.02	2.97	2.9	2.8
22500	700	500	1.49	1.57	1.66	1.76	1.89	2.05	2.22	2.39	2.54	2.67	2.77	2.82	2.82	2.8	2.76	2.71	2.65
22500	1000	10	15.4	15.1	17.3	20.8	23.1	24	24.4	24.7	25.3	26.1	26.4	25.5	23.2	19.9	16.3	12.8	9.33
22500	1000	20	14.1	13.5	15	17.4	19	19.6	19.9	20.1	20.5	21	21.4	21.1	19.7	17.6	15	12.2	9.02
22500	1000	50	11.8	11.9	12.4	13	13.3	13.6	14.1	14.3	14.5	14.5	14.8	14.9	14.6	13.7	12.3	10.6	8.34
22500	1000	100	8.8	8.86	8.75	8.61	8.55	8.74	9.17	9.43	9.46	9.37	9.51	9.74	9.78	9.59	9.14	8.35	7.16
22500	1000	200	5.89	5.97	5.86	5.69	5.59	5.63	5.79	5.93	6.05	6.17	6.35	6.52	6.6	6.6	6.48	6.2	5.69
22500	1000	300	3.73	3.98	4.03	3.99	3.97	4.01	4.13	4.29	4.48	4.68	4.87	4.99	5.03	5.01	4.94	4.81	4.59
22500	1000	400	2.57	2.76	2.88	2.97	3.08	3.25	3.45	3.66	3.88	4.08	4.24	4.33	4.34	4.31	4.24	4.15	4.02
22500	1000	500	2.15	2.27	2.39	2.53	2.71	2.93	3.17	3.41	3.63	3.82	3.96	4.03	4.04	4.01	3.96	3.89	3.79
22500	1500	10	21.4	18.9	22.6	28.6	32	33.2	33.7	34.3	35.3	36.7	37.5	36.4	33.2	28.6	23.9	19.4	15.1
22500	1500	20	19.7	16.7	19.3	23.7	26.2	27.1	27.8	28.5	29.1	29.6	30.1	29.8	28	25.1	21.7	18.2	14.4
22500	1500	50	16.3	15.9	16.7	17.8	18.4	19.6	22.1	23.7	23.4	21.7	20.9	21	20.6	19.4	17.6	15.4	12.7
22500	1500	100	12	12.1	12.1	12	12	13	15.5	17.1	16.6	14.6	13.7	13.8	13.9	13.6	13	12	10.4
22500	1500	200	7.81	7.92	7.92	7.87	7.88	8.18	8.86	9.39	9.47	9.2	9.17	9.33	9.4	9.34	9.15	8.76	8.04
22500	1500	300	4.89	5.07	5.19	5.3	5.46	5.7	5.99	6.29	6.57	6.82	7.02	7.12	7.12	7.05	6.94	6.74	6.4
22500	1500	400	3.48	3.63	3.79	3.98	4.24	4.56	4.91	5.24	5.55	5.82	6.01	6.1	6.09	6.03	5.94	5.8	5.61

P	G	ΔT_w	H_b, kJ/kg																
kPa	Kg/m^{2}s	K	1000	1400	1600	1800	1900	2000	2050	2100	2150	2200	2250	2300	2400	2500	2600	2700	3000
22500	1500	500	2.98	3.11	3.27	3.48	3.76	4.1	4.45	4.79	5.1	5.36	5.55	5.64	5.64	5.59	5.52	5.42	5.29
22500	2000	10	26.7	26.7	32.4	40.6	45.1	45	45.2	46.7	48.7	50.5	51.2	49.4	45.1	39.7	34.8	30.3	25.1
22500	2000	20	24.4	23.8	27.8	33.4	36.4	36.2	36.7	38.2	39.5	40.3	40.7	40.1	37.9	34.6	31.1	27.3	22.3
22500	2000	50	20.3	21.1	22.9	24.6	25.4	26.1	28.9	32.3	32.9	30.5	28.5	28	27.4	25.9	23.8	21.2	17.7
22500	2000	100	15.1	15.7	16.4	16.7	16.6	17.2	20.2	23.8	24.2	21.3	19.1	18.6	18.4	17.9	16.8	15.3	13.1
22500	2000	200	9.65	9.98	10.3	10.5	10.6	11	11.9	13.1	13.5	13.1	12.8	12.8	12.7	12.4	11.9	11.1	9.85
22500	2000	300	6.16	6.39	6.65	6.95	7.31	7.74	8.22	8.7	9.16	9.54	9.81	9.89	9.8	9.61	9.35	8.95	8.32
22500	2000	400	4.61	4.79	5.03	5.34	5.74	6.22	6.73	7.22	7.67	8.06	8.32	8.43	8.4	8.29	8.13	7.92	7.61
22500	2000	500	4.05	4.22	4.44	4.75	5.14	5.61	6.1	6.57	7	7.37	7.63	7.75	7.75	7.68	7.58	7.44	7.24
22500	3000	10	36.6	40.1	51.1	67.4	75.8	69.7	66.4	68.3	70.8	72.4	72.3	69.1	62.7	54.8	47.1	39.7	31.4
22500	3000	20	33.5	35.9	44.3	56.5	62.9	57.1	53.8	55.1	56.5	57.5	57.9	56.6	53.1	47.9	42.2	36	28.5
22500	3000	50	28	31.5	37.3	42.5	44.1	41.9	42.1	44.5	43.9	41.8	40.5	39.9	38.6	36.1	32.6	28.5	23.3
22500	3000	100	20.8	23	26.2	28.2	28	27.4	29.9	33.6	32.7	29.8	27.7	27	26.4	25.3	23.5	21.1	18.1
22500	3000	200	13.3	14.1	15.1	15.8	16.2	16.5	17.7	19.2	19.5	19.3	19.1	19	18.7	18.1	17.2	16	14.2
22500	3000	300	8.73	9.08	9.5	9.99	10.6	11.3	12	12.8	13.5	14.1	14.5	14.6	14.4	14.1	13.7	13.1	12.2
22500	3000	400	6.66	6.92	7.27	7.74	8.34	9.05	9.81	10.5	11.2	11.8	12.2	12.3	12.3	12.1	11.9	11.5	11.1
22500	3000	500	5.86	6.12	6.45	6.9	7.48	8.16	8.88	9.57	10.2	10.7	11.1	11.3	11.3	11.2	11	10.8	10.5
22500	5000	10	50.7	57.7	69.8	87.3	98	95	94.2	97.5	99.9	100	98.8	94.2	85.6	73.8	60.4	46.1	30.6
22500	5000	20	46.9	53.4	62.6	76	84.4	80.8	78.5	80	81.2	81.9	82	79.9	74.4	65.7	55	42.9	29.3
22500	5000	50	38.8	45.8	54.2	61.6	65.2	63.8	62.3	62.1	59.8	58.8	59.3	58.8	56.1	51.1	44.3	36.3	26.8
22500	5000	100	27.8	32.3	38.4	42.9	45	45.4	46.6	46.9	42.5	40.3	40.5	40.3	39	36.6	33.2	29	23.6
22500	5000	200	17.9	19.4	21	22.5	23.7	24.9	26.4	27.6	27.4	27.6	28.1	28.1	27.5	26.4	25	23	20.5
22500	5000	300	12.4	12.8	13.3	14	15	16.2	17.5	18.7	19.8	20.7	21.4	21.5	21.3	20.8	20.1	19.2	18
22500	5000	400	9.84	10.2	10.6	11.3	12.2	13.3	14.4	15.5	16.5	17.4	17.9	18.2	18.1	17.9	17.5	17.1	16.4
22500	5000	500	8.72	9.05	9.52	10.2	11	12.1	13.1	14.1	15.1	15.9	16.4	16.7	16.7	16.5	16.3	16	15.6
23000	100	10	1.53	1.81	2.27	2.77	3.21	3.5	3.64	3.68	3.62	3.49	3.26	2.94	2.54	2.13	1.72	1.32	0.9
23000	100	20	1.43	1.62	1.93	2.27	2.57	2.78	2.89	2.93	2.91	2.82	2.66	2.43	2.15	1.84	1.53	1.21	0.86
23000	100	50	1.22	1.31	1.44	1.59	1.73	1.84	1.93	1.98	1.99	1.96	1.88	1.77	1.61	1.44	1.24	1.03	0.79
23000	100	100	0.94	0.96	0.99	1.04	1.1	1.17	1.24	1.31	1.34	1.34	1.32	1.27	1.21	1.11	0.99	0.85	0.69
23000	100	200	0.65	0.65	0.66	0.68	0.72	0.77	0.84	0.9	0.94	0.96	0.96	0.95	0.93	0.87	0.78	0.69	0.6
23000	100	300	0.46	0.46	0.47	0.49	0.52	0.56	0.61	0.66	0.69	0.72	0.74	0.74	0.72	0.69	0.63	0.58	0.53
23000	100	400	0.36	0.37	0.38	0.39	0.42	0.45	0.49	0.52	0.55	0.57	0.58	0.58	0.57	0.56	0.53	0.5	0.48
23000	100	500	0.32	0.32	0.34	0.35	0.38	0.41	0.44	0.47	0.49	0.5	0.51	0.51	0.5	0.49	0.48	0.47	0.46
23000	200	10	3.53	4.4	5.33	6.19	6.84	7.24	7.4	7.42	7.35	7.18	6.87	6.4	5.78	5.1	4.35	3.52	2.49
23000	200	20	3.22	3.88	4.51	5.05	5.46	5.7	5.8	5.83	5.81	5.73	5.57	5.29	4.9	4.42	3.86	3.18	2.3
23000	200	50	2.74	3.08	3.34	3.53	3.68	3.79	3.85	3.89	3.9	3.88	3.84	3.73	3.55	3.29	2.97	2.54	1.96
23000	200	100	2.12	2.27	2.33	2.35	2.38	2.43	2.48	2.53	2.55	2.57	2.57	2.54	2.47	2.33	2.14	1.9	1.58
23000	200	200	1.47	1.56	1.59	1.58	1.57	1.59	1.63	1.69	1.73	1.76	1.78	1.79	1.75	1.67	1.56	1.42	1.26
23000	200	300	0.97	1.04	1.09	1.11	1.12	1.15	1.2	1.26	1.31	1.35	1.37	1.38	1.35	1.3	1.23	1.16	1.08
23000	200	400	0.73	0.77	0.81	0.85	0.89	0.94	1	1.06	1.11	1.14	1.15	1.15	1.13	1.1	1.07	1.03	0.99
23000	200	500	0.65	0.67	0.7	0.74	0.79	0.85	0.91	0.97	1.01	1.03	1.04	1.04	1.03	1.01	0.99	0.97	0.95
23000	400	10	6.52	8.4	10	11.4	12.3	12.8	13	13	12.9	12.7	12.3	11.6	10.7	9.62	8.5	7.18	5.37
23000	400	20	5.88	7.21	8.3	9.15	9.73	10.1	10.2	10.2	10.2	10.2	9.99	9.6	9	8.29	7.46	6.39	4.83
23000	400	50	4.99	5.63	6.04	6.31	6.5	6.63	6.72	6.78	6.82	6.85	6.82	6.7	6.46	6.1	5.61	4.92	3.88
23000	400	100	3.93	4.09	4.13	4.12	4.14	4.21	4.3	4.37	4.41	4.45	4.46	4.44	4.34	4.17	3.92	3.55	2.99
23000	400	200	2.72	2.78	2.77	2.73	2.71	2.75	2.83	2.9	2.95	2.99	3.02	3.02	2.98	2.89	2.76	2.59	2.33
23000	400	300	1.76	1.86	1.92	1.94	1.95	2	2.08	2.17	2.24	2.29	2.32	2.32	2.29	2.23	2.16	2.07	1.96
23000	400	400	1.31	1.38	1.44	1.5	1.57	1.65	1.76	1.85	1.93	1.98	2	1.99	1.97	1.93	1.88	1.83	1.77

P kPa	G Kg/m²s	ΔT_w K	H_b, kJ/kg 1000	1400	1600	1800	1900	2000	2050	2100	2150	2200	2250	2300	2400	2500	2600	2700	3000
23000	400	500	1.16	1.2	1.25	1.32	1.4	1.51	1.61	1.71	1.78	1.83	1.84	1.84	1.82	1.79	1.75	1.72	1.68
23000	700	10	10.2	12.3	14.4	16.5	18.1	19	19.4	19.5	19.5	19.5	19.1	18	16.4	14.4	12.4	10.4	8.04
23000	700	20	9.42	10.9	12.3	13.6	14.6	15.2	15.4	15.5	15.5	15.5	15.3	14.8	13.7	12.4	11	9.41	7.37
23000	700	50	8.26	8.99	9.47	9.83	10.1	10.3	10.4	10.5	10.5	10.5	10.5	10.3	9.92	9.33	8.55	7.54	6.13
23000	700	100	6.67	6.78	6.72	6.63	6.62	6.7	6.8	6.87	6.9	6.92	6.93	6.88	6.75	6.52	6.18	5.67	4.91
23000	700	200	4.7	4.71	4.61	4.49	4.44	4.49	4.58	4.66	4.69	4.72	4.73	4.71	4.65	4.55	4.42	4.22	3.9
23000	700	300	3.06	3.19	3.23	3.21	3.21	3.26	3.36	3.46	3.54	3.59	3.61	3.6	3.55	3.48	3.41	3.32	3.19
23000	700	400	2.18	2.29	2.37	2.44	2.52	2.64	2.79	2.93	3.03	3.1	3.12	3.11	3.07	3.01	2.96	2.89	2.82
23000	700	500	1.86	1.92	2	2.1	2.23	2.38	2.55	2.7	2.81	2.88	2.9	2.89	2.86	2.81	2.77	2.72	2.66
23000	1000	10	14.6	15.6	18.8	22.6	25.5	27.1	27.8	28.1	28.3	28.3	27.8	26	23.1	19.5	16.2	13.2	10.4
23000	1000	20	13.5	14.2	16.4	19	20.9	21.9	22.4	22.6	22.6	22.5	22.1	21.1	19.3	17	14.6	12.2	9.63
23000	1000	50	11.8	12.5	13.3	14.2	14.8	15.2	15.7	15.9	15.7	15.3	15	14.6	14	13	11.8	10.4	8.51
23000	1000	100	9.42	9.74	9.82	9.8	9.78	9.96	10.3	10.5	10.3	9.84	9.62	9.55	9.41	9.16	8.77	8.15	7.2
23000	1000	200	6.71	6.91	6.85	6.69	6.56	6.55	6.64	6.69	6.64	6.53	6.46	6.42	6.37	6.31	6.24	6.08	5.76
23000	1000	300	4.47	4.72	4.77	4.71	4.66	4.68	4.77	4.87	4.94	4.98	4.98	4.94	4.87	4.81	4.76	4.71	4.63
23000	1000	400	3.18	3.34	3.44	3.52	3.62	3.78	3.97	4.15	4.29	4.37	4.4	4.37	4.31	4.24	4.17	4.11	4.04
23000	1000	500	2.68	2.77	2.87	3	3.19	3.41	3.65	3.86	4.01	4.11	4.14	4.13	4.08	4.01	3.95	3.88	3.81
23000	1500	10	20	17.6	22.5	30.2	35.2	37.4	38.4	39	39.4	39.6	38.9	36.6	32.5	27.7	23.3	19.5	15.9
23000	1500	20	18.7	16	19.5	25.3	28.9	30.5	31.5	32	31.9	31.5	30.8	29.4	27	23.9	20.8	17.7	14.5
23000	1500	50	16.4	16.2	17.6	19.5	20.7	22.1	24.4	25.6	24.8	22.4	21	20.4	19.5	18.1	16.5	14.6	12.3
23000	1500	100	13.1	13.4	13.7	13.9	14	14.9	17.1	18.3	17.4	15	13.7	13.4	13.2	12.7	12.1	11.3	10
23000	1500	200	9.09	9.36	9.44	9.41	9.37	9.57	10.1	10.4	10.2	9.66	9.32	9.17	9.03	8.88	8.72	8.46	7.94
23000	1500	300	5.96	6.15	6.27	6.37	6.5	6.7	6.93	7.13	7.25	7.27	7.22	7.1	6.95	6.82	6.72	6.61	6.42
23000	1500	400	4.33	4.44	4.58	4.76	5.01	5.33	5.66	5.95	6.15	6.25	6.26	6.19	6.08	5.97	5.86	5.76	5.63
23000	1500	500	3.72	3.8	3.94	4.14	4.43	4.77	5.12	5.42	5.64	5.76	5.81	5.78	5.7	5.61	5.52	5.42	5.31
23000	2000	10	24.5	25	31.9	42.4	49.7	51.4	52.2	53.5	54.6	55	54.1	51	46.1	40.5	35.6	31.2	26.1
23000	2000	20	23.1	23	27.9	35.4	40.4	41.3	41.8	42.7	43.1	42.9	42.2	40.5	37.7	34.3	30.9	27.5	22.9
23000	2000	50	20.6	21.7	24.3	27.1	28.6	29.3	31.2	32.9	32.4	30.4	28.6	27.6	26.5	24.9	23	20.8	17.8
23000	2000	100	16.7	17.7	18.7	19.3	19.3	19.6	21.5	23.4	22.8	20.6	19	18.3	17.8	17.1	16.1	14.8	12.9
23000	2000	200	11.5	12.1	12.6	12.8	12.9	13	13.6	14.2	14.1	13.6	13.2	12.9	12.5	12.1	11.6	10.9	9.83
23000	2000	300	7.64	7.94	8.25	8.55	8.86	9.22	9.6	9.94	10.2	10.3	10.2	10.1	9.83	9.56	9.28	8.92	8.38
23000	2000	400	5.78	5.92	6.14	6.44	6.83	7.31	7.79	8.21	8.51	8.68	8.71	8.64	8.49	8.31	8.13	7.92	7.65
23000	2000	500	5.05	5.17	5.37	5.66	6.06	6.53	7.02	7.43	7.74	7.92	7.99	7.95	7.85	7.72	7.59	7.45	7.28
23000	3000	10	33.6	38.3	48.7	66.7	81.6	79.5	77	78.6	79.6	79.3	77.1	72.1	64.6	56.2	48.2	40.7	32.7
23000	3000	20	31.7	35	43.5	57.5	68.3	65	61.8	62.1	62.2	61.8	60.5	57.8	53.5	48	42.4	36.5	29.5
23000	3000	50	28.3	32.6	39.7	46.3	49	47.2	46.4	46.3	44.5	42.8	41.4	40	38.1	35.3	32.1	28.3	23.8
23000	3000	100	22.9	25.8	29.9	32.5	32.3	31.1	32.2	33.4	31.8	29.8	28.2	27.1	26.1	24.7	22.9	20.8	18.1
23000	3000	200	15.9	17.1	18.5	19.4	19.6	19.6	20.3	21	20.9	20.5	20	19.4	18.7	17.9	17	15.8	14.3
23000	3000	300	10.8	11.3	11.9	12.4	12.9	13.5	14.2	14.7	15.1	15.3	15.3	15.1	14.7	14.2	13.7	13.1	12.3
23000	3000	400	8.33	8.56	8.9	9.35	9.94	10.6	11.4	12	12.4	12.7	12.8	12.7	12.5	12.2	11.9	11.6	11.2
23000	3000	500	7.31	7.51	7.8	8.23	8.81	9.51	10.2	10.8	11.3	11.5	11.6	11.6	11.4	11.3	11.1	10.8	10.6
23000	5000	10	46.7	56.4	68.5	87.4	107	110	111	114	114	111	105	97.7	87.1	74.2	60.4	46.1	31
23000	5000	20	44	53.4	63.7	78.7	92.8	93	91	91	90.4	88.7	86	81.6	74.7	65.4	54.5	42.5	29.6
23000	5000	50	38.5	48.3	59.6	68.9	73.8	72.7	69.6	66.3	63.9	62.7	61.6	59.7	56.2	50.8	43.9	36	27.1
23000	5000	100	30.2	36.6	44.6	50.2	52.1	51.4	49.7	46.6	44	43	42.5	41.4	39.5	36.6	33.1	28.9	23.8
23000	5000	200	21.1	23.2	25.4	27	28.1	28.9	29.6	29.8	29.8	29.9	29.7	29.1	28	26.7	25	23.1	20.6
23000	5000	300	15.2	15.7	16.3	16.9	17.9	19.1	20.3	21.4	22.1	22.5	22.5	22.2	21.7	21	20.2	19.3	18.1
23000	5000	400	12.2	12.5	12.9	13.5	14.5	15.5	16.7	17.6	18.3	18.7	18.9	18.7	18.4	18	17.6	17.1	16.5

P kPa	G Kg/m^{2}s	ΔT_w K	H_b, kJ/kg 1000	1400	1600	1800	1900	2000	2050	2100	2150	2200	2250	2300	2400	2500	2600	2700	3000
23000	5000	500	10.9	11.1	11.5	12.1	13	14	15.1	16	16.7	17.1	17.2	17.1	16.9	16.6	16.3	16	15.7
24000	100	10	1.4	1.71	2.2	2.73	3.19	3.5	3.64	3.66	3.59	3.43	3.2	2.88	2.51	2.11	1.72	1.33	0.91
24000	100	20	1.33	1.57	1.91	2.28	2.6	2.81	2.91	2.94	2.9	2.8	2.63	2.4	2.13	1.83	1.53	1.22	0.87
24000	100	50	1.18	1.3	1.46	1.64	1.79	1.91	1.98	2.03	2.04	1.99	1.9	1.78	1.63	1.46	1.26	1.04	0.8
24000	100	100	0.94	0.98	1.03	1.09	1.16	1.23	1.31	1.38	1.42	1.41	1.37	1.33	1.28	1.19	1.04	0.87	0.7
24000	100	200	0.67	0.68	0.7	0.72	0.76	0.82	0.89	0.96	1.02	1.04	1.05	1.05	1.03	0.96	0.85	0.71	0.61
24000	100	300	0.48	0.49	0.5	0.52	0.55	0.58	0.63	0.69	0.74	0.78	0.81	0.82	0.81	0.76	0.68	0.59	0.53
24000	100	400	0.38	0.39	0.4	0.42	0.44	0.47	0.5	0.53	0.57	0.59	0.61	0.61	0.61	0.58	0.55	0.51	0.49
24000	100	500	0.34	0.35	0.36	0.37	0.4	0.42	0.45	0.47	0.49	0.5	0.51	0.51	0.51	0.5	0.49	0.47	0.46
24000	200	10	3.36	4.11	5	5.88	6.6	7.02	7.17	7.13	6.99	6.78	6.48	6.1	5.63	5.07	4.41	3.62	2.63
24000	200	20	3.18	3.75	4.37	4.94	5.37	5.6	5.67	5.65	5.58	5.48	5.33	5.11	4.82	4.44	3.94	3.3	2.47
24000	200	50	2.84	3.14	3.4	3.6	3.74	3.81	3.83	3.83	3.81	3.78	3.73	3.66	3.53	3.34	3.07	2.69	2.16
24000	200	100	2.25	2.4	2.46	2.48	2.48	2.5	2.53	2.54	2.55	2.54	2.53	2.51	2.46	2.36	2.21	2	1.71
24000	200	200	1.56	1.67	1.71	1.7	1.67	1.66	1.69	1.73	1.76	1.77	1.78	1.78	1.75	1.67	1.56	1.43	1.29
24000	200	300	1.03	1.12	1.19	1.21	1.2	1.2	1.23	1.29	1.34	1.37	1.39	1.39	1.37	1.31	1.23	1.15	1.09
24000	200	400	0.78	0.83	0.88	0.92	0.94	0.97	1.02	1.07	1.11	1.14	1.16	1.16	1.14	1.11	1.07	1.03	1
24000	200	500	0.7	0.72	0.75	0.79	0.83	0.87	0.93	0.97	1.01	1.03	1.04	1.04	1.03	1.01	0.99	0.97	0.95
24000	400	10	6.27	7.87	9.39	10.8	11.9	12.6	12.9	12.8	12.6	12.3	11.9	11.2	10.4	9.54	8.54	7.35	5.8
24000	400	20	5.84	7.01	8.04	8.96	9.68	10.1	10.2	10.2	10.1	9.96	9.72	9.36	8.86	8.25	7.52	6.58	5.28
24000	400	50	5.17	5.74	6.15	6.46	6.67	6.81	6.86	6.87	6.85	6.81	6.75	6.63	6.44	6.15	5.74	5.16	4.29
24000	400	100	4.11	4.29	4.35	4.36	4.38	4.41	4.46	4.48	4.47	4.45	4.44	4.4	4.33	4.2	4.01	3.71	3.22
24000	400	200	2.84	2.93	2.96	2.93	2.9	2.91	2.95	2.99	3	3	2.99	2.98	2.93	2.86	2.75	2.61	2.39
24000	400	300	1.88	1.98	2.05	2.07	2.06	2.07	2.13	2.2	2.26	2.29	2.3	2.29	2.26	2.2	2.13	2.06	1.97
24000	400	400	1.42	1.48	1.54	1.6	1.64	1.69	1.77	1.86	1.93	1.97	1.99	1.98	1.96	1.92	1.87	1.83	1.78
24000	400	500	1.25	1.29	1.33	1.39	1.46	1.54	1.63	1.72	1.78	1.82	1.83	1.83	1.81	1.79	1.76	1.73	1.69
24000	700	10	9.87	11.8	13.7	15.9	17.9	19.3	19.8	19.9	19.8	19.6	19	18	16.3	14.4	12.5	10.7	8.75
24000	700	20	9.33	10.7	12	13.4	14.7	15.5	15.8	15.9	15.8	15.6	15.3	14.6	13.6	12.3	11	9.66	8.02
24000	700	50	8.39	9.08	9.6	10.1	10.4	10.7	10.8	10.8	10.7	10.6	10.5	10.2	9.8	9.25	8.58	7.74	6.6
24000	700	100	6.75	6.94	6.99	6.98	6.99	7.03	7.09	7.12	7.08	7	6.91	6.81	6.66	6.45	6.17	5.76	5.13
24000	700	200	4.73	4.8	4.8	4.76	4.72	4.74	4.79	4.83	4.81	4.76	4.7	4.63	4.54	4.44	4.34	4.2	3.95
24000	700	300	3.16	3.28	3.35	3.36	3.36	3.39	3.46	3.55	3.6	3.6	3.57	3.52	3.45	3.38	3.33	3.27	3.21
24000	700	400	2.33	2.41	2.49	2.55	2.62	2.72	2.84	2.96	3.04	3.09	3.09	3.06	3.02	2.97	2.92	2.88	2.83
24000	700	500	2	2.05	2.12	2.2	2.31	2.45	2.59	2.72	2.81	2.86	2.88	2.87	2.84	2.81	2.77	2.73	2.68
24000	1000	10	14.6	15.6	18.4	22.1	25.4	27.5	28.5	28.8	28.9	28.7	27.9	26.1	23	19.6	16.5	13.8	11.3
24000	1000	20	13.6	14.4	16.4	19.1	21.2	22.4	22.9	23	22.9	22.7	22.1	20.9	19.1	16.8	14.6	12.5	10.2
24000	1000	50	11.9	12.5	13.5	14.5	15.2	15.6	15.8	15.9	15.8	15.4	14.9	14.4	13.7	12.7	11.6	10.3	8.75
24000	1000	100	9.44	9.82	10.1	10.2	10.2	10.2	10.3	10.4	10.3	9.97	9.66	9.44	9.2	8.9	8.52	8.01	7.23
24000	1000	200	6.69	6.92	6.97	6.91	6.83	6.78	6.79	6.81	6.77	6.64	6.48	6.33	6.18	6.06	5.99	5.92	5.74
24000	1000	300	4.55	4.73	4.8	4.81	4.8	4.83	4.91	4.99	5.03	5.01	4.92	4.79	4.65	4.56	4.54	4.57	4.63
24000	1000	400	3.36	3.46	3.55	3.63	3.74	3.89	4.05	4.21	4.32	4.36	4.34	4.27	4.19	4.12	4.08	4.06	4.06
24000	1000	500	2.88	2.94	3.03	3.15	3.31	3.51	3.71	3.88	4.01	4.08	4.1	4.08	4.04	3.99	3.94	3.89	3.83
24000	1500	10	19.8	17.7	22.6	30.2	35.6	38.2	39.3	39.7	39.8	39.5	38.4	35.9	32	27.3	23.1	19.3	15.5
24000	1500	20	18.5	16.9	20.6	26.2	29.9	31.5	32.1	32.2	32	31.5	30.5	28.9	26.5	23.4	20.4	17.4	14
24000	1500	50	16.5	15.9	17.8	20.3	21.7	22.3	22.8	23.1	22.9	22	21	20.1	19.1	17.7	16.1	14.3	12
24000	1500	100	13.2	13.5	14.1	14.5	14.6	14.7	15.2	15.6	15.4	14.6	13.8	13.3	12.9	12.4	11.8	11	9.85
24000	1500	200	9.21	9.57	9.77	9.82	9.78	9.74	9.82	9.9	9.83	9.58	9.27	9.01	8.78	8.58	8.41	8.2	7.82
24000	1500	300	6.17	6.36	6.51	6.64	6.76	6.89	7.05	7.18	7.25	7.23	7.1	6.91	6.71	6.57	6.49	6.45	6.38
24000	1500	400	4.61	4.7	4.82	4.99	5.21	5.47	5.75	5.98	6.14	6.2	6.17	6.08	5.96	5.85	5.77	5.71	5.65

P	G	ΔT_w	H_b, kJ/kg																
kPa	Kg/m^{2}s	K	1000	1400	1600	1800	1900	2000	2050	2100	2150	2200	2250	2300	2400	2500	2600	2700	3000
24000	1500	500	4	4.07	4.19	4.37	4.61	4.9	5.19	5.44	5.62	5.72	5.75	5.72	5.66	5.59	5.51	5.43	5.34
24000	2000	10	23.7	24.4	31.5	41.4	48.6	51.9	53.5	54.4	54.5	53.9	52.3	49.5	45	39.6	34.2	28.7	22.4
24000	2000	20	22.7	23.4	28.7	35.9	40.9	43	43.9	44.3	43.8	42.6	41.4	39.7	37	33.7	29.9	25.8	20.4
24000	2000	50	21	21.5	24.7	28.2	30.2	31	31.5	31.5	30.8	29.5	28.3	27.3	26.2	24.6	22.7	20.3	17.1
24000	2000	100	17.4	18.2	19.4	20.2	20.4	20.3	20.7	21.1	20.7	19.9	18.9	18.2	17.7	17	16.1	14.9	13.2
24000	2000	200	12.1	12.8	13.4	13.6	13.6	13.5	13.6	13.7	13.7	13.4	13.1	12.8	12.5	12.2	11.7	11.1	10.2
24000	2000	300	8.14	8.51	8.84	9.12	9.34	9.56	9.8	10	10.2	10.2	10.2	10	9.78	9.56	9.33	9.02	8.55
24000	2000	400	6.21	6.36	6.56	6.82	7.14	7.53	7.92	8.25	8.5	8.62	8.64	8.56	8.44	8.3	8.14	7.96	7.72
24000	2000	500	5.44	5.55	5.72	5.98	6.31	6.71	7.12	7.47	7.72	7.87	7.92	7.89	7.82	7.72	7.61	7.48	7.33
24000	3000	10	32.4	38.7	48.8	61.6	72.2	76.4	78.3	79.7	79.9	78.6	75.8	70.9	63.8	55.4	46.8	38.2	29
24000	3000	20	31.1	36.1	44.6	54.9	62.6	64.6	64.6	64.2	63.4	62	60.3	57.5	53.1	47.5	41.4	34.8	27.1
24000	3000	50	28.6	32.8	39.8	46.2	49.3	49.6	48.6	46.1	44	42.4	41.3	40	38.1	35.3	31.9	28	23.3
24000	3000	100	23.8	26.5	30.2	32.9	33.3	32.8	32.3	30.9	29.5	28.7	27.9	27.2	26.2	24.8	23.1	21.1	18.5
24000	3000	200	16.8	18.2	19.6	20.4	20.6	20.6	20.6	20.5	20.4	20.2	19.9	19.4	18.8	18.1	17.3	16.2	14.7
24000	3000	300	11.6	12.2	12.8	13.3	13.7	14.1	14.5	14.9	15.2	15.3	15.2	15	14.7	14.3	13.8	13.3	12.5
24000	3000	400	8.97	9.22	9.53	9.92	10.4	11	11.6	12.1	12.4	12.6	12.7	12.6	12.4	12.2	12	11.7	11.3
24000	3000	500	7.87	8.06	8.33	8.7	9.19	9.78	10.4	10.9	11.2	11.5	11.5	11.5	11.4	11.3	11.1	10.9	10.7
24000	5000	10	44.9	56.7	71	87	102	110	115	117	116	112	106	97.5	86.4	73.5	60	46.1	31.6
24000	5000	20	42.9	54.3	66.9	79.6	89.8	93.9	94.5	93.2	91.5	89.3	86.1	81.2	74.1	64.8	54.1	42.5	30.1
24000	5000	50	38.6	49	60.3	69	73.7	75	72.6	66.9	63.6	62.5	61.4	59.4	55.8	50.5	43.7	36.1	27.3
24000	5000	100	31.2	37.8	44.9	49.7	51.7	51.9	50	45.5	43.1	42.7	42.3	41.2	39.4	36.6	33.2	29.1	24
24000	5000	200	22.3	24.5	26.5	27.8	28.7	29.4	29.8	29.6	29.6	29.8	29.6	29	28	26.7	25.2	23.3	20.8
24000	5000	300	16.2	16.8	17.3	17.9	18.7	19.6	20.6	21.5	22.1	22.4	22.4	22.1	21.7	21	20.3	19.4	18.3
24000	5000	400	13	13.3	13.7	14.3	15.1	16	16.9	17.7	18.3	18.6	18.7	18.6	18.4	18	17.7	17.2	16.6
24000	5000	500	11.7	11.9	12.3	12.8	13.6	14.4	15.3	16.1	16.6	16.9	17.1	17	16.9	16.6	16.4	16.1	15.8
25000	100	10	1.33	1.64	2.1	2.6	3.04	3.34	3.48	3.5	3.43	3.29	3.08	2.8	2.45	2.08	1.71	1.33	0.92
25000	100	20	1.27	1.51	1.86	2.22	2.52	2.72	2.82	2.84	2.8	2.71	2.55	2.34	2.09	1.82	1.53	1.23	0.88
25000	100	50	1.15	1.28	1.45	1.63	1.78	1.89	1.96	1.99	2	1.95	1.86	1.74	1.61	1.45	1.27	1.05	0.81
25000	100	100	0.94	0.98	1.04	1.11	1.17	1.24	1.3	1.36	1.39	1.38	1.34	1.31	1.27	1.18	1.05	0.88	0.71
25000	100	200	0.68	0.69	0.71	0.74	0.77	0.82	0.88	0.94	1	1.02	1.03	1.03	1.02	0.96	0.85	0.72	0.61
25000	100	300	0.49	0.5	0.51	0.53	0.55	0.58	0.63	0.68	0.72	0.76	0.79	0.81	0.8	0.76	0.68	0.6	0.54
25000	100	400	0.39	0.4	0.41	0.43	0.44	0.47	0.5	0.52	0.55	0.58	0.6	0.61	0.6	0.58	0.55	0.52	0.49
25000	100	500	0.35	0.36	0.37	0.38	0.4	0.42	0.44	0.46	0.48	0.49	0.5	0.51	0.5	0.5	0.49	0.48	0.46
25000	200	10	3.13	3.75	4.58	5.47	6.21	6.68	6.84	6.79	6.6	6.33	6.01	5.65	5.24	4.75	4.16	3.43	2.54
25000	200	20	3.03	3.52	4.12	4.71	5.18	5.44	5.51	5.48	5.38	5.24	5.07	4.86	4.59	4.25	3.8	3.21	2.46
25000	200	50	2.79	3.06	3.32	3.56	3.72	3.8	3.82	3.8	3.78	3.74	3.69	3.62	3.51	3.35	3.1	2.75	2.27
25000	200	100	2.22	2.36	2.45	2.5	2.53	2.55	2.58	2.59	2.59	2.57	2.56	2.53	2.49	2.41	2.28	2.09	1.81
25000	200	200	1.54	1.64	1.7	1.72	1.72	1.73	1.76	1.79	1.8	1.81	1.81	1.8	1.76	1.69	1.59	1.47	1.34
25000	200	300	1.04	1.14	1.21	1.24	1.23	1.23	1.26	1.31	1.35	1.38	1.4	1.4	1.37	1.32	1.24	1.17	1.11
25000	200	400	0.81	0.86	0.91	0.94	0.96	0.98	1.01	1.06	1.1	1.13	1.15	1.15	1.14	1.11	1.08	1.04	1.01
25000	200	500	0.72	0.75	0.77	0.8	0.84	0.87	0.91	0.95	0.99	1.01	1.02	1.03	1.02	1.01	1	0.98	0.96
25000	400	10	5.88	7.05	8.31	9.79	11.2	12.1	12.5	12.4	12.1	11.6	11.1	10.4	9.68	8.81	7.83	6.71	5.38
25000	400	20	5.61	6.53	7.44	8.45	9.38	9.92	10.1	10	9.87	9.63	9.34	8.96	8.47	7.87	7.14	6.26	5.14
25000	400	50	5.1	5.63	6.07	6.45	6.76	6.92	6.98	6.98	6.94	6.89	6.81	6.69	6.51	6.24	5.86	5.31	4.54
25000	400	100	4.07	4.29	4.44	4.53	4.6	4.66	4.7	4.71	4.69	4.66	4.63	4.59	4.52	4.41	4.24	3.95	3.48
25000	400	200	2.84	2.96	3.04	3.09	3.11	3.15	3.19	3.21	3.18	3.15	3.12	3.08	3.03	2.96	2.85	2.71	2.5
25000	400	300	1.96	2.04	2.13	2.17	2.17	2.19	2.23	2.28	2.31	2.33	2.33	2.32	2.28	2.23	2.16	2.09	2
25000	400	400	1.49	1.54	1.6	1.64	1.68	1.72	1.78	1.85	1.91	1.95	1.97	1.97	1.95	1.92	1.88	1.84	1.8

P kPa	G Kg/m^{2}s	ΔT_w K	H_b, kJ/kg 1000	1400	1600	1800	1900	2000	2050	2100	2150	2200	2250	2300	2400	2500	2600	2700	3000
25000	400	500	1.29	1.33	1.37	1.42	1.48	1.54	1.61	1.68	1.74	1.78	1.8	1.81	1.8	1.79	1.77	1.74	1.71
25000	700	10	9.39	10.5	11.5	13.8	16.7	18.7	19.5	19.6	19.3	18.9	18.3	17.1	15.5	13.6	11.8	10	8.18
25000	700	20	9.03	9.87	10.6	12.2	14.3	15.4	15.8	15.8	15.7	15.4	14.9	14.2	13.1	11.9	10.6	9.26	7.74
25000	700	50	8.28	8.9	9.38	9.96	10.5	10.8	11	11.1	11	10.8	10.5	10.2	9.79	9.24	8.58	7.78	6.73
25000	700	100	6.67	6.96	7.13	7.24	7.3	7.34	7.41	7.51	7.45	7.25	7.1	6.96	6.8	6.58	6.29	5.89	5.28
25000	700	200	4.69	4.82	4.92	4.97	4.99	5.02	5.05	5.08	5.03	4.93	4.83	4.74	4.63	4.51	4.39	4.23	3.99
25000	700	300	3.23	3.32	3.41	3.47	3.48	3.51	3.58	3.64	3.66	3.65	3.61	3.55	3.48	3.4	3.34	3.29	3.22
25000	700	400	2.41	2.46	2.54	2.6	2.66	2.74	2.84	2.94	3.01	3.05	3.06	3.05	3.02	2.98	2.94	2.9	2.85
25000	700	500	2.06	2.1	2.16	2.24	2.33	2.44	2.56	2.66	2.75	2.8	2.83	2.84	2.83	2.81	2.78	2.74	2.7
25000	1000	10	14.4	14.9	16.7	20.1	24	26.9	28.1	28.4	28.3	28	27.1	25.3	22.5	19.3	16.3	13.7	10.9
25000	1000	20	13.5	14.1	15.5	18.2	21	22.6	23	23.2	23.1	22.6	21.8	20.6	18.7	16.6	14.5	12.3	9.93
25000	1000	50	12	12.6	13.6	14.7	15.6	16	16.3	17	17	16.1	15.2	14.4	13.6	12.7	11.5	10.2	8.62
25000	1000	100	9.37	9.83	10.2	10.4	10.5	10.5	10.8	11.4	11.4	10.8	10	9.62	9.3	8.93	8.49	7.93	7.12
25000	1000	200	6.51	6.76	6.89	6.95	6.94	6.92	6.98	7.14	7.15	6.96	6.71	6.51	6.31	6.14	6	5.87	5.66
25000	1000	300	4.48	4.61	4.7	4.77	4.83	4.89	4.97	5.05	5.1	5.09	5	4.86	4.71	4.6	4.56	4.57	4.62
25000	1000	400	3.4	3.47	3.55	3.64	3.76	3.89	4.04	4.18	4.28	4.32	4.31	4.26	4.19	4.13	4.09	4.08	4.08
25000	1000	500	2.95	3	3.08	3.19	3.33	3.5	3.66	3.81	3.93	4.01	4.04	4.04	4.02	3.99	3.95	3.91	3.86
25000	1500	10	19.6	18.6	23.2	30.2	35.5	38.2	39.2	39.3	39	38.2	36.8	34.4	30.7	26.4	22.3	18.4	14.1
25000	1500	20	18.4	18.3	22.4	28.1	32.2	33.7	33.6	33.4	32.9	31.8	30.1	28.3	25.9	22.9	19.8	16.7	13
25000	1500	50	16.4	16.6	19.1	22.2	23.9	24.3	24.2	24.8	25.2	24.4	22	20.3	19	17.6	15.9	13.9	11.5
25000	1500	100	13	13.5	14.3	15	15.2	15.2	15.6	16.8	17.6	17	14.9	13.6	13	12.5	11.8	10.9	9.6
25000	1500	200	8.96	9.36	9.64	9.79	9.81	9.76	9.86	10.2	10.4	10.2	9.63	9.22	8.96	8.72	8.48	8.16	7.66
25000	1500	300	6.08	6.27	6.45	6.61	6.74	6.86	6.99	7.11	7.2	7.21	7.12	6.96	6.79	6.65	6.55	6.46	6.35
25000	1500	400	4.67	4.76	4.88	5.03	5.23	5.45	5.67	5.87	6.02	6.1	6.1	6.04	5.95	5.87	5.8	5.74	5.67
25000	1500	500	4.11	4.17	4.28	4.44	4.64	4.88	5.12	5.33	5.49	5.6	5.66	5.66	5.63	5.59	5.53	5.47	5.38
25000	2000	10	23.4	25.1	32.3	41.8	48.8	52.5	54.2	54.5	53.4	51	48.6	45.8	41.7	36.6	31	25	18.3
25000	2000	20	22.6	24.9	31.6	39.7	45.5	48.4	49.8	50	47.8	43.4	40.1	38.1	35.4	31.8	27.8	23.2	17.6
25000	2000	50	21.2	22.5	26.8	31.6	34.6	35.8	36.4	36.8	35.5	32.4	29.2	27.4	26.1	24.3	22.2	19.5	16.1
25000	2000	100	17.3	18.3	19.9	21.1	21.6	21.6	22.2	23.6	23.7	22.3	19.9	18.6	18	17.3	16.4	15.1	13.3
25000	2000	200	12	12.8	13.3	13.7	13.7	13.6	13.7	14	14.2	13.9	13.3	13	12.7	12.4	12.1	11.4	10.4
25000	2000	300	8.23	8.59	8.91	9.15	9.33	9.49	9.67	9.85	10	10.1	10.1	9.97	9.84	9.69	9.48	9.18	8.69
25000	2000	400	6.37	6.52	6.7	6.92	7.18	7.49	7.8	8.08	8.3	8.44	8.5	8.49	8.42	8.32	8.2	8.03	7.79
25000	2000	500	5.61	5.71	5.87	6.08	6.36	6.69	7.02	7.31	7.54	7.7	7.79	7.81	7.78	7.72	7.64	7.53	7.38
25000	3000	10	32	38.9	49.6	61.2	70.5	76.2	78.6	79	77.9	75.4	72	67.1	60.3	52.1	43.4	34.5	24.9
25000	3000	20	31.1	38	48.5	59.4	67.1	70.5	70.6	69.1	66.4	62.3	59	55.9	51.3	45.5	39	32	24.2
25000	3000	50	29	34.3	41.6	48.6	52.6	53.5	52.9	51	48.2	44.2	41.6	40	37.8	34.7	31.1	27	22.2
25000	3000	100	24	27.2	30.8	33.6	34.5	34.2	33.3	31.7	30.3	29.1	28	27.3	26.3	25	23.3	21.2	18.6
25000	3000	200	17	18.4	19.7	20.5	20.6	20.6	20.4	20.1	20	19.9	19.7	19.3	18.9	18.3	17.6	16.5	15.1
25000	3000	300	11.9	12.4	12.9	13.3	13.6	13.9	14.2	14.5	14.8	14.9	15	14.9	14.7	14.4	14	13.5	12.7
25000	3000	400	9.24	9.48	9.75	10.1	10.5	10.9	11.4	11.8	12.1	12.4	12.5	12.5	12.4	12.2	12	11.8	11.4
25000	3000	500	8.14	8.31	8.54	8.86	9.27	9.74	10.2	10.6	11	11.2	11.3	11.4	11.4	11.3	11.1	11	10.7
25000	5000	10	44.8	56.7	72.3	88.4	102	111	115	116	114	110	104	95.7	84.8	72.3	59.4	46.2	32.2
25000	5000	20	43.3	55.3	70.4	84.8	94.8	99	98.1	94	91.1	88.7	85.4	80.2	72.8	63.6	53.3	42.4	30.5
25000	5000	50	39.4	50.3	61	70.2	75.4	76.5	73.4	66.9	63.3	62.2	61	58.8	54.9	49.5	43.1	36	27.7
25000	5000	100	32	39.5	45.4	49.7	51.7	52.1	50	45	42.4	42.1	41.7	40.7	38.8	36.2	32.9	29.1	24.3
25000	5000	200	23	25.3	26.9	28	28.8	29.4	29.6	29	28.9	29.1	29	28.6	27.8	26.6	25.2	23.4	21
25000	5000	300	16.7	17.2	17.7	18.2	18.8	19.6	20.4	21	21.6	21.9	22	21.9	21.5	21	20.4	19.6	18.4
25000	5000	400	13.4	13.7	14.1	14.6	15.2	15.9	16.7	17.4	17.9	18.2	18.4	18.4	18.3	18	17.7	17.3	16.7

P kPa	G Kg/m^{2}s	ΔT_w K	H_b, kJ/kg																
			1000	1400	1600	1800	1900	2000	2050	2100	2150	2200	2250	2300	2400	2500	2600	2700	3000
25000	5000	500	12	12.2	12.6	13	13.7	14.4	15.1	15.7	16.2	16.6	16.8	16.8	16.8	16.7	16.5	16.2	15.9
26000	100	10	1.29	1.59	2.01	2.47	2.87	3.15	3.29	3.32	3.26	3.14	2.96	2.7	2.39	2.05	1.7	1.34	0.93
26000	100	20	1.25	1.49	1.81	2.14	2.42	2.61	2.69	2.71	2.68	2.59	2.46	2.27	2.05	1.79	1.52	1.23	0.89
26000	100	50	1.14	1.28	1.45	1.61	1.74	1.83	1.88	1.9	1.9	1.86	1.78	1.68	1.56	1.42	1.25	1.05	0.82
26000	100	100	0.94	1	1.05	1.11	1.16	1.2	1.24	1.27	1.29	1.28	1.25	1.22	1.18	1.11	1	0.87	0.72
26000	100	200	0.69	0.7	0.72	0.74	0.77	0.8	0.84	0.87	0.9	0.92	0.93	0.92	0.91	0.87	0.8	0.71	0.62
26000	100	300	0.5	0.51	0.52	0.54	0.55	0.58	0.6	0.64	0.67	0.69	0.71	0.72	0.72	0.69	0.64	0.59	0.54
26000	100	400	0.4	0.41	0.42	0.43	0.45	0.47	0.49	0.51	0.53	0.55	0.56	0.57	0.57	0.56	0.54	0.51	0.49
26000	100	500	0.36	0.37	0.38	0.39	0.4	0.42	0.44	0.45	0.47	0.48	0.49	0.49	0.5	0.49	0.49	0.48	0.47
26000	200	10	2.96	3.56	4.36	5.22	5.98	6.48	6.69	6.67	6.5	6.22	5.87	5.45	4.97	4.43	3.82	3.12	2.31
26000	200	20	2.88	3.38	4	4.61	5.1	5.39	5.51	5.49	5.38	5.21	4.99	4.73	4.4	4	3.54	2.98	2.3
26000	200	50	2.65	2.95	3.26	3.53	3.73	3.84	3.88	3.88	3.85	3.79	3.72	3.61	3.46	3.27	3	2.66	2.2
26000	200	100	2.13	2.27	2.38	2.48	2.55	2.6	2.63	2.65	2.64	2.62	2.6	2.56	2.5	2.41	2.28	2.09	1.81
26000	200	200	1.52	1.58	1.65	1.69	1.73	1.76	1.8	1.82	1.82	1.82	1.81	1.79	1.76	1.7	1.61	1.51	1.37
26000	200	300	1.09	1.13	1.18	1.21	1.23	1.25	1.28	1.31	1.34	1.35	1.36	1.36	1.35	1.31	1.25	1.19	1.13
26000	200	400	0.85	0.88	0.91	0.93	0.95	0.98	1.01	1.05	1.08	1.1	1.12	1.13	1.12	1.11	1.08	1.05	1.02
26000	200	500	0.75	0.76	0.79	0.81	0.84	0.87	0.91	0.94	0.97	0.99	1.01	1.02	1.02	1.01	1	0.99	0.97
26000	400	10	5.51	6.58	7.82	9.29	10.7	11.7	12.1	12.1	11.7	11.3	10.7	9.91	9.02	8.04	6.98	5.85	4.58
26000	400	20	5.3	6.23	7.18	8.25	9.21	9.79	10	9.98	9.79	9.49	9.12	8.64	8.05	7.35	6.56	5.66	4.59
26000	400	50	4.84	5.44	5.98	6.46	6.82	7.03	7.12	7.12	7.07	6.99	6.87	6.7	6.47	6.15	5.73	5.18	4.42
26000	400	100	3.93	4.18	4.41	4.6	4.74	4.84	4.9	4.92	4.88	4.83	4.78	4.73	4.65	4.52	4.32	4.01	3.52
26000	400	200	2.85	2.93	3.04	3.15	3.24	3.32	3.38	3.37	3.32	3.27	3.22	3.18	3.13	3.05	2.93	2.78	2.54
26000	400	300	2.07	2.09	2.14	2.2	2.24	2.28	2.33	2.36	2.37	2.36	2.36	2.35	2.32	2.27	2.2	2.13	2.03
26000	400	400	1.57	1.59	1.62	1.66	1.7	1.75	1.8	1.85	1.9	1.93	1.96	1.96	1.96	1.94	1.91	1.87	1.82
26000	400	500	1.34	1.36	1.4	1.44	1.49	1.55	1.61	1.67	1.72	1.75	1.78	1.8	1.8	1.79	1.78	1.75	1.72
26000	700	10	8.84	9.85	10.9	13.1	16	18.1	18.9	19	18.7	18.1	17.3	16.1	14.5	12.6	10.8	8.92	6.9
26000	700	20	8.57	9.42	10.1	11.8	13.9	15.1	15.5	15.6	15.4	15	14.4	13.6	12.5	11.2	9.88	8.44	6.78
26000	700	50	7.96	8.66	9.22	9.88	10.5	10.8	11	11.1	11.1	10.8	10.5	10.1	9.65	9.05	8.33	7.46	6.33
26000	700	100	6.54	6.86	7.1	7.28	7.39	7.46	7.55	7.65	7.58	7.36	7.19	7.06	6.88	6.62	6.29	5.83	5.16
26000	700	200	4.72	4.81	4.92	5.03	5.1	5.16	5.2	5.21	5.14	5.03	4.94	4.86	4.76	4.62	4.46	4.25	3.94
26000	700	300	3.36	3.37	3.44	3.5	3.55	3.6	3.65	3.69	3.71	3.69	3.67	3.63	3.58	3.51	3.43	3.34	3.23
26000	700	400	2.51	2.53	2.58	2.64	2.7	2.77	2.85	2.93	3	3.04	3.06	3.07	3.05	3.03	2.99	2.94	2.88
26000	700	500	2.12	2.16	2.21	2.28	2.36	2.45	2.55	2.63	2.71	2.77	2.81	2.83	2.83	2.82	2.8	2.77	2.72
26000	1000	10	13.6	14.7	16.4	19.5	23.2	26	27.2	27.5	27.2	26.6	25.5	23.6	21	18.1	15.3	12.5	9.42
26000	1000	20	13	14.2	15.6	18	20.6	22.2	22.7	22.8	22.6	22	21	19.7	17.9	15.9	13.7	11.5	8.86
26000	1000	50	11.8	12.8	13.8	14.8	15.6	16	16.4	17.1	17.1	16.1	15	14.2	13.4	12.4	11.2	9.74	7.97
26000	1000	100	9.43	9.91	10.2	10.4	10.5	10.5	10.8	11.6	11.7	10.9	10.1	9.72	9.39	8.97	8.42	7.72	6.73
26000	1000	200	6.52	6.7	6.81	6.87	6.89	6.91	7.01	7.21	7.25	7.08	6.88	6.73	6.58	6.39	6.17	5.88	5.48
26000	1000	300	4.52	4.58	4.66	4.74	4.82	4.9	4.99	5.08	5.15	5.17	5.14	5.08	4.99	4.89	4.8	4.71	4.6
26000	1000	400	3.47	3.51	3.58	3.67	3.78	3.91	4.04	4.16	4.26	4.32	4.35	4.34	4.31	4.27	4.23	4.18	4.12
26000	1000	500	3.03	3.07	3.15	3.24	3.36	3.5	3.64	3.77	3.88	3.96	4.01	4.04	4.04	4.03	4	3.96	3.9
26000	1500	10	18.7	21	25.3	30.5	34.9	37.5	38.5	38.6	38	36.7	34.9	32.4	29	25	21	17	12.5
26000	1500	20	17.9	20.8	24.8	29.1	32.5	33.9	33.7	33.4	32.8	31.3	29.4	27.4	24.9	22	19	15.7	11.9
26000	1500	50	16.3	18.1	20.6	23	24.5	24.9	24.6	25.2	25.7	24.7	22.1	20.2	18.9	17.4	15.6	13.5	10.9
26000	1500	100	13	13.8	14.5	15.1	15.4	15.4	15.8	17.2	18.1	17.4	15.2	13.9	13.3	12.7	11.9	10.8	9.25
26000	1500	200	8.91	9.22	9.46	9.61	9.67	9.69	9.85	10.3	10.5	10.4	9.89	9.56	9.37	9.13	8.79	8.29	7.51
26000	1500	300	6.11	6.24	6.39	6.54	6.68	6.81	6.95	7.08	7.2	7.26	7.26	7.2	7.12	7	6.85	6.65	6.35
26000	1500	400	4.77	4.84	4.94	5.08	5.25	5.44	5.63	5.81	5.95	6.05	6.1	6.1	6.07	6.02	5.95	5.86	5.73

P	G	ΔT_w	H_b, kJ/kg																
kPa	Kg/m^{2}s	K	1000	1400	1600	1800	1900	2000	2050	2100	2150	2200	2250	2300	2400	2500	2600	2700	3000
26000	1500	500	4.22	4.28	4.38	4.51	4.69	4.88	5.08	5.26	5.41	5.53	5.6	5.64	5.65	5.63	5.59	5.52	5.43
26000	2000	10	22.8	27.2	34.3	42.2	48.4	52.1	53.7	53.9	52.3	49.4	46.4	43.1	38.9	33.9	28.5	22.8	16.4
26000	2000	20	22.2	27	33.7	40.7	46	48.9	50.2	50.4	48	43.1	39.3	36.7	33.7	30.1	26	21.5	16.3
26000	2000	50	20.8	23.7	27.9	32.2	35.1	36.4	36.9	37.3	36	32.8	29.3	27.3	25.8	23.9	21.7	19	15.7
26000	2000	100	17	18.3	19.8	21.1	21.7	21.9	22.5	23.9	24.1	22.7	20.2	18.8	18.3	17.6	16.6	15.2	13.2
26000	2000	200	12	12.5	13	13.3	13.5	13.4	13.6	14.1	14.2	14	13.5	13.2	13	12.8	12.4	11.7	10.5
26000	2000	300	8.38	8.59	8.83	9.05	9.23	9.4	9.57	9.75	9.91	10	10.1	10.1	10	9.89	9.69	9.34	8.75
26000	2000	400	6.55	6.65	6.8	6.99	7.22	7.47	7.74	7.98	8.18	8.34	8.43	8.47	8.45	8.39	8.29	8.12	7.86
26000	2000	500	5.78	5.86	6	6.18	6.42	6.69	6.96	7.21	7.42	7.59	7.7	7.76	7.77	7.75	7.69	7.59	7.45
26000	3000	10	31.6	38.6	48.9	60	69.1	74.9	77.2	77.3	75.6	72.5	68.5	63.4	56.7	48.9	40.8	32.3	23.1
26000	3000	20	31	38.4	48.6	58.8	66.4	70	70.3	69	66.1	61.3	57.3	53.7	49	43.2	36.9	30.3	22.8
26000	3000	50	29	34.8	41.5	47.8	51.6	52.8	52.5	51.3	48.7	44.4	41.4	39.5	37.1	34	30.4	26.4	21.7
26000	3000	100	23.9	27	30.4	33.1	34.1	34	33.2	31.7	30.4	29.2	28.1	27.3	26.3	25	23.4	21.4	18.7
26000	3000	200	17.2	18.2	19.2	19.9	20.2	20.2	20	19.8	19.7	19.6	19.5	19.3	18.9	18.5	17.8	16.8	15.3
26000	3000	300	12.2	12.5	12.8	13.1	13.4	13.6	13.9	14.2	14.5	14.7	14.7	14.7	14.6	14.4	14.1	13.6	12.8
26000	3000	400	9.55	9.69	9.9	10.2	10.5	10.9	11.3	11.6	11.9	12.2	12.3	12.4	12.4	12.3	12.1	11.9	11.5
26000	3000	500	8.42	8.54	8.73	9	9.35	9.74	10.1	10.5	10.8	11	11.2	11.3	11.3	11.3	11.2	11.1	10.8
26000	5000	10	45	55.4	70.2	86	99.6	109	113	113	111	107	101	92.9	82.5	70.8	58.7	46.2	32.4
26000	5000	20	43.9	54.5	68.8	82.6	92.5	97.2	96.7	92.9	89.9	87.4	83.7	78.3	70.9	62.1	52.5	42.4	30.8
26000	5000	50	40.4	50.3	59.7	67.8	72.9	74.5	72	66.1	62.8	61.6	60	57.4	53.5	48.4	42.5	35.9	28
26000	5000	100	33.1	39.5	44.6	48.7	51	51.6	49.6	44.5	41.8	41.4	40.9	39.9	38.1	35.7	32.7	29.1	24.6
26000	5000	200	24.2	25.7	27	28	28.8	29.3	29.4	28.6	28.4	28.6	28.6	28.2	27.5	26.5	25.2	23.5	21.2
26000	5000	300	17.6	17.8	18.1	18.4	18.9	19.6	20.2	20.8	21.2	21.6	21.7	21.7	21.5	21.1	20.5	19.7	18.6
26000	5000	400	14	14.2	14.4	14.8	15.3	16	16.6	17.1	17.6	17.9	18.2	18.3	18.2	18.1	17.8	17.4	16.9
26000	5000	500	12.5	12.6	12.9	13.3	13.8	14.4	15	15.5	16	16.3	16.6	16.7	16.7	16.7	16.6	16.3	16
28000	100	10	1.27	1.54	1.92	2.32	2.7	2.97	3.11	3.14	3.1	3	2.83	2.61	2.33	2.02	1.69	1.34	0.95
28000	100	20	1.24	1.47	1.76	2.06	2.32	2.49	2.57	2.59	2.56	2.48	2.37	2.21	2	1.77	1.51	1.24	0.91
28000	100	50	1.15	1.3	1.45	1.59	1.7	1.77	1.81	1.82	1.81	1.77	1.72	1.63	1.52	1.39	1.23	1.05	0.83
28000	100	100	0.96	1.02	1.07	1.11	1.15	1.17	1.19	1.21	1.21	1.21	1.19	1.16	1.11	1.05	0.96	0.86	0.73
28000	100	200	0.71	0.73	0.74	0.75	0.77	0.78	0.8	0.82	0.84	0.85	0.85	0.84	0.83	0.8	0.75	0.7	0.63
28000	100	300	0.52	0.53	0.54	0.55	0.56	0.57	0.59	0.61	0.63	0.64	0.65	0.65	0.65	0.64	0.61	0.58	0.55
28000	100	400	0.42	0.42	0.43	0.44	0.45	0.47	0.48	0.5	0.51	0.53	0.54	0.54	0.54	0.54	0.53	0.52	0.5
28000	100	500	0.37	0.38	0.38	0.4	0.41	0.42	0.44	0.45	0.46	0.47	0.48	0.49	0.49	0.49	0.49	0.48	0.47
28000	200	10	2.89	3.47	4.23	5.03	5.73	6.22	6.47	6.5	6.38	6.14	5.81	5.37	4.84	4.24	3.6	2.91	2.12
28000	200	20	2.8	3.32	3.92	4.5	4.97	5.28	5.41	5.41	5.32	5.15	4.92	4.62	4.23	3.79	3.3	2.75	2.09
28000	200	50	2.58	2.89	3.2	3.48	3.68	3.79	3.85	3.85	3.81	3.74	3.64	3.5	3.31	3.07	2.79	2.44	1.99
28000	200	100	2.12	2.22	2.32	2.41	2.49	2.54	2.58	2.59	2.58	2.56	2.52	2.47	2.4	2.29	2.15	1.96	1.69
28000	200	200	1.56	1.56	1.59	1.63	1.67	1.71	1.75	1.77	1.77	1.76	1.75	1.74	1.7	1.65	1.58	1.48	1.35
28000	200	300	1.14	1.13	1.14	1.17	1.19	1.23	1.26	1.28	1.3	1.31	1.32	1.32	1.31	1.29	1.25	1.2	1.14
28000	200	400	0.89	0.89	0.91	0.93	0.95	0.98	1.01	1.04	1.06	1.08	1.1	1.11	1.11	1.1	1.09	1.06	1.03
28000	200	500	0.78	0.79	0.8	0.82	0.85	0.88	0.91	0.94	0.96	0.98	1	1.01	1.01	1.01	1.01	1	0.98
28000	400	10	5.31	6.44	7.76	9.13	10.3	11.2	11.6	11.6	11.4	11	10.4	9.61	8.65	7.58	6.46	5.27	3.93
28000	400	20	5.13	6.14	7.18	8.19	9	9.51	9.74	9.73	9.55	9.25	8.84	8.31	7.64	6.86	6.01	5.06	3.95
28000	400	50	4.71	5.3	5.86	6.33	6.67	6.88	6.97	6.97	6.9	6.77	6.6	6.37	6.07	5.68	5.21	4.61	3.84
28000	400	100	3.91	4.05	4.23	4.41	4.57	4.68	4.75	4.76	4.72	4.66	4.59	4.51	4.4	4.24	4	3.68	3.21
28000	400	200	2.91	2.86	2.9	2.99	3.1	3.19	3.25	3.26	3.22	3.18	3.15	3.11	3.06	2.97	2.85	2.69	2.46
28000	400	300	2.14	2.07	2.08	2.12	2.18	2.24	2.29	2.32	2.33	2.34	2.34	2.33	2.31	2.27	2.21	2.14	2.03
28000	400	400	1.63	1.61	1.62	1.66	1.7	1.75	1.8	1.85	1.89	1.92	1.94	1.95	1.96	1.95	1.92	1.89	1.83

P kPa	G Kg/m^{2}s	ΔT_w K	H_b, kJ/kg 1000	1400	1600	1800	1900	2000	2050	2100	2150	2200	2250	2300	2400	2500	2600	2700	3000
28000	400	500	1.39	1.4	1.42	1.46	1.51	1.56	1.61	1.66	1.7	1.74	1.77	1.79	1.8	1.8	1.79	1.77	1.74
28000	700	10	8.5	9.9	11.6	13.7	15.8	17.3	18.1	18.2	18	17.4	16.5	15.3	13.7	11.9	10.1	8.17	5.99
28000	700	20	8.29	9.47	10.8	12.2	13.7	14.6	15	15.1	14.9	14.5	13.9	13	11.9	10.6	9.24	7.71	5.91
28000	700	50	7.74	8.45	9.1	9.7	10.2	10.5	10.7	10.7	10.6	10.4	10.1	9.72	9.21	8.56	7.77	6.82	5.62
28000	700	100	6.46	6.64	6.8	6.95	7.07	7.17	7.25	7.28	7.22	7.09	6.97	6.84	6.65	6.36	5.97	5.46	4.77
28000	700	200	4.76	4.69	4.72	4.79	4.87	4.95	5	5.01	4.97	4.92	4.87	4.82	4.73	4.59	4.4	4.16	3.82
28000	700	300	3.44	3.35	3.36	3.4	3.46	3.53	3.59	3.63	3.65	3.67	3.67	3.66	3.63	3.57	3.49	3.37	3.22
28000	700	400	2.59	2.57	2.59	2.64	2.7	2.77	2.84	2.92	2.98	3.03	3.06	3.08	3.08	3.07	3.03	2.98	2.9
28000	700	500	2.2	2.22	2.26	2.31	2.38	2.46	2.55	2.62	2.69	2.75	2.79	2.82	2.84	2.84	2.83	2.8	2.75
28000	1000	10	12.7	14.4	16.8	19.8	22.7	24.9	26	26.2	25.9	25.2	23.9	22.1	19.8	17.2	14.5	11.6	8.38
28000	1000	20	12.4	13.9	15.8	17.9	19.9	21.2	21.7	21.8	21.5	20.9	20	18.7	17	15.1	13	10.7	8.03
28000	1000	50	11.6	12.6	13.5	14.3	15	15.3	15.5	15.6	15.4	15	14.4	13.8	12.9	11.9	10.7	9.22	7.37
28000	1000	100	9.51	9.83	10	10.1	10.1	10.1	10.2	10.3	10.3	10	9.77	9.56	9.27	8.84	8.25	7.45	6.37
28000	1000	200	6.67	6.69	6.7	6.7	6.71	6.74	6.8	6.88	6.91	6.88	6.83	6.79	6.69	6.51	6.25	5.87	5.34
28000	1000	300	4.66	4.63	4.65	4.7	4.77	4.86	4.96	5.05	5.13	5.18	5.21	5.21	5.17	5.1	4.99	4.83	4.6
28000	1000	400	3.59	3.6	3.64	3.71	3.81	3.93	4.04	4.15	4.25	4.32	4.37	4.4	4.4	4.38	4.34	4.26	4.16
28000	1000	500	3.13	3.16	3.22	3.3	3.41	3.53	3.65	3.76	3.85	3.94	4	4.04	4.06	4.06	4.04	4	3.94
28000	1500	10	17.6	20.4	24.4	28.8	32.7	35.4	36.7	36.9	36.3	35.1	33.3	30.7	27.5	23.9	20.1	16.1	11.6
28000	1500	20	17.1	19.8	23.1	26.5	29.2	30.8	31.3	31.2	30.7	29.6	28.1	26.2	23.9	21.2	18.2	15	11.3
28000	1500	50	15.9	17.6	19.4	20.9	22	22.5	22.5	22.5	22.4	21.8	20.7	19.6	18.4	16.9	15.1	13.1	10.5
28000	1500	100	13.1	13.7	14.1	14.5	14.6	14.6	14.7	14.9	15.1	14.8	14.2	13.7	13.2	12.6	11.8	10.6	8.98
28000	1500	200	9.15	9.25	9.34	9.42	9.46	9.5	9.56	9.69	9.8	9.81	9.73	9.66	9.54	9.32	8.94	8.34	7.43
28000	1500	300	6.35	6.36	6.42	6.52	6.65	6.78	6.91	7.04	7.16	7.26	7.33	7.35	7.32	7.24	7.07	6.8	6.39
28000	1500	400	4.94	4.97	5.04	5.16	5.3	5.47	5.63	5.79	5.92	6.03	6.11	6.16	6.17	6.14	6.08	5.96	5.79
28000	1500	500	4.36	4.4	4.48	4.6	4.75	4.91	5.08	5.24	5.37	5.49	5.58	5.64	5.67	5.67	5.64	5.58	5.49
28000	2000	10	22	26.7	33.1	39.9	45.5	49.2	50.9	51	49.9	47.8	45.1	41.7	37.4	32.5	27.4	22	15.9
28000	2000	20	21.7	25.9	31.2	36.6	40.8	43.2	44.1	44	42.8	40.5	38.2	35.7	32.6	29	25.1	20.9	15.9
28000	2000	50	20.5	22.9	25.9	28.7	30.6	31.5	31.7	31.5	30.8	29.6	28.1	26.8	25.3	23.4	21.2	18.6	15.3
28000	2000	100	17	17.9	18.9	19.7	20.2	20.3	20.3	20.5	20.4	19.9	19.2	18.7	18.2	17.5	16.5	15.1	13
28000	2000	200	12.2	12.4	12.7	13	13.1	13.2	13.2	13.3	13.4	13.4	13.3	13.2	13.1	12.9	12.5	11.7	10.4
28000	2000	300	8.71	8.73	8.85	9.01	9.18	9.36	9.52	9.69	9.84	9.96	10.1	10.1	10.1	10	9.8	9.43	8.8
28000	2000	400	6.81	6.83	6.93	7.08	7.28	7.51	7.73	7.94	8.13	8.28	8.39	8.46	8.48	8.45	8.36	8.2	7.94
28000	2000	500	5.98	6.03	6.14	6.3	6.51	6.74	6.96	7.18	7.37	7.52	7.64	7.73	7.77	7.78	7.74	7.66	7.52
28000	3000	10	30.9	37.2	46.2	55.9	64.4	70.1	72.9	73.4	72.1	69.5	65.8	60.8	54.4	47.2	39.6	31.7	22.7
28000	3000	20	30.4	36.2	43.8	51.5	57.5	61.1	62.4	62.1	60.7	58.3	55.4	51.8	47.2	41.8	36	29.7	22.4
28000	3000	50	28.7	32.6	36.9	40.8	43.5	44.8	45	44.6	43.6	42	40.4	38.6	36.2	33.3	29.9	26	21.3
28000	3000	100	24.2	25.7	27.3	28.7	29.4	29.6	29.4	29	28.6	28.2	27.7	27.1	26.1	24.9	23.3	21.2	18.5
28000	3000	200	17.7	18	18.3	18.7	18.9	19.1	19.1	19.2	19.3	19.3	19.3	19.2	18.9	18.4	17.8	16.8	15.2
28000	3000	300	12.7	12.7	12.8	13	13.2	13.5	13.8	14.1	14.3	14.5	14.6	14.7	14.6	14.5	14.2	13.7	12.9
28000	3000	400	9.94	9.96	10.1	10.3	10.6	10.9	11.2	11.5	11.8	12	12.2	12.3	12.3	12.3	12.2	11.9	11.6
28000	3000	500	8.72	8.79	8.94	9.17	9.47	9.8	10.1	10.4	10.7	11	11.1	11.3	11.3	11.3	11.3	11.1	11
28000	5000	10	44.2	53.2	65.9	80	92.7	102	107	108	106	103	97.2	89.7	80.1	69.3	58.1	46.2	32.6
28000	5000	20	43.4	51.7	62.3	73	81.8	87.3	89.3	88.9	87.3	84.9	81.2	75.9	68.9	60.8	52	42.4	31.2
28000	5000	50	40.9	46.9	52.7	57.9	61.6	63.6	63.8	62.5	61.4	60.3	58.6	56	52.2	47.6	42.2	36	28.4
28000	5000	100	34.7	37.2	39.2	41	42.1	42.7	42.6	41.5	41	40.7	40.2	39.2	37.5	35.4	32.7	29.3	24.9
28000	5000	200	25.9	26	26.2	26.5	26.9	27.4	27.7	27.9	28.1	28.2	28.2	28	27.4	26.5	25.3	23.7	21.5
28000	5000	300	18.8	18.6	18.6	18.8	19.1	19.6	20.1	20.6	21	21.4	21.5	21.6	21.4	21.1	20.6	19.9	18.8
28000	5000	400	14.7	14.7	14.8	15.1	15.6	16.1	16.6	17	17.5	17.8	18	18.2	18.2	18.1	17.9	17.6	17.1

P	*G*	ΔT_w	H_b, kJ/kg																
kPa	Kg/m²s	K	1000	1400	1600	1800	1900	2000	2050	2100	2150	2200	2250	2300	2400	2500	2600	2700	3000
28000	5000	500	12.9	13	13.2	13.5	14	14.5	15	15.4	15.8	16.2	16.4	16.6	16.7	16.7	16.6	16.5	16.2
30000	100	10	1.26	1.51	1.85	2.22	2.57	2.84	2.99	3.03	2.99	2.9	2.75	2.55	2.29	1.99	1.68	1.35	0.96
30000	100	20	1.23	1.46	1.73	2.01	2.25	2.41	2.5	2.52	2.49	2.42	2.32	2.17	1.98	1.75	1.51	1.24	0.92
30000	100	50	1.16	1.31	1.45	1.58	1.68	1.74	1.77	1.78	1.76	1.74	1.68	1.61	1.5	1.38	1.23	1.05	0.84
30000	100	100	0.99	1.04	1.09	1.12	1.14	1.16	1.17	1.18	1.19	1.18	1.16	1.13	1.09	1.03	0.96	0.86	0.73
30000	100	200	0.73	0.75	0.75	0.76	0.77	0.78	0.8	0.81	0.82	0.82	0.82	0.82	0.8	0.78	0.74	0.7	0.63
30000	100	300	0.54	0.54	0.55	0.55	0.56	0.58	0.59	0.6	0.61	0.62	0.63	0.63	0.63	0.62	0.61	0.58	0.55
30000	100	400	0.43	0.43	0.44	0.45	0.46	0.47	0.48	0.5	0.51	0.52	0.53	0.53	0.53	0.53	0.53	0.52	0.5
30000	100	500	0.38	0.38	0.39	0.4	0.41	0.43	0.44	0.45	0.46	0.47	0.48	0.48	0.49	0.49	0.49	0.48	0.48
30000	200	10	2.84	3.42	4.14	4.88	5.52	5.99	6.24	6.29	6.2	6	5.7	5.28	4.75	4.15	3.51	2.83	2.03
30000	200	20	2.77	3.28	3.86	4.4	4.84	5.13	5.27	5.28	5.19	5.04	4.82	4.52	4.13	3.68	3.18	2.63	1.97
30000	200	50	2.56	2.86	3.16	3.41	3.6	3.71	3.76	3.76	3.72	3.64	3.53	3.38	3.18	2.93	2.64	2.28	1.84
30000	200	100	2.15	2.2	2.28	2.35	2.41	2.46	2.5	2.51	2.5	2.48	2.44	2.39	2.3	2.19	2.04	1.85	1.59
30000	200	200	1.61	1.56	1.55	1.57	1.61	1.65	1.69	1.71	1.72	1.72	1.71	1.7	1.67	1.62	1.55	1.46	1.33
30000	200	300	1.17	1.13	1.12	1.14	1.17	1.2	1.24	1.26	1.28	1.29	1.3	1.3	1.3	1.28	1.25	1.21	1.15
30000	200	400	0.91	0.9	0.91	0.92	0.95	0.98	1.01	1.03	1.06	1.08	1.09	1.1	1.1	1.1	1.09	1.07	1.04
30000	200	500	0.8	0.8	0.81	0.83	0.86	0.88	0.91	0.93	0.96	0.98	0.99	1.01	1.01	1.02	1.01	1	0.99
30000	400	10	5.22	6.36	7.66	8.94	10	10.7	11.1	11.2	11	10.7	10.1	9.4	8.46	7.39	6.26	5.05	3.66
30000	400	20	5.08	6.06	7.08	8.01	8.73	9.19	9.41	9.41	9.26	8.98	8.59	8.05	7.37	6.58	5.71	4.74	3.59
30000	400	50	4.7	5.2	5.69	6.11	6.42	6.63	6.73	6.73	6.65	6.51	6.32	6.06	5.71	5.29	4.79	4.17	3.39
30000	400	100	3.95	3.95	4.03	4.15	4.29	4.42	4.5	4.52	4.49	4.44	4.37	4.28	4.14	3.95	3.7	3.38	2.93
30000	400	200	2.95	2.78	2.74	2.79	2.89	2.99	3.06	3.09	3.09	3.07	3.05	3.02	2.97	2.88	2.76	2.6	2.38
30000	400	300	2.16	2.02	1.99	2.03	2.09	2.16	2.22	2.26	2.28	2.3	2.31	2.31	2.3	2.26	2.21	2.14	2.03
30000	400	400	1.65	1.61	1.61	1.64	1.69	1.74	1.79	1.84	1.88	1.91	1.93	1.95	1.96	1.95	1.93	1.9	1.85
30000	400	500	1.42	1.42	1.44	1.48	1.52	1.57	1.61	1.66	1.7	1.73	1.76	1.78	1.8	1.8	1.8	1.78	1.75
30000	700	10	8.31	9.76	11.6	13.6	15.4	16.7	17.4	17.6	17.4	16.9	16	14.9	13.4	11.7	9.86	7.92	5.69
30000	700	20	8.15	9.32	10.7	12.1	13.3	14.1	14.6	14.7	14.5	14.1	13.5	12.7	11.6	10.3	8.93	7.38	5.54
30000	700	50	7.63	8.21	8.78	9.31	9.78	10.1	10.3	10.4	10.3	10.1	9.81	9.42	8.88	8.19	7.38	6.41	5.17
30000	700	100	6.4	6.42	6.45	6.52	6.66	6.81	6.93	6.98	6.95	6.87	6.78	6.64	6.43	6.12	5.71	5.19	4.49
30000	700	200	4.74	4.55	4.47	4.49	4.58	4.68	4.77	4.81	4.82	4.8	4.79	4.75	4.67	4.53	4.34	4.08	3.74
30000	700	300	3.45	3.29	3.25	3.27	3.34	3.42	3.5	3.56	3.6	3.63	3.65	3.66	3.64	3.58	3.5	3.39	3.22
30000	700	400	2.63	2.58	2.58	2.62	2.69	2.76	2.83	2.9	2.96	3.01	3.05	3.08	3.09	3.08	3.05	3	2.92
30000	700	500	2.25	2.26	2.29	2.34	2.4	2.48	2.55	2.62	2.69	2.74	2.78	2.82	2.84	2.85	2.84	2.81	2.77
30000	1000	10	12.1	13.9	16.4	19.2	21.9	23.9	25	25.3	25	24.3	23.1	21.4	19.2	16.7	14.1	11.3	8.09
30000	1000	20	11.9	13.4	15.3	17.3	19.1	20.3	21	21.1	20.8	20.2	19.4	18.2	16.6	14.7	12.7	10.5	7.78
30000	1000	50	11.2	12.1	13	13.8	14.4	14.7	14.9	14.9	14.7	14.4	14	13.4	12.6	11.6	10.4	8.97	7.14
30000	1000	100	9.43	9.61	9.71	9.76	9.79	9.82	9.84	9.84	9.8	9.7	9.58	9.42	9.14	8.71	8.1	7.31	6.23
30000	1000	200	6.78	6.67	6.59	6.55	6.56	6.6	6.66	6.72	6.76	6.78	6.79	6.77	6.69	6.51	6.24	5.85	5.3
30000	1000	300	4.78	4.68	4.65	4.68	4.74	4.84	4.93	5.03	5.11	5.17	5.22	5.24	5.22	5.16	5.05	4.87	4.62
30000	1000	400	3.68	3.66	3.68	3.75	3.83	3.94	4.05	4.15	4.24	4.31	4.37	4.41	4.43	4.42	4.38	4.3	4.19
30000	1000	500	3.21	3.22	3.27	3.35	3.44	3.55	3.65	3.76	3.85	3.92	3.99	4.04	4.07	4.08	4.07	4.03	3.96
30000	1500	10	16.5	19.2	23	27.1	30.9	33.7	35.2	35.5	35	33.9	32.2	29.8	26.8	23.4	19.7	15.8	11.4
30000	1500	20	16.2	18.6	21.6	24.7	27.2	29	29.8	29.8	29.3	28.5	27.2	25.5	23.2	20.7	17.9	14.7	11
30000	1500	50	15.4	16.8	18.3	19.7	20.6	21.2	21.3	21.2	20.9	20.5	19.9	19	17.9	16.4	14.8	12.8	10.2
30000	1500	100	13	13.4	13.7	13.9	14.1	14.1	14	14	13.9	13.8	13.6	13.4	13	12.4	11.5	10.4	8.83
30000	1500	200	9.38	9.3	9.27	9.28	9.31	9.35	9.39	9.45	9.52	9.57	9.61	9.59	9.49	9.26	8.88	8.29	7.41
30000	1500	300	6.58	6.49	6.49	6.54	6.64	6.77	6.89	7.02	7.14	7.24	7.32	7.36	7.35	7.27	7.11	6.85	6.43
30000	1500	400	5.09	5.08	5.13	5.22	5.35	5.49	5.64	5.78	5.91	6.02	6.11	6.16	6.19	6.18	6.12	6.01	5.83

P	G	ΔT_w	H_b, kJ/kg																
kPa	Kg/m^{2}s	K	1000	1400	1600	1800	1900	2000	2050	2100	2150	2200	2250	2300	2400	2500	2600	2700	3000
30000	1500	500	4.46	4.49	4.56	4.66	4.8	4.95	5.1	5.24	5.36	5.47	5.56	5.63	5.67	5.69	5.67	5.62	5.53
30000	2000	10	21.3	25.6	31.4	37.6	42.9	46.7	48.6	48.9	48.1	46.5	44	40.8	36.6	32	27.1	21.8	15.8
30000	2000	20	21.1	24.8	29.4	34.1	37.9	40.2	41.2	41.2	40.4	39.1	37.3	34.9	31.9	28.4	24.7	20.5	15.6
30000	2000	50	20.1	22.3	24.8	27	28.5	29.3	29.5	29.2	28.8	28.2	27.3	26.2	24.7	22.8	20.7	18.1	14.8
30000	2000	100	17.1	17.8	18.4	19	19.4	19.5	19.4	19.2	19.1	19	18.7	18.4	17.9	17.2	16.1	14.7	12.7
30000	2000	200	12.6	12.6	12.6	12.8	12.9	12.9	13	13	13.1	13.1	13.2	13.1	13	12.8	12.3	11.6	10.3
30000	2000	300	9.03	8.9	8.91	9.01	9.16	9.33	9.49	9.65	9.8	9.93	10	10.1	10.1	9.98	9.79	9.44	8.84
30000	2000	400	7.01	6.98	7.04	7.16	7.34	7.54	7.74	7.93	8.1	8.25	8.37	8.45	8.49	8.47	8.4	8.25	7.99
30000	2000	500	6.12	6.16	6.25	6.39	6.57	6.78	6.98	7.17	7.35	7.5	7.62	7.72	7.78	7.8	7.77	7.7	7.58
30000	3000	10	30.2	36.1	44.2	53	61	66.8	69.9	70.7	69.7	67.5	64	59.3	53.3	46.4	39.2	31.5	22.7
30000	3000	20	29.8	35	41.5	48.1	53.6	57.2	58.8	59	58.2	56.5	54.1	50.7	46.2	41.1	35.5	29.4	22.1
30000	3000	50	28.5	31.7	35.1	38.2	40.4	41.7	42.1	42	41.5	40.8	39.6	37.9	35.6	32.7	29.4	25.6	20.8
30000	3000	100	24.5	25.4	26.3	27.1	27.7	27.9	28	27.9	27.8	27.7	27.3	26.7	25.8	24.5	23	20.9	18.1
30000	3000	200	18.4	18.2	18.2	18.3	18.5	18.6	18.8	18.9	19.1	19.1	19.2	19	18.8	18.3	17.6	16.6	15.1
30000	3000	300	13.2	13	12.9	13	13.2	13.5	13.8	14	14.2	14.4	14.6	14.6	14.6	14.4	14.2	13.7	12.9
30000	3000	400	10.2	10.2	10.2	10.4	10.7	11	11.3	11.5	11.8	12	12.2	12.3	12.3	12.3	12.2	12	11.7
30000	3000	500	8.92	8.96	9.09	9.3	9.57	9.87	10.2	10.4	10.7	10.9	11.1	11.2	11.3	11.3	11.3	11.2	11
30000	5000	10	43.3	51.9	63.5	76.4	88.4	97.5	103	104	103	99.5	94.5	87.5	78.6	68.5	57.8	46.2	32.8
30000	5000	20	42.8	50.4	59.7	69.1	77.3	82.9	85.8	86.3	85.3	83	79.5	74.4	67.8	60.2	51.8	42.5	31.4
30000	5000	50	40.9	45.8	50.5	54.7	58	60	60.9	61	60.5	59.5	57.8	55.2	51.6	47.2	42.2	36.2	28.7
30000	5000	100	35.7	36.9	37.9	38.8	39.4	40	40.3	40.5	40.6	40.4	39.9	38.9	37.3	35.3	32.7	29.5	25.1
30000	5000	200	27.2	26.6	26.3	26.3	26.5	26.8	27.2	27.6	27.9	28.1	28.1	27.9	27.3	26.5	25.4	23.8	21.6
30000	5000	300	19.6	19.1	18.9	19	19.3	19.7	20.2	20.6	21	21.3	21.5	21.5	21.4	21.2	20.7	20	19
30000	5000	400	15.1	15	15.1	15.4	15.7	16.2	16.6	17	17.4	17.7	18	18.1	18.2	18.2	18	17.7	17.2
30000	5000	500	13.2	13.2	13.4	13.7	14.1	14.6	15	15.4	15.8	16.1	16.4	16.6	16.7	16.8	16.7	16.6	16.3

APPENDIX G

PAPERS RELATED TO THIS THESIS AUTHORED OR CO-AUTHORED BY H. ZAHLAN

Zahlan, H., D.C. Groeneveld and S. Tavoularis, "Measurements of convective heat transfer to vertical upward flows of CO_2 in circular tubes at near-critical and supercritical pressures", Nuc. Eng. Des., submitted for publication, 2015.

Zahlan, H., S. Tavoularis and D.C. Groeneveld, "A look-up table for trans-critical heat transfer in water-cooled tubes", Nuc. Eng. Des., accepted for publication, 2015.

Zahlan, H., D.C. Groeneveld and S. Tavoularis," A transcritical heat transfer look up table for water-cooled tubes", International Meeting of Specialists on Heat Transfer to Fluids at Supercritical Pressure, Manchester, UK, 30th June/1st July 2014b.

Zahlan, H., D.C. Groeneveld and S. Tavoularis, "Fluid-to-fluid scaling for convective heat transfer in tubes at supercritical and high subcritical pressures", Int. J. Heat Mass Tran.73, 274–283, 2014a.

Zahlan, H., K. Jiang, S. Tavoularis and D.C. Groeneveld, "Measurements of heat transfer coefficient, CHF and heat transfer deterioration in flows of CO2 at near-critical and supercritical pressures", 6th Int. Sym. SCWR (ISSCWR-6), March 3-7, Shenzhen, Guangdong, China, 2013.

Zahlan, H., D.C. Groeneveld and S. Tavoularis, "A look-up table for trans-critical heat transfer in water-cooled tubes", the 3rd China-Canada Joint Workshop on Supercritical-Water-Cooled Reactors, CCSC-2012, Xi'an, China, April 18-20, 2012.

Zahlan, H., D.C. Groeneveld and S. Tavoularis, "Derivation of a look-up table for trans-critical heat transfer for water-cooled tubes", NURETH-14, Toronto, Ontario, Canada, September 25–30, 2011a.

Zahlan, H., D.C. Groeneveld, S. Tavoularis, S. Mokry and I. Pioro, "Assessment of supercritical heat transfer prediction methods", Proc. 5th Int. Sym. SCWR (ISSCWR-5), Vancouver, British Columbia, Canada, March 13–16, 20 pages, 2011b.

Zahlan, H., D.C. Groeneveld and S. Tavoularis, “Look-up table for trans-critical heat transfer”, the 2nd CCSC-2010, Toronto, Canada, April 25–28, 18 pages, 2010.

Jackson, J.D., M. Anderson, X. Cheng, **H. Zahlan**, Y.Y. Bae and K. Yamada, “Review of progress on the development of new empirical correlation equations under the framework of the IAEA Coordinated Research Programme on heat transfer in SCWR’s”, Proc. of ICAPP ’12, Chicago, USA, June 24–28, Paper 12268, 2012.

Jackson, J.D., editor, (**H. Zahlan contributed to this study**), “Section 6.2 of IAEA CRP report on heat transfer behaviour and thermohydraulics code testing for SCWRs”, IAEA TECDOC-1746, 2012.

Zahlan, H., D.C. Groeneveld and S. Tavoularis, “Validation of a transcritical HEAT Transfer look up table**”,** 1000 Islands Fluid Mechanics Meeting, 2014.

Zahlan, H., S. Tavoularis and D.C. Groeneveld, “Measurements of heat transfer and pressure drop in pipe flow of carbon dioxide at near-critical and supercritical pressures”, 1000 Islands Fluid Mechanics Meeting, 2013.

Zahlan, H., D.C. Groeneveld and S. Tavoularis, “Progress on the development of a look-up table for trans-critical heat transfer in water-cooled heated tubes”, 1000 Islands Fluid Mechanics Meeting, 2012.

Zahlan, H., D.C. Groeneveld and S. Tavoularis, “A skeleton look-up table for trans-critical heat transfer in water-cooled heated tubes”, 1000 Islands Fluid Mechanics Meeting, 2011.

Zahlan, H., D.C. Groeneveld and S. Tavoularis, “Look-up table for trans-critical heat transfer: Skeleton table construction”, 1000 Islands Fluid Mechanics Meeting, 2010.

Jiang, K., **H. Zahlan**, S. Tavoularis and D.C. Groeneveld, “Commissioning tests of the University of Ottawa Supercritical CO_2 Facility”, 6^{th} Annual CNS/CNA Student Conference, TCU Place, Saskatoon, Saskatchewan, June 10 – 13, 2012.